The Tailored Production of Small Diameter Fibres and Their Applications in Wound Healing

A thesis submitted for the partial fulfilment of the requirements for transferring to the degree of

Doctor of Philosophy

By

Jubair Ahmed

Department of Mechanical Engineering

University College London

Torrington Place

London WC1E 7JE

2022

Declaration

I, Jubair Ahmed, confirm that the work presented in this thesis is my own. Where information has been derived from other sources, I can confirm that this has been indicated in the thesis.

Abstract

Thinner fibres benefit from a high surface area to volume ratio which is valuable in many biomedical applications ranging from tissue engineering to drug delivery and wound healing. Fibre forming technologies such as electrospinning and pressurised gyration rely on the careful manipulation of solution properties as well as working parameters to obtain the most optimal fibre morphology for their intended applications. In deeply understanding how these fibre manufacturing technologies work, there can be highly optimised and tailored production of polymeric biomaterials.

Natural substances represent a class of materials that fail to be forgotten for use in health-related applications. Honey and cinnamon have gained significant interest not only for their physical and chemical properties but also for their antibacterial activity. Manuka Honey UMF 20+ was examined for its antibacterial properties against *Escherichia coli* and *Staphylococcus epidermidis* using flow cytometry where the active agent is thought to be the high methylglyoxal content. The inhibitory effect of manuka honey on bacterial growth was evident at concentrations ranging from 10 to 30 v/v%, where higher concentrations benefited from additional honey loading. The incorporation of Manuka honey as an antibacterial agent was explored as a potential route for manufacturing wound dressing components. Using pressurised gyration, scaffolds of sub-micrometre fibres were formed from 10, 20 and 30 v/v% Manuka honey which were incorporated into the polycaprolactone polymer solutions. The composite fibres were analysed for their morphology and topography using scanning electron microscopy. The average fibre diameter of the Manuka honey-polycaprolactone scaffolds was found to be in the range of 437 to 815 nm. The antibacterial activity of the most potent 30 v/v% scaffolds was studied against *S. epidermidis*. The scaffolds showed strong antibacterial activity with a bacterial reduction rate of over 90%. The results here show that honey composite fibres can be considered a natural therapeutic agent for wound healing applications.

Fibrous bandage-like constructs made with incorporated cinnamon extract have been previously shown to have potent antifungal abilities which surpass even the raw material itself. The question remains as to whether these constructs are useful in the prevention of bacterial infections and what the antimicrobial effect means in terms of toxicity to native physiological cells. In this work cinnamon-extracted fibres are tested against *Staphylococcus epidermidis* to assess their antibacterial capacity; it was found that the fibres were able to successfully kill the bacteria. The constructs were also tested under indirect MTT cytotoxicity tests involving the L929 mouse fibroblast cell line, where they showed no variation from the control groups in terms of toxicity. Additionally, cell viability imaging showed no significant toxicity issues with the fibres, even at their tested highest concentration. Here I present a viable method to produce wound healing products made from non-toxic and abundant naturally occurring materials such as cinnamon.

Two fibre forming techniques, pressurised gyration and electrospinning have been combined to create a manufacturing process where advanced wound healing bandages can be created. This new hybrid process leverages the rapid production rate of pressurised gyration to create the bulk portion of the bandages and exploits the precise nature of electrospinning to directly print a bioactive fibrous patch onto the active site of the bandages. Polycaprolactone bandages have thus been created which have a bioactive patch consisting of collagen and chitosan with a poly(ethylene oxide) support. The patches have an average fibre diameter of 173 ± 27 nm and closely resemble the extracellular matrix in its structure, together with the active collagen and chitosan, this will be crucial in their ability to facilitate advanced wound healing. Additionally, synthetic materials such as antimicrobial nanoparticles can be added to the patches which demonstrate that the manufacturing technique is not limited to only using natural materials. Patches with these nanoparticles had an average fibre diameter of 142 ± 31 nm and demonstrated that very uniform and thin fibres could be created with these materials. The process has a great degree of automation and has potential for industrial scalability.

The advancement of manufacturing processes needs to be supported by the discovery of novel materials and novel combinations of existing materials.

Graphene possesses many properties that have predominately been investigated for commercial applications. For the first time, porous graphene (PG) has been incorporated into polymer matrices produced by a high-output manufacturing process. Graphene and its other derivates such as graphene oxide have been shown to provide an antibacterial surface that can mechanically kill pathogens that encounter it. For this reason, graphene nanopores presents itself as a viable additive for wound healing materials. This overarching work focuses on the production of small diameter fibres via multiple techniques to achieve the most control over the final fibre morphology for uses in advanced wound healing materials.

Impact Statement

The cost of wound care for healthcare providers marks a significant portion of overall expenditure. Over 30% of hospital beds are occupied by patients having wounds, whilst those not requiring beds are still treated for wounds [1]. With the rise in global average life expectancy, chronic wounds have shown a strong correlation with increasing age [2]. Together with the rise of antibiotic-resistant bacteria, there is growing pressure for the development of advanced wound care that has the capacity to meet the soaring demands [3].

Even with the abundance of novel materials which show antibacterial properties, little can be done to avoid the side effects which can occur when using these materials *in vivo* [4, 5]. By utilising naturally derived products in antibacterial settings, many of these side effects can be avoided. Materials such as bacterial cellulose, collagen, chitosan and cinnamon from natural sources offer tremendous bioactive wound healing properties that have not yet been properly leveraged. These materials can be incorporated into flexible and easy to apply bandage-like constructs that possess both antibacterial and wound healing properties. However, for these materials to be produced, expertise in fibre forming technologies is needed and their subsequent optimisation will lead to cost-effective healthcare solutions.

Small diameter fibres can be produced by various methods and have for centuries been used for various applications. Today, many specialist techniques are used in the laboratory and in industry that can produce highly fine fibres which benefit from remarkable mechanical properties suitable for wound healing and other healthcare applications.

There is an ever existing need to progress manufacturing technologies to be able to keep up with the demands and requirements of their customer base. For healthcare, there is a great need for better dressings and filtration materials that can adapt to the shifting landscape of antimicrobial resistance and ergonomic designs. The successful modern manufacturing techniques such as electrospinning and pressurised gyration could be stifled by stagnant progress, therefore a thorough investigation into its mechanisms of forming

and modification to the original design will serve to forward materials-based healthcare.

The work presented here is a detailed investigation into different fibre manufacturing techniques and how their operating parameters, polymer solution properties and optimisations can yield a revolution in producing functional biomaterials. There is a lot to be gained from producing low-cost biomaterials for healthcare. High costs prevent mass adoption and increase the financial burden of governments. By targeting cost and biological performance, healthcare providers will be given with additional choices when requiring wound-care materials. Globally, reduction of costs for biomaterials translates into better adoption of technologies that serves to improve the quality of life for patients, increase average life expectancy and reduce offer up more budget towards other impactful activities such as education and public policy making.

Additionally, there is a secondary focus of this work on creating environmentally friendly polymeric systems, the polymers used as biodegradable and sustainable and often come from natural sources. This focus on the environment allows for a groundwork of sustainability, bringing a longevity to the work and facilitating mass adoption to countries all over the world.

By producing novel techniques to produce polymeric fibres, such is presented in this work, this can influence policy makers to begin to optimise manufacturing and have beneficial targets such as reducing final costs, scale-up production and increase funding to specific impactful projects such as manufacturing healthcare biomaterials. Finally, this work represents many scholarly outputs which have already led to several publications beneficial inside and outside of academia. These publications serve to influence professional practice within medicine and healthcare, as well to influence public health and clinical policies.

Publications, Conferences and Awards

Publications

Ahmed J, Matharu RK, Shams T, Illangakoon UE, Edirisinghe M. A Comparison of Electric-Field-Driven and Pressure-Driven Fiber Generation Methods for Drug Delivery. Macromolecular Materials and Engineering 2018:1700577.

Heseltine PL, **Ahmed J**, Edirisinghe M. Developments in Pressurized Gyration for the Mass Production of Polymeric Fibers. Macromolecular Materials and Engineering 2018;0(0):1800218.

Altun E, Aydogdu MO, Crabbe-Mann M, **Ahmed J**, Brako F, Karademir B, Aksu B, Sennaroglu M, Eroglu MS, Ren G, Gunduz O, Edirisinghe M. Co-Culture of Keratinocyte-Staphylococcus aureus on Cu-Ag-Zn/CuO and Cu-Ag-W Nanoparticle Loaded Bacterial Cellulose:PMMA Bandages. Macromolecular Materials and Engineering 2018:1800537.

Altun E, Aydogdu MO, Togay SO, Sengil AZ, Ekren N, Haskoylu ME, Oner ET, Altuncu NA, Ozturk G, Crabbe-Mann M, **Ahmed J**, Gunduz O, Edirisinghe M. Bioinspired Scaffold Induced Regeneration of Neural Tissue. European Polymer Journal 2019;114(2019):98-108.

Aydogdu OM, Altun E, **Ahmed J**, Gunduz O, Edirisinghe M. Fiber Forming Capability of Binary and Ternary Compositions in the Polymer System: Bacterial Cellulose–Polycaprolactone–Polylactic Acid. Polymers 2019;11(7):1148.

Ahmed J, Altun E, Aydogdu MO, Gunduz O, Kerai L, Ren G, Edirisinghe M. Anti-fungal bandages containing cinnamon extract. International Wound Journal 2019;16(3):730-6.

Ahmed J, Gultekinoglu M, Edirisinghe M. Bacterial cellulose micro-nano fibres for wound healing applications. Biotechnology Advances 2020:107549.

Ahmed J, Harker A, Edirisinghe M. COVID-19: Facemasks, healthcare policies and risk factors in the crucial initial months of a global pandemic. Medical Devices & Sensors 2020:e10120.

Ahmed J. Electrospinning for the manufacture of biosensor components: A mini-review. Medical Devices & Sensors 2020;n/a(n/a):e10136.

Cam ME, Hazar-Yavuz AN, Cesur S, Ozkan O, Alenezi H, Turkoglu Sasmazel H, Sayip Eroglu M, Brako F, **Ahmed J**, Kabasakal L, Ren G, Gunduz O, Edirisinghe M. A novel treatment strategy for preterm birth: Intra-vaginal progesterone-loaded fibrous patches. International Journal of Pharmaceutics 2020;588:119782.

Khan AH, Jiang X, Surwase S, Gultekinoglu M, Bayram C, Sathisaran I, Bhatia D, **Ahmed J**, Wu B, Ulubayram K, Edirisinghe M, Dalvi SV. Effectiveness of Oil-Layered Albumin Microbubbles Produced Using Microfluidic T-Junctions in Series for In Vitro Inhibition of Tumor Cells. Langmuir 2020;36(39):11429-41.

Afshar A, Yuca E, Wisdom C, Alenezi H, **Ahmed J**, Tamerler C, Edirisinghe M. Next-generation Antimicrobial Peptides (AMPs) incorporated nanofibre wound dressings. Medical Devices & Sensors 2020:e10144.

Ahmed J, Tabish TA, Zhang S, Edirisinghe M. Porous Graphene Composite Polymer Fibres. Polymers 2021;13(1).

Ahmed J, Alenezi H, Edirisinghe U, Edirisinghe M. Perspective: Covid-19; emerging strategies and material technologies. Emergent Mater 2021:1-6.

Ahmed J, Gultekinoglu M, Bayram C, Kart D, Ulubayram K, Edirisinghe M. Alleviating the toxicity concerns of antibacterial cinnamon-polycaprolactone biomaterials for healthcare-related biomedical applications. MedComm 2021;2(2):236-46.

Kelly A, **Ahmed J**, Edirisinghe M. Manufacturing Cyclodextrin Fibers Using Water. Macromolecular Materials and Engineering 2022:2100891.

Altun E, **Ahmed J**, Onur Aydogdu M, Harker A, Edirisinghe M. The Effect of Solvent and Pressure on Polycaprolactone Solutions for Particle and Fibre Formation. European Polymer Journal 2022:111300.

Conferences

Edirisinghe, M and **Ahmed, J.** Production of Wound Repair Biomaterials with Combined Manufacturing Techniques. Materials Science & Technology 2019, Portland Oregon. Oral Presentation.

Ahmed, J. and Edirisinghe, M. Anti-fungal Bandages Containing Cinnamon Extract. Department of Mechanical Engineering PhD Students Conference, University College London, London, U.K. June 2019. Oral and poster presentation.

Ahmed, J., Mahalingam, S. and Edirisinghe, M. Production of Antibacterial Bandages using Pressurised Gyration and Electrospinning. Department of Mechanical Engineering PhD Students Conference, University College London, London, U.K. June 2018. Oral and poster presentation.

Awards

1st Place at the Young Persons Lecture Competition, London Materials Society, Institute of Materials, Minerals and Mining. London, U.K. February 2020.

Associate Fellowship of the Higher Education Academy. London, U.K. June 2018.

Armourers and Brasiers Company Biomaterials Prize. March 2019.

Acknowledgements

Without Professor Mohan J Edirisinghe, none of this would have been possible. He took me in when I did not have the correct grades for any respectful MSc. programme. It is this belief in his students that sets Professor Edirisinghe apart and his tenacity to motivate (not forgetting his unmatched ability to publish). He is therefore the first person that I would like to thank.

I would also like to thank the friends I have made along the process for providing the support and comfort that is required during such pivotal years a PhD programme delivers. I especially want to acknowledge Dr. Phoebe Heseltine, Mr. Hussain Alenezi (Dr. soon), Miss Ayda Afshar (Dr. soon too, you see the trend), Miss/Dr. Esra Altun, Mr./Dr. Onur Aydogdu and Dr. Keith Lau. Special mention to Dr. Rupy Matharu who is a large part of my success. In addition, I would like to acknowledge Miss Paresha Lily Thind for her help and support of things outside of academia.

I would also like to thank and acknowledge my parents, even though we barely see eye-to-eye, you have supported me greater than any and I am always thankful and grateful for this.

I would like to thank University College London for being a great host, not only for its great catering facilities and events, but for providing excellent resources and being so responsible during the pandemic of 2020 to pending. On the topic of a pandemic, I believe it’s important to acknowledge this as it shows that nothing should be taken for granted and that science cannot stop, as people lives will always depend on it.

Lastly, I would like to thank the people that have come and gone and given me memorable experiences. Without such people, my life would have less value and I believe it is important to meet as many people as you can (when it's safe doing so, of course).

Table of Contents

Chapter 1 : Introduction 26

1.1 Background 26

1.2 Aims and Objectives 28

1.2.1 Produce fibrous membranes suitable for wound healing applications 28

1.2.2 Manufacture functional bioactive wound healing dressings 29

1.2.3 Develop novel routes for manufacturing technologies which can produce materials for biomedical applications 29

1.3 Structure of the thesis 31

1.4 The current landscape 33

Chapter 2 : Literature Review 35

2.1 Introduction 35

2.2 Fibre Production Methods 35

2.2.1 Overview of spinning technologies 36

2.2.2. Electrospinning 40

2.2.3 Pressurised Gyration 44

2.3 Characteristics of Small Diameter Fibres 48

2.3.1 Surface Area 48

2.3.2 Mechanical Properties 48

2.3.3 Morphology, Porosity and topography 49

2.3.4 Applications of Small Diameter Fibres 56

2.4 Fibre Production and Working Parameters 63

2.4.1 Solution Properties 63

2.4.2 Effect of Solvent 64

2.4.3 Effect of Electric Field 66

2.4.3 Effect of Rotation Speed 67
2.4.4 Effect of Pressure 67
2.4.5 Effect of Collection Distance 68
2.5 Uses of Natural Materials as Fibres 68
2.5.1 Antimicrobial Naturally Occurring Spices 69
2.5.2 Cinnamon 70
2.5.3 Honey 71
2.5.4 Collagen 72
2.5.5 Chitosan 73
2.5.6 Alginate 74
2.6 Wound Healing 75
2.6.1 Principles of Wound Healing 75
2.6.2 Requirements of a Wound Healing Material 77
2.6.3 Advanced Wound Healing 79
2.6.3.1 Pro Wound Healing 79
2.6.3.2 Reduction of Scarring 81
2.6.3.3 Antimicrobial 81
Chapter 3 : Experimental Details 84
3.1 Introduction 84
3.2 Effect of working parameters and solution properties on polymeric fibre production 84
3.2.1 Effect of Solvent and Pressure 85
3.2.2 Effect of Binary and Ternary Polymer Systems 88
3.3 Antimicrobial Natural Materials 90
3.3.1 Antibacterial Honey Fibres 91
3.3.2. Antifungal Cinnamon Fibres 96
3.4 Advancements in manufacturing technologies and Materials Selection 100

3.4.1 Bandage Production with Novel Manufacturing Route 101
3.4.2 Production of Fibres Using an Updated Vessel Design 103
3.4.3 Advanced Material selection: Porous Graphene Composite Fibres 106
Chapter 4 : Investigating the Effect of solution properties and working parameters on polymeric fibre production 109
4.1 Introduction 109
4.2 Effect of Solvent on Fibre Morphology 109
4.2.1 Solubility 109
4.2.2 Physical and Rheological Properties Influenced by Solvent 112
4.2.3 Effect of Solvent on the Morphology of the fibres 114
4.3 Effect of Gas Pressure on Fibre Morphology 120
4.4 Effect of Binary and Ternary Polymer Blends on Fibre Production 124
4.4.1 Production Yield 124
4.4.2 Morphology 126
4.4.3 Mechanical Properties 132
Chapter 5 : Antimicrobial Natural Materials 136
5.1 Introduction 136
5.2 Honey 136
5.2.1 Antibacterial Activity of Honey 136
5.2.2 Honey Composite Bandage-like Fibres 139
5.2.3 Antibacterial Activity of Honey Composite Fibres 146
5.3 Cinnamon 148
5.3.1 Antifungal ability of Cinnamon 148
5.3.2 Cinnamon Bandage-like Fibres 152
5.3.3 *In-Vitro* Testing on Cinnamon-extracted Fibres 156
5.3.4 *Cytotoxicity* Testing on Cinnamon-extracted Fibres 157
5.3.5 Antibacterial activity of Cinnamon Extracted Fibres 159

Chapter 6 : Advancements in Manufacturing Technologies and Materials Selection 164
6.1 Bandage Production with Novel Manufacturing Approaches 164
6.1.1 Bandage Production 164
6.1.2 Collagen and Chitosan Patches 166
6.1.3 Collagen, Chitosan and Antimicrobial Nanoparticles Patches 168
6.2 Gyratory Fibre Production with an Updated Vessel Design 170
6.3 Advanced Material Selection for Novel Wound Healing Approaches 178
6.3.1 Characterisation of Fibres 179
6.3.2 Chemical Composition of Fibres..... 183
Chapter 7 : Conclusions and Future work..... 189
7.1 Conclusions 189
7.1.1 The effects of Solution and Working Parameters in Fibre Production 189
7.1.2 Bandage production using natural materials 192
7.1.3 Advancements in Manufacturing Technologies and Materials Selection 196
7.2 Future work and Limitations 199
7.2.1 Analyse non-major working parameters 199
7.2.2 Develop polymer systems avoiding organic solvents 200
7.2.3 Extensive mechanical testing 201
7.2.4 Further chemical and morphological testing 201
7.2.5 Further discovery of natural materials which have antimicrobial effects..... 202
7.2.6 Further discovery of natural materials with healthcare benefits.. 203
7.2.7 Antimicrobial tests 204
7.2.8 Mechanism of Action 204
7.2.9 Further Purification and Isolation Studies 205

7.2.10 Wound Healing Models 205
7.2.11 Further Development of Fibre Forming Technologies 206
7.2.12 Materials Discovery and Novel Combinations 206
References 208

List of Tables

Table 1: Table summarising the key properties and their desired ranges for optimal wound healing 78
Table 2: Physical properties of the solvents investigated in this work; values have been reported at 25 °C. 110
Table 3: Physical properties of the PCL solutions with different solvents used in the study, values have been reported at 25 °C and a constant sheer rate of 3 mPa.s was used. 113
Table 4: Solution properties of the binary systems and the ternary samples investigated in this study. 131
Table 5: Viscosity and surface tension measurements of the studied polymer solutions and Manuka honey. 139
Table 6: Temperature values of virgin PCL, C1, C2 and C3 gyrospun polymeric fibre materials in terms of weight loss %. 157
Table 7: Solution properties of the three polymer solutions used in this study, all dissolved in chloroform 170
Table 8: Collected Raman bands (cm^{-1}) and their corresponding assignments for PCL-based graphene nanocomposite at 532 nm laser excitation [555-557]. 184

List of Figures

Figure 2.1: Schematic representation of woven and non-woven fibre products, woven structures are interlaced at right angles whilst non-woven materials are not bonded during the initial process. 36
Figure 2.2: Diagrammatic overview of the melt blowing process. 38
Figure 2.3: Diagrammatic overview of the dry spinning process. 39
Figure 2.4: Diagrammatic overview of the wet spinning process. 40
Figure 2.5: Illustration of the major forces in equilibrium in a stable Taylor cone produced by electrospinning. Adapted from [68]. 41
Figure 2.6: Schematic representation of the basic electrospinning setup, depicting the high voltage power supply, metallic nozzle, high precision continuous syringe pump and the grounded plate where fibres are collected. 42
Figure 2.7: Diagrammatic representation of the basic pressurised gyration laboratory setup showing the rotating drum, gas supply inlet, high-speed motor and the variable speed controller. 45
Figure 2.8: Diagrammatic summary of the main forces acting on the polymer solution to cause a polymer jet and subsequent thinning into fibres. 47
Figure 2.9: Diagram showing intra-fibre porosity in a non-woven fibre mat with red arrows indicating pores between fibre strands. 51
Figure 2.10: Scanning electron micrograph images showing surface pores of polymeric fibres. 52
Figure 2.11: Scanning electron micrograph images showing; a) smooth surface fibres, b) rough surface fibres, c) fibres with surface grooves and d) fibres with pits resembling valleys. 53
Figure 2.12: Scanning electron micrograph images showing polymeric fibres which have unidirectional alignment. 54
Figure 2.13: Scanning electron micrograph images showing the characteristic bead-on-string morphology in small diameter fibres. 55
Figure 2.14: Scanning electron micrograph image showing a hollow fibre strand. 56

Figure 2.15: Diagrammatic overview of tissue engineering, showing how a three-dimensional fibrous can be used to support and encourage cellular growth. 57
Figure 2.16: Diagrammatic overview and principle of solid dispersion of pharmaceuticals in polymeric fibres. 59
Figure 2.17: Diagrammatic overview of the basic principles of water filtration using a polymeric fibrous membrane to trap particulates, a similar approach can be used for air filtration where the air is passed through the same setup. 61
Figure 2.18: Diagram summarising the thinning mechanism of polymer jets in pressurised gyration, volatile solvents will allow less thinning than less volatile solvents. 65
Figure 3.1: Photograph showing honey-PCL composite fibres surrounding the pressurised gyration vessel, ready to be collected. 93
Figure 3.2: Photograph showing the manufacturing route combining electrospinning (top right corner) and pressurised gyration (centre); the collection walls can be seen to aid bandage production and a grounded collection ring allows the electrospinning needle to focus bioactive material onto a specific target site of the bandage. 102
Figure 3.3: Photograph showing a) general view and b) front view of the updated pressurised gyration vessel design (left); the inner and outer walls have been curved as opposed to the standard flat wall of the original (right). 105
Figure 4.1: Schematic diagram of the polymer dissolution process. 112
Figure 4.2: Scanning electron micrograph images of PCL fibres in different solvents. Constituting of a macroscopic view of; a) DMF, d) THF, g) Toluene, j) DCM, m) Chloroform, a surface view of; b) DMF, e) THF, h) Toluene, k) DCM, n) Chloroform and the close-up fibre view of; c) DMF, f) THF, i) Toluene, l) DCM, o) Chloroform. 116
Figure 4.3: Diagrammatic representation of the polymer jet under pressurised gyration when using a) a volatile solvent, b) a less volatile solvent. Differences in the solvent systems used in spinning fibres give rise to changes in fibre morphology which can be beneficial for different applications. 119

Figure 4.4: Scanning electron micrograph images of PCL fibres in different solvents; a), b) DMF 0 MPa and 0.1 MPa pressure, c) - f) THF 0 MPa to 0.3 MPa pressure, g) -f) Toluene 0 MPa to 0.3 MPa pressure, k) - n) DCM 0 MPa to 0.3 MPa pressure and o) - r) Chloroform 0 MPa to 0.3 MPa pressure. For all instances, n = 100. 120
Figure 4.5: Graph showing the overview and relationship between increasing gas pressure and the resulting fibre diameters, for each case n = 100. 122
Figure 4.6: Percentage yield values for binary systems showing a) PLA-BC b) PCL-BC and c) PLA-PCL bandage-like fibrous samples, differences in yield are a direct result of changing the binary composition of the polymer system. 125
Figure 4.7: Scanning electron micrograph images of the PLA-BC binary fibres, showing; a) 90:10 PLA-BC, b) 80:20 PLA-BC, c) 70:30 PLA-BC, d) 60: 40 PLA-BC, e) 50:50 PLA-BC, f) 40:60 PLA-BC, g) 30:70 PLA-BC, h) 20:80 PLA-BC and i) 10:90 PLA-BC. 127
Figure 4.8: Scanning electron micrograph images of the PCL-BC binary fibre, showing: a) 90:10 PCL-BC, b) 80:20 PCL-BC, c) 70:30 PCL-BC, d) 60:40 PCL-BC, e) 50:50 PCL-BC, f) 40:60 PCL-BC, g) 30:70 PCL-BC, h) 20:80 and i) 10:90 PCL-BC. 128
Figure 4.9: Scanning electron micrograph images of the PLA-PCL fibres produced with: a) 100:0 PLA-PCL, b) 90:10 PLA-PCL, c) 80:20 PLA-PCL, d) 70:30 PLA-PCL, e) 60:40 PLA-PCL, f) 50:50 PLA-PCL, g) 40:60 PLA-PCL, h) 30:70 PLA-PCL, i) 20:80 PLA-PCL, j) 10:90 PLA-PCL and k) 0:100 PLA-PCL. 129
Figure 4.10: Graphical representation of the average fibre diameters for each material combination used: a) binary systems of (PLA-BC, PCL-BC, and PLA-PCL), b) Virgin PLA, PCL and optimised ternary composite (70:30 (PLA-PCL)-BC). 130
Figure 4.11: Tensile strength values of samples: a) Ultimate tensile strength of the binary systems, b) Young's modulus of the binary systems, and b) Ultimate tensile strength and Young's modulus of the ternary sample. 133
Figure 5.1: Antibacterial activity of S. epidermis and E. coli against Black Forest Honeydew and Manuka honey at concentrations of 10, 20 and 30 (v/v%). The antibacterial efficiency is given here as the percentage proportion

of dead cells following incubation. **** indicates a significant difference with a p-value <0.0001. 137
Figure 5.2: Scanning electron microscope image of fibres produced; a), Virgin PCL fibres, b), 10% honey-composite fibres, c), 20% honey-composite fibres, d), 30% honey-composite fibres. High magnification images of e), Virgin PCL fibres, f), 10% honey-composite fibres, g), 20% honey-composite fibres, h), 30% honey-composite fibres, along with corresponding fibre diameter distribution histograms i to l. 141
Figure 5.3: FTIR spectra of virgin PCL fibres, 30% honey-loaded fibres and pure Manuka honey. Specific peaks associated with Manuka Honey and with PCL are highlighted using arrows in the composite fibres. 144
Figure 5.4: Antibacterial activity of 10, 20 and 30% Manuka honey-PCL composite fibrous meshes compared to the negative control of virgin PCL fibres, antibacterial effectiveness is expressed as a percentage bacterial reduction. The data was compared using an unpaired t-test **** $p < 0.0001$; ** $p < 0.05$..... 147
Figure 5.5: Pictures following 48 hours of incubation showing plates containing; a): ground cinnamon powder, b): virgin PCL fibres, showing lack of an inhibition area, c): C1 cinnamon extracted fibres, d): C2 cinnamon extracted fibres, e): C3 cinnamon extracted fibres and, in each case, 100mg of sample was investigated. For each plate, the inhibition area value is given. 150
Figure 5.6: Graph comparing inhibition areas of the different samples, shown in figure 2, n=3. 151
Figure 5.7: Scanning electron microscopy images of pressure spun fibres at 0.1 MPa: a) virgin PCL fibres b) diameter distribution of the virgin PCL fibres c) cinnamon-extracted PCL fibres (C2) d) diameter distribution of the cinnamon-loaded PCL fibres, in all cases, n= 100. 153
Figure 5.8: Fluorescence microscopy video stills of: a) C1 extracted cinnamon fibre showing a clear inhibition zone with no fungal growth, SEM images of: b), c), candida growth over virgin PCL fibres, arrow marked in b), d) high magnification image showing close-up of C. albicans cell growth on virgin PCL fibre surface. 154

Figure 5.9: Images taken 504 hours after initial incubation comparing: a), C1 extracted cinnamon containing fibres (RHS) compared with raw cinnamon powder (LHS) with raw cinnamon powder b), C2 extracted cinnamon containing fibres c), C3 extracted cinnamon containing fibres. All petri-dishes shown are 90mm in diameter..... 155
Figure 5.10: TGA thermograms of PCL, C1, C2 and C3 gyrospun polymeric fibres..... 157
Figure 5.11: Cytotoxicity-MTT test results indicating the cell viability (%) of PCL fibres and cinnamon-extracted fibres at the tested concentrations. ... 158
Figure 5.12: Live/dead staining test results for a) control, b) PCL Fibres, c) C1 fibre sample, c) C2 fibre sample and e) C3 fibre sample. 159
Figure 5.13: Antibacterial test results for control (virgin PCL), C1, C2 and C3 samples against S. aureus, MRSA, E. coli and E. faecalis bacteria species (* $p < 0.05$). 160
Figure 5.14: Antibacterial test results captured by scanning electron micrographs for the control (virgin PCL), C1, C2 and C3 samples against S. aureus, MRSA, E. coli and E. faecalis species. For each micrograph, the scalebar corresponds to 5 μm. 162
Figure 6.1: a), b) high magnification scanning electron micrographs of PCL fibrous bandages; c) fibre diameter distribution graph for the corresponding micrographs. 165
Figure 6.2: a), b) high magnification scanning electron micrographs of: PEO fibres loaded with collagen and chitosan within the polymer matrix; c) fibre diameter distribution graph for the corresponding micrographs 167
Figure 6.3: a), b) high magnification scanning electron micrographs of: PEO fibres loaded with collagen, chitosan and antimicrobial nanoparticles; c) fibre diameter distribution graph for the corresponding micrographs. 169
Figure 6.4: SEM micrographs of: a) PCL, c) PLA and e) PMMA fibres spun at 0.0 MPa additional gas pressure with the P0 pot design, g) PCL, i) PLA and k) PMMA fibres spun at 0.0 MPa additional gas pressure with the P0 pot design. b),d), f), h), j) and l) are fibre diameter distributions to the corresponding SEM micrographs. 173
Figure 6.5: SEM micrographs of: a) PCL, c) PLA and e) PMMA fibres spun at 0.1 MPa additional gas pressure with the P1 pot design, g) PCL, i) PLA and k)

PMMA fibres spun at 0.1 MPa additional gas pressure with the P0 pot design. b),d), f), h), j) and l) are fibre diameter distributions to the corresponding SEM micrographs. 174
Figure 6.6: High speed video camera snapshots of a transparent gyration pot with the original P0 design. a) – f) shows 6 frames from when t=0 after the gyration motor starts to t= 590 ms when the fibre generation begins. 176
Figure 6.7: Scanning electron micrograph images of fibres; a), b) 15% pristine PCL fibres without the incorporation of PG, c), d) 3 wt% PG incorporated fibres showing surface porosity and unidirectional alignment, red circles and arrows indicate the presence of surface particles e), f) 4 wt% PG incorporated fibres showing surface topography and random orientation alignment and g, h)) 5 wt % PG incorporated fibres with surface and full view, all images come with accompanying diameter distribution graphs, i), j), k) and l). For each graph, 100 fibre strands were measured at random. 181
Figure 6.8: Raman spectra of 3,4 and 5 wt% PG-PCL composite fibres. .. 185
Figure 6.9: Fourier Transform Infrared (FTIR) spectra comparing the chemical compositions of pristine PCL fibres along with 3, 4 and 5 wt% PG-PCL fibres. 186
Figure 6.10: Fourier Transform Infrared (FTIR) spectra comparing the chemical compositions of pristine PCL fibres along with 3, 4 and 5 wt% PG-PCL fibres. 187

Abbreviations

BC: Bacterial Cellulose

DCM: Dichloromethane

DMF: Dimethylformamide

FTIR: Fourier-transform infrared spectroscopy

kV: Kilovolt

MPa: Megapascal

nm: Nanometre

PCL: Polycaprolactone

PG: Porous Graphene

PLA: Poly(lactic acid)

PMMA: Poly(methyl methacrylate)

rpm: Revolutions per minute

SEM: Scanning electron microscope

TGA: Thermal gravimetric analysis

THF: Tetrahydrofuran

v/v% Volume by volume percentage

w/v%: Weight by volume percentage

wt.%: Mass fraction percentage

µm: Micrometre

Chapter 1 : Introduction

1.1 Background

Fibres are a class of materials defined by having a significantly higher length than width. Owing to their unique shape, fibres have been historically used in clothing and protection due to their numerous characteristic properties. The high length to width ratio of fibres gives them high mechanical strength in bundles, high flexibility and are a class of materials that possess high uniformity [6-8]. Moreover, fibres have been extensively utilised in biomedical applications ranging from tissue engineering, antibacterial filtration, drug delivery to use as biomaterials [9-12]. In these applications, fibres are highly suited due to their structure and properties [13]. The use of polymeric fibres opens the vast potential for biomedical applications owing to their biocompatibility and highly customisable nature.

Many techniques exist to produce small diameter fibres, common methods are centrifugal spinning, wet spinning, dry spinning, solution blowing and electrospinning [14]. Of all the laboratory fibre production methods, electrospinning has gained the most attraction from academia and industry for its ability to consistently produce fine fibres [15]. The hybrid technique pressurised gyration has also seen much interest recently in the manufacturing of fine fibres for use in biomedical applications [16]. As with all technologies, optimisation can transform the output capabilities and provide superior products which are highly suited to end-use case scenarios.

Synthetic chemistry has revolutionised the way in which humans live thanks to the superior properties of these polymers and their ability to be readily produced [17, 18]. However, there has been a recent shift towards using naturally occurring polymers as they are more environmentally friendly and are often more biocompatible than their synthetic counterparts [19, 20]. Naturally occurring polymers have long been known for their ability to be antibacterial, anticancer, antidiabetic and pro wound healing [21-24]. Naturally derived polymers are abundant and biodegradable but they fall short in their

reproducibility methods and they demonstrate batch-to-batch variation [25]. By combining synthetic and naturally derived polymers, advantageous properties can be merged and exploited.

The cost of wound care for any healthcare provider marks a significant portion of overall expenditure. Over 30% of hospital beds are occupied by patients having wounds, whilst those not requiring beds are still treated for wounds [1]. With the rise in global average life expectancy, chronic wounds have shown a strong correlation with increasing age [2]. Furthermore, with the increase in global antimicrobial resistance, there is a huge concern for the spread of microbial infection, which is especially prevalent in open-wound scenarios [26]. There is growing pressure for the development of advanced wound care that can prevent the spread of infection and provide an advanced recovery. This type of wound care product must be able to meet the soaring demands of the healthcare industry.

Fibres produced by electrospinning and other methods have been successfully used as wound dressing materials [27, 28]. These fibres are highly suited to wound healing as they can resemble the extracellular matrix and encourage cell development, they provide adequate protection to the wound site and they permit for the free movement of exudate, allowing the wound healing process to occur [29-31]. Electrospinning exploits an electric field applied to its metallic nozzle which overcomes various forces in the polymer solution to create a polymer jet [32]. Fibres produced by pressurised gyration provide high strength and flexibility which are very beneficial as bandage-like materials [33]. Unlike electrospinning, pressurised gyration uses centrifugal force and an external gas pressure to form the polymer jet required for spinning fibres [34]. Pressurised gyration has the unique ability of all the laboratory fibre manufacturing techniques, to produce bandages with excellent mechanical properties at a substantial production rate which significantly outpaces all other technologies. By utilising the benefits from different practices, there can be an advanced process that can provide the necessary output materials for wound healing and other specific biomedical applications.

In this work, small diameter fibres are produced with an emphasis on properties relating to use in wound healing. The manufacturing process of these fibrous constructs will be thoroughly analysed to determine the effects of solution properties and working parameters which will allow for the tailoring of fibres for use in antimicrobial wound healing and other biomedical applications. Furthermore, natural and synthetic polymers will be used in conjunction with each other to produce antimicrobial bandages which will target hospital-related infections that are more prevalent in environments where wounds are widespread. The manufacturing process of Pressurised gyration will also be combined with electrospinning to enable the creation of bandages with a highly specific active site where the active region come into contact directly with the wound. This sort of technology would contain nanofibrous materials capable of advanced wound healing.

1.2 Aims and Objectives

The research carried out here has a focus on the production of fibrous membranes suitable for wound healing applications. The aims and objectives of this work can be broken down into core segments.

1.2.1 Produce fibrous membranes suitable for wound healing applications

Extensive research will be undertaken to optimise for the ideal materials in order to optimise the production of bandage-like fibrous constructs for wound healing applications. In order to best optimise the production system using pressurised gyration, the effects of several key working parameters will be investigated including the effect of polymer solution, solvent and applied gas pressure. The produced polymeric materials will then be evaluated using scanning electron microscopy and ImageJ software where the fibre morphology and diameter distribution will be assessed with respect to their ability to sustain a good wound healing environment. Furthermore, the mechanical behaviour of these fibrous bandage-like constructs will be

assessed using tensile-testing in order to evaluate their suitability as wound healing materials.

1.2.2 Manufacture functional bioactive wound healing dressings

Naturally occurring materials have remarkable antibacterial and pro-wound healing abilities that can be utilised in modern wound-care materials with the benefit of having low toxicity, less likely to result in rapid antimicrobial resistance and having a lower impact on the environment. The optimised polymer solutions will be used to manufacture bioactive fibrous constructs, which are to be antimicrobial in nature using a range of natural additive such as honey and cinnamon extract. These fibrous materials will then be tested for their ability to elicit antimicrobial activities against a range of different microbial species. For example, the antifungal ability of these bandage-like structures will be tested against *Candida albicans* and the antimicrobial ability with both gram-positive *Staphylococcus aureus* and gram-negative *Escherichia coli.* Antimicrobial materials can often be toxic to self-cells of the body and therefore cytotoxicity studies will then have to be undertaken. For cytotoxity tests LIVE/DEAD™ Viability/Cytotoxicity tests will be used to estimate the proportion of live and dead cells. Natural materials will be discovered and a novel methodology to effortlessly produce high-yield fibrous meshes will be created. Natural spices such as cinnamon will be extracted and used in polymeric bandage-like constructs aimed at providing an antimicrobial recovery environment for wounds, the action of these antimicrobial additions will be studied for their efficacy and how they affect the healing process.

1.2.3 Develop novel routes for manufacturing technologies which can produce materials for biomedical applications

Improvements to the field of manufacturing fibrous biomedical scaffolds will serve to reduce costs and increase access to better wound healing materials for all. A novel combination of manufacturing techniques for bioactive bandages will be made. The study will elucidate the necessity for improvements to original designs, especially pertaining to pressurised gyration and the requirement for the discovery of novel materials and their subsequent

exploitation in manufacturing. In order to achieve this, a combination of the pressurised gyration and electrospinning systems will be showcased which will allow for the highly customised and specific creation of wound healing products that will leverage the advantages from both manufacturing techniques. A novel pressurised gyration design will be compared to the original and the incorporation of novel material approaches such as polycaprolactone-porous graphene fibres will be produced. These comparisons will take made via comparing the fibre morphology of the produced fibres using the different techniques and asses the fibre morphology and diameter distribution.

All in all, this work focuses on the production of such fibrous materials with an emphasis on how these final products can be used to advance the field of wound healing by providing wound specific activity. Antimicrobial testing will be used to assess the ability of these materials to restrict or inhibit microbial growth of both bacterial and fungal species. Chemical analysis will be used to confirm the presence of important compounds including certain bioactive substances which are essential to the proper functioning of the polymeric structures in wound healing environments. The thorough investigation into the tailored production of small diameter fibres will pave the way for the advancement in wound healing strategies that can be utilised in healthcare settings and other important biomedical engineering applications such as in drug delivery and tissue engineering.

1.3 Structure of the thesis

This thesis is structured in the following way:

Chapter 1

Provides a concise summary of the background behind the chosen project as well as the aims and required objectives for successfully carrying out the work presented in this thesis.

Chapter 2

Presents an in-depth look at the exciting knowledge on fibre production methods, the detailed characteristics of fibre morphology and how desirable properties relating to wound healing can be produced by utilising modern production techniques. This section also contains original diagrams and micrographs that detail fibre morphology from additional experiments carried out by the author which have not been published elsewhere.

Chapter 3

Contains a detailed account of the materials, reagents and methodology used in this work along with the names of the related suppliers and their locations. Details regarding antimicrobial testing procedures and other cell-based testing are included here as well as characterisation techniques crucial for analysing any microstructures.

Chapter 4

Is a thorough investigation into the effects of polymer solution properties and manufacturing working parameters on the morphology and properties of polymeric fibres. In this section, the solubility of solvents, physical properties of solutions, the effect of working parameters and the blending of different polymer systems are studied experimentally, and the produced constructs are characterised.

Chapter 5

Is focused on the manufacture of bandage-like fibrous scaffolds from naturally occurring materials which are both antimicrobial and pro-wound healing. These natural materials are composited with purposeful polymers to produce bandages, they are then characterised, and a series of *in vitro* tests are carried out to show the antimicrobial and cytotoxic properties.

Chapter 6

Concludes the work encompassing this thesis. It thus incorporates all the elements found in the previous chapters. The data gathered from optimising manufacturing and producing healthcare biomaterials are used to develop a novel manufacturing route to produce bioactive bandages, improved design and implementation for the pressurised gyration process and work carried out with novel material combinations to advance the field of healthcare materials.

Chapter 7

Concludes the work by summarising key findings from each of the experimental phases and the future work that should be carried out in order to continue the progress in manufacturing functional healthcare biomaterials and overcome some of the limitations of the current work.

1.4 The current landscape

Currently, the state of the art of producing fibres is limited to electrospinning. Although recent strides have been made in electrospinning such as the nanospider electrospinning system, allowing it to be used in mass production applications, there is still room for improvement [35]. Multi-nozzle configurations do exist and can improve the production rate, however, there are complications with the electrical interference of neighbouring nozzles. Other techniques which mass-produce polymeric nanofibers such as melt spinning can produce large masses of fibrous product and are also not perfect, these technologies do not offer highly custom designs to be made.

The current gold standard for low-cost wound management strategies is mostly confined to using bandages and gauzes for multiple intended effects such as the stoppage of bleeding, protecting the immediate wound environment and the application of pressure over the wound site. These low-cost materials do little to protect against many microbial species, both fungal and bacterial, which can cause serious complications later and then be difficult to treat. This work focuses on the optimised production of advanced wound healing constructs that can provide a wound healing environment capable of fighting microbial infection, whilst also providing suitable chemical cues to improve the quality of healing down to the cellular level. Consequently, it is important to work closely with the manufacturing and production side as, any addition to the beginning of the line, will result in disproportionally higher costs to the final design. Therefore, an extensive analysis of the manufacturing is provided in this thesis.

Most importantly, various physical characterisations will be made to investigate the effect of important operating parameters and solution properties on the final fibre morphology of the produced bandage-like fibres. The work presented will therefore operate as a thorough guide for future work based on this initial offering. This work will present the extensive effects of important operating parameters and solution properties on the physical and chemical characteristics of fibres. With the intended application of wound healing in mind, the characterisation and subsequent deep analysis will yield

useful data that will allow for advanced wound care materials to be made in an optimised manner. In relation to the analysis of working parameters which influence fibre morphology for wound healing products, there is very little definitive literature and work. This work will thus focus on the important operating and solution parameters that work together to provide the utmost control over polymeric fibrous products for their intended use in biomedical engineering and healthcare.

Chapter 2 : Literature Review

2.1 Introduction

The use of fibres in civilisation has been of great importance for many millennia. Cotton, wool and silk as textile fibres can be dated as far back as the ancient Egyptians [36]. Their unique shape and flexibility allowed them to be woven into clothing which minimally restricted free movement for the wearer, provided protection against the environment and also served as status symbols in many cultures [37]. The versatility of fibres allowed them to be used in other applications such as fishing nets, ropes, agriculture and netting [38]. Today, fibres are routinely used in various commercial applications, however, the use of fibres for biomedical applications and medicine has seen a steep rise in interest [39]. The literature surrounding the production of small diameter fibres for use in biomedical applications such as wound healing is thoroughly surveyed, with an emphasis on how to achieve desirable characteristics. Also, in this chapter, natural and synthetic polymers are researched for their ability to provide advanced wound care which can support new cell growth and provide antimicrobial action.

2.2 Fibre Production Methods

Many production methods have existed to produce fibres for lifestyle applications such as clothing and insulation. Cotton is the most commonly used natural fibre for textiles [40]. Raw seed cotton is removed, purified and then formed into functional fibrous textiles in a well-known process called spinning [41]. Modern fine-diameter fibre production methods work on dissimilar principles as the choice of materials are different along with their applications. This section will discuss prominent modern techniques and how each technology addresses modern requirements.

2.2.1 Overview of spinning technologies

Fibrous products can be categorised into two main types, woven and non-woven (**Figure 2.1**). Traditional fibre products are woven, where weaving many threads together perpendicularly with each other creates woven fabrics. Woven products generally benefit from increased uniaxial tensile strength due to the arrangement of their fibres [42]. Non-woven materials are long fibres that have not been constructed together during manufacturing, but which typically are later bonded together using chemicals, heat or other mechanical treatment [43]. Both categories of products have their distinct advantages and disadvantages. The non-woven industry was valued at 14 million dollars in 2004 and is expected to continue growing [44]. Non-woven fibres can generally be produced at a lower cost and have useful properties such as water-repellence, thermal insulation, material stretch and can also act as a barrier against microbes [45-48].

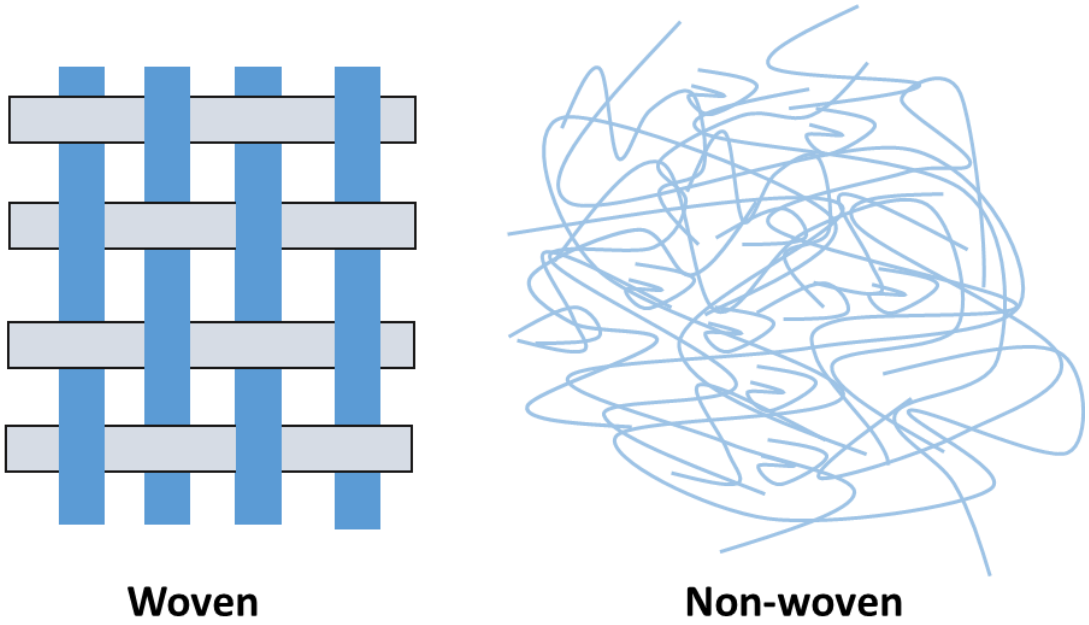

Figure 2.1: Schematic representation of woven and non-woven fibre products, woven structures are interlaced at right angles whilst non-woven materials are not bonded during the initial process.

In recent decades, there has been a shift in consumer medical technology as personalised and wearable medical devices have seen increased demand and investment [49]. Materials that come in contact with the skin or bodily fluids must be biocompatible. Biocompatibility can be defined as materials that are not toxic to living tissue by way of not causing an immunological rejection [50]. The material choice for use in medicine is therefore heavily dependent on its ability to be non-toxic to cells and other crucial characteristics discussed later in (**section 2.3**). Both woven and non-woven structures can be used in biomedicine, but careful consideration must always be carried out to suit to end application, small diameter fibres have had a large increase in interest. In order to produce finer fibres, newer methods have been invented which aim to balance production with average fibre diameter, yield, production rate and fibre diameter uniformity.

Melt blowing is a fabrication method allowing for the production of micro- and nanofibres. In this technology, fibres are essentially extruded through small nozzles by a high-velocity gas stream [51]. The overview of the technology is shown in (**Figure 2.2**). The high-speed gas causes the polymer melt inside the machinery to be manipulated at a greater velocity through the nozzles creating ultrafine fibres as they are forced through the openings. In order for this technology to operate, the processed material must be a polymer with thermoplastic behaviour, common examples are polypropylene, polystyrene and polyurethane [52]. This technology has many benefits; it is a one-step process that can be automated, does not require the use of solvents and is able to produce fibres down to an average of about 36 nm [53]. The fibres are usually collected on rotating collectors and thus the end product is a mat of non-woven fine fibres. These fibre mats can have direct applications in filtration, as sorbents, medical gowns and drug delivery [54-56]. The melt blowing technology is not without its drawbacks. The polymer that is to be spun, must be a thermoplastic and be able to form a melt to be processed into fibres, this greatly limits the choice of working materials, as many useful polymers for biomedical applications may not exhibit this property. Furthermore, the process relies on very high temperatures (between 230 - 390°C) which makes it a highly energy-intensive process. Investment in heavy

and expensive machinery is required, when compared to other smaller fibre forming methods, which limits its ability to be used in many laboratory environments and as an *in-situ* form of producing nanofibres in a hospital environment.

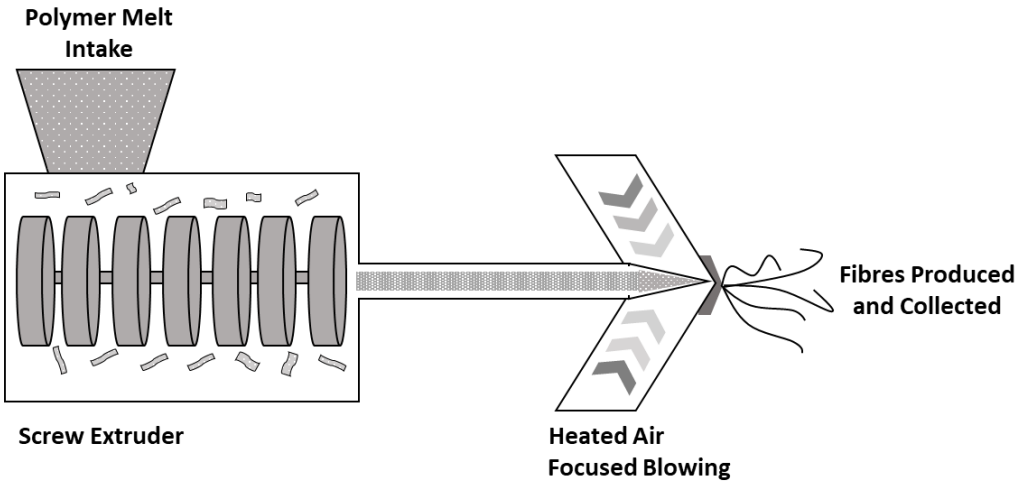

Figure 2.2: Diagrammatic overview of the melt blowing process.

Dry spinning is another fibre manufacturing process where a polymer in the form of a dissolved solution, is pumped through a spinneret where an evaporating chamber is responsible for providing a stream of hot air onto the emerging jets [57]. The key principle behind its fibre production is the control over evaporation of the polymer in the spin line were the key variables are mass transfer, heat transfer and filament stress [58]. The process is summarised in (**Figure 2.3**). The produced non-woven fibres can be utilised in many different applications such as tissue engineering and drug delivery. The most common polymer to be used by dry spinning is cellulose acetate where the polymer has had much success [59]. The advantages of this technology are that fine fibres below the micrometre range can be easily produced. The drawbacks, however, are mainly due to the use of harsh solvents. High vapour pressure volatile solvents are required which can pose health and safety concerns as well as environmental problems. Furthermore, the polymer solution is often blended with additives and needs to be filtered which adds processing steps and ultimately increased costs to the production line. This process is fundamentally more complex than melt spinning and thus

the fibres are more expensive to produce, in a field where cost per unit determines mass adoption, this can be very undesirable.

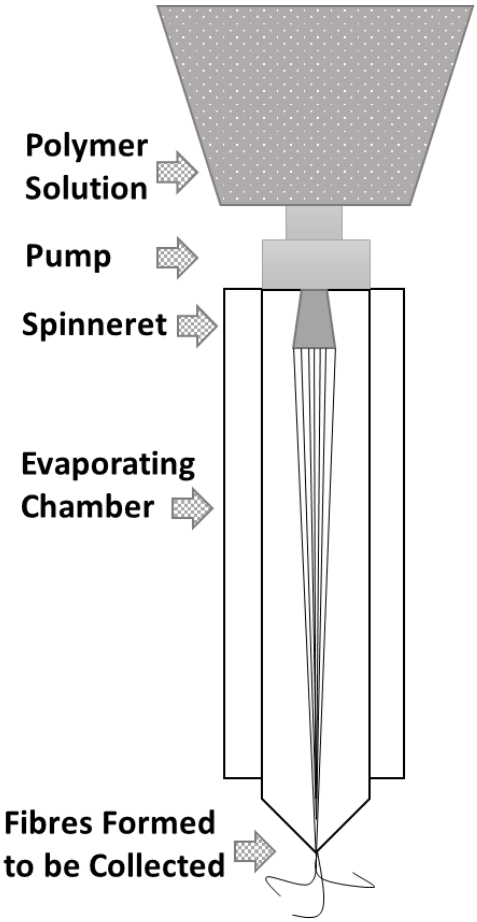

Figure 2.3: Diagrammatic overview of the dry spinning process.

Wet spinning is similar in design to dry spinning but differs in some crucial ways and is the oldest of the modern fibre production techniques. The polymer is fed through a pump to a spinneret, having been dissolved in a suitable solvent. The spinneret is submerged in a coagulating bath which causes the emerging polymer jet to precipitate and solidify, creating long continuous non-woven fibres [60]. The overview of the technique can be seen in (**Figure 2.4**). The technology can produce microfibers for a wide range of applications such as in the development of conductive polymeric fibres [61]. The process has seen many successful materials being spun with it, including materials with the trade names: Acrylic, Aramid, Chitosan, Rayon and Spandex [62-65]. The process benefits from the lack of high temperatures and all the spinning and

post-spinning can occur in one continuous loop which makes this method favourable. The technology is however unable to produce nanofibers, to add to this, the production rate is very low due to the slow spooling speeds and the requirement for post-processing of the polymeric fibres.

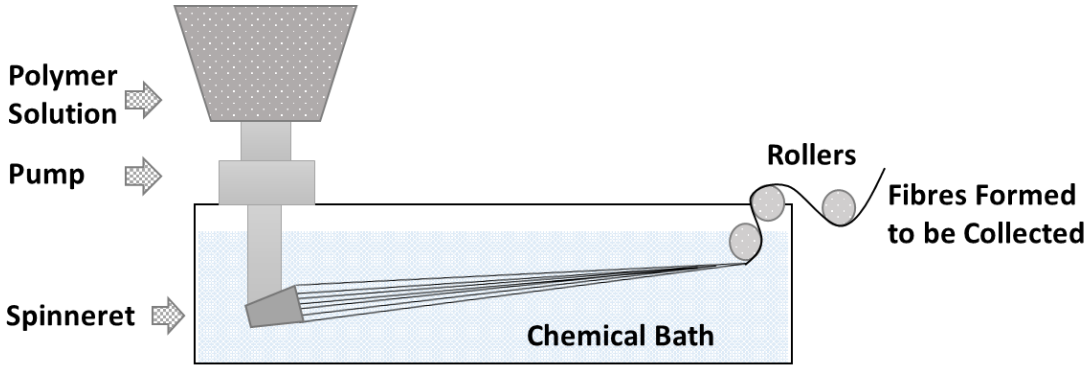

Figure 2.4: Diagrammatic overview of the wet spinning process.

Melt, dry and wet spinning are examples of three conventional fibre manufacturing processes that have been designed for commercial applications but can output material to be used for biomedicine too. However, more purpose-built processes can create finer fibres with a high degree of customisability that is required in wound healing applications.

2.2.2. Electrospinning

Electrospinning is arguably one of the most preferred and established fibre forming techniques for the production of nanofibres and has seen exponential growth in the number of scientific journals since its re-interest in the 1990s [66]. In electrospinning, a polymer solution is pumped through tubing into a metallic nozzle where a high-voltage electric field is applied directly to it [67]. The electric field has a remarkable effect on the fluid as various forces become balanced to form a stable Taylor cone [68]. The Taylor cone and the major forces can be seen in (**Figure 2.5**). When the electric field overcomes the surface tension of the polymer solution, a polymer jet erupts from the liquid

cone where it is attracted towards a grounded collector due to the difference in electrical potential [69]. As the solvent from the emerging jet evaporates, dry fibres are formed which then can be collected in several ways such as via a static collector or a rotating collector [70, 71].

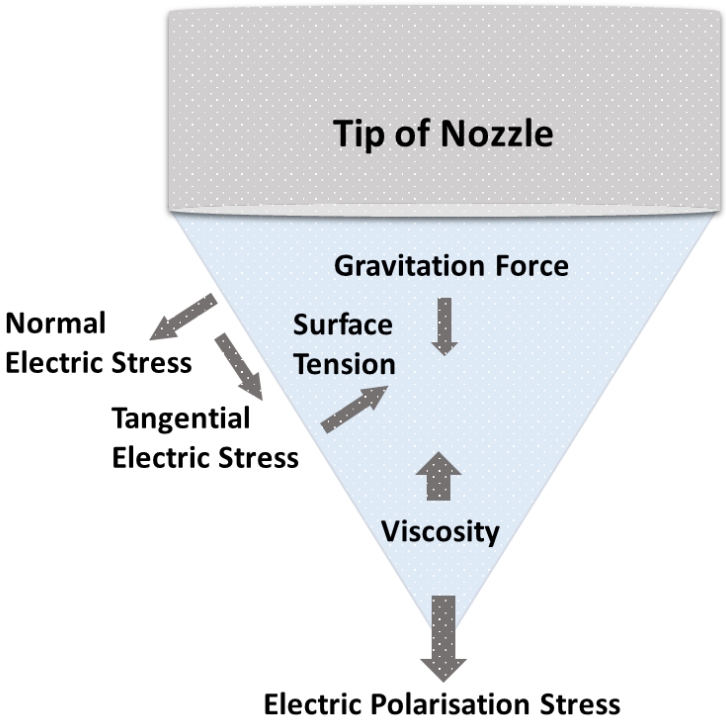

Figure 2.5: Illustration of the major forces in equilibrium in a stable Taylor cone produced by electrospinning. Adapted from [68].

What makes electrospinning so popular is its ease of use in both the initial setup and also in normal operation, allowing it to be used in laboratories across the world [72]. A polymer solution that is dissolved in a suitable solvent is attached to a syringe pump, where it is fed through a metallic nozzle. A high voltage power supply is connected directly to this nozzle, which provides a very low current to ensure the safety of the operator [69]. The setup (summarised in **Figure 2.6**) is therefore basic in nature and maintenance which has contributed somewhat to its large popularity.

Electrospinning has several vital working parameters which allow customisability and tailoring of the final fibre production to be highly specific to the desired application. As the electric field interacts with the ions in the

polymer solution, this important operating parameter can be altered to a very high degree of granularity, typically in 0.1 kV increments, but with more modern power supplies, even tighter controls exist [73]. Allowing small steps in voltage to be applied, there is precise control over the fibre production. The electrical gradient is the main driving force for fibre production. A sufficient charge potential is necessary for overcoming the surface tension of the polymer solution. Typically upon exceeding 0.3 kV/cm, fibre production usually proceeds, increases in the electric field beyond that value can significantly reduce the fibre diameter [74]. In surpassing 1.2 kV/cm, however, jet instability increases and the size-reducing effect ceases. The necessary magnitude of applied voltage varies dramatically from different polymers at differing concentrations [75]. Therefore, being able to regulate the electric field with a high degree of control is crucial to tailor the final fibre morphology.

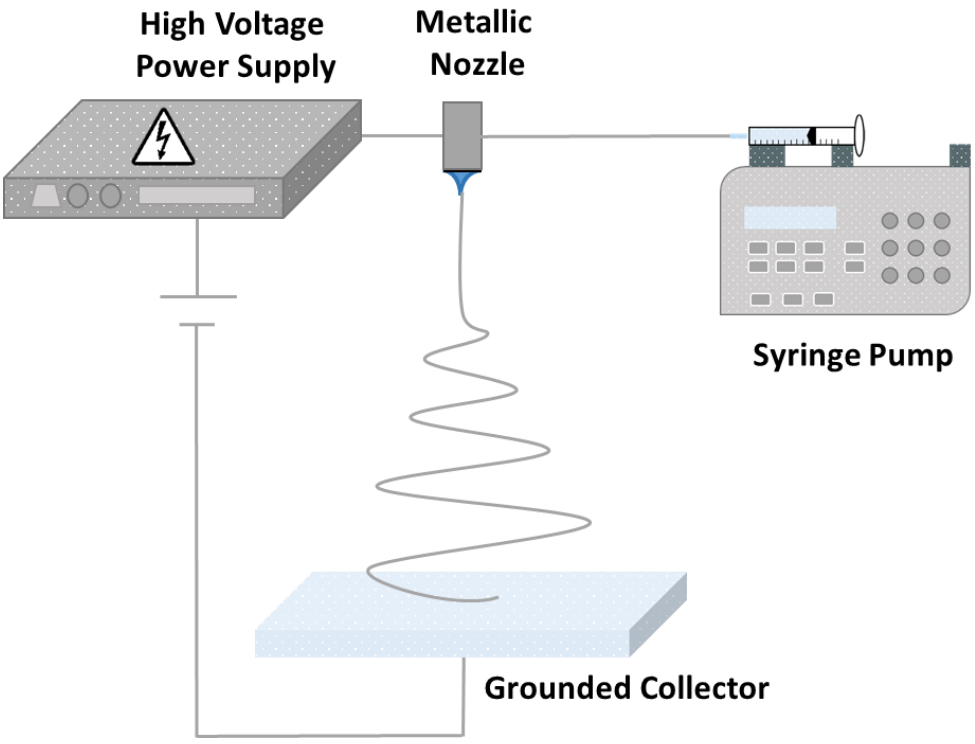

Figure 2.6: Schematic representation of the basic electrospinning setup, depicting the high voltage power supply, metallic nozzle, high precision continuous syringe pump and the grounded plate where fibres are collected.

The flow rate of the solution determines the mass transfer of polymer through the tubing and into the nozzle. This particular working parameter has a direct influence on the final fibre diameter and size, as well as other morphological features such as surface porosity [76]. There must be adequate flow into the nozzle to maintain a stable Taylor cone, but an oversupply may lead to an increase in fibre size and diameter [77]. The use of a precise syringe pump in the electrospinning setup is essential and permits finer control over the final fibre diameter and morphology.

The distance between the tip of the nozzle and the collector also plays a notable role in the fibre production process [78]. During fibre formation, the jet draws the polymer solution into thin strands via the motion of whipping instability, the solvent then subsequently dissolves and fibres in their dry form are produced [79]. If the collection distance is increased, it provides the jet with additional time for its solvent to evaporate and this may lead to thinner fibres being formed. Additionally, collection distance influences topological features of the fibres such as groves and pores as it governs the regime of solvent evaporation [80].

The benefits of electrospinning are vast. Firstly, this is a one-step process setup that does not require additional processing, this allows it to not only be managed easily but can provide low-cost fibres for various applications. The process can be terminated at any time, allowing for a safe working environment and reducing waste. The fibres produced by electrospinning are highly uniform in their size distribution and have often been produced with diameters below 100 nm [81-83]. The technology however does not come without some limitations. The polymer solution to be spun must possess conductivity or would otherwise not spin [84]. Moreover, the setup is not compatible with spinning biological polymers such as cells as the high voltage can disturb them [85]. By far one of the greatest obstacles that have prevented the technology from mass production is in its scalability, as increasing the number of needles leads to charge interferences and single needle production throughput is very low [86].

2.2.3 Pressurised Gyration

Pressurised gyration is a fibre manufacturing technique that combines centrifugal spinning with solution blow spinning to produce fine fibres with an emphasis on high production throughput [34]. The technology has seen a large number of publications that rivals and exceeds similar technologies such as centrifugal spinning for spinning fibres with biomedical applications. Pressurised gyration is a rapid-forming technology where production rates of 6 kg/h can be achieved with a single setup and has the potential of high scalability by increasing the number of units [87].

The pressurised gyration setup consists of a cylindrical rotating drum, made of aluminium at a width of only 60 mm. The drum has 24 small 0.5 mm orifices through its walls which allow polymer solution to be extruded through it. The drum is closed with a lid containing a gas supply that is capable of infusing nitrogen gas of up to 0.3 MPa [88]. The bottom of the aluminium vessel is connected to a high-speed DC motor which is capable of reaching speeds of up to 36,000 rpm [89]. Via the use of a speed controller, the speed at which the drum rotates can also be configured during operation. A polymer solution, such as one that is prepared for electrospinning is placed into the vessel before the spinning occurs. The basic pressurised gyration setup is summarised in (**Figure 2.7**).

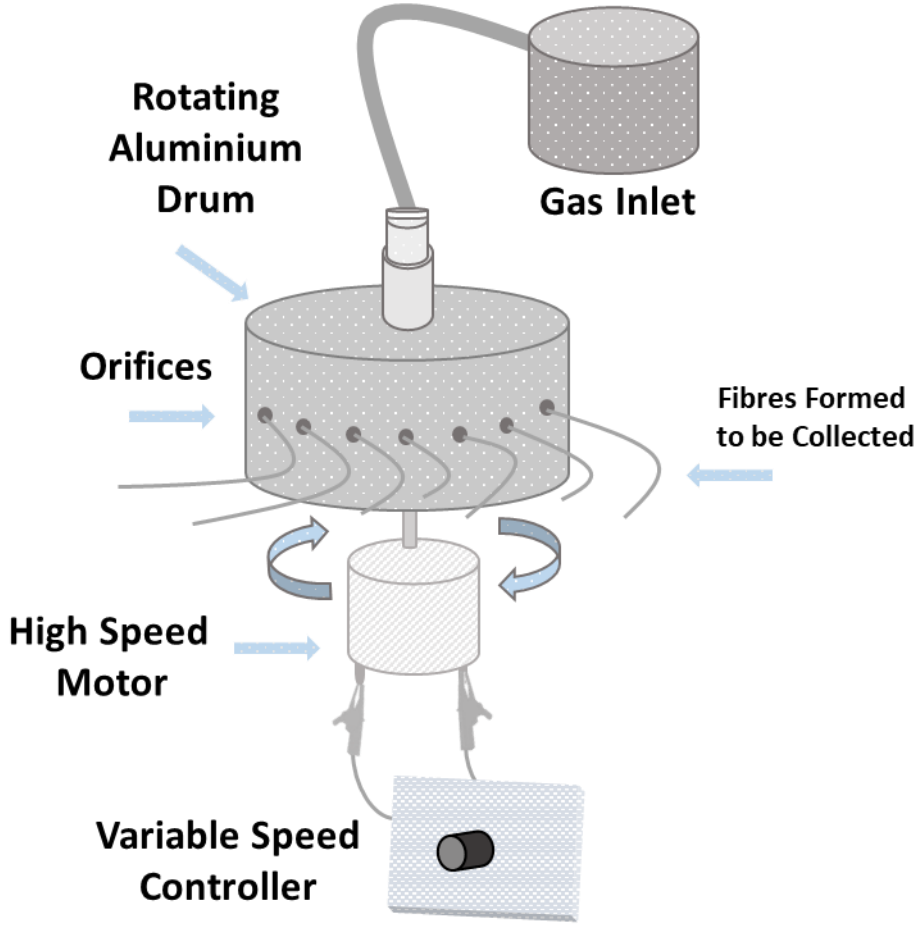

Figure 2.7: Diagrammatic representation of the basic pressurised gyration laboratory setup showing the rotating drum, gas supply inlet, high-speed motor and the variable speed controller.

Fibre production ensues when the motor is initiated, and the gyration pot begins to rotate. The high-speed rotation of the pot causes a build-up of centrifugal force in the pot which acts upon the polymer solution causing it to be manipulated through the pot, when this force exceeds the surface tension forces of the polymer solution, a polymer jets erupt at the orifices [16, 90]. The polymer jet is similar to what occurs in electrospinning, this jet is responsible for fibre production and it is solvent evaporation which leads to fibre production [91]. The applied gas pressure works in tandem with the rotation of the pot to provide an additional force which is responsible for the extrusion of the polymer through the orifices, it creates a pressure differential in the vessel that causes the solution to be forced out with higher kinetic energy. The gas

pressure works to reduce the fibre diameter in most cases as it is responsible for additional jet thinning leading to thinner fibres.

The technology is beneficial in a few key ways, firstly it allows for a high production rate of fibres to meet the demands of biomedical applications. It is a single step process with very little setup and maintenance cost. It operates in ambient conditions and does not require a high-voltage electric field which allows it to spin a wide range of natural and synthetic polymers without exposure to a direct electrical current [92]. Whilst the technology is capable of producing nanofibres, many of the materials that have been spun are largely in the micrometre range [16, 93]. In later discussed sections, optimisation of both the polymer solutions and the operating parameters will be carried out to achieve smaller diameter fibres.

As with all fibre manufacturing methods, many operating parameters crucial to end-product morphology exist. The rotation speed of the motor provides the principal driving force for spinning, which is the centrifugal force. Given the mass of the gyration pot, at 6000 rpm, the centrifugal force is estimated to be 650 N. An increase in centrifugal force, with higher rotational speeds causes the polymer jet to exit at a higher velocity, this energy is then carried through the emerging polymer jet where it is responsible for travelling through the open environment and solvent evaporation. There exists a critical minimum rotation speed in order to generate a polymer jet. Therefore, being able to control the rotation speed allows there to be a regulation over fibre morphology. As the motor is starting up, the critical speed is not met instantaneously at t=0, in this phase, the gas pressure is capable of extruding the polymer out through the orifices. The gas pressure contributes to polymer jet elongation and thus the thinning of the fibres. At high gas pressures, the kinetic energy of the jet also increases, contributing to thinner fibres [94]. A summary of forces on jet thinning can be seen in (**Figure 2.8**).

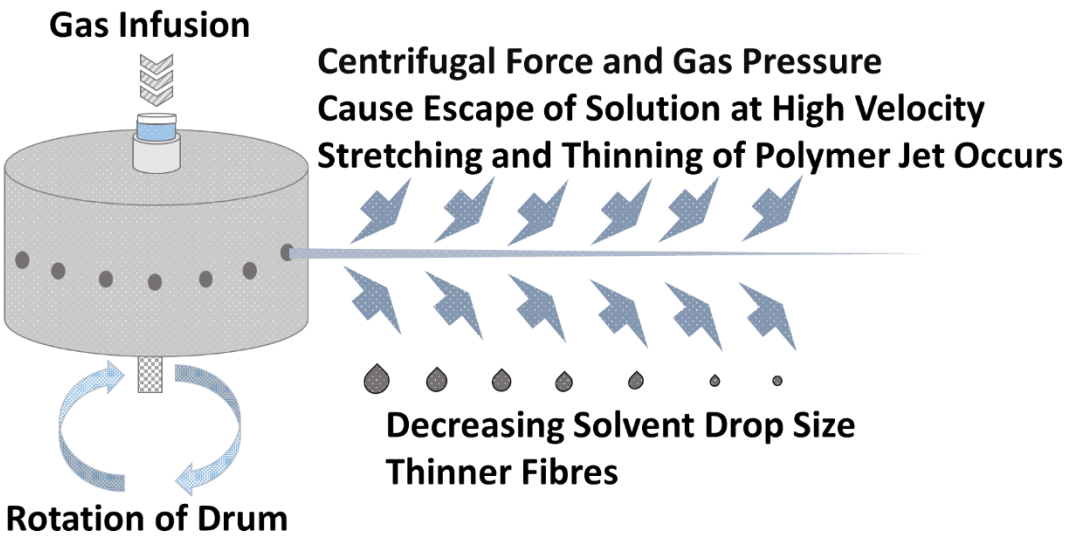

Figure 2.8: Diagrammatic summary of the main forces acting on the polymer solution to cause a polymer jet and subsequent thinning into fibres.

Manufacturing techniques that form fibres from a polymer solution have distinct advantages, the polymer solution can consist of more than one material. Firstly, polymer blends can easily be created in solution form, these allow two or more blends of polymers with one common solvent, hybridising their mechanical properties and morphological behaviours [95]. Furthermore, additives can be added to the polymer solution which can provide additional advantages such as an increased surface area, improved sensitivity, antimicrobial action and fluorescent abilities [96-98]. Pressurised gyration can also be used to spin fibres with cells as it doesn't rely on an applied electric field which could otherwise disrupt the cell wall. Pressurised gyration also differs from electrospinning with its production yield, being superior and its control over fibre morphology via the use of rotational speed and applied gas pressure. Cell electrospinning and aerodynamically assisted bio-threading are techniques that can be used to spin scaffolds consisting of animal cells, cell electrospinning works on the same principle as electrospinning but includes a conducting coaxial needle which is situated above a collection grill or a rotating mandrel [99].

2.3 Characteristics of Small Diameter Fibres

As the diameter of the fibre strands falls below the micron level, many appreciable characteristics become apparent. The reduction in diameter brings a great increase in the surface area-to-volume ratio, increases the mechanical strength of the fibres as bundles and affords a greater ability in functionalisation compared to fibres with larger diameters [72, 100].

2.3.1 Surface Area

The specific surface area of a fibre strand is defined in terms of surface area per unit volume [101]. The thinner the fibre strand, the greater its specific surface area. A higher specific surface area translates to a greater available area of contact between fibre strands and the intended environment, leading to greater cohesion.

A nanofibrous network with a large surface area also enhances ion conductivity which can be utilised to improve the packing efficiency of energy storage devices such as batteries, these advancements will allow consumer and medical technology to be powered on for longer [102].

2.3.2 Mechanical Properties

The production of fibres with below-micron sized diameters allows for the functionalisation of the mechanical properties in the final fibrous products. Mechanical properties are an important consideration in every application as the fibres must be able to carry out the intended action whilst maintaining their original form and structural integrity.

Tensile strength is a measurement of the maximum stress a material can withstand whilst being stretched, before it fails due to breakage [103]. Fibres typically do well in tensile strength tests as the orientation and diameter of individual strands work well to increase the stress they can endure. In wound healing, a bandage must be able to have adequate tensile strength, so it does not fail during normal operation and the forces that come from flexing joints.

The tensile strength and extensibility of wounded skin is noticeably lower than that of normal healthy skin. Consequently for efficient wound healing, the backing material must have a sufficient tensile strength to provide an adequate mechanical support to the regenerating cells of the skin [104]. In dermal wound healing, collagen fibres begin to form in the wound area, as they develop in thickness and number, their tensile strength increases which directly correlates to the progression of the wound back to a healthy state [105].

The Young's modulus shows the elastic properties of a material that undergoes tension and compression in one direction. This number is also known as the stiffness and it measures the tensile or compressive stiffness of a material when a lengthwise force is applied to it [106]. The stiffness of fibrous materials depends on the fibre length and the fibre orientation distribution [107]. Cells are highly sensitive to the stiffness of materials that they come into contact with, following dermal injury, the native tissue architecture is compromised and mechanically altered [108]. Mechanical cues in the wound environment can act to guide cells needed for wound healing, such as immune cells and fibroblasts [109]. It was found that by varying the stiffness of alginate/collagen in three-dimensional fibre scaffolds, there was an effect on the fibroblast biology in a wound microenvironment. When the stiffness changed, there were dramatic changes in the morphology of the fibroblasts which triggered differing wound healing genetic mechanisms such as the expression of different inflammation mediators [110]. It is therefore important to note that the mechanical properties, such as tensile strength and stiffness are valid considerations when developing a material that is purpose-made to be used in environments that contains cells such as in tissue engineering and wound healing.

2.3.3 Morphology, Porosity and topography

Functionalisation of fibres at the microscale and below is easy to achieve with the aforementioned fibre manufacturing techniques, morphology and surface functionalisation plays a key role in its applications as it provides the basis of

interaction with the target environment [111]. Many important morphological features are discussed in this section and how these features are beneficial to their intended applications.

Intra-fibre porosity created by the overlapping of fibres is a highly desirable property of fibre mats as they can provide a niche for cells in tissue engineering or act as the filter membrane for the filtration of various substances (**Figure 2.9**). The formation of intra-fibre porosity in electrospinning is formed via the competition between the solidification and the phase separation of the fluid polymer jet [112]. Fibre porosity can also be found in fibres formed by other techniques. For any given application, there exists an optimal pore diameter. In tissue engineering, small pore sizes can hinder efficient cellular growth whilst too large of a pore size will also prevent cell growth as the cells will be too far apart [113]. Interconnected and open porous fibre networks are essential for cell nutrition, tissue vascularisation as well as in cell migration and proliferation [114]. Porosity can also work to increase the mechanical stability of an implant by providing the physical interlocking between the scaffold and the surrounding tissue [115]. The structure and network of the porosity of a fibrous scaffold can assist in guiding new tissue formation and high porosity can enable the effective release of bio factors such as genes and proteins to provide adequate nutrient exchange [116, 117]. The porosity of a fibrous sample can refer to the void fraction or the total void space within the volume of the fibrous mat and can serve as a useful measurement for potential tissue ingrowth in *in vivo* systems [118]. The porosity in fibrous filtration membranes places a crucial role in the efficiency of small particle entrapment. Membranes with a high level of porosity have a greater filtration efficiency and can trap smaller particulates [119].

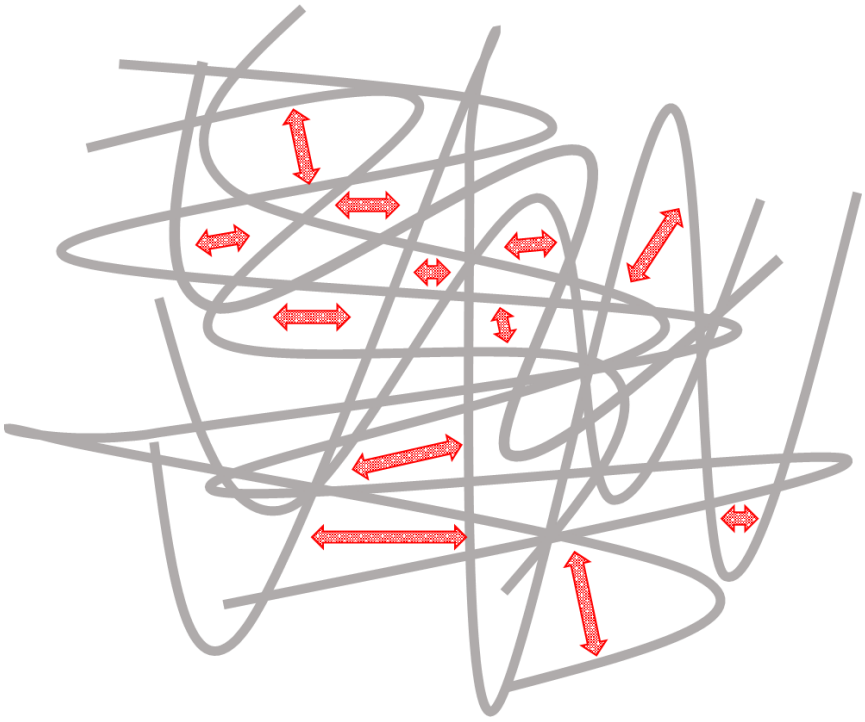

Figure 2.9: Diagram showing intra-fibre porosity in a non-woven fibre mat with red arrows indicating pores between fibre strands.

Cells are sensitive to the topography of materials that are presented to them [120]. A wide range of characteristic topographies exists when analysing polymeric small diameter fibres. Surface pores are formed when a volatile solvent is used in the fibre production process, the high volatility causes a temperature difference as it rapidly evaporates which causes water droplets to deposit on the surface of the polymeric fibres. These droplets consequently evaporate which creates pores on the surface [121]. Depending on the manufacturing conditions, these pores can be superficial or even penetrate through the fibre. Examples of surface pores are shown in (**Figure 2.10**).

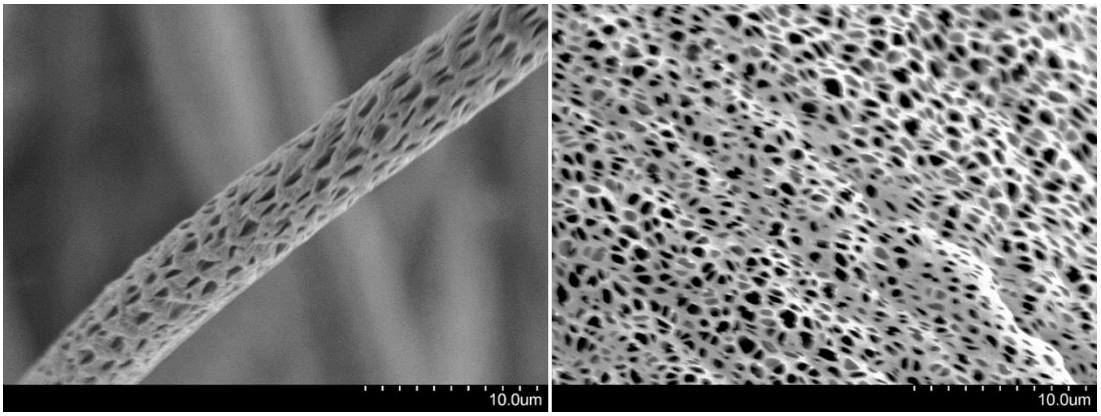

Figure 2.10: Scanning electron micrograph images showing surface pores of polymeric fibres.

Surface pores act to increase the available surface area of the polymeric fibres, thus can increase the dissolution rate in aqueous solutions of drug delivery fibres, promoting enhanced cell attachment in tissue engineering and increasing particle entrapment in use as filters [122-124]. As surface features are crucial in biological environments, fibres can be functionalised to also have other surface features such as smoothness, roughness, grooves and even pits. Examples of these topological features can be seen in (**Figure 2.11**). Macrophages and astrocytes that were seeded onto smooth-surface fibres showed a more elongated morphology than those same cells growing on rougher fibres [125, 126]. Cells specific to certain tissues and niches will not behave the same and will not respond to the same topological stimuli. An investigation into the growth of chick dorsal root ganglion on various fibre topographies found that on smooth surface fibres, the neurites extended by about 65% farther than that seen on rougher surfaces with grooves [127]. Fibres with surface roughness have many benefits in cell-based environments, as the roughness can increase the available surface area for cell attachment and also provide topological cues for cell growth. Surface roughness has been shown to modulate the responsiveness of mesenchymal stem cell signalling and thus its cell differentiation in murine C2C12 cell lines [128]. Fibres with pits and grooves can also act as a guideline for cell growth and differentiation [129]. Therefore, in this work, fibres with morphologies which tend to increase the surface area are beneficial such as a high degree

of surface porosity and fibres having a smaller overall fibre diameter throughout.

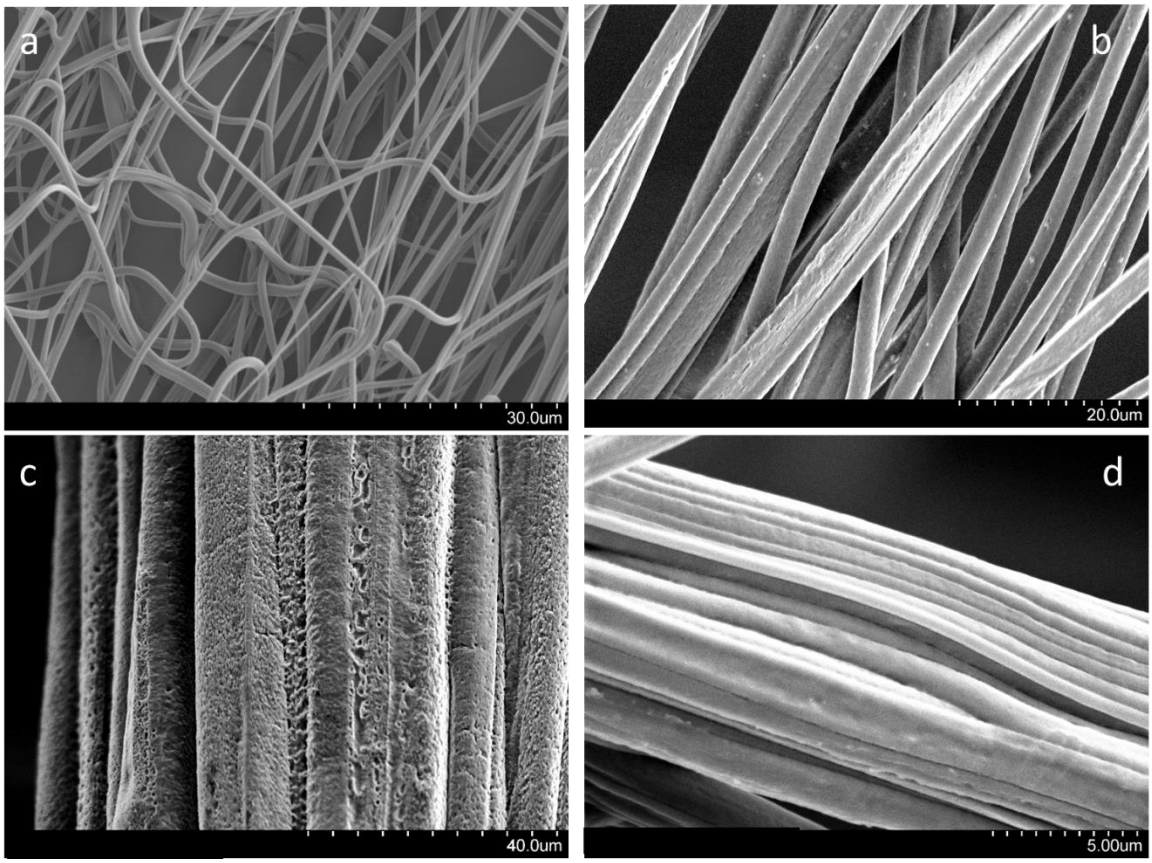

Figure 2.11: Scanning electron micrograph images showing; a) smooth surface fibres, b) rough surface fibres, c) fibres with surface grooves and d) fibres with pits resembling valleys.

Fibres are said to be unidirectionally aligned if the majority of the strands follow in the same orientation and direction. Aligned fibres can increase cellular interaction in many tissue systems by providing directionality for cell growth [130]. Fibroblasts, the most common cells for skin tissue repair, have been found to show a difference in directional spreading as a response to a greater unidirectional alignment of fibres [131].

Highly aligned fibres display a more isotropic mechanical behaviour and have shown to have greater stiffness, tensile strength and greater bending strength than randomly aligned fibres [132]. A study into the effect of the fibre alignment on the behaviour of rat periodontal ligament cells found that aligned scaffolds

maintained higher structural integrity compared to the control, following an incubation period of 6 weeks, fibre alignment also influenced cell orientation [133]. The aligned fibres additionally promoted a directionality in the cell growth as randomly oriented fibres were found to hamper the migration of the cells. The surface coverage of cells was, as a result, increased on the aligned fibres. Another study showed that glioma cells on fibres that were unidirectionally aligned migrate at a higher velocity compared to the fibres with different alignments, the alignment acts as a “highway” which cells use as a guide for growth [134]. Examples of highly aligned polymeric fibres are shown in (**Figure 2.12**).

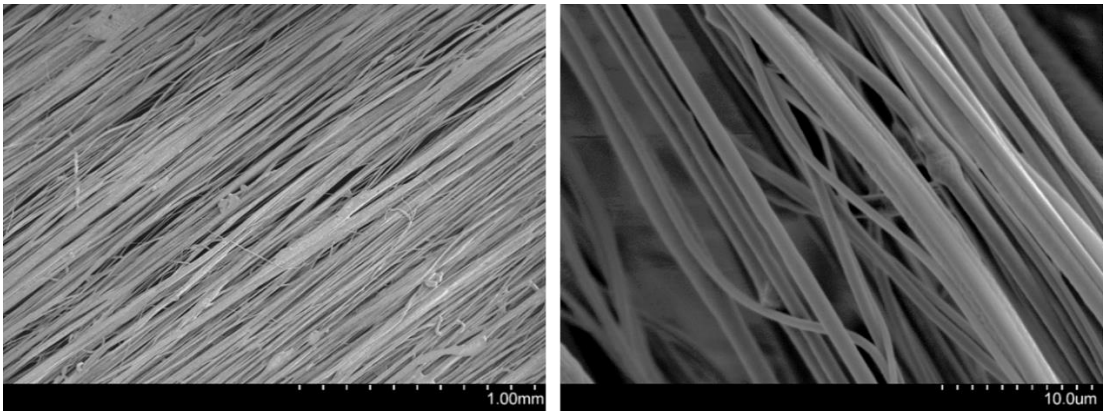

Figure 2.12: Scanning electron micrograph images showing polymeric fibres which have unidirectional alignment.

The bead-on-string morphology of small diameter fibres is grouped by the unique and characteristic morphology which depicts the fibre strands with a reoccurring ball or bead-like assemblies (**Figure 2.13**) [135]. This particular morphology has been of keen interest in many studies, and it often can be seen as undesirable as it alters fibre diameter and makes for less uniformity in fibre production. In electrospinning, the bead-on-string morphology can be attributed to the instabilities of the emerging jet due to low charge densities of the surface tension of the polymer solution [136, 137].

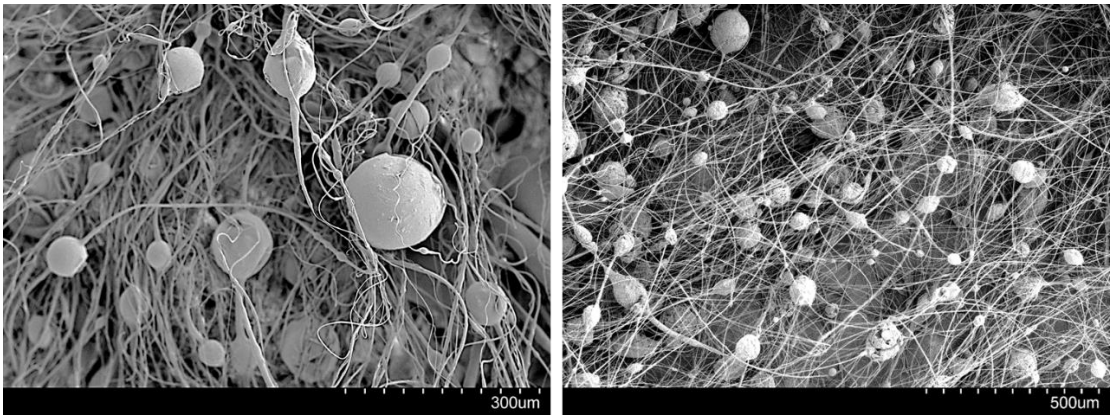

Figure 2.13: Scanning electron micrograph images showing the characteristic bead-on-string morphology in small diameter fibres.

Hollow Fibres and other hollow materials can be effective building blocks in many applications such as biosensors, catalysts and energy storage [138, 139]. Hollow fibres have many beneficial properties; the hollow core increases the surface area to volume ratio of the fibres which makes them desirable in any biomedical application where a higher surface area is advantageous. Furthermore, hollow fibres can provide the necessary active sites for physiochemical reactions to take place with the surrounding environment, where there is higher sensitivity and superior kinetic efficiency [140, 141]. Hollow fibre membrane bioreactors for tissue engineering can also be used where it offers a viable alternative to traditional culture flasks due to the increased area where lower volumes of media are required [142]. Hollow fibre membranes have been shown to provide cells with growth guidance and have some nerve tissue engineering applications [143]. An example of a hollow fibre can be seen in (**Figure 2.14**). Hollow fibres are also desirable in technological applications such as in fibre optics, where light can be used to send signals through the hollow tract [144].

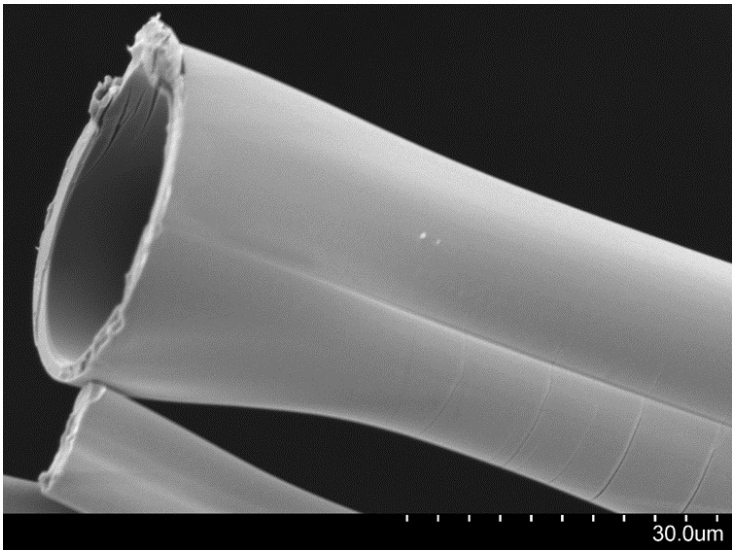

Figure 2.14: Scanning electron micrograph image showing a hollow fibre strand.

2.3.4 Applications of Small Diameter Fibres

The numerous characteristics of small diameter fibres give them beneficial properties that can be specifically leveraged in many biomedical applications. For use in each specific application, the properties must be carefully evaluated to maximise and tailor to the end-use application. Polymeric fibres spun by electrospinning and other manufacturing techniques can produce nanofibers for optical sensors [145]. The sensitivity of sensors increases with higher surface areas per unit mass.

2.3.4.1 Tissue Engineering

Tissue engineering is a field of science that focuses on the fabrication of scaffolds in three-dimension that can facilitate cellular growth and proliferation [146, 147]. The basic principle is to be produce materials that can support and promote cell growth as summarised in (**Figure 2.15**). Recent advances in biocompatible polymeric nanofibre technology have led to a greater focus on tissue engineering. An ideal scaffold should have the appropriate porosity to allow for cell migration whilst having a sufficient surface area for cell adhesion

and growth [148]. The manufacturing techniques discussed previously (**section 2.2**) can generate thin fibres that fall into this category.

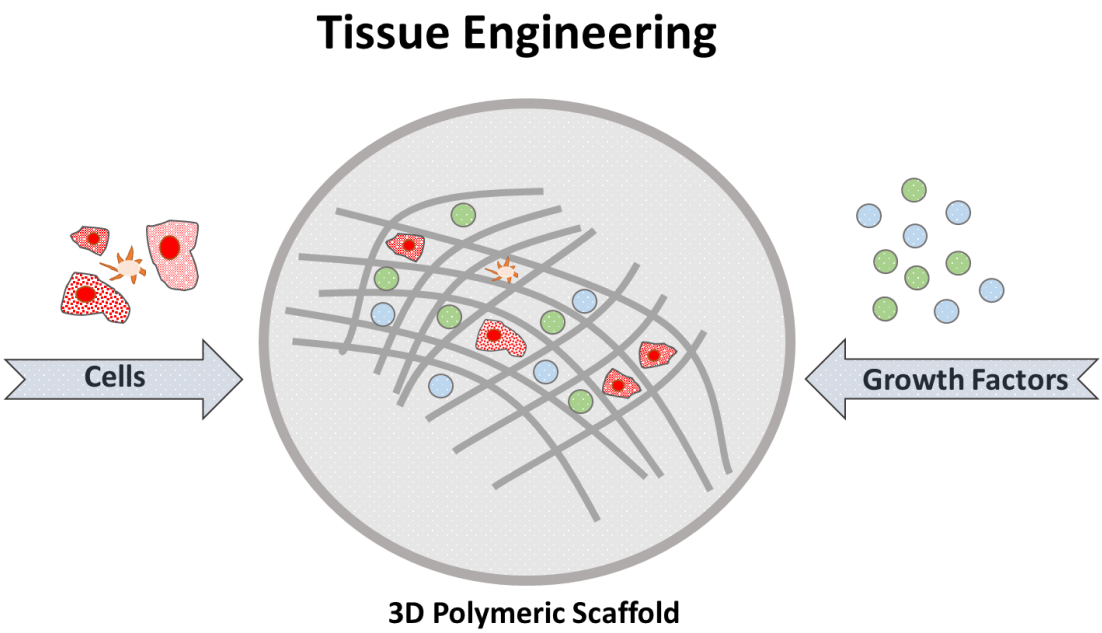

Figure 2.15: Diagrammatic overview of tissue engineering, showing how a three-dimensional fibrous can be used to support and encourage cellular growth.

Thin fibres can provide a biomimetic cellular niche where cells can attach, proliferate and migrate in order to regenerate faulty tissues. Extracellular matrix mimicking fibrous mats have been produced which have been shown to increase cellular activity [149, 150]. For bone tissue engineering, pore size distribution between 100 - 350 µm and porosity of over 90% is preferred [151]. A high surface area thus allows for a high degree of cellular attachment and also allows for multiple focal adhesion points [152].

Surface modification of fibres can be carried out as a cost-effective way to alter the surface properties of a fibrous scaffold without significantly affecting its bulk properties. A popular tissue engineering approach is to incorporate bioactive molecules onto the surface of the fibres, as cells only interact with the surface of materials, it is otherwise wasteful to incorporate expensive molecules within the fibre [87, 122, 153]. Surface modification is a post-

processing technique; soaking is a method where the surface of fibres can be cost-effectively modified by dipping into a solution with a high concentration of bioactive components [154]. Soaking works based on physical entrapment; the high surface area of thin fibres can increase the uptake of these beneficial molecules.

Mechanical and topological properties are crucial considerations in tissue engineering, as cells are sensitive to certain properties such as stiffness and roughness [155]. An example is found in the basement membrane of the corneal epithelium where the nano topography consists of small elevations ranging from 76 to 379 nm and pores in the size of 22 to 216 nm [156]. This specific nano topography can increase the surface area by over 400% [157]. In order to produce a good tissue engineering scaffold, a few important criteria should be met. The scaffold must match the host tissue in terms of elastic modulus, fatigue properties, degradation rate and compressive strength [158]. A scaffold should have sufficient tensile and compressive strength to maintain its integrity as the tissue regenerates and the original porosity should remain constant [159]. Furthermore, the scaffold should match the stiffness of the original tissue as closely as possible to avoid stress shielding [160]. Mechanotransduction is a phenomenon where a cell converts mechanical stimuli into chemical activity which can promote or prevent growth, therefore the scaffold should provide similar mechanical cues to the native tissue [161].

2.3.4.2 Drug Delivery

One prevalent obstacle in the pharmaceutical industry is the delivery of drugs that have poor water solubility. Poorly water-soluble drugs thus cannot be taken orally, the simplest of delivery techniques with the highest level of patient compliance [162]. To increase the solubility of a drug, there must be control over the physical form of the active pharmaceutical ingredient. Conversion from the crystalline, tough to dissolve form to the easy to dissolve amorphous state increases the dissolution rate [163].

Small diameter fibres can be engineered to be used as drug delivery vehicles. A poorly water-soluble drug can be distributed in its amorphous form into a

hydrophilic polymer, in a process known as a solid dispersion [164]. When a solid dispersion is exposed to an aqueous environment, the hydrophilic polymer readily dissolves and the drug is released as fine colloidal particles with a low energy barrier to dissolution [165]. The amorphous state of a drug is not stable and the conversion back to a crystalline form is the favourable state, by dissolving a drug into a polymer solution, the polymer matrix physically prevents the reversal via steric hindrance [166]. The basic principle of using polymeric fibres in drug delivery is summarised in (**Figure 2.16**).

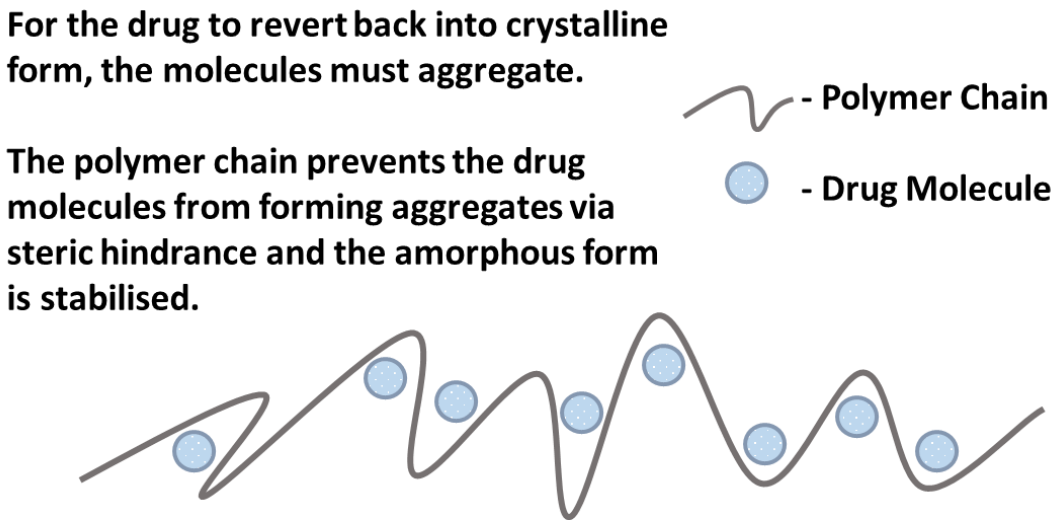

Figure 2.16: Diagrammatic overview and principle of solid dispersion of pharmaceuticals in polymeric fibres.

Utilising small diameter polymeric fibres in drug delivery is especially advantageous due to its numerous beneficial properties. Thin fibres have a very large surface area which increases their ability to dissolve in an aqueous environment and release the drug with higher efficiency [167]. One can control the release rate of a drug by adjusting the fibre diameter during manufacturing.

The production of polymeric fibre-based drug delivery allows for a high degree of control of the drug release kinetics. The choice of polymer can determine the release kinetics, release profile and targeted release. The degradation rate of a polymer regulates how long a drug will take to release into the body. Polyvinylpyrrolidone (PVP) is a water-soluble polymer that is capable of being

dissolved in the buccal cavity in a matter of seconds to minutes, depending on the surface area [168]. Conversely, poly(lactic-co-glycolic acid) is a copolymer made of poly(lactic acid) (PLA) and poly(glycolic acid) (PGA) monomers, as a hydrophobic polymer, PLGA can release drugs over a longer time period, providing a sustained release [169]. PLA has a long degradation time and whilst PGA degrades quicker, by altering the ratio of PLA and PGA, there can be control over the release rate of the pharmaceutical ingredient [170, 171].

Targeted drug delivery allows for lower doses to be prescribed which reduces the dangers of overdosing [172]. In the case of drug delivery to the stomach, an enteric polymer could be used which does not dissolve at low PH's but later in the intestine at a more neutral pH, will dissolve and release the drug at the intended site [173]. Methacrylic acid, which is known by its tradename Eudragit, is a synthetic polymer that exhibits pH-dependant solubility [174]. The polymer thus can be used to dispersed drugs into the matrix for targeted delivery into the intestine where the bioavailability would be higher for certain drugs.

2.3.4.3 Filtration

Sub-micron fibres can be produced with beneficial characteristics that make them suitable for use as filtration membranes. A filtration membrane is a barrier that is capable of separating two distinct phases [175]. The main function of a filtration membrane is therefore to trap particulates or other matter within its membrane whilst permitting the secondary phase (feed) through [176]. Filters require a driving force to function, typically being pressure, water and concentration gradients. Filters can perform many kinds of separation that other conventional separation processes can also perform such as extraction, distillation and adsorption, but they present themselves as low cost and energy-efficient methods capable of high throughput. The requirement of filters in biomedical applications are vast and can range from air and water purification to antimicrobial meshes [11, 97, 119].

Fibres produced by electrospinning and other manufacturing techniques possess several key attributes which make them highly suitable for use as

filters. Their characteristics include high porosity, presence of surface pores, high permeability for gases and their large surface area to volume ratio [176]. High porosity and interconnected pore structures allow for the efficient entrapment of particulates and microbes but still allow for the passage of water, air and other liquids (**Figure 2.17**).

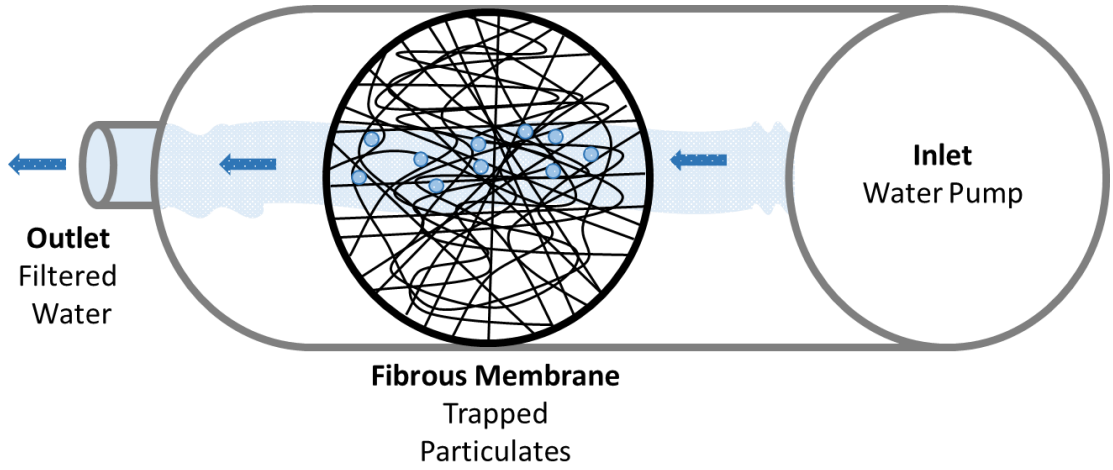

Figure 2.17: Diagrammatic overview of the basic principles of water filtration using a polymeric fibrous membrane to trap particulates, a similar approach can be used for air filtration where the air is passed through the same setup.

The higher the porosity, the smaller the mesh size and its ability to entrap fine particulates more efficiently. The presence of surface pores leads to an increase in surface area, surface area improvements allow for higher flow rates to be used and consequently reduce processing times and cost [177]. Permeability is the ability of a material to allow molecules to pass through and is highly dependent on the thickness of the membrane [178]. Fibres with thickness below the micro-level have a high permeability for gasses and this allows air and other gas filtration to occur through their membrane [179].

The transmission of infections in hospital settings is a growing problem that needs addressing as it is associated with a notable mortality and morbidity rate for many patients [180]. Hospitals routinely employ filters for both

ventilation and water supply, but these filters only trap bacteria, which can later grow and accumulate [181]. Bacteria that are not killed on contact can form biofilms and aggregate to become a continuous source of pathogens for immunocompromised patients [182]. Novel approaches to filtration problems are to use membranes that are antimicrobial that can kill bacteria upon contact. Using fibre forming methods such as pressurised gyration, antimicrobial nanoparticles have been loaded into polymeric fibrous meshes for use as antibacterial filters for air and water [183]. The produced fibres had surface pores in the range of 36 - 300 nm, which both increased the surface area and the ability to trap finer particles. The fibres were found to be effective against gram-negative *P. aeruginosa* cells, which leads to a common hospital acquired infection in the U.K. This novel approach to filtration is not limited to the use of nanoparticles, as polymer solutions can easily incorporate many different antimicrobial additions.

2.3.4.4 Wound healing

The wound healing process is extremely complex and can differ tremendously from person to person, its requirements are based on the type of wound the patient has sustained. Therefore, a single treatment modality for wound healing, in general, does not exist [184]. Plain gauzes are the most commonly used wound dressing material, as they address the basic requirements for a wound, protection from the external environment and the stoppage of bleeding [185].

The function of a wound dressing is primarily to protect the wound site from the external environment in the event when the skin barrier is compromised [186]. The wound dressing should also provide the optimum conditions for wound healing whilst also preventing infection. Ideal characteristics of a wound dressing include being able to maintain high humidity at the wound site, remove exudate, be nontoxic and non-allergenic, be impermeable to pathogens, be thermally insulative, be cost-effective and allow gaseous exchange [187]. Antimicrobial dressings can have different physical characteristics, the antibacterial agent applied to the dressings can have the ability to kill or inhibit bacterial strains, the toxicity of these applied agents need

to be considered to see if they would be potentially toxic to new cell growth [188].

Non-woven fibre mats created using fibre production methods are highly suitable as wound healing materials due to their numerous characteristics such as porosity, biocompatibility, nano-topography, mechanical properties and bioactivity. Like with tissue engineering, the multilevel cellular processes that occur during the healing process require a specific niche and proliferation and differentiation of these cells must be encouraged [189]. The requirements of a wound-healing material and the specifics of wound healing are analysed in more detail in (**section 2.6**)

2.4 Fibre Production and Working Parameters

Having multiple working parameters in any machinery allows for fine-tuning of the end product. In this section, the two focal fibre forming techniques, electrospinning and pressurised gyration will be discussed in terms of how working parameters can be tuned to tailor fibres with specific morphologies and properties. Although the two technologies work in dissimilar principles, they share similarities such as the ability to form fibres with a polymer solution.

2.4.1 Solution Properties

Although not a physical working parameter, the solution properties of the polymer solution play a pivotal role in fibre production and final morphology. A polymer is typically dissolved in a compatible solvent at given concentrations to form a solution that can then be processed into fibres.

Polymer concentration is a property of a solution that influences fibre production greatly in both techniques. There is a minimum concentration that exists, separately for both electrospinning and gyration that must be met for

fibre production. Upon exceeding the critical minimum concentration, the molecular chains of the polymer are entangled enough and will prevent the jet from a breakup during spinning [15]. There is also a direct link between polymer concentration and solution viscosity, where an increase in the polymer concentration generally results in an increase in solution viscosity [190]. This increase in viscosity is linked with the increased number of polymer chains which are more likely to be entangled given that they occupy the same volume. More viscous polymer solutions also tend to produce thicker fibres as they are a result of polymers with higher concentrations being used. The molecular weight of a polymer indicates the average length of the polymer chains, using a higher molecular weight polymer will lead to more chain entanglements and thus thicker fibres [191].

The surface tension of a liquid can be defined by the force required per unit area to expand the surface of the liquid and this important property plays a crucial role during fibre production [192]. The surface tension of the polymer solution must be overcome to form the polymer jet responsible for fibre production; in electrospinning, the electric field overcomes this and in gyration, the centrifugal force is ultimately responsible. A polymer solution that has a lower surface tension will therefore have a lower energy barrier in forming a polymer jet. One method of reducing the surface tension of a liquid is via the use of surfactants [193].

2.4.2 Effect of Solvent

During the spinning of the polymer solution, the choice of solvent is highly influential in determining the solution properties. With pressurised gyration based techniques, the main driving force for the production of fibres are the centrifugal force exerted by the rotating pot and the gas pressure inside this vessel, for this reason, properties such as dipole moment and dielectric constant are not important properties [90, 194]. As the polymer jet escapes the orifices of the gyration vessel, it is elongated by the motion of the

centrifugal force and the momentum from its exit velocity, this causes thinning of the jet which can result in thinner fibres.

Volatility describes how readily a substance vaporises, in liquids the boiling point is directly related to volatility where a lower boiling point indicates rapid evaporation [195]. Solvent volatility is thus a key factor in fibre morphology. Volatile solvents will cause rapid evaporation in the solvent portion of the polymer jet which can lead to changes in fibre diameter. Often a volatile solvent is desired in electrospinning as it ensures that the fibre is dry before hitting the collector [196]. However, in gyration-based technologies, the additional time for solvent evaporation of less volatile solvents such as water can lead to the production of thinner fibres [89]. The jet thinning process for pressurised gyration is summarised in (**Figure 2.18**) and can also apply to electrospinning. Furthermore, as discussed earlier, the use of volatile solvents can lead to a difference in topography such as the presence of surface pores.

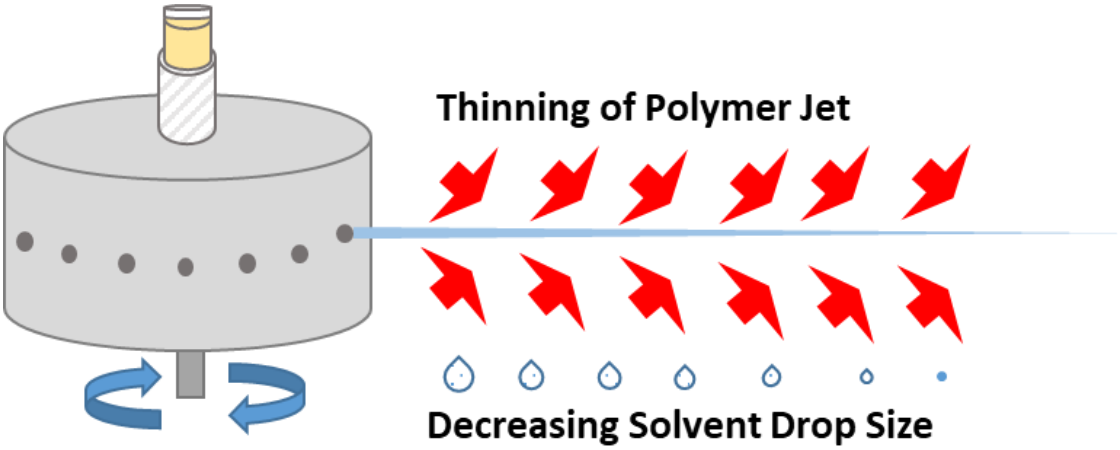

Figure 2.18: Diagram summarising the thinning mechanism of polymer jets in pressurised gyration, volatile solvents will allow less thinning than less volatile solvents.

Solvent choice in creating polymer solutions is another important consideration to make when tailoring fibre production. Polymers do not dissolve instantly, and their dissolution process is complex and highly dependent on processing conditions and solvents used. The complete dissolution of a polymer in a solvent involves two transport processes which

are solvent diffusion and the disentanglement of the polymer chains [164]. The solvent must then be dynamically compatible with the polymer. Solubility parameters exist to show an estimate between solutes and solvents on how well they are expected to be miscible. For example, the Hildebrand solubility parameter (δ), is a numerical value that indicates the solubilising power of specific solvents, it is derived from the cohesive energy densities of known solvents and shows the relationship between vaporisation, van der Waals forces and solubility [197]. A small difference in the values between the solvent and the polymer indicates that there should be good miscibility between them. Therefore, the Hildebrand solubility parameter is a useful tool to select an optimal solvent to create a polymer solution. Many polymers such as polycaprolactone, may have many redundant solvents which show complete dissolution, however, some solvents have higher solubilising powers than others and this will affect the surface tension and viscosity of the solution which in turn affects fibre morphology [198].

2.4.3 Effect of Electric Field

The applied electric field is specific to electrospinning and is the electrical potential difference between the droplet of the polymer solution and the grounded collector. If the electric field overcomes the surface tension of the polymer droplet, it becomes charged and the ejected jet contains bending instabilities triggered by repulsive forces between the charges on the jet [199]. The high voltage power supply of the electrospinning setup allows for fine control in the magnitude of voltage (kV), this is necessary, as a small window exists for each different polymer solution where there is an optimal voltage to produce fine fibres [200]. Usually, fibres are produced when the applied electric field exceeds 0.3 kV/cm, further increasing the voltage can significantly reduce the fibre diameter [74]. Beyond the specific window, a further increase in the applied voltage would reduce the volume of the drop and thus the Taylor cone would disappear and displace to the edge of the needle tip [73]. At very high voltages, the jets have large diameters and multiple jets can erupt from the needle causing non-uniform fibre production [201].

2.4.3 Effect of Rotation Speed

As the rotational speed increases, so does the centrifugal force. Given the mass of the gyration pot, at 6000 rpm, the centrifugal force is estimated to be 650 N. The centrifugal force is responsible for the movement of the polymer solution within the gyration pot, as this force increases so does the velocity of the polymer [202]. The small orifices of the pressurised gyration pot prevent the polymer from escaping; however, when the centrifugal force overcomes the surface tension of the solution, it can now escape and be extruded through the openings. Generally, once the surface tension has been overcome, there is enough kinetic energy in the solution to form a polymer jet [203].

Increasing the rotational speed causes the polymer jet to be stretched further, jet thinning is ultimately responsible for thinner fibres and so rotational speed is a direct parameter to yield lower diameter fibres. A critical minimum rotational speed exists which must be exceeded in order to produce fibres [16]. Solution properties such as viscosity and surface tension can influence the critical minimum rotational speed. it is not known if further increases in rotational speed would lead to finer fibres, or if there is a physical limit to reducing fibre size.

2.4.4 Effect of Pressure

In pressurised gyration, the applied gas pressure acts as a supplementary external force that participates in jet elongation and jet thinning. The addition of gas pressure sees the reduction of fibre diameter as a result of the increased travel of the emerging droplet [204]. With a Poly(ethylene oxide) polymer system using water as the solvent, it is observed that the fibre diameter reduces with each increment of applied pressure [34]. As the polymer jet escapes the orifices of the gyration vessel, it is elongated by the motion of the centrifugal force and the momentum from its exit velocity, this causes thinning of the jet which can result in thinner fibres. With solvents of high

volatility, it can reduce the effect of jet thinning as the jet rapidly solidifies as the solvent evaporates. In this thesis, the effects of pressure on fibre diameter are observed as well as the effect of applied pressure on solvents with varying volatilities.

2.4.5 Effect of Collection Distance

The distance between the point the fibre exits, and the collector can greatly affect the morphology of fibres in electrospinning and pressurised gyration. A greater collection distance usually affords the drying polymer jet with more time, further jet thinning can thus occur and thinner fibres can be produced [205]. Changes in the collection distance can also give rise to morphological features such as the bead-on-string morphology [16]. At short collection distances, there is less available solvent evaporation and unevaporated droplets remain in the fibre chain. Collector type can also affect the fibre morphology, by incorporating a collector that mimics the rotation of the pot in pressurised gyration, highly aligned fibres can be produced. Similarly, in electrospinning, fibres are spun directly onto a rotating mandrel which allows control over its speed to produced fibres with the desired level of alignment for biomedical applications [206, 207].

2.5 Uses of Natural Materials as Fibres

Even before the discovery of modern medicine, bioactive and medically beneficial ailments existed in nature that could be found in a consumable form [208]. Several commonly eaten foods have the uncultivated ability to inhibit microbial growth and provide relief from disease, which remained unknown to the consumer. These spices are not only abundant but come at relatively little cost whilst being completely natural and having a minor impact on the environment.

2.5.1 Antimicrobial Naturally Occurring Spices

As bacteria continue to develop and evolve, the search for novel drugs to counter the resistant strains provides a continuous challenge. A large number of plants have been used to battle different diseases [209]. Plants also have been shown to have antimicrobial activity and new chemical components are discovered in nature frequently. Spices are highly desirable food ingredients that have also seen historic use as currency for the trading of goods. No specific definition exists to differentiate between spices and herbs, however. Spices are obtained from different parts of plants such as the seed from cardamom and the fruits of pepper [210]. In small quantities, spices provide little to no nutritional value compared to other foods such as vegetables, however, spices can have secondary compounds that have medicinal, antioxidant and antimicrobial properties [211, 212].

India is often referred to as being the king of spice, owing to its exhaustive use of spices for culture, culinary arts and medicinal properties. Turmeric is one of the most common and characteristic spices of India and is obtained from a flowering plant called *Curcuma longa* [213]. First characterised in 1910, curcumin (diferuloylmethane), is considered the most active constituent of turmeric [214]. The principal active ingredient within turmeric is known to be the chemical compound curcumin. Curcumin is known to have antidiabetic, anti-inflammatory and anti-cancer effects [215, 216]. In a study of the antimicrobial activity of curcumin against the bacterial species *Helicobacter pylori*, it was revealed that the principle component of turmeric was able to significantly inhibit bacterial growth [217].

Cistus incanus, a species of herb is used as an anti-inflammatory agent in northern parts of Greece against local inflammation of the skin [218]. Aqueous extracts of the herb are obtained by boiling the ground material in water or by extracting it with ethyl acetate. The main active agents of *Cistus incanus* are believed to be several flavonoid compounds, including flavonol glycosides and tannins [219]. It is found that the extract with ethyl acetate shows a more active anti-inflammatory action than the boiled extract [220]. Solvent extraction

techniques have been widely investigated and used to acquire valuable chemical compounds from plants for commercialisation [221]. Solvent extraction is therefore a tried and tested method to obtain important chemical compounds from spices without having to use the bulk material.

2.5.2 Cinnamon

Cinnamon (*Cinnamomum),* is a spice acquired from the inner dried bark of several species of trees indigenous to South Asia and China and belongs to the genus *Cinnamomum* [222]. Cinnamon is grown commercially, and its uses range from cosmetics, cuisine components worldwide, flavouring additives and aromatic condiments. The history of cinnamon usage dates back thousands of years where references to it are found in the Bible. The ancient Egyptians even used the spice as embalming fluid for the wealthy deceased [222]. Arguably, two predominant types of cinnamon exist, *Cinnamomum verum* (Ceylon) *and Cinnamomum cassia.* Ceylon cinnamon is considered amongst most to be the “true cinnamon” whilst Cassia cinnamon is most commonly found in international commerce and thus holds a lower trading value [223]. The principal chemical component of cinnamon, cinnamaldehyde, gives the spice its unique aroma and flavour, cassia variants contain more cinnamaldehyde in their essential oil [224]. Historically, cinnamon has been long used as traditional medicine in the treatment of many conditions such as bronchitis, rheumatism and neuralgia [225]. Furthermore, many modern scientific papers report on the ability of cinnamon to be antidiabetic, antioxidant, anti-inflammatory, anti-fungal, anti-HIV, improve heart function, anticancer and even pro-wound healing [226-231]. It has also been reported that cinnamaldehyde holds remarkable antimicrobial activity [232-235].

2.5.3 Honey

As far back as the 16th century BC, the medicinal applications of honey can be dated to the ancient Egyptian civilisations. In the Smith Papyrus, the earliest record of medicinal honey used can be found in wound balm which consisted of mrht (grease), byt (honey) and ftt (lint/fibre) [236]. In fact, in over half of all discovered ancient Egyptian remedies, honey was found as a component [237]. The Egyptians were not the only ancient group found to be using honey, it was also found in the ancient Greek, Romans, Assyrians and Chinese as a means to treat pain, fever, dehydration, ocular issues and gastrointestinal diseases [238]. Today, honey still sees use in modern medicine which can be found in topical agents for treating chronic wounds [239-243]. Honey has been shown to accelerate the wound healing process in a short amount of time following its initial application. Honey has also been found to encourage re-epithelisation in gangrenous tissue and in sloughs, its use can even prevent the need for some surgical interventions [244].

There are over 200 different substances that make up the components of honey. These substances include proteins, amino acids, carbohydrates, antioxidants, vitamins, minerals, and many different enzymes. Honey is however composed of mostly carbohydrates (approximately 82-99%) which are predominantly in the form of glucose and fructose [245]. The antibacterial action of honey is theorised to be attributed to its very high sugar content. Further theories for its antibacterial mechanism are thought to be from its low pH and production of hydrogen peroxide [246-248]. The high sugar and low moisture content of honey create high osmolarity, in this environment, the bacterial cytoplasm can be drawn, causing damage to the cell wall and killing the bacteria [249]. The high osmolarity of honey can also compete for water with bacteria, which rely on it for survival [250]. The low pH of honey is also capable of neutralising the high pH of wound environments leading to a reduction in protease activity, an increase in fibroblast activity and higher oxygen release [251, 252].

The main mechanism of antimicrobial action of honey is via the production of its active agent hydrogen peroxide and other non-peroxide compounds from

glucose oxidase, produced from bees [246-248]. These compounds contain antiseptic properties and have the ability to speed up the wound repair process. Hydrogen peroxide gradients in wounds have been shown to increase the prevalence of macrophages secreting vascular endothelial growth factors which contribute to angiogenesis (new blood vessel architecture) [253-255]. Furthermore, honey can also provide macrophages of the wound site with substrates for glycolysis, allowing restoration of tissue at low oxygen conditions, especially relating to damaged vessel architecture. In a wound site, the low pH of honey and its hydrogen peroxide production contribute to keeping the area sterile.

2.5.4 Collagen

Collagen is the most abundant protein in animals and is the major component for the majority of tissues including the skin, muscles, tendons and ligaments [256]. Many synthetic and naturally occurring polymers are used as biomaterials, but collagen is distinct in its mode of interaction in the body [257]. Collagen works as a structural component in the formation of tissue as well as being responsible for many functional expressions of cells [258, 259]. Collagen demonstrates the ability to penetrate through lipid-free interfaces and is a good surface-active agent [260]. Compared to other natural polymers such as gelatin and albumin, collagen has an unmatchable level of biocompatibility, great biodegradability and weak antigenicity [261]. Through its self-aggregation and cross-linking, collagen can form fibres with high strength and stability, one of the reasons why it is so sought after in biomedical applications [262].

Collagen is involved in all the phases of wound healing where it stimulates the migration of the involved cells and contributes to the formation of new tissue [263]. Wound dressings that incorporate collagen encourage the further formation of collagen which creates a microenvironment that has chemotactic properties on fibroblast cells [264]. When collagen is found in wound healing, it can stimulate and recruit fibroblasts and macrophages which enhances and

influences wound healing. Collagen-based wound dressings are also very easy to apply and are conformable to the patient's skin [265]. Cellulose combined with collagen has been used to produce a wound dressing that can protect and bind to growth factors by inactivating matrix metalloproteinases in the wound microenvironment [266]. Modern classes of collagen and growth factor biomaterials can target specific defects in a wound, laboratory data shows that these materials alter the wound biochemistry that is capable of stimulating healing.

2.5.5 Chitosan

In the 1950s, studies into accelerated wound healing found that shark cartilage contained a component that lead to rapid recovery of wounds [267]. It was suggested that the presence of glucosamine in the shark cartilage was responsible for the accelerated healing effect [268]. Glucosamine is one of the most abundant monosaccharides and makes up part of the structure of chitin and chitosan [269]. Used as supporting material for crustaceans and insects, chitin is an abundant natural mucopolysaccharide that consists of 2-acetamido-2-deoxy-β-d-glucose through a β 1→4 linkage [270]. Chitosan, however, is the *N*-deacetylated derivative of chitin and due to its high percentage composition of nitrogen compared to synthetic cellulose, it has much commercial interest and is widely used as a chelating agent [271]. Compared to most synthetic polymers, chitosan has superior biocompatibility which is comparable to that of cellulose [272].

Chitosan is now used widely for its wound management properties. It is a bioactive polymer that promotes macrophage function leading to faster wound healing [273]. Additionally, chitosan can stimulate histoarchitectural tissue organisation and stimulate cell proliferation [274]. The application of chitosan hydrogels on mice full-thickness skin incisions shows a significant wound contraction and an accelerated wound closure compared to the untreated mice [275-277]. In another study using half chitosan and half a conventional wound dressing, it was found that chitosan facilitated rapid regeneration of the nerves

and allowed for rapid re-epithelisation [278]. Chitosan used in wounds has been associated with an early return of normal colour back to the skin following injury [277]. Furthermore, wound treatment with chitin and chitosan demonstrates a reduction in healing times whilst also reducing scarring that would otherwise have occurred via natural healing in various animals [279].

Chitosan has many other useful biological properties that make it an ideal material to be used in wound healing. In the biochemistry of chitosan, a silver sulfadiazine bilayer exists which gives the polymer excellent oxygen permeability, good water uptake capability and controlled water vapour transition rates [280]. In addition to all the benefits this material has in wound healing applications, chitosan demonstrates excellent antibacterial and fungicidal activity *in vivo* [281, 282].

Although chitosan has many properties that would make it the ideal material to be used in wound care, the poor solubility of the material becomes a major obstacle in its commercial utilisation. The material cannot, therefore, be readily mixed with other polymers and processing can take additional steps, but chitosan materials are still being made. Fibres made from chitin have been used in absorbable sutures and in wound dressing materials [283, 284]. Electrospinning has been used to form chitosan-containing and pure chitosan fibres from dissolved chitosan, the production with electrospinning allow morphological and topological tailoring of the material for wound healing [285].

2.5.6 Alginate

Alginate is an anionic linear polysaccharide that consists of manuronic acid (M units) and Guluronic acid (G units) connected by β 1→4 linkages. The ratio and distribution of these units along the polymer depend on the source of alginate [286]. Alginate is derived from brown algae and bacteria. In the presence of divalent cations such as ca2+, alginate undergoes reversible gelation to form a hydrogel via cross-linking [287]. Treatment with a chelating agent such as EDTA will reserve the gelation [288].

Alginate is ideal for cell-based systems because it is highly biocompatible, non-toxic and biodegradable [289]. Alginate also allows for a simple and rapid cell immobilisation process which makes it ideal for cell transplantation. Alginate is a highly abundant polymer that can be utilised to bring down costs in wound care products. Cells immobilised in alginate display good long-term viability thanks to the mild environment of the gel network. The high absorbency of alginate minimises bacterial contamination permitting use in wound dressings [290]. Wound dressings made from alginate can maintain a physiologically moist environment and facilitate wound healing [291]. In its dry form, alginate dressings can absorb wound fluids which can cause the alginate to re-gel which can later be used as a reservoir for the wound [292]. Many bioactive alginate-based wound materials have been studied, and it was found that oxidised alginate produced dibutyryl cyclic adenosine monophosphate, a regulator of human keratinocyte proliferation which reduced healing times in rat models [293].

2.6 Wound Healing

A wound can be defined as a compromise in living tissue caused by physical trauma which typically occurs when the skin is cut or broken. The cost of wound care in the UK alone exceeds £5 billion and is a market valued at over $25 billion [185, 294]. In this section, the basics of wound healing will be discussed relating to how these steps can be addressed to achieve advanced wound healing.

2.6.1 Principles of Wound Healing

The stages of wound healing in the microenvironment of a wound can be broadly divided into three phases; inflammation, cellular proliferation and remodelling [295]. In understanding these cellular processes, more can be done to achieve a higher quality of healing.

The first phase of wound healing is haemostasis and inflammation where the exposed collagen of the open wound is responsible for activating the blood clotting pathways [296]. Cell membranes release vasoconstrictors upon injury, the clot formed is made of collagen, fibronectin and thrombin which release growth factors, initiating inflammation of the wound [297]. This clot acts as a scaffold for cells of the wound response such as fibroblasts, endothelial cells, monocytes and neutrophils [298]. The first phase of the wound healing can therefore govern the overall process and by improving each phase, advanced wound healing can be achieved. By incorporating collagen into a wound dressing, structural and biochemical support can be provided [299]. Additionally, important molecules such as growth factors and signalling proteins can be seeded with the wound material to accelerate healing [300].

The second major phase of wound healing is proliferation, where epithelisation and angiogenesis occur. A complex chemical and signalling pathway exists here and collagen is a key component. Epithelisation occurs early in the repair process where epithelial cells migrate upward to repair the compromised skin and re-establish the natural protective barrier [301]. Angiogenesis also occurs in which a network of new blood vessels to the affected site is established, critical for proper wound healing [302]. Also in this stage, granulation and tissue deposition occur which require an adequate supply of nutrients from the capillaries, if this supply fails, it may result in a chronic wound [303]. Advanced wound care materials can provide essential nutrients and act as a scaffold to guide the important proliferation of the cells responsible for wound healing.

In the final stage of wound healing, maturation and remodelling occur. This phase can ultimately determine the physical appearance and functionality of the repaired wound and is therefore especially important as a clinical consideration for patients [304]. Collagen deposition is central in this process, and it is required that a well-organised network should be formed. Issues in the collagen matrix deposition can result in a loss of wound strength when too little collagen is deposited and hypertrophic scarring when too much is deposited [305, 306]. The collagen that is first laid down is oriented parallel to the skin but is thinner than that found in uninjured skin. Over time, the collagen threads will become reabsorbed and be deposited as thicker strands which

will be organised along the stress lines of the wound, this increased thickness results in higher tensile strength [303].

2.6.2 Requirements of a Wound Healing Material

Wounds cause pain, loss of normal function and increased exposure to infections. An ideal wound healing dressing must possess some basic characteristics in order to facilitate good wound healing. Firstly, a wound-healing material must act as a barrier against pathogenic infiltration whereby physically limiting the entry of harmful microbes which can cause infection and prolong healing [307]. Whilst providing this barrier, the material must also be able to allow efficient gas exchange such as allowing oxygen into the wound site which has been shown to increase healing rates as oxygen is an important metabolic gas [308].

A good wound dressing material must be able to maintain a suitable wound environment, by managing exudate absorption [309]. Exudate is a key element in wound healing which must be able to flow freely in and out of the wound [310]. The exudate must not completely dry out and the material must be able to also maintain a moist environment [311]. Porous dressings are beneficial in maintaining a good environment as they can drain excess exudate [312]. The water-holding and uptake capabilities of wound dressings are therefore very beneficial to healing.

Furthermore, the biocompatibility of any material encountering skin or bodily fluids is a necessary consideration and must not adversely cause an immune response or rejection. The material should be able to prevent necrosis in the wound environment and be able to facilitate the movement of important growth factors and cells such as tumour necrosis factors [313]. Some other key properties of wound dressing materials are summarised in (

Table 1).

Table 1: Table summarising the key properties and their desired ranges for optimal wound healing

Property	Specific benefits to wound healing	References
Biodegradability (*Degradation between 6 weeks to 2 years*)	Bandage for chronic wounds potentially doesn't require removal	[314, 315]
ECM Resembling Matrix (*Fibre porosity between 250 to 500 μm)*	Biomimetic structure promotes prompt wound healing	[316, 317]
Excellent Biocompatibility (Cell viability above 70%)	Reduces complications with immune rejection	[318, 319]
High Stiffness for high movement areas (*Between 1MPa – 2 KPa, depending on wound area)*	Maintain correct pressure on wound, depending in wound location	[320, 321]
High Tensile Strength (*Above 1 MPa ultimate tensile strength)*	Resistance against tearing as a wound dressing	[322, 323]
High Water Uptake Ability *(Above 30 g water/g sample)*	Maintains moist environment and flow of wound exudate	[324-326]
Large Surface Area *(Above 100 m^2/g)*	Increased interactions with cells of wound response	[327, 328]
Minimal Pain During Application	Should not cause the patient pain during application or removal	[329]
Conformability	Should be able to take shape of the wound area and not restrict patient movement	[330]

2.6.3 Advanced Wound Healing

Traditionally in the past, wound management materials only aimed to cover and conceal the wound. These materials were passive in that they did and very little was done to encourage the wound healing process [331]. In 1891, Johnson and Johnson first began to mass-produce a wound dressing where they sterilised cotton yarns, following this sterile gauze became the most used surgical dressings [332]. Bandages and gauzes have proven to change the landscape in wound management, however more advanced forms of wound healing have been practised recently and are greatly required.

Advanced wound healing allows for the treatment of wounds that result in greater healing compared to conventional methods. This advancement can be in the time required to heal, the reduction of scarring and the antimicrobial ability of the wound dressings. Therefore, an advanced wound healing dressing should be able to do the following: 1) eliminate infection 2) reduce external bleeding by restoration of nerve function 3) promote epithelisation and wound restoration.

2.6.3.1 Pro Wound Healing

Modern gauze dressings are available to purchase with impregnated active substances such as zinc, iodine, petroleum and bismuth. These additions can make the dressing semi-occlusive and non-adherent, therefore reducing pain associated with standard coverings and decreasing moisture loss from the wound [333]. A dressing is occlusive if it can maintain a moist wound surface which is crucial for full recovery [334]. Transparent film dressings also exist where thin flexible sheets made of synthetic polymers such as polyurethane that are permeable to water vapour and gasses but impermeable to bacteria [335]. They are commonly used to cover donor skin graft sites and are reported to improve healing and reduce pain. Foam dressings made from a

polyurethane base allow gas and water vapour permeability, the hydrophobic nature of the polymer gives high absorbance whilst also providing thermal insulation [336]. Foam dressings are highly versatile as they can be used on wounds with moderate to heavy exudate, full-thickness wounds and with diabetic ulcers [337].

Hydrogels are a complex network of hydrophilic cross-linked polymer chains that consist of about 80-92% water. Hydrogels can absorb and donate moisture to a dry wound and facilitate autolytic debridement, which is the removal of dead, damaged or infected matter [338]. Hydrogels have been found to be able to reduce the wound bed temperature by 5°C and promote granulation and epithelisation [339, 340]. Hydrogels soften and loosen slough and necrotic wound debris, they can be used in pressure ulcers, partial to full-thickness wounds and in vascular ulcers. Hydrocolloids, on the other hand, are a class of dressings that have an inner self-adhesive, gel-forming layer and are composed of hydrophilic colloidal particles such as sodium carboxymethylcellulose, gelatin and pectin [341]. The special layer can provide a moist environment whilst providing thermal insulation. The outer layer made of a synthetic polymer contains the seal which protects the wound from foreign invasion [342]. As mentioned previously alginates are another class of dressings that form a hydrophilic gel when the sodium and calcium ions come into contact with the serum found in wounds [343].

Hydrofibre dressings are a non-woven dressing pad made of sodium carboxymethylcellulose and can interact with wound exudate and serum to form a gel [344]. Hydrofibres are similar to alginates and share common properties, they are comfortable, amenable and easy to remove. Hydroconductive dressings are a novel class of dressings products that were introduced in 2011, they provide capillary action that can lift and move exudate away from the wound site to the second layer [345]. Hydroconductive dressings can also remove and displace debris away from the wound surface. These dressings are capable of moving fluid either vertically or horizontally and can hold up to 50 times their weight in liquid. Advanced and novel approaches to wound healing and improved engineering allows for the wound to heal faster and more effectively as shown by these examples, the

incorporation of synthetic and natural materials can further the field of advanced wound healing [346].

2.6.3.2 Reduction of Scarring

Scarring is a natural process in the recovery of wounds, it is however an unwanted cosmetic consequence that can significantly reduce a patient's quality of life. Advanced wound care materials aim to improve the quality of healing, one major aspect is therefore scarring. Researchers believe that the inflammatory phase of wound healing may be the most crucial in the reduction of scarring and for the improvement of appearance in healed skin injuries. Investigations into the healing of scarless embryonic wounds have influenced the interest in the inflammation stage [347]. Fetal skin is capable of rapid reepithelialisation with minimal inflammation [348, 349].

Scarring as a result of surgical intervention totals to over 100 million cases annually worldwide creating a huge market for materials that tackle this [350]. Current treatments for scar therapy include topical therapy and steroidal injections which has a success rate of over 50%, but is associated with hypopigmentation, dermal atrophy and delayed wound healing [350, 351]. More recently, work has been carried out with gene targeting where the genes and growth factors have been identified. Polypeptide growth factors such as TGF-ßs are used in conjunction with scar reduction strategies to promote fibroblast to myofibroblast transition in the production of the wound extracellular matrix [352, 353]. The fact remains that novel approaches must be created that would improve the quality of healing of a wound without the current drawbacks.

2.6.3.3 Antimicrobial

Infections due to microbial interference provides a huge problem to wound healing as they can affect the wound healing process and lead to chronic wounds. Infections of the skin and soft tissue are the most common and affect nearly 14 million people in the USA alone [354]. In

the early stages of the infection process, gram-positive microbes such as *Staphylococcus aureus* and *Streptococcus pyogenes* are predominant whilst gram-negative microbes such as *Escherichia coli* and *Pseudomonas aeruginosa* can be found later and especially when a chronic wound is developed [355]. Antimicrobial wound dressings are highly favoured to prevent wound contamination.

Antibiotics are used as antibacterial agents to enhance wound dressings, although thousands of antibiotics have been discovered, only 1% of those can be used in clinical application due to their toxicity [356]. Aminoglycosides, glycoproteins, sulphonamides and tetracyclines have been used in dressings that display antimicrobial activity [357-359]. However, the practice of overusing antibiotics in a clinical environment can lead to an increased rate of bacterial resistance due to the selection pressure it causes on the microbes [360]. Alternatively, metallic nanoparticles have been used as alternatives to conventional antibiotics, they display bactericidal activity against many strains [361]. Nanoparticles typically kill bacteria through direct contact with their cell wall, by releasing toxic metallic ions and through the generation of reactive oxygen species [362]. Typical antimicrobial nanoparticles include silver, iron, zinc oxide and titanium oxide [363]. There are however safety concerns due to the toxicity of these nanoparticles as they can leach ions and affect healthy cells [364]. Furthermore, as mentioned before, some naturally derived polymers such as chitosan have also been used in potential wound dressings as they exhibit antimicrobial capacity.

Antifungal dressings are also an important class of materials. *Candida albicans* is found in abundance in the human gut flora of around 50% of all healthy adults and is an opportunistic pathogenic yeast [365, 366]. *C. albicans* is known to cause human infections such as candidiasis which occurs as a result of its overgrowth and is a contributing factor in tooth decay [367, 368]. Furthermore, *C. albicans* is the most common fungal species found to form as a biofilm on medical implants and is the cause of many implant failures [369]. The cost of treatment for patients only increases due to the rise of hospital-acquired infections [370]. The usage

of bandages and gauzes remains a highly prevalent method of wound care in many countries and thus there must be novel wound healing materials that address the threat of fungus instead of focussing all the resources on antibacterial materials. Therefore, the antimicrobial ability of a wound dressing is a very desirable and important feature, this work will heavily investigate the production of wound healing biomaterials with specific antimicrobial compounds mentioned in this chapter. The work will thoroughly investigate the efficacy of these produced bandage-like materials to prevent both bacterial and fungal infection from occurring in wounds and to facilitate advanced wound healing.

Chapter 3 : Experimental Details

3.1 Introduction

This chapter describes the materials used, the procedures followed, and any details of equipment utilised in the duration of the different tests. This section has been compartmentalised into three main segments that describe the materials and testing procedures for chapter four to chapter six.

The following section contains experimental details and details of materials and methods used in experimental process of the work. Based on previous and preliminary testing, the choice of primary polymer and processing conditions had been determined. For example, polycaprolactone of molecular weight 80,000 was selected because it has a sufficient polymer chain entanglement which ensured that viable fibre production would ensue with pressurised gyration. Multiple different solutions of this polymer were prepared and spun to determine that 15% (w/v) was the optimal concentration where there was an ideal compromise between fibre yield and fibre diameter. The pressurised gyration operating parameters were kept constant, where otherwise mentioned. For the following tests, the rotational speed and collection distance were kept the same, that is maximum speed and a collection distance of 150mm as they were deemed optimal to ensure sufficient centrifugal speed for spinning and collecting dried fibres. All tests were carried out in ambient conditions or otherwise stated, and the room conditions were kept constant between 22-24 °C, with a relative humidity between 35-55%.

3.2 Effect of working parameters and solution properties on polymeric fibre production

In this study, the effects of varying working parameters and solution properties on the pressurised gyration setup are analysed to be able to produce fibres that can be tailored to suit a range of different applications which require

different morphological and topological features, as well as surface area and uniformity in the fibre production. Secondly, the effects of using binary and ternary polymer blends to produce bandage-like fibres using pressurised gyration were investigated to see the differences in fibre morphology and production yield.

3.2.1 Effect of Solvent and Pressure

3.2.1.1 Materials

Polycaprolactone (PCL) is an important biomedical polymer due to its mechanical properties and its excellent miscibility with other polymers and organic solvents. PCL is a biodegradable polyester with a melting point of about 60°C, high in flexibility and has a relatively high tensile strength [371]. PCL was used in these tests as it shows good solubility in a large range of organic solvents which have distinguished physical properties [372]. The polymer used in this work had an average molecular weight of 80,000 and was obtained from (Sigma Aldrich, UK).

For the second phase of the study, the effect of binary and ternary polymer blends on the manufacturing of bandage-like fibres was carried out. Poly(lactic acid) (PLA) of molecular weight 60,000 was used

3.2.1.2 Solvents

Chloroform, also known as trichloromethane, is a sweet-smelling and dense solvent that is commonly used as a precursor in the production of Teflon [373]. Chloroform is produced naturally in the environment at about 650 kilotonnes annually, many types of seaweed and fungi can produce it through an abiotic process [374, 375]. Chloroform (CAS: 67-66-3) was used to dissolve PCL, purchased and supplied by (Sigma Aldrich, UK).

Dichloromethane (DCM) is similar in its chemical structure to chloroform but has one fewer chlorine group. DCM, also known as ethylene dichloride, is a colourless liquid with a sweet smell. DCM is used in the production of polyvinyl

chloride materials which have a large number of applications in waste piping and houseware [376]. As a solvent, DCM forms azeotropes with many other solvents such as water, an azeotrope has a mix of boiling points that are not native to either solvent in the composition [377]. DCM (CAS: 75-09-2) was used to dissolve PCL and was obtained from Sigma Aldrich, (Gillingham, U.K.).

N,N-dimethylformamide, (DMF), is a colourless and odourless solvent that has good miscibility in a large range of organic solvents and water [378]. DMF has a very high boiling point and is thus used in applications where low evaporation rates are required such as in the development and production of pesticides, adhesives and synthetic leathers [379]. DMF (CAS: 68-12-2), was used to dissolve PCL and was obtained from Sigma Aldrich, (Gillingham, U.K.). Tetrahydrofuran, (THF), is a low viscosity colourless organic liquid that demonstrates good miscibility with water, its most common use is as a precursor in the production of other polymers [380]. THF is also an industrial solvent for use in varnishes and polyvinyl chloride materials, it can dissolve in a wide range of chemical compounds and can form clathrate hydrate structures with water at low temperatures [381, 382]. THF (CAS: 109-99-9), was used to dissolve PCL and was obtained from Sigma Aldrich, (Gillingham, U.K.)

Toluene is a colourless liquid that has a distinct strong odour commonly associated with paint thinners [383]. Toluene is an aromatic carbon and does not demonstrate any solubility in water [384]. Toluene is a common solvent for use in paints, paint thinners, silicone sealants, printer ink and disinfectants [385].

3.2.1.3 Solution Preparation

PCL solutions in DMF, THF, Toluene, DCM and Chloroform were all prepared at a constant concentration of 15 % (w/v). This concentration was selected due to giving optimal yield in preliminary studies. The solutions were stored in an airtight 50 mL glass vial where they were subjected to high-speed mixing at 3600 rpm for 20 minutes (Hauschild SpeedMixer DAC 150.1 FVZ-K,

Germany), at 5-minute intervals to ensure heat did not accumulate and cause expansion of the solutions. Solutions of DMF required further heating at 60 °C to ensure complete dissolution. Complete dissolution was indicated by the presence of a clear solution.

3.2.1.4 Solution Characterisation

The physical properties of the polymer solutions were measured. The surface tension of the solutions was characterised via a tensiometer (Tensiometer K9, Kruss GmbH, Germany) and was repeated three times to find the average value. These values were all taken at a sheer rate of 3 mPa.S to ensure comparison between the samples. Viscosity was measured using a programmable rheometer (DV-III Ultra, Brookfield Engineering Laboratories INC, Massachusetts, USA), readings were taken at a shear stress of ≈ 5 Pa, measurements were repeated 3 times to find the average value.

3.2.1.5 Experimental Setup - Fibre Production

The solutions were all subjected to spinning before beginning the main experiments to determine spinnability when using differing solvents. All solvents but Acetone managed to form fibres in the test run, for this reason, Acetone was excluded from the solvent list from this point onwards.

The spinning process was carried out with a pressurised gyration laboratory setup. This involved a small aluminium cylindrical vessel measuring 60 mm in diameter which had 24 small 0.5 mm drilled holes through its wall, into which a polymer solution was placed. The vessel was connected to a nitrogen gas supply and a high-speed motor. For these experiments, rotation speed was kept constant at 36000 rpm to observe differences owing to solvent and gas pressure only. The gas pressure was then varied from 0 to 0.3 MPa in 0.1 MPa increments. All experiments were carried out in ambient conditions (20 - 22°C) with a relative humidity range of (41 - 46 %).

3.2.1.6 Characterisation of Fibres

The produced fibres were gold sputter-coated (Q150R ES, Quorum Technologies) for 3 minutes preceding SEM imaging (Hitachi S-3400n). The SEM images were then surveyed using Image J software, 100 fibres were measured at random, and the mean diameter was calculated. High magnification SEM images allowed visualisation of surface topography such as porosity and presence of beads which have been analysed in his paper.

3.2.2 Effect of Binary and Ternary Polymer Systems

3.2.2.1 Materials

Bacterial cellulose (BC) is a form of cellulose produced by certain species of bacteria, it has remarkable suitability as a wound-healing material due to its high water uptake ability, robust mechanical properties and high affinity for biological cells of the wound response [386-388]. BC was obtained from the Centre for Nanotechnology & Biomaterials Research, Marmara University (Istanbul Turkey). PLA (MW = 110 $x10^3$ g mol^{-1}), PCL (MW = 80 $x10^3$ g mol^{-1}) and Chloroform (CAS: 67-66-3) was purchased from Sigma-Aldrich (Gillingham, UK). Poly (lactic acid) of molecular weight ~ 60,000 Da.

3.2.2.2 Preparation of Solution Blends

The BC membranes were cut into small pieces and placed onto a napkin, pressed for 30 seconds to remove excess water. Samples were placed in a beaker with chloroform and subjected to high-frequency sonication for 1h using a sonifier (Branson SFX550, BRANSON Ultrasonics Corporation, USA). The BC was centrifuged with ethanol to remove any excess water and was subsequently stored in an airtight vial at ambient temperature (22-24^{o}C). 12 wt. % PLA and 12 wt.% PCL solutions were used and prepared in chloroform which was stirred for 24h at ambient temperature (22-24^{o}C). BC blends were

created (0 to 100 wt. ratio) with PLA and PCL to make binary Prepared PLA and PCL solutions with different ratios (10 to 90 wt. ratio) were blended. In order to increase the solubility of BC, 1mL of DMF was used in polymer solutions where BC was used. BC concentration within the (PLA-PCL)-BC ternary system was systematically increased (0 to 90 wt. ratio). All blend solutions for binary and ternary systems were used without further treatment.

3.2.2.3 Fibre Production

Fibre production utilised the pressurised gyration setup as mentioned before at an operating pressure of 0.1 MPa and a rotation speed of up to 36,000 rpm. All runs were timed at 15 seconds and were carried out at ambient temperature (23-24^{o}C) and relative humidity (51-54%). Following the experiments, a vacuum oven was used to evaporate any residual chloroform that may have remained in the bandage-like fibrous scaffolds. At the end of the experiments, the optimal blending ratio was found by characterisation tests and calculations of the yield.

3.2.2.4 Characterisation

3.2.2.4.1 Physical

A Brookfield DV-III ULTRA viscometer (Brookfield Viscometers Ltd, Harlow, UK) was used to measure the viscosity using a small sample adapter with a volume of 3 mL. A digital tensiometer (K9, Kruss GmbH, Hamburg, Germany) was used to evaluate the surface tension of the solutions via the Wilhelmy's plate method. All equipment was calibrated before use and all measurements were repeated three times at ambient temperature (22-24°C) and a relative humidity of 40–50 %.

3.2.2.4.2 Morphological

For visualisation of the fibres in bandage-from, a ZEISS MA EVO 10 scanning electron microscopy (SEM, Zeiss, USA) was used at an accelerating voltage

of 10 kV. Before imaging, samples were sputter-coated with gold for 60 seconds using a Quorum SC7620 Mini Sputter Coater. The diameters of the fibres were measured at random with the image processing program, ImageJ.

3.2.2.4.2 Mechanical Testing

In order to perform mechanical testing, the fibrous samples were prepared into uniform thicknesses of 2mm strips via even rolling into bundles. The fibre bundles were then cut into equal length of 70mm. The thickness of each fibrous scaffold was measured three times at different points using a Mitutoyo, High-Accuracy Digimatic Micrometer (USA). The average thickness of each sample (2 mm) was used for the determination of tensile strength. The stress-strain properties of the samples were calculated using a tensile extension with a 30 mm gauge length by a uniaxial tensile test machine (INSTRON 4411, Massachusetts, USA). Test cycles were performed using a load sensor of 50 N and a loading speed of 5 mm/min at ambient conditions (temperature 22-24°C). The stress-strain curves were recorded, the maximum tensile strength and Young's modulus were obtained. For each fibrous sample, the tensile loading was repeated three times and the mean and standard deviation was calculated and plotted onto graphs.

3.3 Antimicrobial Natural Materials

Natural materials can provide antimicrobial support whilst retaining their biocompatibility and support for wound healing. In this section, two main natural materials; honey and cinnamon were explored and incorporated into bandage-like fibrous meshes for use in wound healing. Honey is a great material against harmful bacterial species whilst cinnamon is potent against pathogenic fungi found in open wound scenarios. The materials and methodology follow.

3.3.1 Antibacterial Honey Fibres

3.3.1.1 Materials

3.3.1.1.1 Honey

Two types of honey were initially screened for their antimicrobial activity: Black Forest Honeydew Honey and Manuka honey. According to literature, Black Forest Honey showed one of the highest levels of antibacterial activity when compared to other common kinds of honey [389]. The antibacterial activity of Black Forest Honeydew Honey and Manuka Honey UMF 20+ was determined against two known commonly occurring wound pathogens: *E. coli* and *S. epidermidis*, and the most potent honey was then incorporated into polymeric fibrous meshes using pressurised gyration. Black Forest Honeydew Honey was purchased from Bulgarian Bee (Okorsh, Bulgaria). Manukora Manuka Honey of UMF 20+ was obtained from Manukora (Auckland, New Zealand). Both honey jars were stored at a dry temperature-managed cupboard to prevent crystallisation.

3.3.1.1.2 Polymers

The polymer of choice for the fibre production was PCL (mn 80,000) and was obtained from Sigma Aldrich, (Gillingham, U.K.). Chloroform (CAS: 67-66-3) was used to dissolve the PCL into a polymeric solution and was obtained from Sigma Aldrich, (Gillingham, U.K.). All solvents and chemicals were of analytical grade and used as received.

3.3.1.1.3 Bacteria Strains and Media

Antibacterial activity was assessed against *Staphylococcus epidermidis* NCTC 11047 and *Escherichia coli* K12. LB Broth Base (Lennox L Broth Base) was purchased from Sigma-Aldrich (Gillingham, U.K.). LIVE/DEAD BacLight Bacterial Viability and Counting Kit were purchased from ThermoFisher Scientific (Paisley, UK). Media were prepared as instructed by the manufacturer.

3.3.1.2 Solution Preparation

Chloroform was used to dissolve PCL at a concentration of 15% (w/v) which from previous studies and optimisation, was deemed the optimal concentration for production yield and mechanical properties. Manuka honey was then added at to the PCL at concentrations of 10, 20 and 30% (v/v) with a syringe, the pressure of which allowed the honey to penetrate deep into the PCL solution. The mixtures of honey and PCL were then subjected to high-speed mixing using a (SpeedMixer DAC 150.1 FVZ-K, Germany) at a speed of 3600 rpm for a duration of 5 minutes. It should be noted that if the honey was subjected to high heat from the speed mixer for a prolonged duration, it would cause solidification of the honey, rendering the polymer solution unusable.

3.3.1.2 Methods

3.3.1.2.1 Antibacterial Mesh Production

The honey polymer solutions were subjected to spinning via pressurised gyration at a gas flow pressure of 0.1 MPa and a rotational speed of 36,000 rpm. The fibres formed a ring around the gyration vessel which resembled large bandage-like scaffolds as seen in (**Figure 3.1**). The fibres were then collected via sterile utensils and stored for characterisation and antibacterial studies. The fibre manufacturing process occurred at ambient conditions (22 ± 2°C, 45-55% relative humidity).

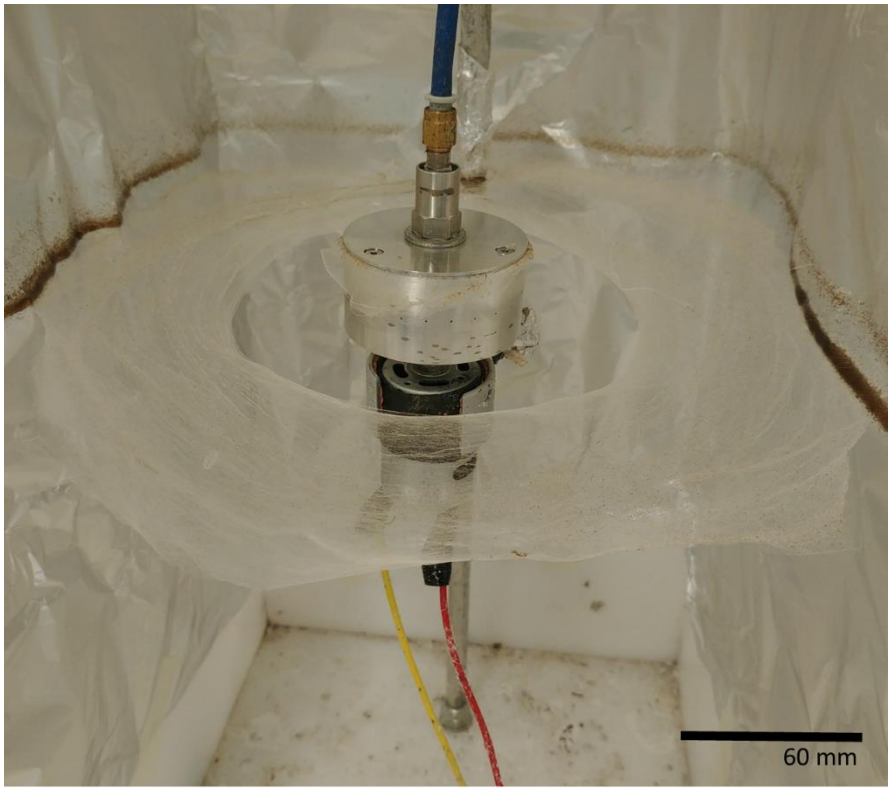

Figure 3.1: Photograph showing honey-PCL composite fibres surrounding the pressurised gyration vessel, ready to be collected.

3.3.1.3 Characterisation

3.3.1.3.1 Viscosity

The viscosity of the solutions was measured using a Brookfield Viscometer DV-III (Brookfield, Middleboro, MA, USA). A small-sample spindle was used with a polymer volume of 3mL. For the Manuka honey readings, the lowest spindle speed was selected (0.01 rpm) due to the high viscosity range of these solutions, measurements were taken at a constant torque value to ensure comparability within the samples. All viscosity measurements were taken at ambient conditions (22 ± 2°C) and repeated 3 times to give an average value. The viscosity of the pure Manuka honey could not be determined as it fell above the viscosity range of the apparatus, for this reason, I have assumed it is larger than 60000 mPa s.

3.3.1.3.2 Surface Tension

The interfacial surface tension of prepared solutions was characterised via a tensiometer (Tensiometer K9, Kruss GmbH, Germany). The Du Nouy ring method was employed to measure the surface tension, a glass vial was filled with polymer solution and a platinum-iridium ring with a 6 cm diameter was submerged into the solution. The ring in the solution was raised to enable a fluid meniscus to form, the variation of forces was measured using a force tensiometer. These readings were repeated 5 times to find the average surface tension values for each solution of varying concentrations.

3.3.1.3.3 Fibre Morphology

The virgin PCL fibres and the honey composite fibres were characterised for their diameter distribution and their surface topography. The samples were examined by scanning electron microscopy (SEM) (Hitachi S-3400n, Japan) which were gold sputter-coated (Q150R ES, Quorum Technologies) for 90 seconds before imaging at various high magnifications. The SEM images were then surveyed using Image J software, 100 fibre strands were measured at random, and the mean diameter was calculated. The frequency distribution of the fibre diameters was calculated using OriginPro graphical software.

3.3.1.3.4 Fourier Transform Infrared Spectroscopy

Fourier Transform Infrared Spectroscopy (FTIR) was carried out on a Perkin Elmer Spectrum-2 FTIR Spectrophotometer (PerkinElmer Inc., Beaconsfield, UK). The infrared spectra of the fibres and the honey were taken in transmittance mode between the wavenumbers of 4000 to 450 cm^{-1}. All measurements were taken at ambient temperature and conditions (22-24°C). For each sample, four scans were taken at a resolution of 4 cm^{-1}. The spectra were analysed with Essential FTIR software and plotted into graphs using OriginPro.

3.3.1.4 Antibacterial Activity of Honey and Honey Fibre Meshes

The antibacterial activities of Manuka Honey and Black Forest Honeydew Honey were determined against *S. epidermidis* and *E. coli*. Stock cultures of

these microorganisms were stored in LB broth supplemented with 10% glycerol at -80°C until use. The antibacterial activities of the honey samples were determined by evaluating the survival of the bacteria strains after incubation with 10, 20 and 30 v/v% of honey/PCL for 24 hours at 37 °C and 150 rpm. Honey concentrations of 10, 20 and 30 v/v% were chosen, as previous studies have shown the minimum inhibitory concentration of honey to range from 4.2 to 25% [390, 391]. Overnight *S. epidermidis* and *E. coli* cultures were added to sterile LB broth at 10 v/v%. Manuka Honey or Black Forest Honeydew Honey was added to the cultures at either 10, 20 or 30 v/v% and incubated for 24 hours at 37°C and 150 rpm. Post incubation, flow cytometry was used together with the LIVE/DEAD BacLight Bacterial Viability and Counting Kit to quantify the proportion of live and dead bacteria cells in the suspensions. This method relies on the use of fluorescent stains, SYTO®9 and propidium iodide (PI). SYTO®9 is a green, fluorescent nucleic dye that can penetrate both live and dead cells; whilst PI is a red fluorescent intercalating stain that can only penetrate cells with damaged membranes (non-viable cells) to displace the SYTO®9. Therefore, viable cells appear green whilst non-viable cells have a red colouration. A stock solution of PI and SYTO®9 was prepared according to manufacturers' instructions. 180 µL of the stock staining solution was added to 20 µL of diluted sample and incubated at ambient temperature in the dark for 15 minutes. After incubation, cells were acquired using a calibrated Guava easyCyte® flow cytometer and InCyte software. Gates were set up using positive (media and bacteria only), negative (media only) and fluorescent minus one control (single stained positive controls). 50,000 events were collected, and bacteria acquisition gates were determined using forward scatter and side scatter channels to eliminate background noise and debris from the sample. The gated population of bacteria was then analysed using fluorescent channels. FlowJo was used to gate the live and dead bacterial cell counts where proportions of live and dead bacteria cells were calculated. All experiments were repeated at least three times. The prepared honey-PCL composite fibrous meshes were tested for antibacterial activity against S. epidermidis. An overnight S. epidermidis culture was added to sterile LB broth at 10 v/v%. To this, honey-PCL scaffolds were added at 10 wt% and incubated for 24 hours at 37°C and 150 rpm. Pure

PCL fibrous scaffolds were used as the negative control. The number of live bacteria in the suspension post-exposure was enumerated using the colony counting method and compared to the negative control, which was set to 0%.

3.3.1.5 Statistical Analysis

The antibacterial activity of both honey types was statistically analysed and compared using unpaired t-tests. The different concentrations, honey types and potency against different strains were compared. The antibacterial activity of the prepared honey-PCL fibres was statistically analysed and compared to the control fibres using an unpaired t-test. The difference was considered significant when $p < 0.05$.

3.3.2. Antifungal Cinnamon Fibres

3.3.2.1 Fibre Preparation

Solvent extraction via chloroform (CAS Number: 67-66-3, Sigma Aldrich, UK) was carried out to formulate varying concentrations of cinnamon in solution form. Three cinnamon (cassia) extractions (C1, C2 and C3) of differing concentrations were prepared from ground cinnamon powder (JustIngredients, UK). The extraction process involved mixing 6g, 9g and 12g into 24 mL of chloroform; the solution was vortexed, excess cinnamon that was not dissolved into the solvent was separated by the addition of 10 mL distilled water and centrifugation at 2000 rpm for 15 minutes. Four concentrations of fibres were tested in this investigation: virgin PCL fibres with no cinnamon, C1, C2 and C3 fibres with 6g, 9g and 12g cinnamon per 24 mL of chloroform respectively. C1, C2 and C3 fibres therefore have an effective cinnamon content of 250, 375 and 500 mg/mL. Polycaprolactone (Mn 80,000, Sigma Aldrich, UK), was added to the cinnamon extract solutions to make a concentration of 15% (w/v) and magnetically stirred overnight to produce a polymer solution. The solutions were spun with a laboratory pressurised gyration set up which consists of a small (35 mm × 60 mm) aluminium

cylindrical vessel with multiple, narrow (0.5 mm) perforations that is connected to a gas inlet and high-speed motor to produce fibre meshes. 4 mL of the polymer solution was spun with pressurised gyration for 20 seconds to obtain a fibrous bandage-like mat at ambient conditions (24°C and 42% relative humidity).

3.3.2.2 Anti-fungal Testing Procedure

The zone of inhibition method was used to investigate the antibacterial activity of the scaffold samples against Candida albicans (*C. albicans*) yeast strain as the model organism. The yeast cultures from the colony were cultivated in Sabouraud Dextrose Agar (SDA, SIGMA-Aldrich, USA) overnight at 37°C. Colonies were taken with a sterile loop and suspended in 7 mL of sterile saline 0.145 mol/L (8.5 g/L NaCl, 0.85% saline). The resulting suspension was vortexed for 15 seconds and the cell density was adjusted to 1 $x10^6$ to 1 $x10^6$ colony-forming units (cfu)/ml. The yeast strain (1 $x10^6$ to 1 $x10^6$ colony-forming units (cfu)/ml) were inoculated on a previously prepared Mueller-Hinton (MH) agar (MH broth with 38g/l agar) plate using a sterile glass spreader.

100mg of cinnamon-containing fibres (C1, C2 and C3 samples) were tested at differing concentrations in 10 mL of agar (Sigma Aldrich, UK) at 37°C for 48h. After the incubation period, zones of inhibition of the scaffold samples were evaluated by measuring the clear area that formed around each scaffold sample. 250 µL of *C. albicans* (population 4-5 x 10^6) was distributed within the standard petri-dish. The fibres were placed in the centre of the petri-dish to determine any inhibition zones between the fungus and the samples. The agar plates were incubated at 37° C. As a negative control, the fibres containing polycaprolactone only were also used and inhibition zones were analysed. As a positive control, the raw material of cinnamon in powder form was tested as described previously. Images of the agar plates were taken following 48 hours after incubation, inhibition zones were calculated as areas using Image J software. Scanning electron microscopy (Hitachi S-3400n) was utilised to analyse the morphology of the fibres.

3.3.2.3 Cytotoxicity Testing

Cytocompatibility tests were performed for PCL and PCL-cinnamon gyro spun fibres according to the ISO10993-5 standard “Biological evaluation of medical devices-Part 5. Tests for *in vitro* cytotoxicity: Indirect MTT cytotoxicity test” regulation. During the study, L929 (ATCC-NCTC clone 929:CCL1) mouse fibroblast cell line was used. Incubation conditions were kept constant at >% 90 humidity, 5% CO_2 atmosphere and 37°C. Dulbecco’s modified Eagle’s medium (DMEM) (90 % (v/v)), Fetal Bovine Serum (FBS) (10% (v/v)) was used as cell culture medium in the presence of 0.1 % penicillin-streptomycin. Fibre samples were incubated in cell culture medium for 3 days with the 0.2 g/mL fibres/cell culture medium ratio in the incubator at 37 °C. L929 cells were seeded into a 96-well plate with the $1x10^4$ numbers of cells to each well. Extracted cell medium solutions interacted with the cell line in the 96-well plate for 24 h. 10 % dimethyl sulfoxide (DMSO) containing cell medium was used as positive control and DMEM-FBS medium was used as the negative control. At the end of the study, L929 cells were incubated with 10 % (4,5-Dimethylthiazol-2-yl)-2,5-diphenyltetrazolium bromide (MTT) solution for 3.5 hours at 37°C and afterwards, MTT crystals were dissolved by DMSO. Cell viability percentages were determined by the ELISA microplate reader at an absorbance of 570 nm.

Additionally, direct cell-material interactions were investigated by LIVE/DEAD™ Viability/Cytotoxicity test. The same cell culture conditions and the number of cells were used which were used during the MTT test. $1x10^4$ numbers of L929-cells were seeded to each well onto the fibre samples directly. After a 3-day incubation period, LIVE/DEAD™ Viability/Cytotoxicity staining kit was used to obtain live and dead cell fluorescent images of samples. Ethidium homodimer-1 (EtdH-1) (4 µM, red) and Calcein AM (2 µM, green) fluorescent dyes were mixed in phosphate buffer saline (PBS) and incubated with the samples for 45 minutes. At the end of the incubation period, samples were examined by fluorescent microscopy (Leica Microsystems, Germany). Fluorescence microscope images were obtained red for dead cells

and green for live cells and then the obtained images were overlaid (ImageJ 1.52a, USA).

3.3.2.4 Antibacterial Activity of Cinnamon-Extract Containing Fibre Constructs

The antibacterial activity of cinnamon–extract containing bandage-like fibres were investigated by a 24h bacterial adherence/biofilm formation assay. *Escherichia coli* (*E. coli* ATCC 25922), *Staphylococcus aureus* (*S. aureus* ATCC 29213), *Methicillin-Resistant Staphylococcus aureus* (MRSA ATCC 43300) and *Enterococcus faecalis* (*E. faecalis* ATCC 29212) strains were used. Tested bacterial isolates were dissolved from stocks kept at -80 °C in glycerol medium and sub-cultured twice before use. Each of the strains was adjusted to approximately $1x10^6$ colony-forming units (CFU/mL) as a final inoculum suspension concentration. 1 cm^2 of the samples were placed into a 48-well plate. 1 mL of bacterial suspension was added to the samples in each well. Well-plates were incubated at 37°C for 24 hours in a shaking incubator. After 24 hours, samples were rinsed with sterile PBS, moved into a new sterile well-plate and sonicated (Branson Sonifier SFX250, USA) in 1 mL sterile PBS medium (15 min). Sample solutions were serially diluted and placed into Petri dishes. Tryptic soy agar (TSA) medium was poured onto the dishes and stirred. After the 24-hour incubation period, each petri dish was counted for dilutions and biofilm formation was investigated.

For SEM analysis (SEM, GAIA 3; Tescan, Brno, Czech Republic), 24 hours after incubation with bacterial suspensions, samples were rinsed with PBS and fixed. Samples were kept in glutaraldehyde (G.A) solution (2.5% v/v, GA/PBS) for 15 mins. Samples were washed with serial alcohol dilutions for 15 min time intervals (25, 50, 70, 80, 90, 95 and 100% ethanol) and hexamethyldisilazane (HMDS) was added to the top of completely dry samples [46]. Before SEM analysis, samples were coated in a thin layer of gold via sputter coating (Edwards, UK).

3.3.2.5 Fibre Characterisation

The chemical structures of the cinnamon-extract containing bandage-like fibre constructs were characterised by Thermogravimetric analysis (TGA) (TA Instruments Q600-SDT, USA) to investigate and compare the thermal characteristics of PCL and cinnamon extract containing-PCL fibre samples. The virgin PCL fibres and the cinnamon containing fibres were characterised for their diameter and their surface topography. The samples were examined by scanning electron microscopy (SEM) (Hitachi S-3400n, Japan) which were gold sputter-coated (Q150R ES, Quorum Technologies) for 90 seconds before imaging at various high magnifications. The SEM images were then surveyed using Image J software, 100 fibre strands were measured at random, and the mean diameter was calculated. The frequency distribution of the fibre diameters was calculated using OriginPro graphical software.

3.4 Advancements in manufacturing technologies and Materials Selection

As discussed in (**2.2 Fibre Production Methods**), different methods of fibre forming have their unique advantages and disadvantages. The novel production of bandages by combining two manufacturing techniques has been carried out in this work. Flexible and strong polycaprolactone (PCL) bandages produced at a large scale can be created using pressured gyration which combines centrifugal spinning with solution blowing [16, 34, 392, 393]. Concentrated bioactive patches made of collagen and chitosan, which directly cover the wound have been produced by electrospinning, a technique that exploits a high voltage electric field to form fine and uniform fibres [72, 90]. These patches can also be incorporated with antimicrobial nanoparticles which have been shown to have a 100% kill rate with certain bacteria [394]. The collagen and chitosan composition has been established before with many studies showing excellent results [27, 395, 396]. This opens up the

possibility to use natural or a combination of synthetic materials to target antimicrobial and advanced wound healing.

3.4.1 Bandage Production with Novel Manufacturing Route

3.4.1.1 Materials

Polycaprolactone pellets, Mw 80,000 (Sigma-Aldrich, UK) were used as the selected polymer to be spun into the bandages. Chloroform, CAS: 67-66-3, (Sigma-Aldrich, UK) was used as-is to dissolve the pellets to form a homogenous polymer solution. Polyethylene oxide, Mw 1,000,000 (Sigma-Aldrich, UK), was used as the carrier polymer for the spray-on patches. Pure pigskin type I collagen extracted from feet bone tendons and ligaments, Mw 300,000, was obtained from (Hebei Aineng Biotechnology Co., Ltd, China). Chitosan powder made of shellfish was obtained from (Hebei Aineng Biotechnology Co., Ltd, China); the degree of deacetylation (%DD) 86%DD, dynamic viscosity 6000 mPa.s, MW= 30,000. Glacial acetic acid, CAS: 64-19-7 (Sigma-Aldrich, UK), was diluted with distilled water and used as a solvent for the collagen and chitosan found bioactive patches. Antimicrobial nanoparticles, (AMNP 8.1) were obtained from the University of Hertfordshire and used in conjunction with the collagen and chitosan solution in the secondary patches. The nanoparticles came suspended in chloroform as 1% (wt/v) chloroform, they contained NF CuO rods and an alloy of copper and zinc.

3.4.1.2 Novel Production Assembly for Bioactive Bandages

Electrospinning and pressurised gyration are both excellent fibre production techniques with their own unique advantages and disadvantages. For example, electrospinning is great at printing highly targeted bioactive nanofibres on other surfaces and pressurised gyration excels at its high production speed an ability to quickly produce bandage-like fibrous constructs. A new fibre producing setup was therefore constructed that combines two manufacturing techniques: electrospinning and pressurised gyration (**Figure**

3.2). In this setup, the pressurised gyration vessel is placed in the centre where the gyration vessel is surrounded by 4 repositionable “L- shaped” collection walls (200 x 130 x 280 mm). These walls allow for the collection distance to be easily altered and allow for easy sectioning of the produced bandages where the segments intercept following fibre generation. Initially pressurised gyration starts, producing the Saturn-ring like polymeric bandage-like structure (**Figure 3.2**), following this, electrospinning is used to print active material onto the formed bandage surface. The electrospinning jet is focused onto the bandage using a grounded aluminium ring (Outer diameter 280mm, inner diameter 140 mm) of high electrical conductivity (3.5×10^{7} S/m). Once the printing is completed, the bandages can be sectioned into quarters using the junctions between the collection walls as guides.

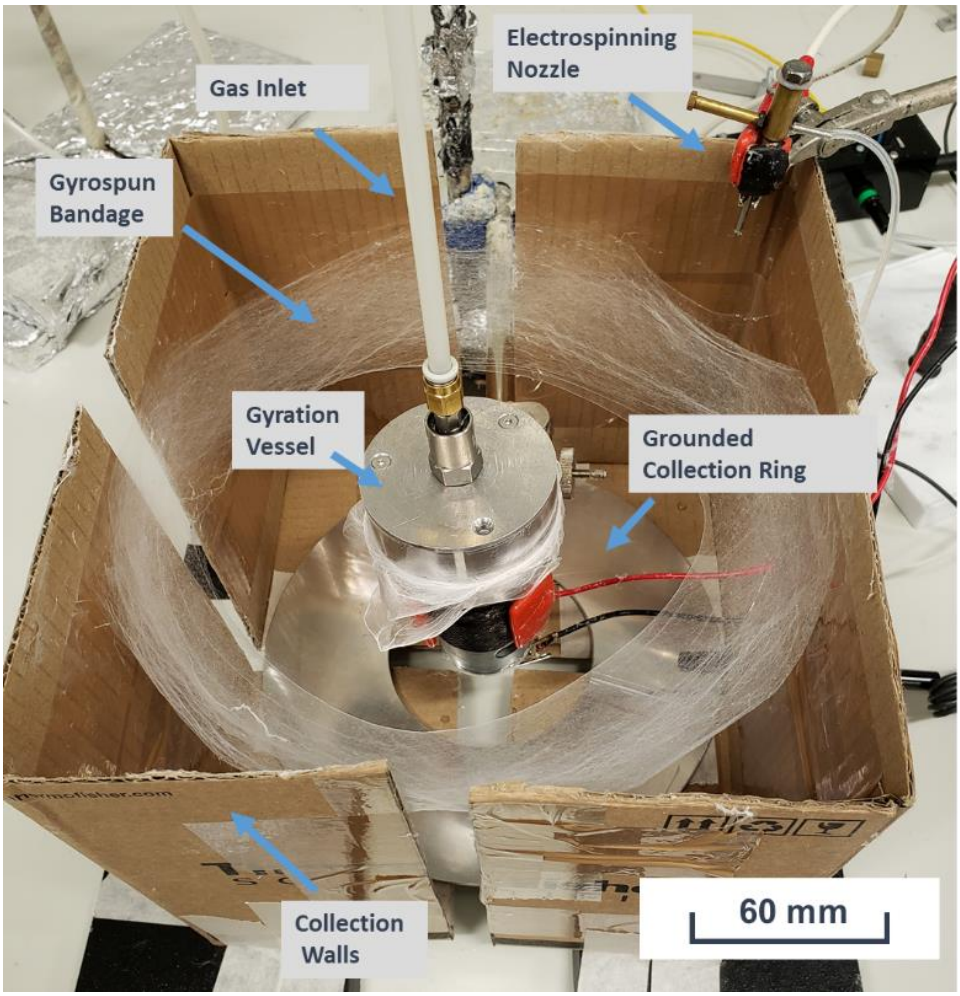

Figure 3.2: Photograph showing the manufacturing route combining electrospinning (top right corner) and pressurised gyration (centre); the collection walls can be seen to aid bandage production and a grounded

collection ring allows the electrospinning needle to focus bioactive material onto a specific target site of the bandage.

3.4.1.2 Production of Bioactive Bandages

From previous work, polycaprolactone has shown to provide a high yield of fibres which could also sustain the wear and tear of bandage environments [397]. Polycaprolactone solution was dissolved in chloroform to form a solution with a concentration of 15% (w/v), the solution was mechanically stirred for 24 hours and kept in ambient conditions to form a homogenous polymer solution. 4 mL of the PCL polymer solution was placed inside the pressurised gyration vessel and spun at 30,000 rpm with a flow pressure of 0.1 MPa for 20 seconds. A collection distance of 120 mm was used, this allowed the fibres to be deposited as a bandage-like ring surrounding the gyration setup.

Collagen and chitosan were both dissolved in 0.5M acetic acid at different ratios and weights. PEO was used to decrease the conductivity of the collagen and chitosan solution and add polymer chain entanglement to ensure that fibres could be formed. Patches of collagen, chitosan and PEO were then deposited directly onto the PCL bandages via electrospinning, a template can be used to ensure uniform deposition and size of the patch. The polymer solution was spun using a voltage of 12.0 kV, an infusion rate of 75 µL/min and at a working distance of 120 mm. The second set of bandages was created with the incorporation of antimicrobial nanoparticles (AMNP). The same method mentioned above was used with the addition of AMNP in the collagen/chitosan solution.

3.4.2 Production of Fibres Using an Updated Vessel Design

3.4.2.1 Updated Vessel Design

Advances in technology are needed to keep pace with the demands and evolving requirements of consumers. Even small adjustments to a manufacturing device can lead to large gains in output performance, especially

when scaled up to great volumes. An updated gyration vessel (**Figure 3.3**) has been re-designed to incorporate curved walls. This updated design takes into consideration the parabolic nature of the polymer solution within the pressurised gyration vessel, normally with straight walls the right angles formed under the parabola of the solution could lead to areas of vortices and introduce turbulence into the vessel. By incorporating curved walls, the time taken for the polymer solution to reach the orifices also reduces, meaning that fibre production can be more efficient. Furthermore, the design of the P1 pot also allows for more volume of gas to be controlled during the pressurised gyration process. Even given the slightly larger dimensions and volume, the updated gyration vessel manages to be more lightweight (35 g) than the original design (53g), thanks to its thinner walls. Having a lower density will positively affect the rotational capability of the gyratory vessel. The P1 design furthermore has a slightly larger volume, owing to the larger dimensions (340mm in height and 660 mm in width, compared to 300mm height and 600mm width of the P0 pot).

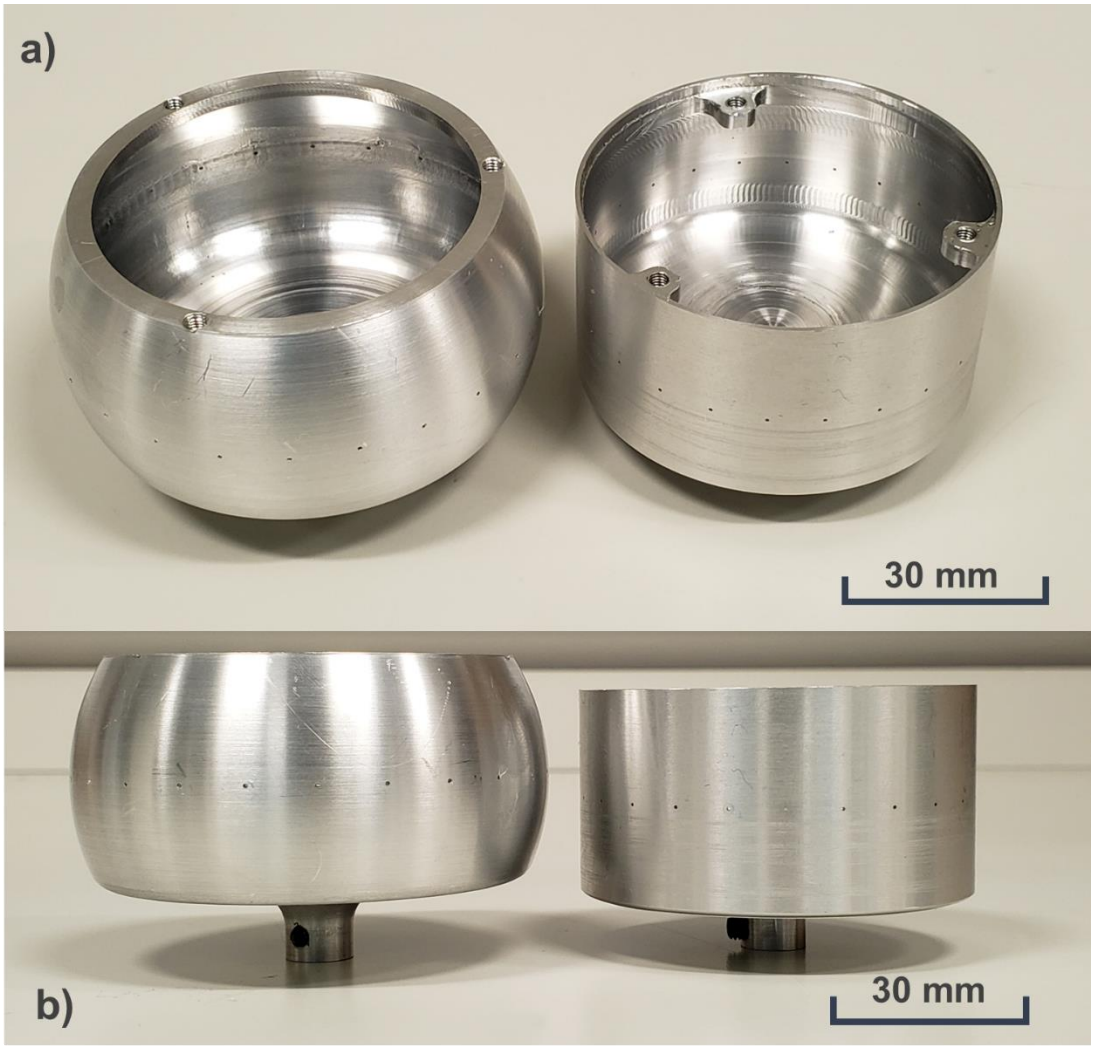

Figure 3.3: Photograph showing a) general view and b) front view of the updated pressurised gyration vessel design (left); the inner and outer walls have been curved as opposed to the standard flat wall of the original (right).

3.4.2.2 Fibre Production

Fibres were produced via the two different designs to compare how changes in pot design could affect fibre morphology. For this testing, three different polymer solutions were spun with the same solvent to eliminate differences based on solvent selection. PCL, PLA and PMMA Poly(methyl methacrylate) (PMMA) (Sigma-Aldrich, UK) were dissolved into Chloroform, CAS: 67-66-3, (Sigma-Aldrich, UK) to make solutions of 15% (w/v) for the PCL and PLA

polymers and 20% (w/v) for PMMA. These solutions were then spun with the original pot (P0) and the updated pot (P1) at no additional pressure and 0.1 MPa of additional pressure to discern how the two pots handled pressure infusion.

3.4.2.3 Comparison and Analysis

SEM micrographs were taken of the fibrous samples and their fibre diameter distribution was calculated. In addition to this, a transparent acrylic pot (of the original design), was used in conjunction with a high-speed camera (Photron, FASTCAM SA1.1, Japan) to capture the solution kinetics of the P0 pot, details of this pot can be found here [398].

3.4.3 Advanced Material selection: Porous Graphene Composite Fibres

3.4.3.1 Materials

PCL pellets, Mw 80,000 (Sigma-Aldrich, UK) were used as the carrier polymer to form graphene-loaded fibres. Chloroform, CAS: 67-66-3, (Sigma-Aldrich, UK) was used to dissolve the pellets to form a homogenous polymer solution. Porous Graphene (PG) was synthesised by following our previously reported methods [399, 400]. Briefly, in the first step, graphene oxide was prepared using a modified Hummers method [401]. Exfoliated graphite oxide flakes (of lateral size ~0.5 - 20 μm and ~1.5 nm thickness) were prepared by oxidising graphite flakes in concentrated H_2SO_4, in the presence of $NaNO_3$, H_2O_2, and $KMnO_4$. Graphite oxide was further exfoliated to form graphene oxide (of size 0.8 - 1 nm). Hydrazine was used as a reducing agent to reduce graphene oxide into reduced graphene oxide (average thickness of 1.5 nm). To obtain PG (average pore size of 3 - 5 nm), the filtered product of reduced graphene oxide was oven-dried in a vacuum overnight. Thermal treatment was then applied at 200ºC in Argon for 12 hours. The surface morphology (using high-resolution transmission electron microscopy), surface area study (using Brunauer-Emmett-Teller-BET theory method), composition and structural analysis (using X-ray photoelectron spectrometer – XPS, X-ray diffraction,

Fourier transform infrared (FT-IR spectroscopy, Raman spectroscopy). PG is especially beneficial in wound healing applications due its enhanced adsorption capacities owing to its microporous and mesoporous interconnected network [399].

3.4.3.2 Preparation of Graphene Polymer Solution

As-prepared PG powder was weighed (3, 4 and 5 wt%) into chloroform where it was suspended, ready for homogenisation. Branson SFX 550 Sonifier (Cole-Parmer, UK) was used to disrupt the graphene platelets within chloroform to form a fine suspension of graphene, the output was set to 65% (~ 325 Watts), and the solution was subjected to ultra-sonication for 6 hours. PCL pellets were then added to the PG suspension following ultrasonication to allow the thorough dissolution of the polymer. The polymer solutions were stirred mechanically for 24 hours at room temperature (20 - 22 °C).

The prepared solutions were subjected to surface tension measurements using a calibrated tensiometer (Tensiometer K9, Kruss GmbH, Germany). In these measurements, the Du Nouy ring method was used to attain the surface tension, a glass vial was filled with polymer solution and a platinum-iridium ring with a diameter of 60 mm was submerged into each polymer solution. The ring was then slightly raised to enable a fluid meniscus to form, the variation in the forces was measured using a force tensiometer which gave the surface tension values. These readings were carried out at ambient temperature (22-24°C) and were repeated five times to find the average surface tension values for each solution and concentration.

The viscosity of the solutions was also measured using a Brookfield Viscometer DV-III (Brookfield, Middleboro, MA, USA). A small-sample spindle was used with a polymer volume of 3 mL. The samples were all taken at the same shear rate of ~ 5 Pa which ensured comparability between the samples. All viscosity measurements were done under ambient conditions (22 ± 2°C) and repeated three times to give an average value.

3.4.3.3 Preparation of Graphene-loaded Fibres

Pressurised gyration was used to form the graphene-loaded fibres. 4 mL of the polymer solutions were placed in the gyration vessel and subjected to a rotation speed of 30,000 rpm at an operating pressure of 0.1 MPa. The production process was carried out at ambient conditions (20-22 °C, 45-55% relative humidity).

3.4.3.4 Characterisation of fibres

Following the production of the fibres, they were collected, placed on aluminium studs and gold sputter-coated for 180 seconds (Q150R ES Quorum Technologies Ltd., Laughton, England). The gold coated samples were then analysed via scanning electron microscopy (SEM) (Hitachi S-3400n) using an operating voltage of 5 kV. The SEM images were used to detect the structure of the composites, 100 fibres were measured at random, and the mean diameter was calculated using Image J software. The frequency distribution of the fibre diameters was modelled using OriginPro software. Raman spectra of samples were measured in backscattering mode at a 532 nm laser excitation and 6 mW power. Samples were placed on glass slides to collect Raman spectral signatures. FTIR spectra were measured using a spectrometer in the wavenumber range of 4000 - 500 cm^{-1} (Bruker Optics Tensor-27 IR, Ettlingen, Germany). The samples were prepared by mixing composites with KBr (of spectroscopic grade) to make pellets of about 2 mm in thickness and 5 mm in diameter. X-ray diffraction (XRD) analysis of composites was measured using Cu Kα radiation (at 40 kV and -40 mA).

Chapter 4 : Investigating the Effect of solution properties and working parameters on polymeric fibre production

4.1 Introduction

For fibres to be formed via pressurised gyration, a polymer solution containing the desired polymer must be formed, the solution characteristics and physical properties play a key role in the end fibre morphology as alluded to in **Chapter 2**. In this chapter, the effect of important solution properties and working parameters of the pressurised gyration setup will be analysed and discussed in the creation of fibres with differing morphologies.

4.2 Effect of Solvent on Fibre Morphology

Each solvent inherently has a differing solubility power due to the differences in functional groups, polarity and hydrogen bonding abilities [402]. It is therefore important to consider the solubility of a polymer within a solvent, as just the solubility alone may considerably change the rheological behaviour of the polymer solution.

4.2.1 Solubility

In order to produce fibres, a critical minimum concentration (c_e) needs to be met [403]. Once the c_e is achieved and exceeded, it is said that an adequate degree of polymer chain entanglement occurs; which is required when the polymer forms a jet at the tip of the orifice and fibres are formed [78, 404]. The value of c_e is not universal and will vary depending on the molecular weight of the polymer and the solvent used, for this reason, the polymer molecular weight and concentration remained constant during testing. Solubility parameters can be used in the selection of a suitable solvent for dissolving a polymer. The Hildebrand solubility parameter (δ) is a numerical model which

estimates the extent of interaction between a solvent and a solute, the closer the values match, the more likely the two materials will be miscible, it is calculated by the taking square root of the cohesive energy density [405]. The delta in the Hildebrand solubility parameter values for the solvents in this work and PCL are shown in (**Table 2**). A solvent that demonstrates a high level of solubility with a selected polymer has a specific balance in its hydrogen bonding, dispersion forces and polar forces [75, 406].

Table 2: Physical properties of the solvents investigated in this work; values have been reported at 25 °C.

Solvent	Boiling Point (°C)	Density (g/cm^3)	Surface Tension ($mN\ m^{-1}$)	Viscosity (mPa S)	Vapor Pressure (KPa)	Difference in Solubility Parameter $(MPa)^{1/2}$ [390]
DMF	152.8	0.95	37.10	0.80	0.35	+ 5.6
THF	66.0	0.89	26.40	0.53	19.34	- 0.6
Toluene	110.6	0.87	28.52	0.56	3.79	- 0.7
DCM	39.6	1.33	26.50	0.42	58.40	+ 1.0
Chloroform	62.1	1.49	26.67	0.79	20.90	- 0.5

The solvents used in this investigation (THF, Toluene, DCM and chloroform) all demonstrated good solubility in forming homogenous polymer solutions of PCL at a concentration of 15% (w/v). However, DMF showed only partial solubility when subjected to the same conditions as the other solvents. The delta in the solubility parameters between PCL and DMF in this testing is the greatest at + 5.6 $MPa^{1/2}$, this large difference indicates that DMF is not the

most suitable solvent for dispersing the PCL polymer chain. However, by heating the DMF-PCL solution to 60°C, the solution displayed complete solubility. Increasing the temperature of a solution increases the kinetic energy of the particles, this leads to an increased frequency of collisions which results in complete dissolution [407].

The lowest difference in solubility parameter between PCL was with chloroform at only - 0.5 $MPa^{1/2}$. Chloroform is one of the most common solvents used to dissolve PCL and is used in the study of many biomedical applications [408]. It was observed that THF, Toluene, DCM and chloroform all manage to dissolve the polymer quickly and efficiently as expected from their low deviation in solubility parameter which were all equal to or less than 1.0 $MPa^{1/2}$.

The dissolution of a low molecular weight solute such as sucrose can occur almost immediately when placed in a compatible solvent such as water. This is a commonly known phenomenon; the sugar molecules leave their crystal lattice and disperse in the water to form a solution. However, the dissolution process of polymers is much more complex as these molecules typically consist of long chains with many segments that from tightly folded coils, these coils can even be entangled between each other [409]. These coils are held together by many intra- and intermolecular cohesive and attractive forces such as dipole-dipole interactions, inductions, dispersive forces, hydrogen bonding and van der Waals forces [410, 411]. The dissolution of polymers can thus be said to occur in two main steps, firstly the swelling and then dissolution [412]. When a polymer is submerged into a solvent, dispersion and attraction forces act between the segments and are dependent on their chemical characteristics, polarity and even their solubility parameters. When the polymer-solvent interactions exceed the polymer-polymer interactions, the chain segments begin to absorb solvent molecules which increases the volume of the polymer matrix and loosens the coil. The segments are then said to be in a solvated state instead of an aggregated solid state. The unfolding and swelling process can occupy a long time period and is not influenced by mechanical stirring or temperature increases. The polymer dissolution process is summarised in (**Figure 4.1**).

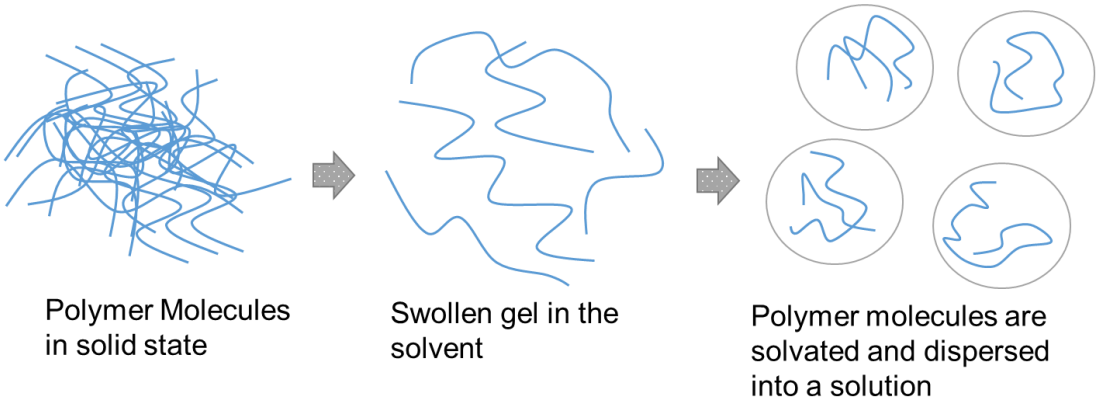

Figure 4.1: Schematic diagram of the polymer dissolution process.

The solubilising power of the selected solvents are expected to alter the physical properties of the polymer solutions and will be analysed in the next section. The difference in dissolution due to the choice of solvent can create molecular differences in the polymer solution which become apparent when measuring the physical properties of the polymer solution.

4.2.2 Physical and Rheological Properties Influenced by Solvent

As chloroform is the most widely used solvent for PCL and because it had the lowest difference in solubility parameter, this will be the base solvent for comparisons between the difference in physical properties between the different solvents. At a concentration of 15% (w/v), the chloroform solution had a surface tension of 30.3 ± 0.7 mN m^{-1} and a viscosity of 2383 ± 34 mPa.S. The choice of solvent can affect both these properties which in turn influences the behaviour of the polymer jet and fibre production [89]. All the solutions used in this study had high relative viscosities, viscosity affects the movement of the polymer solution within the pressurised gyration vessel as it responds to two predominant opposing forces; normal stress and shear stress [398]. The measured surface tension and viscosity values for the different polymer solutions are given in (**Table 3**).

Table 3: Physical properties of the PCL solutions with different solvents used in the study, values have been reported at 25 °C and a constant sheer rate of 3 mPa.s was used.

Solvent Used	Surface Tension ($mN\ m^{-1}$)	Viscosity (mPa S)
DMF	34.3 ± 0.5	2523 ± 35
THF	25.3 ± 0.4	1887 ± 26
Toluene	32.3 ± 0.6	3465 ± 39
DCM	29.7 ± 0.4	1553 ± 38
Chloroform	30.3 ± 0.7	2383 ± 34

Of all the solvents used, DMF has the highest surface tension at 37.1 $mN\ m^{-1}$, this results in the respective polymer solution also having the highest surface tension value at 34.3 ± 0.5 $mN\ m^{-1}$. We can see that the surface tension of a polymer solution is governed by the surface tension of the solvent. The surface tension of the polymer solutions is lower than that of the solvent because of the energetic adsorption of polymers close to the surface [413]. In considering the flat surface of a polymer solution, at the surface, the micro-Brownian motion is restricted and entropy is decreased, if there are no other energetic interactions with the surface, the concentration near it decreases which leads to an increased surface tension [413]. Brownian motion is described as the random motion of particles in a liquid that results in constant collisions [414]. We also see that THF has the lowest surface tension value, and the resulting polymer solution also has the lowest surface tension. Differences in surface tension of the polymer solutions are likely to lead to a difference in fibre morphology [415].

The viscosities of the different polymer solutions did vary significantly when using different solvents, even whilst using the same concentration and mass of polymer in preparing them. When a polymer concentration is increased, there is greater polymer chain entanglement and this increases its viscosity [416]. This suggests that solvents may undergo different dissolution paths based on their solubilising powers and solvent-polymer interactions which will

lead to changes in the polymer chain entanglement. Solutions with higher viscosities are expected to produce fibres with larger diameters when spun under identical conditions.

4.2.3 Effect of Solvent on the Morphology of the fibres

Initially, the five solvent-polymer systems were spun with the pressurised gyration setup with no external gas pressure, just operating as centrifugal spinning. The resulting fibres were analysed for their morphologies owing to differences purely in the use of solvent, the scanning electron micrographs are presented in (**Figure 4.2**). Fibres spun with DMF, shown in (**Figure 4.2 a**) showcase a highly beaded form, interconnected by very fine fibres. The bead sizes range from 20 - 240 µm and are highly polydisperse in their size distribution. Here is an extreme example of the bead-on-string morphology which according to literature, can be attributable to viscoelasticity and surface tension of the polymer solution [417]. Of all the solvents, DMF had the highest surface tension which could explain its beaded nature. As all the solutions were spun at the same rotational speed, they would have the same centrifugal force acting upon them and thus a higher surface tension would hinder fibre formation and possibly give rise to a bead-on-string morphology. This notion is also supported when we look at the product of the solvent having the second-highest surface tension reading, Toluene, shown in (**Figure 4.2 g**)**.** It is seen by the macroscopic view that the dominant structures are the beads. The beads formed by the Toluene-dissolved-PCL ranged in sizes between 10 - 160 µm, polydisperse to a lesser extent than those of the DMF fibres. The toluene solution had a significantly higher viscosity of 3465 mPa S compared to that of DMF at 2523 mPa S, this higher viscosity could aid in reducing the disparity of the beads as it counteracts the high surface tension during spinning.

DCM and chloroform, shown by (**Figure 4.2 j**) and **m)**) both have very similar surface tension values and thus produce similar morphologies when spun. Beads are present in the macroscopic views but are not high in numbers as with DMF and Toluene. For these solvents, the product morphology is mostly

fibrous, which are also unidirectionally aligned overall. The alignment is due to the rotation of the gyration pot and how the fibres are collected [16]. The fibres formed from the THF, having the lowest surface tension, are completely devoid of beads as can be seen in (**Figure 4.2 d**). The results presented here strongly point towards surface tension as having a dominant effect on the formation of beads during spinning as THF had the lowest surface tension of all the polymer solutions.

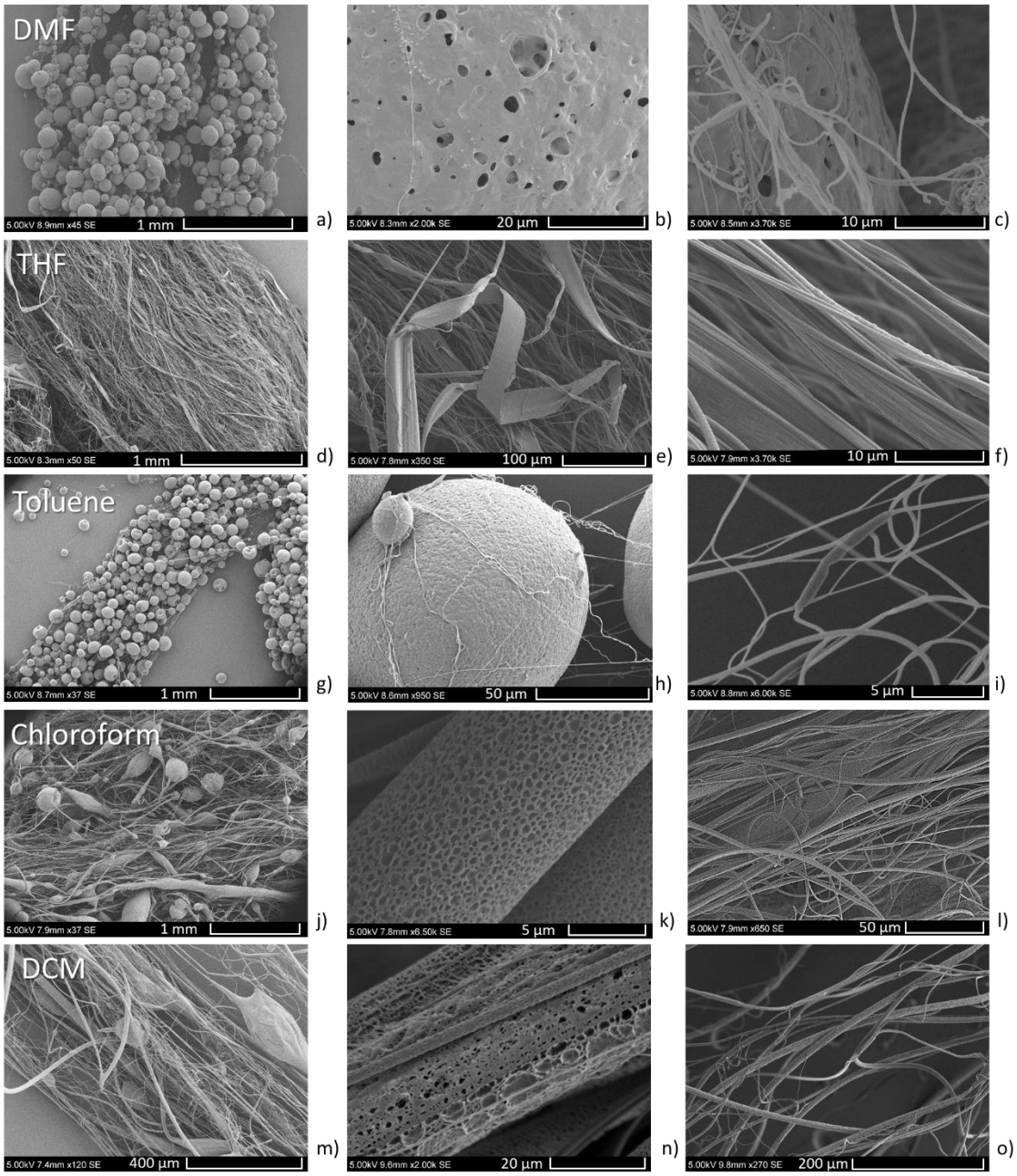

Figure 4.2: Scanning electron micrograph images of PCL fibres in different solvents. Constituting of a macroscopic view of; a) DMF, d) THF, g) Toluene, j) DCM, m) Chloroform, a surface view of; b) DMF, e) THF, h) Toluene, k) DCM, n) Chloroform and the close-up fibre view of; c) DMF, f) THF, i) Toluene, l) DCM, o) Chloroform.

High magnification images showing the surface of the produced fibres can be seen in (**Figure 4.2 b, e), h), k)** and **n)**). Surface pores are readily found in polymeric structures following the use of highly volatile solvents which cause condensation as they evaporate, these droplets then form dimples as they too evaporate at a later stage [121]. DCM and Chloroform (**Figure 4.2 k** and **n**) have the highest boiling points and thus are the most volatile, and from the surface of the fibres, we can see the resulting pores. In the DCM system, the pore sizes range from 40 to 840 nm whereas, in the Chloroform system, the range is between 0.1 to 2.1 µm. The difference in the pore range between the two solvents is likely due to the size of the condensation droplets which is formed from the evaporation. These pores can be useful in biomedical applications where their small size can inhibit cell growth in three-dimensional scaffolds [418]. Furthermore, surface pores increase the available surface area to volume ratio of the fibres which is beneficial in a multitude of applications such as drug delivery, filtration and tissue engineering [4, 5, 122, 419].

Looking closer at the morphology of the Toluene fibres shown in (**Figure 4.2 h**), it is noticed that the surface is free from porosity, instead, we can see that there is a slightly rough topography with small dimple-like indentations covering the bed of the beads. Having low volatility, surface nanopores are not expected to form here. However, when observing the surface of beads formed by DMF (**Figure 4.2 b**), we can observe craters and pores which penetrate deeper than the surface. DMF has the highest boiling point of all the solvents tested the formation of its pores is unlikely attributable to condensation droplets formed by rapid evaporation. Instead, the observed pores could be the result in the solubility parameter difference which is largest in the DMF system with a difference of 5.6 $MPa^{1/2}$ [420].

Fibres produced from THF, which is a relatively volatile solvent, resulted in very small diameter fibres which appear to not possess a porous morphology as can be seen in (**Figure 4.2 f**)**.** It is possible however that with higher magnification, pores may start to be visible. Nonetheless, the morphology observed in (**Figure 4.2 e**) resembles a flat ribbon-like structure, which is not found with the use any of the other solvents tested. Ribbon-like fibres have

been known to be produced in special cases with electrospinning [32, 421, 422]. The ribbon-like polymeric structure is likely due to a non-axisymmetric change in the shape of transverse sections of the polymer jet, due to an irregularity in rotation, whilst the rapid evaporation of the solution allowed it to retain this form after drying [423].

Upon closer magnification, we can focus on fibrous areas which were present in all the samples (**Figure 4.2 c, f, i, l** and **o**). (**Figure 4.2 c** and **i**) show unaligned fibres formed by DMF and Toluene, the least volatile solvents. The slow-drying nature of these solvents could be responsible for the lack of unidirectional alignment that the pressurised gyration system usually affords [204]. As the polymer jet travels through the air, it is stretched by the motion of an emerging droplet, slower evaporation leads to a greater distance being covered by the jet. As the jet becomes thinner, the forces acting on the droplet become greater and the top of the jet becomes more unstable, causing the random alignment. The fibre alignment can be quantified using OrientationJ computer software. Highly volatile solvents generally show an overall unidirectional alignment (**Figure 4.3 a**), whilst less volatile solvents often show more random orientations (**Figure 4.3 b**)**.** Fibres produced from THF, DCM and Chloroform (**Figure 4.2 f, l** and **o**) all demonstrated aligned morphologies which can be credit to the fast-drying nature of the solvents and the unidirectional rotation of the pressurised gyration vessel.

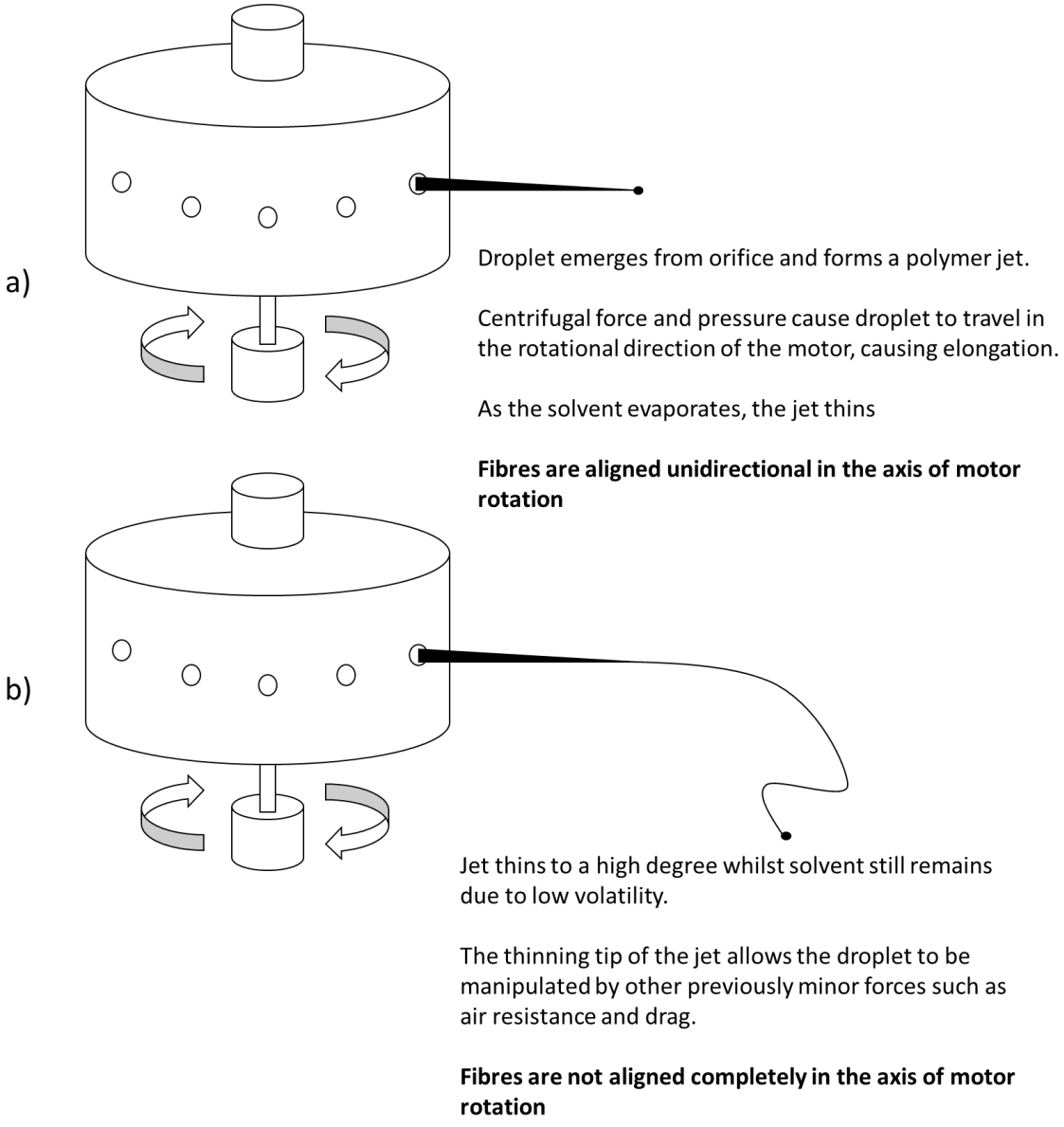

Figure 4.3: Diagrammatic representation of the polymer jet under pressurised gyration when using a) a volatile solvent, b) a less volatile solvent. Differences in the solvent systems used in spinning fibres give rise to changes in fibre morphology which can be beneficial for different applications.

4.3 Effect of Gas Pressure on Fibre Morphology

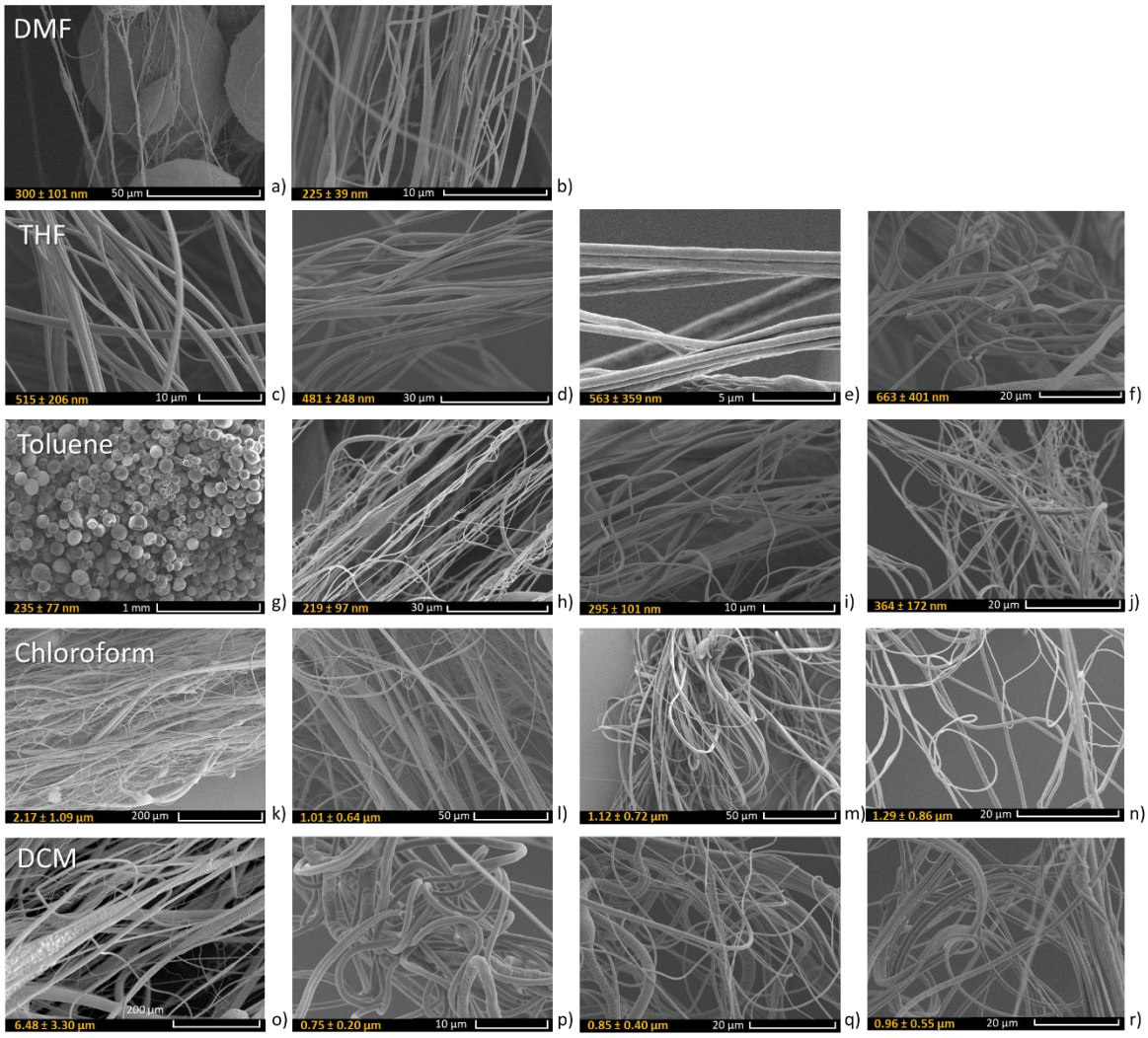

Figure 4.4: Scanning electron micrograph images of PCL fibres in different solvents; a), b) DMF 0 MPa and 0.1 MPa pressure, c) - f) THF 0 MPa to 0.3 MPa pressure, g) -f) Toluene 0 MPa to 0.3 MPa pressure, k) - n) DCM 0 MPa to 0.3 MPa pressure and o) - r) Chloroform 0 MPa to 0.3 MPa pressure. For all instances, n = 100.

The five solvent-polymer systems were then subjected to spinning under a range of gas pressures from 0.0 to 0.3 MPa, they are summarised in (**Figure 4.5**) and their average fibre diameters are shown. DMF systems did not show the presence of fibres after the application of 0.1 MPa pressure. With the lack of pressure, DMF fibres had an average diameter of 300 ± 101 nm (**Figure 4.4 a**), at 0.1 MPa, the fibres thinned significantly to 225 ± 39 nm (**Figure 4.4 b**).

The reduction in fibre diameter is the result of the external gas pressure working in tandem with the centrifugal force to extrude the polymer solution out of the orifices with greater energy, this energy overcomes the surface tension of the polymer and causes additional thinning of the jet [424]. The resulting gas pressure also has two effects, causes alignment and reduces the bead-on-string morphology of the fibres in the DMF systems. As discussed, due to the low volatility of DMF, the emerging droplet from the gyration orifices thins until the initial exit energy is lost and air resistance causes random alignment. The addition of pressure allows for a higher exit velocity of the jet and thus more energy is conserved until evaporation is complete. Additionally, pressure can cause a reduction in solvent volatility which causes faster drying of the jet, this can aid in maintaining the extruded form of the polymer, causing more uniform fibres to be formed, as seen with DMF fibres spun at 0.1 MPa [425]. Bead-on-string morphology is thought to be caused by axisymmetric instabilities in the production process, the application of gas is likely to have counteracted these instabilities to produce fewer beads [426].

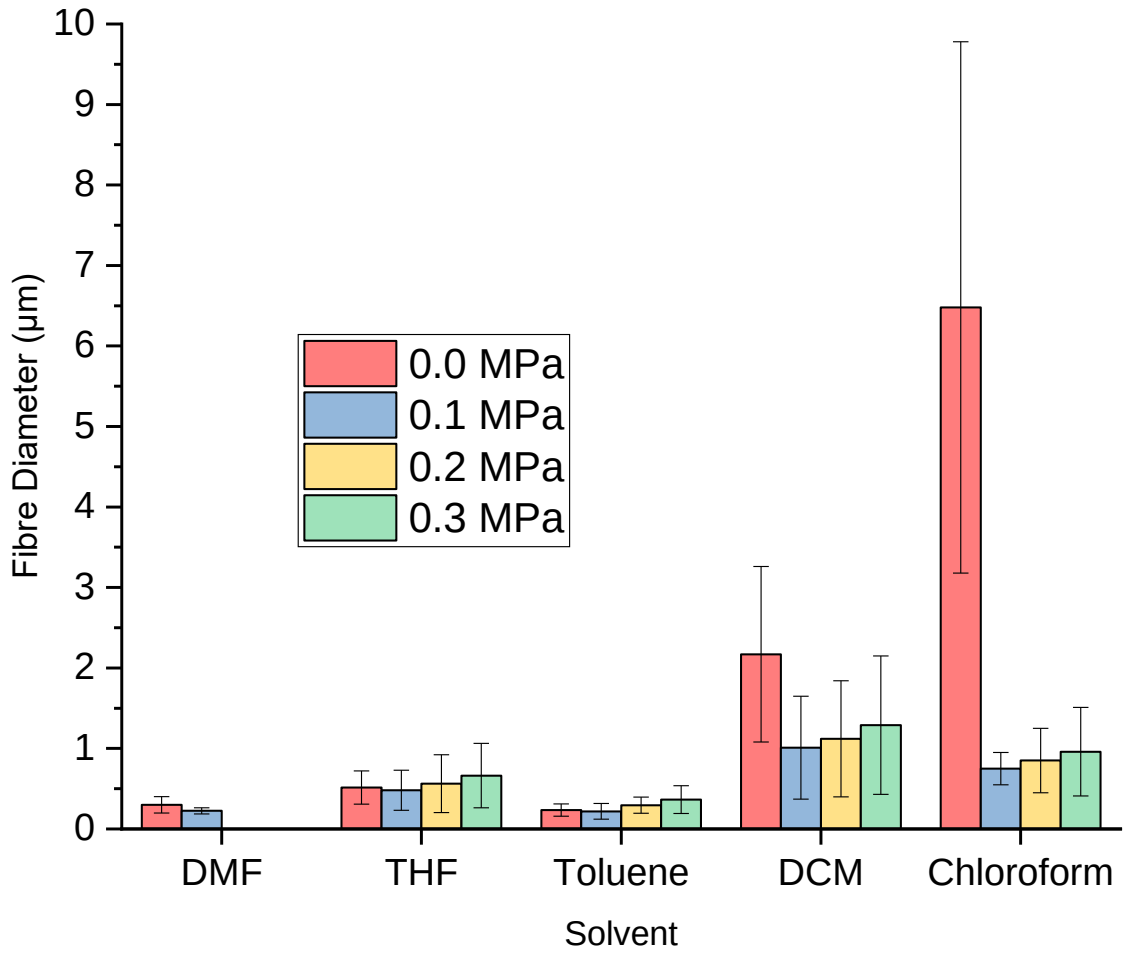

Figure 4.5: Graph showing the overview and relationship between increasing gas pressure and the resulting fibre diameters, for each case n = 100.

THF fibres had an average diameter of 515 ± 206 nm when spun at zero additional pressure (**Figure 4.4 c**), at 0.1 MPa of applied pressure, the fibres thinned to 481 ± 248 nm (**Figure 4.4 d**). However, beyond 0.1 MPa, the fibres began to become coarser and less uniform. This could be explained by the high pressure in the small volume of the vessel causing instabilities in the jet. With volatile solvents such as THF, the pressure can cause rapid and sporadic evaporation which leads to thicker, less uniform fibres.

With Chloroform and DCM, similar trends are observed. Increasing the gas pressure from 0 to 0.1 MPa causes a significant reduction in average diameter, however, further increases cause thicker fibres to be formed. Both solvents form aligned fibres without external gas pressure, the addition of gas causes

fibres to be less aligned, due to the volatile nature of the solvents and the evaporation behaviour. Toluene fibres (**Figure 4.4 g** - **j**), show a highly beaded morphology with no additional pressure, the pressure causes the beaded morphology to disappear.

Solvent and pressure thus have a marked effect on fibre diameter distribution. (**Figure 4.5**) summarises the effect of solvent and pressure on the diameters of the investigated fibres. Firstly, it can be noticed that the role of the solvent has a deterministic effect on the resulting fibre diameters. Chloroform produced the thickest fibres whilst Toluene produced the thinnest fibres, at no added pressure, the difference in diameter is over 25 times. The physical properties of the solvents differ considerably, and this data is shown in **Table 2**. For instance, the volatility of the solvents is vastly different with DCM being the most volatile with a boiling point of 39.6 °C and DMF being the least volatile with a boiling point of 152.8 °C. DMF therefore produces thinner fibres due to two main reasons: the low volatility and large difference in solubility parameter between it and the polymer. A solvent with low volatility results in reduced evaporation during the jet thinning process, leading to greater elongation and thinner deposited fibres [427]. Additionally, the large difference in solubility parameter indicates a lower level of polymer chain entanglement during dissolution, which leads to thinner fibres being produced [78].

The data doesn't seem to suggest that in this case, there is a link between the vapor pressure and the diameter of the fibres. However, the thinnest fibres were produced from the solvents with the lowest vapor pressure, namely DMF and Toluene which all had a vapor pressure of 0.35 and 3.79 KPa respectively. In this study using the same polymer, there isn't a direct indication that surface tension and viscosity played major roles in the diameter of the produced fibres. This is likely due to the fact that when using differing solvents, the degree of polymer chain entanglements plays a more substantial role in the fibre diameter than its physical properties. There does not seem to be a strict correlation between the average fibre diameters achieved and the viscosity and surface tension of the solutions. Typically, we see that with the same polymer and solvent, the increase in concentration leads to an increase in viscosity, this results in thicker fibres being deposited. The viscosity of the

solvents differed very slightly and therefore had little effect on the final solution viscosity. The surface tension of the solutions does differ based on the solvent used, but a lower surface tension does not seem to lead to lower fibre diameters, as evidenced by DCM and Chloroform, which attained the thickest overall fibres.

Furthermore, adding pressure inside the gyration vessel caused the fibre diameters to decrease with each solvent system at 0.1 MPa. Pressure is thus a viable processing parameter that yields smaller diameter fibres compared to using no pressure at all. However, at pressures beyond 0.1 MPa, the fibre diameter increases again in all the systems, likely due to the instabilities it causes on the polymer jet. This trend is observed with all the four solvents that could be spun at the entire pressure range. Overall, it was found that highly volatile solvents such as Chloroform and DCM produced the larger diameter fibres and that the less volatile solvents were able to form much thinner fibres, this was also true at the differing levels of applied gas pressure too.

Having used the same polymer and concentration for all fibres in this study, physical properties such as surface tension and viscosity was not found to have a link to the final fibre diameter. Toluene fibres produced the thinnest fibres, but the solution also has the highest viscosity. A higher viscosity can be an indication of greater polymer chain entanglement [428, 429]. DMF fibres had the highest surface tension but did not produce the largest diameter fibres.

4.4 Effect of Binary and Ternary Polymer Blends on Fibre Production

4.4.1 Production Yield

In this phase of the study, the blending behaviour between three polymers PLA, PCL and BC was investigated for fibre morphology and production yield with the pressurised gyration technology. Having investigated PCL fibres thoroughly in the previous phase, the incorporation of a polymer blend should yield differing morphologies. Both PCL and PLA dissolve completely in chloroform [430]. However, BC was additionally subjected to sonication in a

small volume of DMF in order to increase its solubility within the solution. The addition of DMF can lead to small differences in the final fibre morphology as DMF has a lower solvent volatility which contributes to elongated jet thinning, this could result in thinner fibres being observed. (**Figure 4.6**) shows the trend in production yield of the different binary polymer blends.

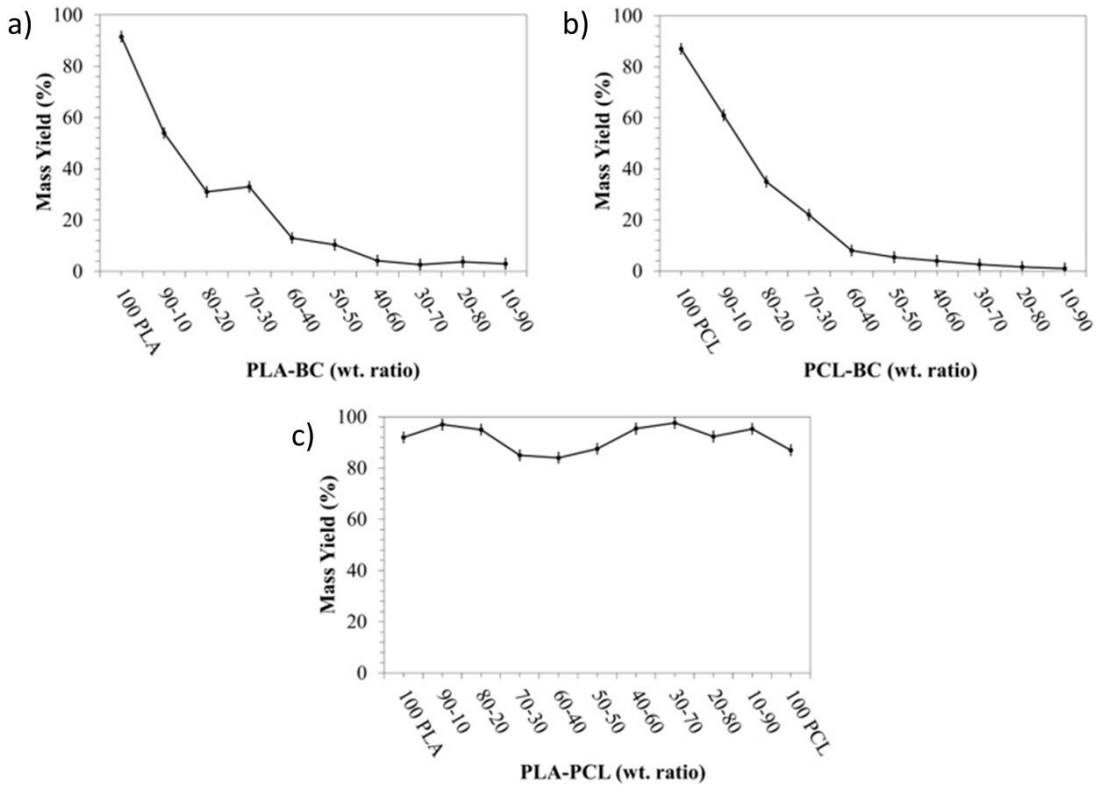

Figure 4.6: Percentage yield values for binary systems showing a) PLA-BC b) PCL-BC and c) PLA-PCL bandage-like fibrous samples, differences in yield are a direct result of changing the binary composition of the polymer system.

The percentage yield results for the PLA-BC binary samples are given in (**Figure 4.6**). For PLA alone, the yield is maximal at 91.5 ± 1.2%. Incorporating even just 10% of BC to a ratio of 90:10 PLA-BC sees a steep decrease of yield to 54.0 ± 1.4 %. This number only decreases further to 33.0 ± 1.4 % for the 70:30 PLA-BC sample before falling to 3.0 ± 0.4% for the 10:90 PLA-BC sample. A yield of 87.0 ± 1.4 % was obtained for the 100% PCL sample after which there is an observed drop to 61.0 ± 1.2% for the 90:10 PCL-BC sample

(**Figure 4.6 b**). There is a reduction of yield down to 22.0 ± 1.4 % for the 70:30 PCL-BC ratio sample before dropping to 1.0 ± 0.4% for the 10:90 PCL-BC sample. Forming PCL and PLA into a binary composite shows appreciable results. At the starting point of 90:10 PLA-PCL, there was a high production yield of 97.0 ± 1.5%, suggesting that the two polymers were highly compatible in a blend. The yield did then subsequently decrease to 84.0 ± 1.9% at 60:40 PLA-PCL. The rise in yield was observed for the 50:50 PLA-PCL composite at 87.5 ± 1.8 % and then a peak at 97.6 ± 0.8 % for the 30:70 PLA-PCL. The results shown here shows that PCL and PLA can be blended to improve fibre production yield which results from the interaction of the polymer group chains.

The production yield decreases drastically as BC is introduced to the two polymers. It is assumed to be due to the change in polymer chain interaction, collisions in its matrix and change in the physical properties of the polymer solution. A BC concentration of 30 wt. % was selected as the optimal blend with the PLA-PCL binary system since otherwise, a significant drop in production yield would be observed. In producing viable bandages, production yields can affect the end pricing. Furthermore, the bandage-like shape can be compromised at higher concentrations of BC, as the yield decreases. The 30:70 PLA-PCL samples were chosen as the most optimal binary polymer system and were then investigated with BC to produce the best (PLA-PCL)-BC ternary in terms of yield and mechanical integrity. The addition of BC at any concentration causes a reduction in percentage yield which could be from the use of DMF as a partial solvent to increase BC solubility.

4.4.2 Morphology

The produced fibre mats comprising of the binary systems (PLA-BC, PCL-BC and PLA-PCL) were characterised using SEM. (**Figure 4.7**) shows the micrographs of the PLA-BC fibrous samples. At the lowest BC concentration of 90:10 PLA:BC, fibres were observed with a low bead frequency and were not uniaxially aligned. With increases in BC concentration, there was a higher instance of beaded fibres, distinguished by demonstrating a bead-on-string

morphology.

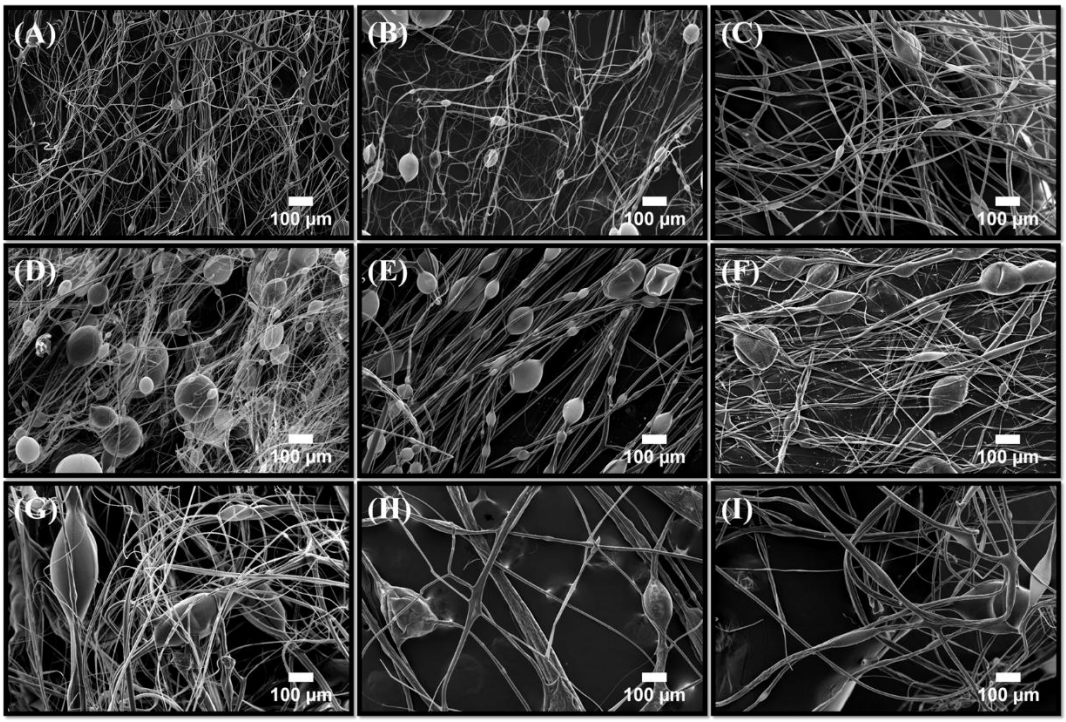

Figure 4.7: Scanning electron micrograph images of the PLA-BC binary fibres, showing; a) 90:10 PLA-BC, b) 80:20 PLA-BC, c) 70:30 PLA-BC, d) 60: 40 PLA-BC, e) 50:50 PLA-BC, f) 40:60 PLA-BC, g) 30:70 PLA-BC, h) 20:80 PLA-BC and i) 10:90 PLA-BC.

Similar outcomes were also observed with PCL-BC where its corresponding micrographs are given in (

Figure *4.8*), which shows the micrographs of PCL-BC fibres from a starting ratio of 90:10 to 10:90 PCL:BC. Fibres without a uniaxial alignment and infrequent bead occurrence were detected at the highest PCL mix. By gradually increasing the amount of BC in the polymer system, the bead density in the fibres increased. Previous studies have also corroborated this by reporting that increases in BC content lead to an increased frequency of beads and the addition of BC in other polymeric mixes, resulting in comparable conclusions, but high BC loadings of 30% have not yet been achieved [33, 431, 432]. When the production yield was low, the fibre density also reduced, indicating that the beaded nature of the fibres could have influenced a reduction in yield. Comparing the microstructures of the different polymer blends, we can see that the fibre diameter increases with BC content, likely

due to the higher viscosity of the polymer solution. The surface appears to be absent of surface roughness and does not possess grooves, pits or nanopores. This smoothness is not necessarily a feature of the fibres, as surface indentations could be beneficial in wound healing scenarios.

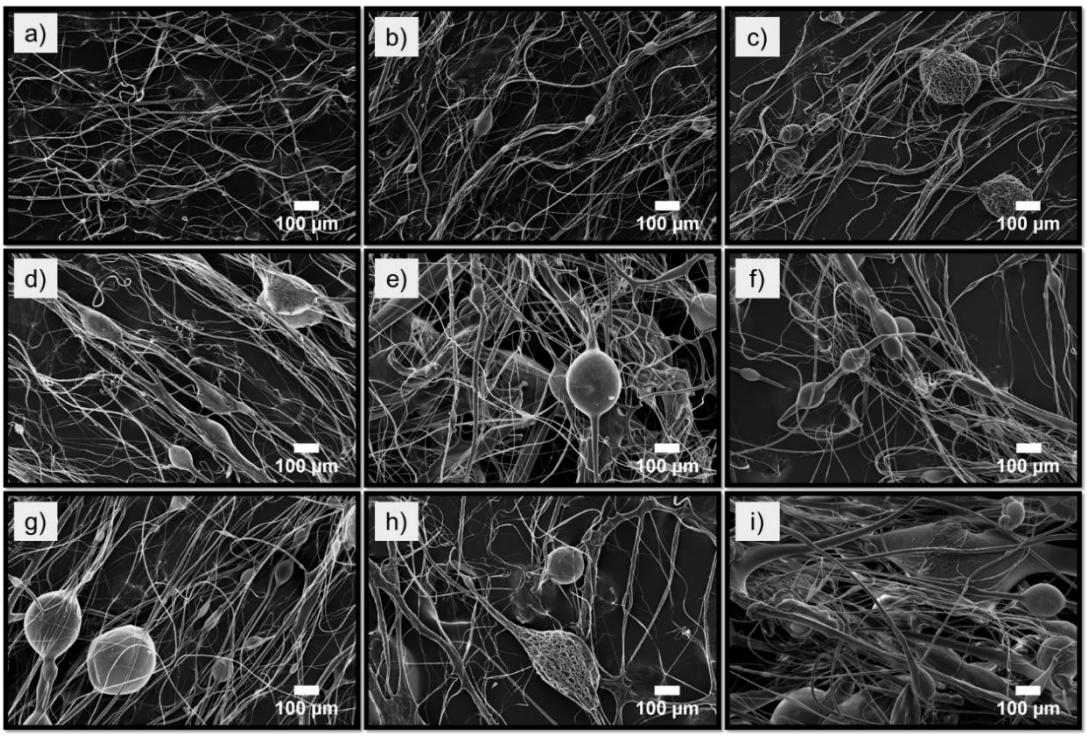

Figure 4.8: Scanning electron micrograph images of the PCL-BC binary fibre, showing: a) 90:10 PCL-BC, b) 80:20 PCL-BC, c) 70:30 PCL-BC, d) 60:40 PCL-BC, e) 50:50 PCL-BC, f) 40:60 PCL-BC, g) 30:70 PCL-BC, h) 20:80 and i) 10:90 PCL-BC.

The morphological analysis of the PLA-PCL binary systems is shown in (**Figure 4.9**). The results indicate that bead frequency increased with increases in the PCL concentration. This phenomenon has already been established in other PLA-PCL composite structures; PCL presence amplifies the beaded frequency when forming a fibre matrix with other blended polymers. Previous studies have also confirmed the same interactions between PLA and PCL, and have thus reported comparable bead forming mechanisms when constituent polymer concentrations are varied [433].

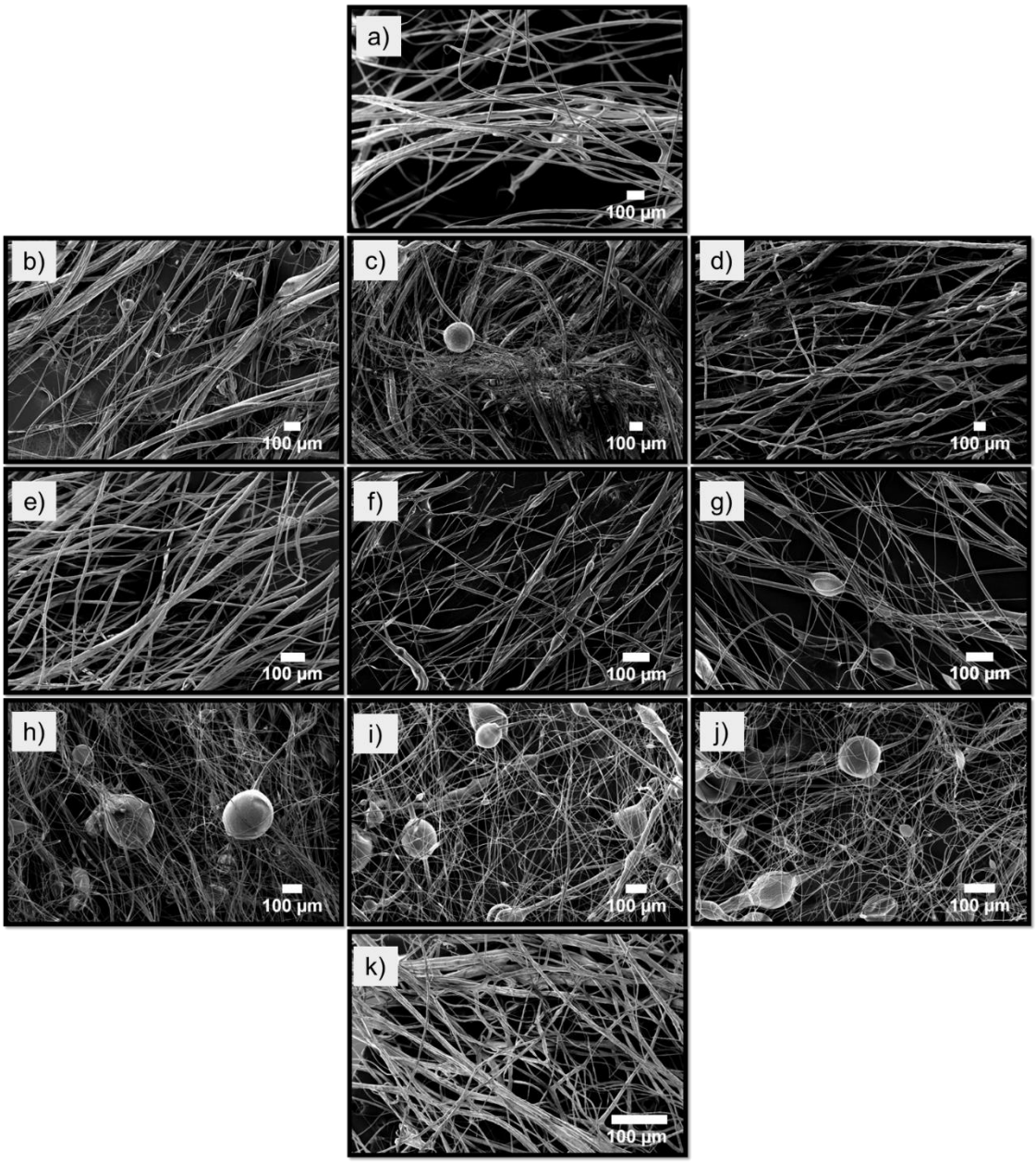

Figure 4.9: Scanning electron micrograph images of the PLA-PCL fibres produced with: a) 100:0 PLA-PCL, b) 90:10 PLA-PCL, c) 80:20 PLA-PCL, d) 70:30 PLA-PCL, e) 60:40 PLA-PCL, f) 50:50 PLA-PCL, g) 40:60 PLA-PCL, h) 30:70 PLA-PCL, i) 20:80 PLA-PCL, j) 10:90 PLA-PCL and k) 0:100 PLA-PCL.

(**Figure 4.10**) shows the average fibre diameter values for the composite polymer systems (PLA-BC, PCL-BC, and PLA-PCL) and their corresponding average fibre diameters, it also shows the average diameter of the optimised

ternary samples containing BC (70:30 (PLA-PCL)-BC). Diameters of 100% PLA and 100% PCL had an average thickness of 18 µm and 5 µm, respectively whilst the binary combinations fluctuated, ranging from 5.0 µm to 18.5 µm.

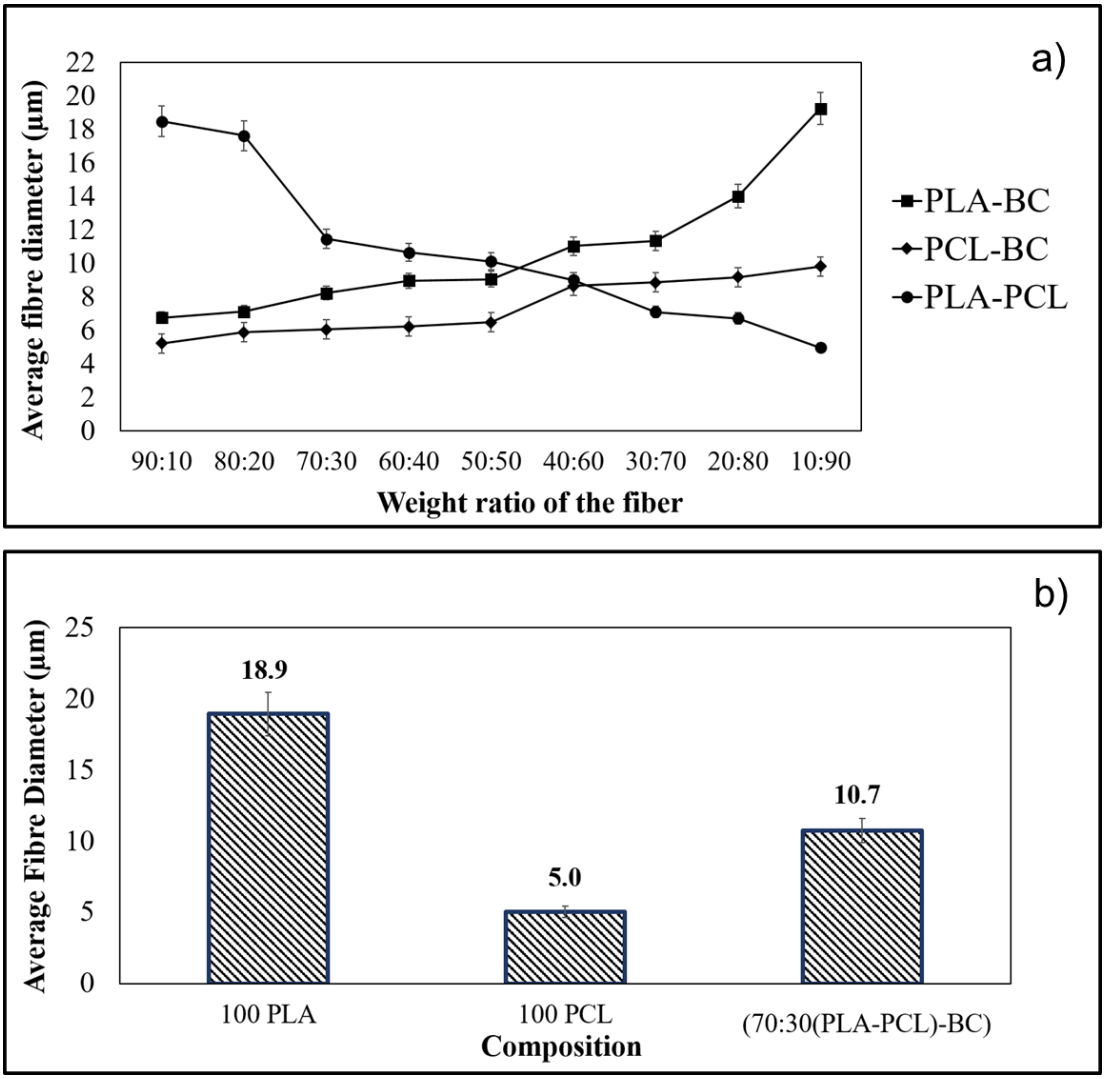

Figure 4.10: Graphical representation of the average fibre diameters for each material combination used: a) binary systems of (PLA-BC, PCL-BC, and PLA-PCL), b) Virgin PLA, PCL and optimised ternary composite (70:30 (PLA-PCL)-BC).

In this study, the fibre diameters of the PLA-BC composite fibres varied between 6 µm and 19 µm. The diameters of the PCL-BC binary fibres varied between 5 and 9 µm. Fibre diameters for each binary group and the ternary product (70:30 (PLA-PCL)-BC) increased with elevated levels of BC. This increase can be ascribed to the differences in the physical properties of the polymer solution such as in its viscosity, surface tension and polymer weights,

as all other environmental parameters were kept constant. When the viscosity and surface tension of the solutions are higher, fibre diameters are comparatively higher in samples containing BC [33]. The addition of BC within the polymer system results in an increase in the viscosity and a slight increase in the surface tension (**Table 4**), this change in physical properties caused thicker fibres whenever the BC proportion was increased. It is well established that a higher viscosity and surface tension of a solution has important effects on the production of thicker fibres [34]. PLA had a higher measured viscosity than PCL and as such, has a larger influence in producing thicker fibres when the PLA ratio was higher. Other studies using centrifugal spinning reported similar findings in terms of the fibre diameters and ratio of PLA and PCL [87, 434, 435].

Table 4: Solution properties of the binary systems and the ternary samples investigated in this study.

Solution ratio (wt. ratio)	**PLA-BC**		**PCL-BC**		**PLA-PCL**	
	Viscosity (Pa S)	**Surface Tension (mN m^{-1})**	**Viscosity (Pa S)**	**Surface Tension (mN m^{-1})**	**Viscosity (Pa S)**	**Surface Tension (mN m^{-1})**
100:0	363±1	52.8±0.1	258±1	38.4±0.1	363±1	52.8±0.1
90:10	368±2	53.9±0.1	269±2	39.2±0.2	358±1	51.3±0.2
80:20	375±2	55.2±0.2	288±3	41.4±0.3	351±2	50.8±0.2
70:30	403±1	57.2±0.3	301±1	43.3±0.1	346±1	49.5±0.1
60:40	445±01	59.5±0.3	342±1	46.4±0.1	331±2	48.2±0.2
50:50	462±2	60.1±0.2	371±2	48.8±0.2	321±2	47.1±0.1
40:60	481±1	61.5±0.3	432±2	51.3±0.3	314±1	44.2±0.1
30:70	503±1	63.3±0.1	476±3	54.2±0.3	301±3	43.8±0.1
20:80	521±2	65.5±0.2	525±3	57.6±0.4	295±2	41.4±0.2
10:90	544±3	67.2±0.1	573±2	59.4±0.1	284±2	39.2±0.2
0:100	N/A	N/A	N/A	N/A	258±1	38.4±0.1

4.4.3 Mechanical Properties

Mechanical strength is a crucial consideration for a suitable wound dressing. The dressings must be able to project the wound mechanically but also allow freedom of natural movement [436]. Tensile testing was carried out for the binary systems and the optimised ternary to determine the effect of polymer concentration and BC composition on its resulting mechanical properties. The ultimate tensile strength and Young's modulus values of each binary system and the ternary systems are displayed in (**Figure 4.11**).

a)

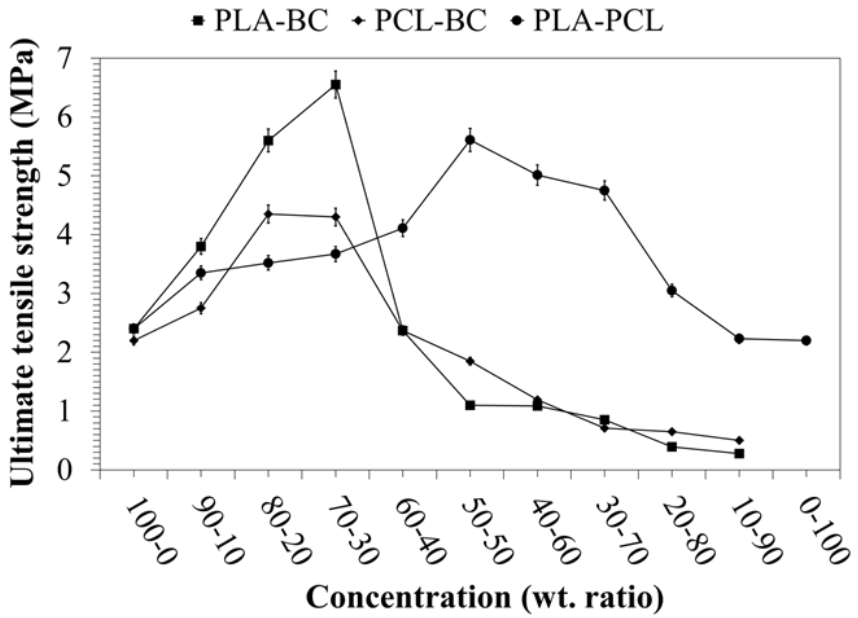

b)

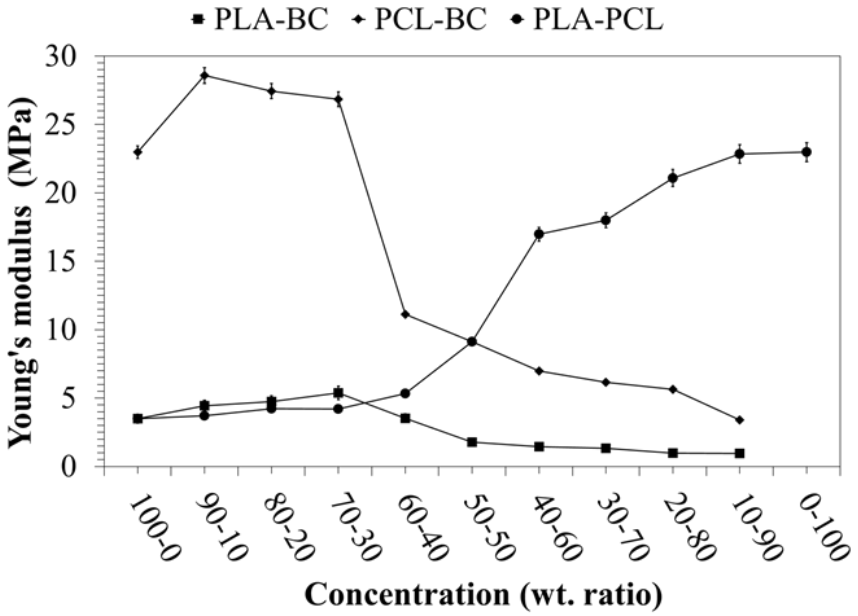

c)

Sample name	Ultimate tensile strength (MPa)	Young's modulus (MPa)
70:30 (PLA-PCL)-BC	9.05 ± 0.04	19.61 ± 0.10

Figure 4.11: Tensile strength values of samples: a) Ultimate tensile strength of the binary systems, b) Young's modulus of the binary systems, and b) Ultimate tensile strength and Young's modulus of the ternary sample.

For the PLA-PCL binary polymeric systems, the ultimate tensile strength values varied between 2.2 MPa and 5.6 MPa and the stiffness between 3.5 MPa and 22.3MPa. PLA-PCL blends are good examples of a composite polymer system that shows high mechanical compatibility and stability [437]. PLA is known for its good tensile strength, but it suffers from low toughness, the incorporation of PCL into its matrix can counteract this downfall in its mechanical properties. PCL is a flexible polymer and therefore demonstrates significant elongation at break; when composited with PLA, their beneficial mechanical properties can be merged [438-440]. PLA-PCL blend systems in this study exhibited good tensile and elongation properties at the ratio of 50:50 PLA-PCL.

In all the observed cases, an increase in BC content led to increases in the tensile strength, seen up to a limit of 30 wt.% BC. Beyond this limit, a fall in the tensile strength is observed that is also accompanied by a fall in production yield which highlights the difficulties in increasing BC content to high amounts. The Young's modulus of the PLA composite systems also rises with increasing BC content. An inverse pattern however is seen in PCL binary systems where the stiffness decreases. This decrease in stiffness can be explained by the role of relative slippage in the PLA-PCL polymeric matrix. PCL being a highly elastic polymer interacts with the PLA polymer, where the existing bonding forces prevent the structure from stretching, resulting in strong mechanical characteristics [70, 320, 437, 441].

Samples containing BC displayed similar results when integrating with the PLA and PCL composites. Measured stiffness decreased from 23.0 MPa to 3.4 MPa for the PCL binary systems whilst the PLA binary systems had stiffness values ranging from 1.0 MPa to 3.5 MPa, as the BC concentration increased. However, the tensile strength values of PLA-BC binary systems ranged between 0.3 MPa and 6.6 MPa whilst the PCL-BC displayed a range from 0.5 MPa and 4.4 MPa.

The addition of BC into the composite polymer systems leads to increases in tensile strength. The network of ultra-fine fibres of BC has very high stiffness,

as a composite, this network can mesh with other polymers to produce superior mechanical properties such as high tensile strength [320]. In all the polymer blends produced in this study, it is expected that the incorporation of BC caused interactions between the BC microfibrils and the polymers chains, increasing the mechanical strength [442]. The optimised ternary sample produced in this study had a tensile strength of 9.1 MPa and stiffness of 19.6 MPa. This optimised ternary composite had the beneficial elasticity of PCL whilst retaining the high mechanical strength of PLA and BC. This ternary was also able to maintain a high level of yield and structural integrity during the manufacturing process. After reaching a critical point (30 wt.%) however, the production yield drastically falls off to undesirable levels with higher BC loadings. This significant diminishing of the yield and ultimate tensile strength can be explained with similar reasons as to before, that adding too much bacterial cellulose to the composites effects the fibre forming mechanism during spinning, hindering both the quality and quantity of the fibres being produced.

Chapter 5 : Antimicrobial Natural Materials

5.1 Introduction

The wound healing aid from naturally occurring materials has long been exploited across all cultures and lands. These natural materials have the ability to increase the wound healing quality as mentioned in (**2.5 Uses of Natural Materials as Fibres**). In this Chapter, two naturally occurring materials, honey and cinnamon will be investigated into their ability in wound healing as antimicrobial (against bacteria and fungus) additives.

5.2 Honey

5.2.1 Antibacterial Activity of Honey

The sensitivity of *S. epidermidis* and *E. coli's* sensitivity towards Black Forest Honeydew Honey and Manuka honey were assessed to decide which from source of honey was more suitable for antimicrobial applications. As shown in (**Figure 5.1**), the antibacterial activity of the two honey types was concentration-dependant, where higher concentrations lead to greater antibacterial activity. Manuka honey was superior in its antibacterial activity for both the Gram-positive *S. epidermidis* and Gram-negative *E. coli*.

Black Forest Honeydew honey exhibited potent antibacterial activity against *S. epidermidis* at 30 v/v% (97.4 ± 0.026%), whilst Manuka honey was very effective at all tested concentrations (>90% cell death post-incubation). The Black Forest Honeydew Honey showed mild cytotoxic properties against *E. coli* as only 37.19 ± 0.07%, 45.3 ± 0.24% and 57.4 ± 0.17% of the bacterial population were dead following incubation with 10, 20 and 30 v/v% of honey, respectively. Manuka honey in comparison, showed stronger antibacterial

properties at 30 v/v% as 91.40 ± 0.07% of the bacterial population were shown to have died.

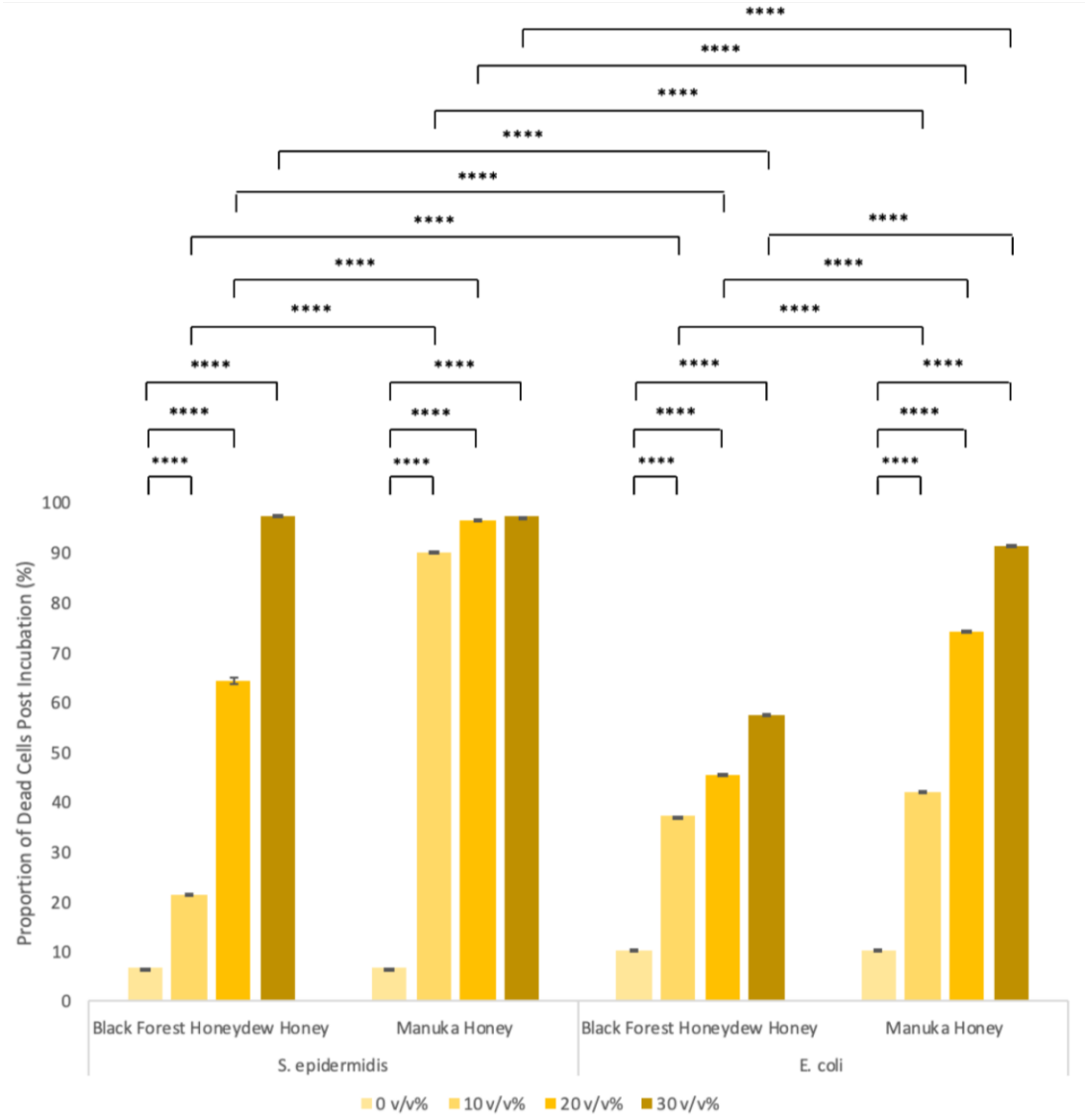

Figure 5.1: Antibacterial activity of S. epidermis and E. coli against Black Forest Honeydew and Manuka honey at concentrations of 10, 20 and 30 (v/v%). The antibacterial efficiency is given here as the percentage proportion of dead cells following incubation. * indicates a significant difference with a p-value <0.0001.***

Variances seen in the presented antibacterial activity are thought to result from differences in the chemical composition of the two honey sources. The interaction between the hydrogen peroxide and polyphenolic compounds in Black Forest Honeydew honey is responsible for the antibacterial activity [248]. Glucose oxidase mediated conversion of glucose to gluconic acid under

aerobic conditions is responsible for hydrogen peroxide in honey [443]. Black Forest Honeydew honey contains high concentrations of glucose oxidase, which plays an important role in the generation of hydrogen peroxide leading to its antibacterial activity [444]. In the presence of transition metal ions and peroxides, the polyphenolic compounds of Black Forest Honeydew honey act as pro-oxidants. These polyphenolic compounds work in two principal antibacterial ways: by producing hydrogen peroxide directly; and by reducing iron, triggering the Fenton reaction to generate more potent reactive oxygen species such as hydroxyl radicals. The chemical interactions between the hydrogen peroxide and the polyphenols of the honey can additionally result in the production of components used in the degradation of bacterial DNA [445, 446]. These synergistic effects can further induce oxidative stress-related responses in bacteria [447].

Conversely, for Manuka honey, which has a lower concentration of hydrogen peroxide producing components, the principal bactericidal activity is thought to be from methylglyoxal. Compared to conventional honey, Manuka honey contains over 100 times the concentration of a reactive metabolite, methylglyoxal [448-450]. Nonenzymatic conversion of nectar-derived dihydroxyacetone produces Methylglyoxal; where nectar taken from manuka trees show very high concentrations [449, 450]. Methylglyoxal can be toxic to cells via inhibition of protein synthesis by reacting with quinine residues [451-453]. Many studies attribute the sole mechanism of antibacterial activity of Manuka Honey methylglyoxal [448, 450, 454].

Overall, both sources of honey were more effective against Gram-positive *S. epidermidis* than Gram-negative *E. coli*. This difference in potency is due to the difference in the cell wall structures. Although Gram-positive bacteria have a thicker multi-layered cell wall, they lack an outer membrane and lipopolysaccharide content, making them more vulnerable to attack. As the Manuka honey samples show greater antibacterial efficacy, from here onwards, Manuka honey was chosen as the sole honey source to be studied.

5.2.2 Honey Composite Bandage-like Fibres

It is important to know the physical characteristics of the polymer solutions as they can explain the consequential fibre morphology. (**Table 5**) shows the measurements of viscosity and surface tension of the used polymer solutions and Manuka honey. These measurements show changes due to the increase in honey concentration and can explain how the rheology affects the spinning of polymers.

Table 5: Viscosity and surface tension measurements of the studied polymer solutions and Manuka honey.

Solution	Viscosity (mPa.S)	Surface Tension (mN m^{-1})
15% PCL	7638 ±128	33.1 ± 1.1
10% Honey/PCL	44091 ±56	33.6 ± 1.1
20% Honey/PCL	49265 ±89	34.4 ± 1.2
30% Honey/PCL	54096 ±69	35.1 ± 0.8
Pure Manuka Honey	> 60000	32.5 ± 1.6

Honey is very thick and known to be one of the most vicious naturally occurring products [455]. In this study, Manuka honey composite fibres were formed by combining 15% PCL polymer solutions with different concentrations of Manuka honey. From (**Table 5**), we see that all the polymer solutions were high in viscosity. Virgin PCL had the lowest viscosity at about 7638 mPa.S. Even with the addition of only 10% v/v Manuka honey, the viscosity increases over five times the original PCL value to 44091 mPa s. The Manuka Honey fell above the viscosity range of the equipment used; it is assumed that the viscosity is well over 60000 mPa.s. Further addition of Manuka honey to the PCL solution of 20% and 30% v/v, lead to a predictable increase in viscosity which is due to the increase in volume fraction of high viscosity honey. In the cases shown above, all the composite solutions displayed extremely high viscosity. The implications of high viscosity have been found to lead to thicker fibres; however, such viscous solution behaviour has not been previously explored in gyration-based manufacturing processes.

The surface tension of any polymer solution plays an essential role during polymer jet formation of any fibre forming technique, this polymer jet subsequently dries to give rise to fibres [90, 200]. (**Table 5**) shows the recorded surface tension values for the tested honey solutions. It was found that the surface tension of both the PCL and Manuka Honey solutions were very closely matched, this explains the small deviation in number for the composite solutions, all solutions gave very similar surface tension readings. From the given values, we can deduce that the centrifugal force from the pressurised gyration could easily overcome the interfacial surface tension of all the solutions and that viscosity played the more significant role for fibre production and its resulting morphology. The solutions were spun with the gyration setup, their morphology and structure were analysed using SEM. The micrographs of all the produced and tested samples can be found in (**Figure 5.2**).

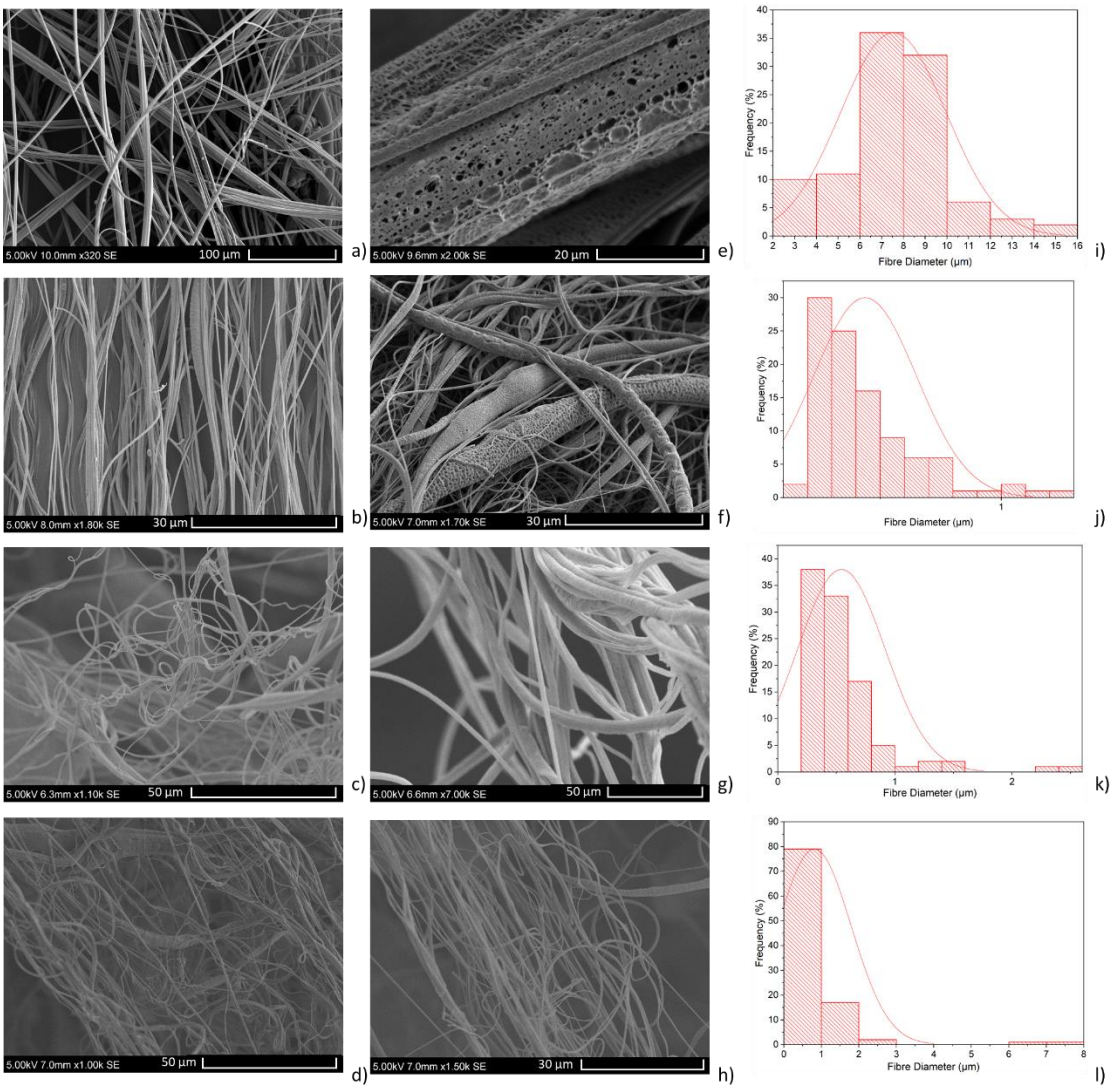

Figure 5.2: Scanning electron microscope image of fibres produced; a), Virgin PCL fibres, b), 10% honey-composite fibres, c), 20% honey-composite fibres, d), 30% honey-composite fibres. High magnification images of e), Virgin PCL fibres, f), 10% honey-composite fibres, g), 20% honey-composite fibres, h), 30% honey-composite fibres, along with corresponding fibre diameter distribution histograms i to l.

Solvent evaporation is a key mechanism in the formation of polymeric fibres in both electrospinning and pressurised gyration [456]. The resulting fibres differ in morphology due to the properties of the original solution such as the solvent volatility, viscosity, degree of polymer chain entanglement and surface tension [78, 457-459]. The SEM micrographs of the fibrous samples can be seen in (**Figure 5.2**). The average fibre diameter of the virgin PCL fibres was 7.5 ± 2.4 µm, these fibres coincide with typical values from PCL based fibres

at higher molecular weights of over 60000 mn [392]. Due to the high viscosity and high molecular weight (80000 mn) of the tested PCL solutions, there is a high degree of polymer chain entanglement, which leads to relatively thick fibres being produced. The average diameter for the 10% honey composite fibres was 437 ± 21 nm, this unexpected steep and sudden drop in fibre diameter does not coincide with normal trends where the increase in polymer viscosity leads to thicker formed fibres [460]. It is not fully understood what causes the large reduction in fibre diameter, however very high viscosity solutions do differ in rheology to lower viscosity solutions. The highly thick solution could have reduced the available orifice aperture of the gyration pot to subsequently cause thinner fibres to be extruded from the orifices.

The average diameter for the 20% honey composite fibres was 543 ± 374 nm, we can see that the move from 10-20% w/w honey caused a noticeable increase in fibre diameter, this is expected as the honey concentration is now larger and thus the fibres contain more of the viscous medium. The average diameter for the 30% honey composite fibres was 815 ± 98 nm, again the increase in honey content and viscosity of the solution yielded another sizable increase in average fibre thickness. These fibres are however still very thin, compared to the PCL fibres and thus afford a very high surface area to volume ratio which is exceptionally suitable for a wide range of biomedical applications, and beneficial in wound healing [461]. In a wound environment, thinner fibres can closely resemble the surrounding extracellular matrix and provide a suitable niche for fibroblasts and other essential cells of the wound response to attach and proliferate [462-465]. At the highest Manuka honey concentration of 30 v/v%, there is a trade-off between fibre diameter and available honey concentration. The initial honey antibacterial tests found that 30% of Manuka honey killed over 90% of both Gram-positive and Gram-negative bacteria, for these reasons 30% Manuka honey-PCL scaffolds were chosen as the sole optimal antibacterial structures to be tested in this study.

High magnification images of the fibre surface revealed the surface topography of the scaffolds in more detail (**Figure 5.2**). The fibres can be seen to have many nanopores. The presence of nanopores arises from the use of a volatile solvent (chloroform) which causes condensation through rapid

temperature change as it evaporates, these condensation droplets then dry to leaves small craters, characterised as surface pores [121]. Nanopores can further increase the available surface area of the fibres and may even contain pockets of Manuka Honey that are able to trap small microbes and release active ingredients (such as antimicrobial peptides from the honey) as a function of time.

The structures of the virgin PCL, Manuka honey and the honey-loaded fibres were analysed via FTIR to confirm the presence and uptake of honey into the fibrous scaffolds, this can be seen in (**Figure 5.3**). The virgin PCL fibres show characteristic peaks at 2950 cm^{-1}, 1725 cm^{-1}, and 1165 cm^{-1}. The peak at 2950 cm^{-1} is linked with the asymmetric CH_2 stretching, at 1165 cm^{-1}, the peak related to the symmetric COC stretching and the peak at 1725 cm^{-1} corresponds to the carbonyl vibration region of the PCL polymer [466, 467]. Pure Manuka honey on its own, shows characteristic bands at 3240 cm^{-1}, 1645 cm^{-1} and 1020 cm^{-1}. The peak around 3240 cm^{-1} is likely to belong to the O-H stretching group of the honey, where the peak can cover a broad range because of the intramolecular bond type [468, 469]. At a wavelength of 1645 cm^{-1}, the peak is likely to be attributed to a carbonyl bond group belonging the honey, the peak at 1020 cm^{-1} would correlate to the C-O and C-O stretching vibrations of honey [470]. The absorbance profiles of all the honey-loaded fibres where similar.

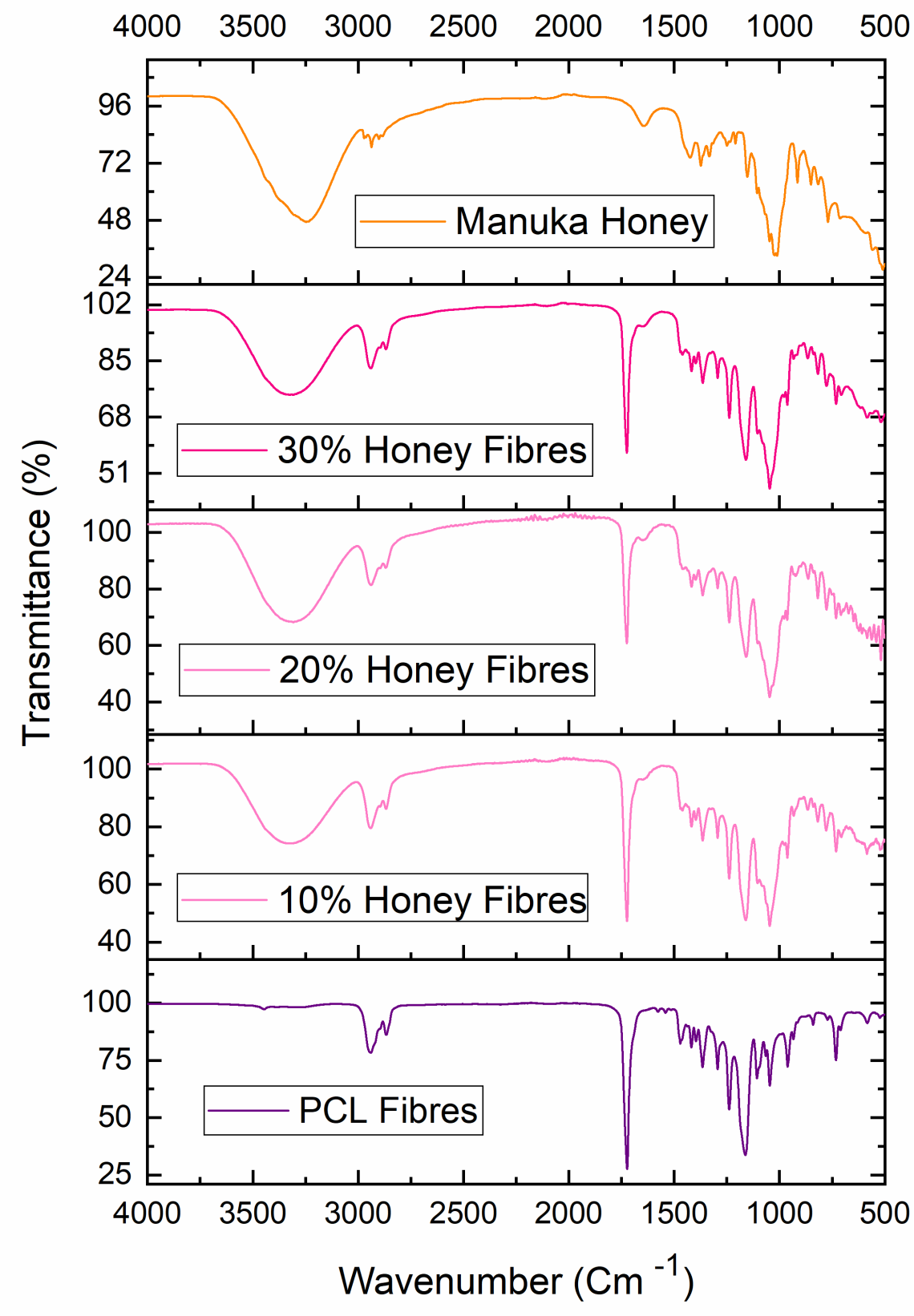

Figure 5.3: FTIR spectra of virgin PCL fibres, 30% honey-loaded fibres and pure Manuka honey. Specific peaks associated with Manuka Honey and with PCL are highlighted using arrows in the composite fibres.

We can see that by overlaying the spectrum of the Manuka honey fibres, there is an overlap of prominent peaks at around 3220 - 3360 cm^{-1} between the Manuka honey and the Manuka honey fibres. This peak is due to the O-H bonds in the Manuka honey and appears only in honey, confirming the successful uptake of Manuka honey in the PCL fibres. Additionally, samples containing PCL show characteristic bands at 2950 cm^{-1} confirming the presence of CH_2 stretching that is typically found in the polymer. The honey-loaded fibres and pure Manuka honey overlap at wavenumbers of around 1055 cm^{-1} confirming the presence of honey in the fibres.

As Manuka Honey was found to perform the strongest against bacteria in this study, it was incorporated into polymeric fibres at concentrations of 10, 20 and 30% v/v. 30% honey composite fibres had the largest diameter but also were the most uniform of the fibres tested, there was a narrow distribution of their fibre diameter, which can be beneficial in producing bandage-like structures when ensuring the final product meets strict conditions in the manufacturing process.

During the fibre production process, 4 mL of honey-PCL solution was spun for 10 seconds. During this time, an average of 0.4 grams was produced in each run, as this process relies on solvent manipulation, loss of product yield can be ascribed to solvent evaporation. Theoretically and based on current results, if the production technique was scaled up and run continuously, it would be capable of outputting over 8.6 kg/hour of honey-composite nanofibres, this value is much larger than a single set-up of any electrospinning device [471]. As the gyration setup also takes very little floor space, yield can be improved by increasing the number and volume of the pots. Unlike with electrospinning, multiple gyration setups are viable to be in operation simultaneously, as there is no electrical interference between neighbouring devices [86].

5.2.3 Antibacterial Activity of Honey Composite Fibres

The antibacterial activity of the produced Manuka honey composite fibres was tested against both *S. epidermidis* and *E. coli* and the results are shown in (**Figure 5.4**). The honey-loaded fibres were highly effective against the Gram-positive *S. epidermidis* as compared with the negative control (which did not show any antibacterial activity, $p = 0.0041$). The 10, 20 and 30 % v/v honey-based scaffolds were able to reduce the bacterial concentration by 41.1%, 81.4 %, and 97.0 %, respectively. This high reduction in bacterial viability showcases the strong antibacterial activity of the honey fibres at low concentrations. The honey composite fibres also demonstrated some antimicrobial effect against the Gram-negative *E. coli*, but not as potent as seen against *S. epidermidis*. The 10, 20 and 30 % v/v honey fibrous scaffolds were able to reduce the *E. coli* bacterial numbers by 1.2%, 5.7 %, and 22.8 %, respectively. PCL alone is not known to be antimicrobial and therefore shows no antibacterial capability. The fibres tested here were spun at 36000 rpm with a gas flow pressure of 0.1 MPa and were successfully able to carry the honey into the polymeric structure whilst retaining a high antibacterial activity.

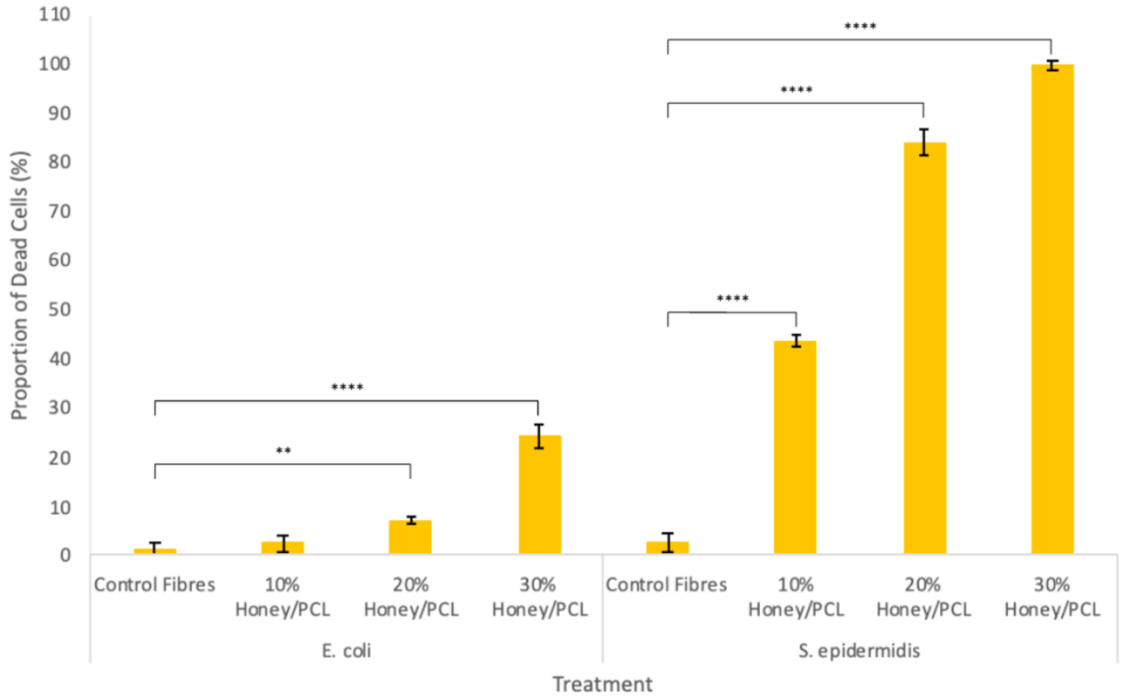

Figure 5.4: Antibacterial activity of 10, 20 and 30% Manuka honey-PCL composite fibrous meshes compared to the negative control of virgin PCL fibres, antibacterial effectiveness is expressed as a percentage bacterial reduction. The data was compared using an unpaired t-test **** $p < 0.0001$; ** $p < 0.05$.

S. epidermidis infections are becoming increasingly prevalent in hospital settings, partially due to the high density of immunocompromised patients where weaker but resistant strains thrive [472]. Although not directly pathogenic, *S. epidermidis* forms impenetrable biofilms which can protect other bacterial species [473]. *S. epidermidis* can also function as a gene reservoir that allows gene transfer to *Staphylococcus aureus* which can lead to further antibiotic resistance [474]. As *S. epidermidis* is native to the skin microbiome, these honey-containing fibrous meshes provide a protective layer whilst the honey comes in contact with the bacterial niche to reduce the populations of pathogens.

As described before, the mechanism of Manuka Honey's anti-bacterial action is thought to be a combination of its low pH and its osmotic effects on invading bacterial cells [240]. As a wound healing additive, honey is also known to be anti-inflammatory allowing for a smoother healing process and stimulating the

immune response [475]. In *in vitro* studies using Manuka honey, show that cells integral to the wound healing process, such as tumour necrosis factor-alpha, interleukin- 1beta and interleukin-6, have been seen in increased levels, which results in improved overall healing [476].

In fibrous form, honey is significantly easier to store, package and apply evenly to a wound site. The PCL fibres in these composites allow for the even distribution of honey within the fibre surface and polymer matrix. As a biodegradable material, PCL can degrade as a function of time releasing honey over long periods, requiring fewer bandage applications and removal. This can reduce the risk of trauma, which is typical during the removal process. Additionally, the honey in the fibres will draw wound exudate to the fibres through osmosis, thus maintaining the moisture content of the wound. Furthermore, the fibres produced here demonstrate sub-micrometre thickness, providing a large surface area for cell attachment during the wound healing process and reepithelisation. The application of honey over a wound often causes a stinging pain to the patient, by incorporating honey into a fibrous scaffold, honey content is vastly reduced whilst retaining a high (> 90%) killing rate, reducing pain associated with pure honey. The cytotoxicity of the prepared fibres is of no concern as both honey and PCL are routinely used in the medical field as topical treatments and have centuries of after effect data available [477, 478].

5.3 Cinnamon

5.3.1 Antifungal ability of Cinnamon

The antifungal capability of the raw cinnamon powder and the fibre samples was tested against *C. albicans*, where inhibition areas were used to determine the effectiveness of each anti-fungal substance [397]. Larger inhibition zones were indicative of a greater ability for the material to kill the fungal population, these have been compared in the following results. (**Figure 5.5**) shows an overview of all the samples tested in this investigation including pure PCL, raw cinnamon powder and the three cinnamon-extracted fibre samples.

Three cinnamon extract concentrations were used in this work to show the effect of concentration on the anti-fungal power of the fibres, but also as a precaution for toxicity concerns, it may have an active chemical compound [479]. The three concentrations where given names: C1, C2 and C3 where their cinnamon-extract concentrations were 0.250 mg/mL, 375 mg/mL and 500 mg/mL respectively.

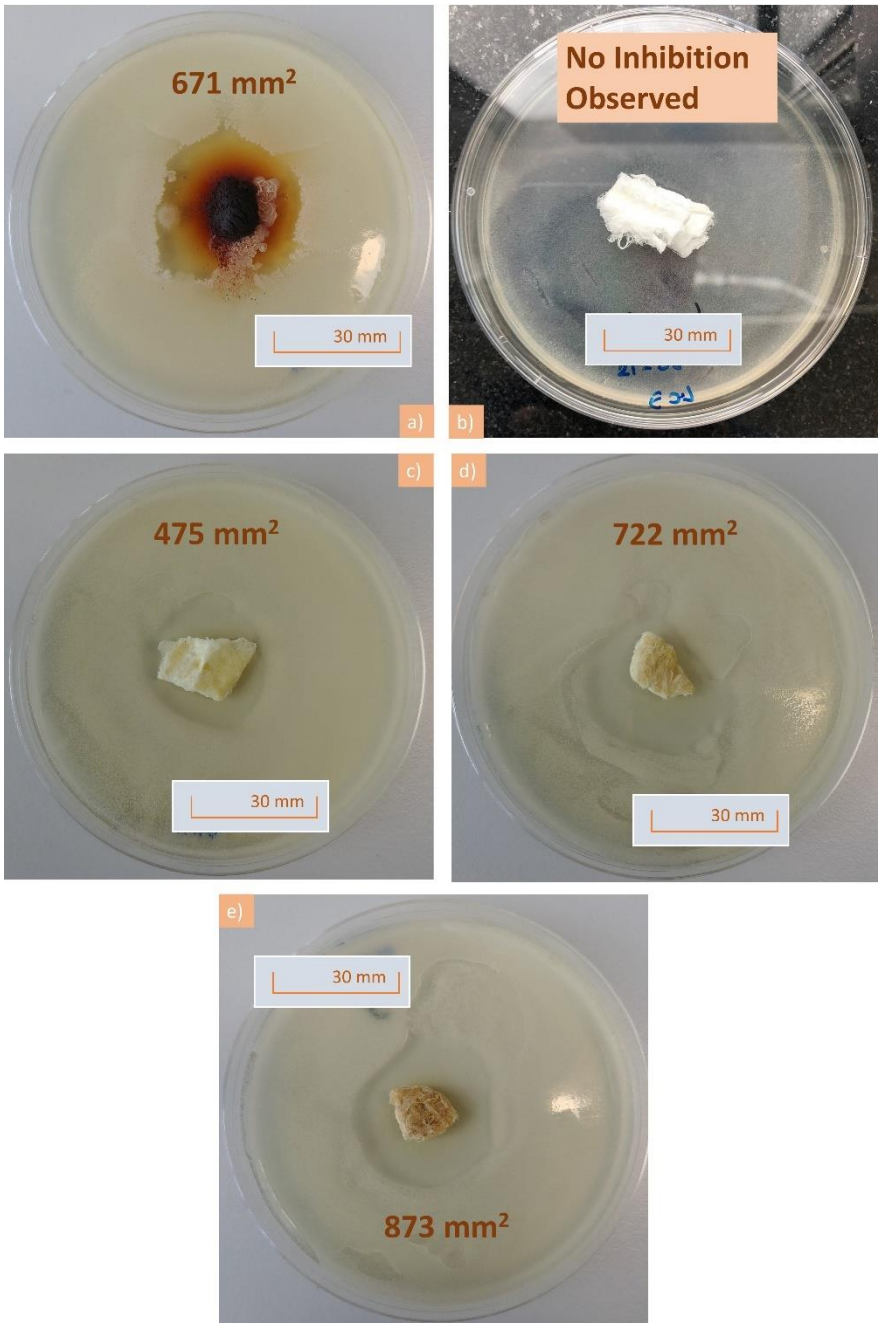

Figure 5.5: Pictures following 48 hours of incubation showing plates containing; a): ground cinnamon powder, b): virgin PCL fibres, showing lack of an inhibition area, c): C1 cinnamon extracted fibres, d): C2 cinnamon extracted fibres, e): C3 cinnamon extracted fibres and, in each case, 100mg of sample was investigated. For each plate, the inhibition area value is given.

We can see from (**Figure 5.5**) that all cinnamon-containing samples are found with a clear inhibition zone surrounding them, this indicates that these fibrous

meshes were able to prevent the inward growth of *C. albicans.* We also see that the pure PCL fibres do not demonstrate an inhibition zone, as expected. PCL as a polymer itself has no antimicrobial activity and thus will not prevent the growth of fungus, which validates that the chloroform from the fibre manufacturing process has completely evaporated as otherwise, this would have led to an inhibition zone. What is also obvious is that by increasing the concentration of cinnamon extract within the fibres, even at the same weight, there is an increase in antifungal strength. The results are summarised graphically in (**Figure 5.6**).

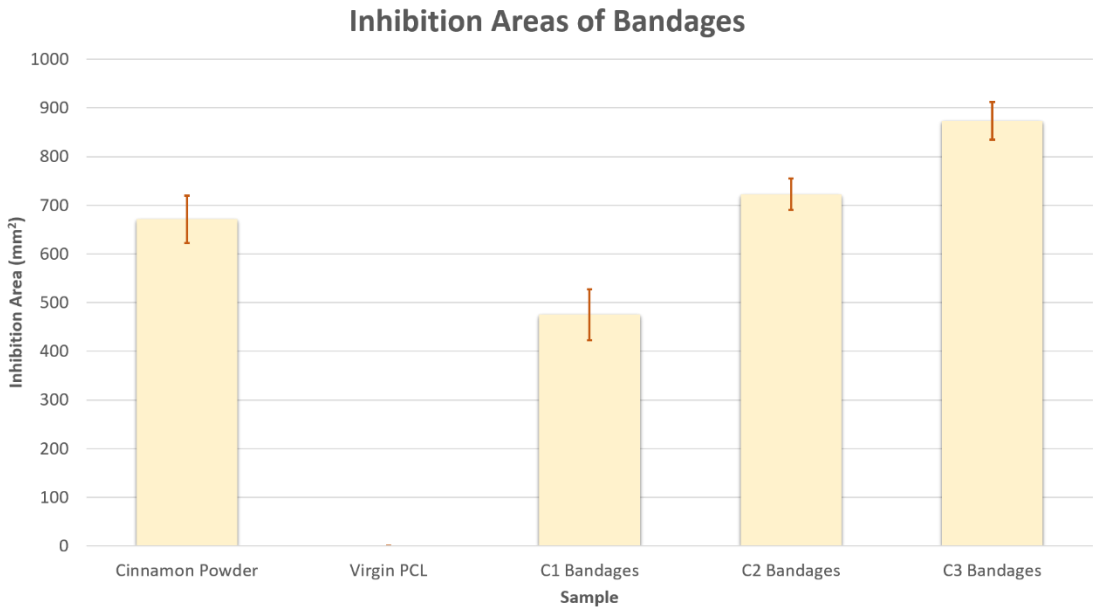

Figure 5.6: Graph comparing inhibition areas of the different samples, shown in figure 2, n=3.

We see from (**Figure 5.6**) how all the samples behaved on the Petri dishes that were fully coated with a population of *C. albicans.* Inhibition areas were used in this study to eliminate the effects of having different shaped fibrous meshes in the testing procedure, however, an inhibition area in these instances follows the same principles as one may carry out in standard antimicrobial testing procedures [480]. Cinnamon powder of 100mg showed a potent antimicrobial effect against the fungal population with an inhibition area of 671 ± 49 mm^2. C1 fibres also showed a strong inhibition ability with an area of 475 ± 52 mm^2, compared to the raw powder this was lower, showing that there is great

potential in being able to increase the concentration within the same mass of fibre to be able to control antifungal ability. C2 and C3 fibres demonstrated very high inhibition areas of 671 ± 32 mm^2 and 873 ± 39 mm^2 respectively, indicating that indeed the increase of extract concentration plays a role in proportionately increasing the antifungal ability, all the while keeping the volume and mass of the fibres constant.

Extracts of cinnamon contain several active compounds including cinnamaldehyde and tannins [481]. Tannins are known to inhibit the growth of certain bacterial strains such as *Staphylococcus aureus [482]*. Cinnamaldehyde too is antimicrobial due to its activity in inhibiting cell wall synthesis of microbes [483]. During the extraction process, the powder and cellulose of the cinnamon were discarded leaving only the chemical extract. The results here, therefore, suggest that the anti-fungal effect may indeed be of chemical origin. Having a lower minimum non-cytotoxic concentration than many other natural antimicrobial materials, it is unlikely that the anti-fungal effect is due to a toxic effect [484].

5.3.2 Cinnamon Bandage-like Fibres

Fungus, like all other microbes, come into contact with the surface of materials that they are exposed to. It is therefore important to study the fibres to identify if any differences in fibre morphology could have affected the antifungal activity. (**Figure 5.7**) shows the micrographs of the produced cinnamon-extracted fibres.

The average fibre diameter for the virgin PCL fibres was 6.0 ± 2.6 μm, the diameter distribution of these fibres is shown in (**Figure 5.7 b**)**.** These thin fibres can carry the active ingredients of cinnamon whilst acting as a physical barrier to microbes such as fungi. These fibres contain nano-pores which are the result of rapid solvent evaporation and subsequent micro droplet formation on the fibre surface as discussed earlier [121]. These pores increase the available surface area to volume ratio of the bandages and also allow for the free movement of exudate in and out of the bandage, which is a highly desired characteristic for a wound

dressing [485, 486]. (**Figure 5.7 c**) shows cinnamon-extracted PCL fibres (C2) which have an average fibre diameter of 2.3 ± 1.3 µm. Compared to the virgin PCL fibres, the cinnamon-loaded fibres are thinner and have a smaller diameter distribution (**Figure 5.7 d**) meaning that the fibre thicknesses are more uniform. Lower diameter fibres can be more beneficial in releasing active ingredients due to the higher surface area to volume ratio they afford [90].

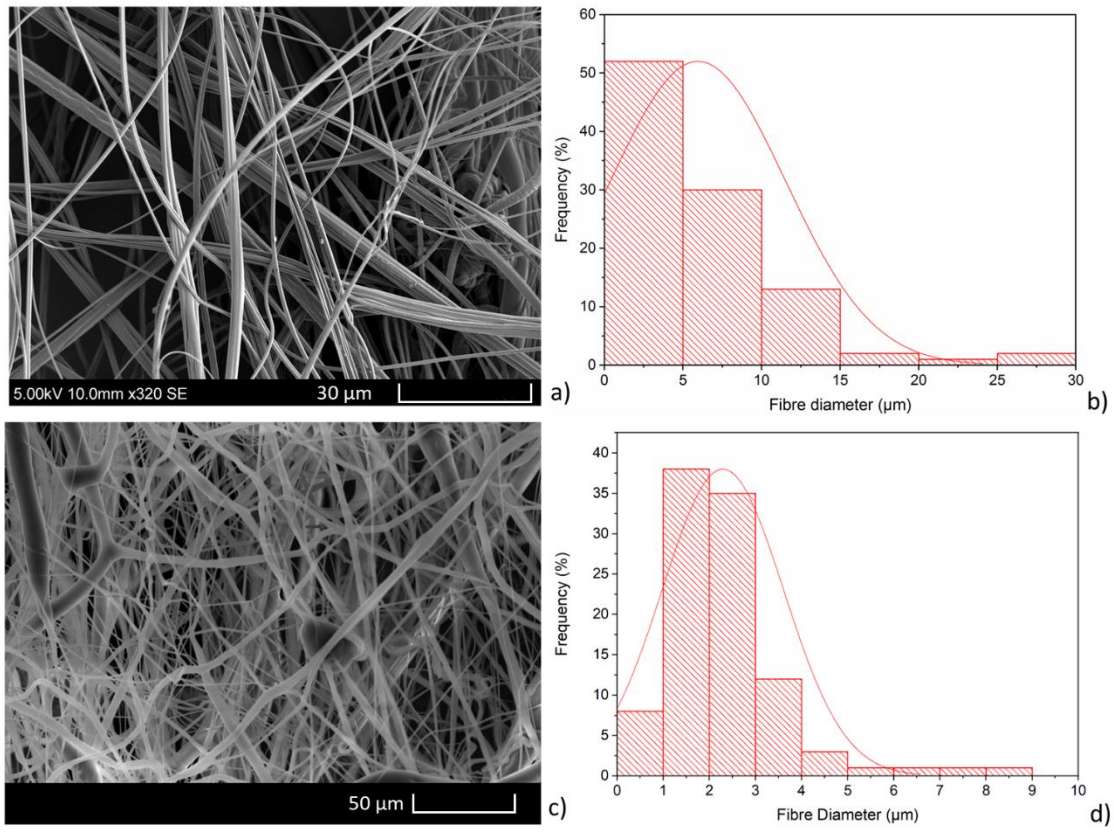

Figure 5.7: Scanning electron microscopy images of pressure spun fibres at 0.1 MPa: a) virgin PCL fibres b) diameter distribution of the virgin PCL fibres c) cinnamon-extracted PCL fibres (C2) d) diameter distribution of the cinnamon-loaded PCL fibres, in all cases, n= 100.

Inhibition zones clearly show antimicrobial effects, but this could be due to several factors other than the cinnamon extract. To eliminate the doubt of the antifungal ingredient, virgin PCL fibres containing no cinnamon extract were seen under microscopy and compared with cinnamon-extracted PCL fibres

these are shown in (**Figure 5.8**). The images consist of three frames taken from a video clip that pans an area between the fibre and the fungi. There is a clear inhibition zone in between the extracted cinnamon containing fibres and the surviving fungi where *C.albicans* cells have failed to survive. The extracted cinnamon containing fibres are successful in denying fungal growth here.

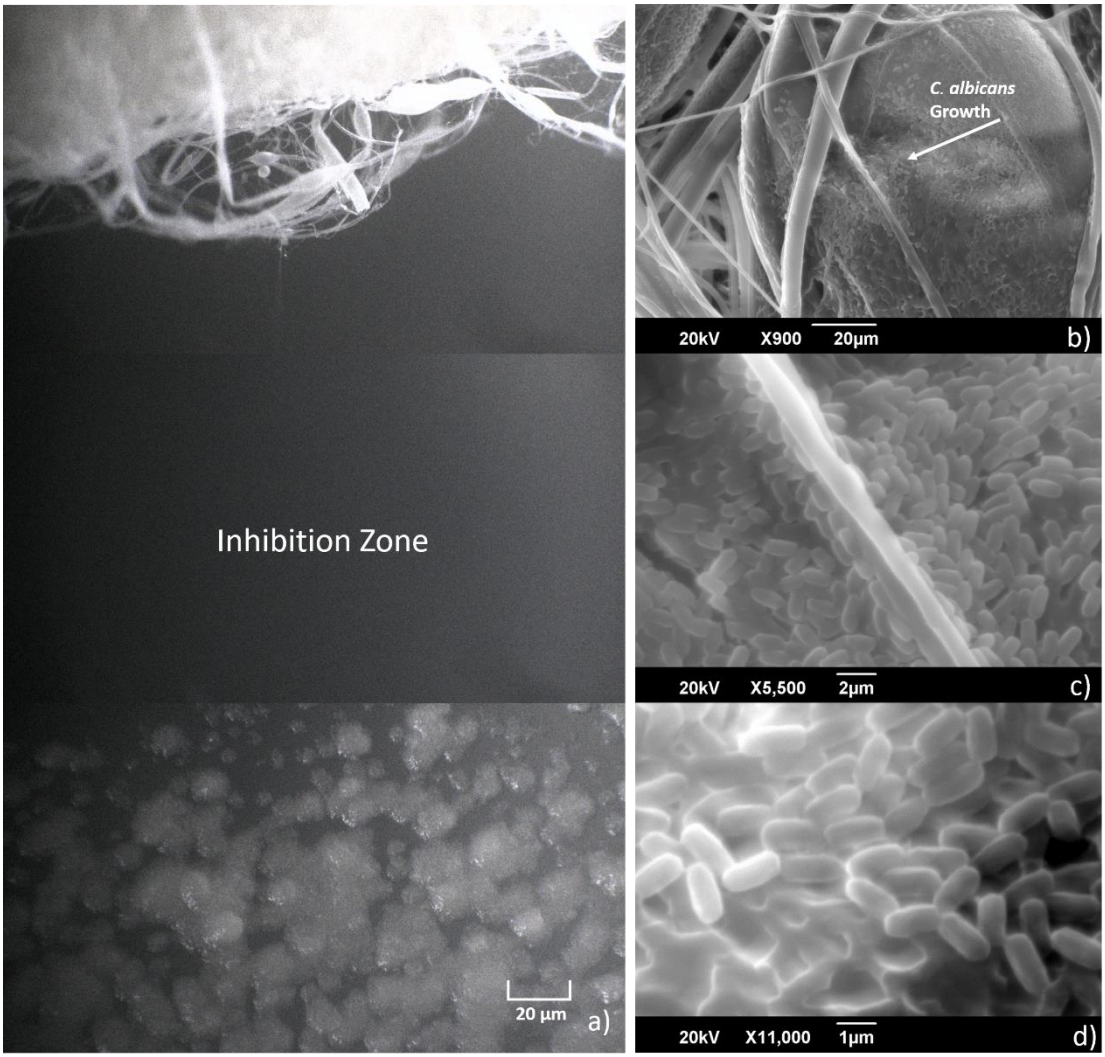

Figure 5.8: Fluorescence microscopy video stills of: a) C1 extracted cinnamon fibre showing a clear inhibition zone with no fungal growth, SEM images of: b), c), candida growth over virgin PCL fibres, arrow marked in b), d) high magnification image showing close-up of C. albicans cell growth on virgin PCL fibre surface.

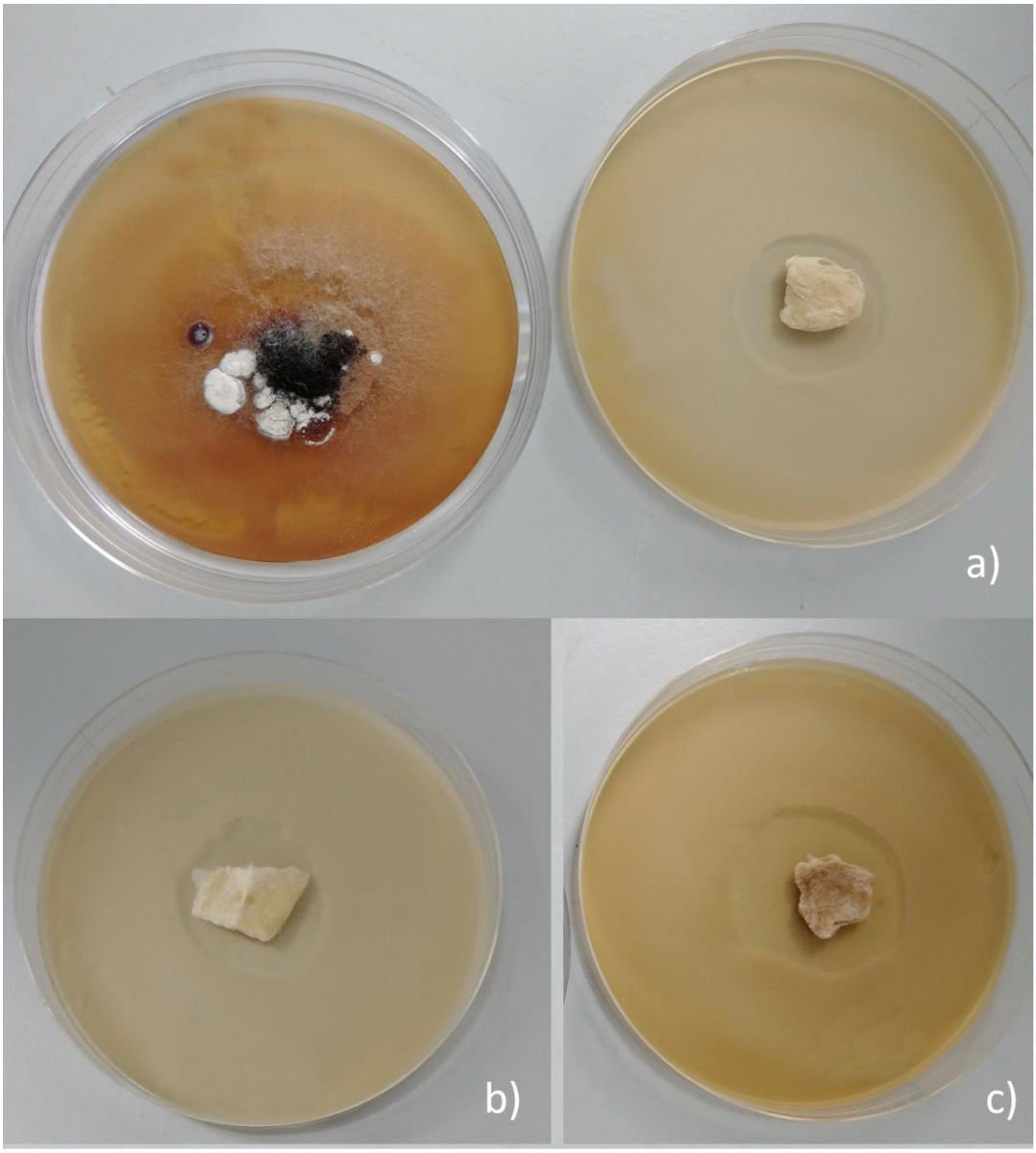

Figure 5.9: Images taken 504 hours after initial incubation comparing: a), C1 extracted cinnamon containing fibres (RHS) compared with raw cinnamon powder (LHS) with raw cinnamon powder b), C2 extracted cinnamon containing fibres c), C3 extracted cinnamon containing fibres. All petri-dishes shown are 90mm in diameter.

The longevity of the antifungal effect is also an important consideration for use as a wound dressing. Following the 504 hours of initial incubation, the samples were re-photographed to observe the longevity of the antifungal influence as shown in (**Figure 5.9**).

Very interestingly, following 3 weeks of incubation, the cinnamon powder solutions show a regrowth of fungal colonies, indicating that the antifungal effect of the ground cinnamon powder is only temporary and given time, fungi can grow into the previously established inhibition zones (**Figure 5.9**). All the extracted cinnamon fibres (C1, C2 and C3) still retain the same inhibition zones, demonstrating that the antifungal effect is not short-term and even after 3 weeks of 37°C incubation, there is no regrowth of fungal communities. One possible explanation for the regrowth of fungi in the cinnamon powder is that the fungi are initially repelled from the powder, but the surviving fungi can grow in numbers and invade the cinnamon powder which acts as their food source for further growth. In any case, I have successfully demonstrated that we can get lasting antifungal activity with cinnamon-loaded fibres. Compared to raw cinnamon powder alone, there is no regrowth of fungi following 3 weeks.

5.3.3 *In-Vitro* Testing on Cinnamon-extracted Fibres

Thermal decomposition temperatures and weight loss % data obtained by thermal gravimetric analysis (TGA) (**Figure 5.10**) shows that the blending of PCL with cinnamon extract causes a slight reduction in the thermal stability of the fibres. The starting decomposition temperature was reduced with the increasing concentration of cinnamon extract. The C1, C2 and C3 blends lost 5% of their weights at a temperature of 368.1°C, 354.4°C and 348.7°C, respectively, whereas PCL lost its 5% of weight at 372.7°C. The temperatures of the PCL, C1, C2 and C3 weight loss at $T_{X\%}$ are given in detail in (**Table 6**) for $T_{5\%}$, $T_{10\%}$, $T_{15\%}$, $T_{20\%}$, $T_{50\%}$, $T_{75\%}$, $T_{90\%}$ and $T_{100\%}$ (°C) respectively. The results presented here show a discernible difference in the thermogravimetric values for the differing samples, suggesting that the increase in cinnamon concentration may affect the adsorption of the samples [487, 488].

Table 6: Temperature values of virgin PCL, C1, C2 and C3 gyrospun polymeric fibre materials in terms of weight loss %.

	$T_{5\%}$ (°C)	$T_{10\%}$ (°C)	$T_{15\%}$ (°C)	$T_{20\%}$ (°C)	$T_{50\%}$ (°C)	$T_{75\%}$ (°C)	$T_{90\%}$ (°C)	$T_{100\%}$ (°C)
PCL	372.7	382.5	387.8	391.8	407.2	418.8	430.3	479.9
C1	368.1	379.5	385.8	390.2	406.9	419.8	438.0	480.0
C2	354.4	374.5	382.7	387.8	405.3	416.9	426.4	474.6
C3	348.7	369.8	378.6	384.2	402.4	414.0	423.3	478.7

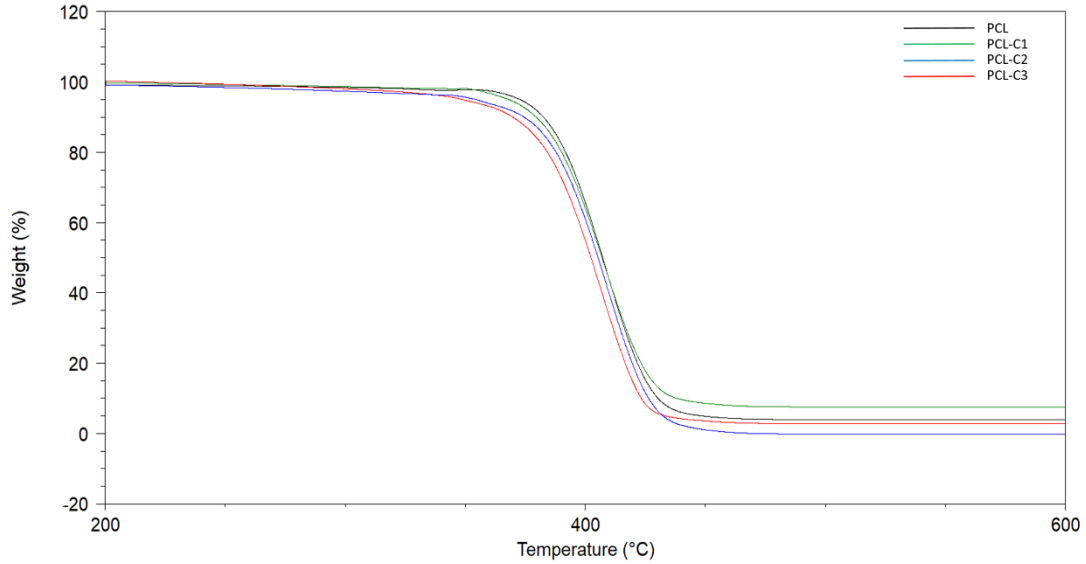

Figure 5.10: **TGA thermograms of PCL, C1, C2 and C3 gyrospun polymeric fibres**

5.3.4 *Cytotoxicity* Testing on Cinnamon-extracted Fibres

Testing the toxicity of any antimicrobial compound is of great interest to any healthcare provider as a chemical that can kill microbes may also have the same effect on native cells that are not desired to be damaged [489]. Cytotoxicity tests results (**Figure 5.11**) showed that there is no toxic effect neither for virgin PCL gyrospun fibres nor the cinnamon-extracted fibres. It has been observed that virgin PCL fibres showed 88.1±6.7 % cell viability compared to the negative control (100 % cell). Additionally, C1 fibre samples

had 88.1±8.1 %, C2 fibres has have 91.8±9.2 % and C3 fibres had 106.6±10 % cell viability which is deemed to be a highly cytocompatible result compared to the positive control (46.7±1.1 % cell viability). According to the ISO10993-5 standard, the cytotoxicity limit is 70 % cell viability where all samples have the results above this threshold value [490]. As a result, the cinnamon blended PCL has promising potential for the use of gyro spun fibres as biomaterials, especially for advanced wound care materials.

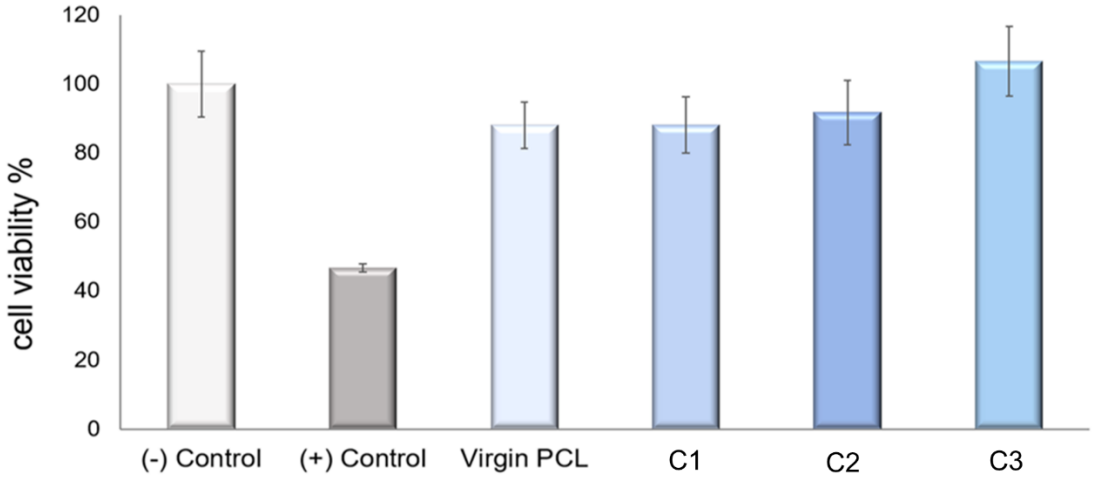

Figure 5.11: Cytotoxicity-MTT test results indicating the cell viability (%) of PCL fibres and cinnamon-extracted fibres at the tested concentrations.

(**Figure 5.12**) demonstrates that all sample groups showed high cell viability with a very small number of dead cells. Direct live/dead staining test results supported the results obtained from the indirect MTT cytotoxicity test. C1, C2 and C3 fibres showed high cell proliferation/viability as much as the control group and the virgin PCL samples. PCL is widely used in biomaterial science and tissue engineering as it is FDA (Food and Drug Administration) approved and affordable material, as well as being biocompatible, biodegradable and easy to manufacture [491]. Cinnamon is also a well-known natural anti-inflammatory agent with low solubility and has very low dose-dependent allergic reactions [492]. Salehi and co-workers also indicated that cinnamon as an ingredient is very effective for wound healing applications both *in vitro* and *in vivo* with great importance to the dosage limit of cinnamon content [493].

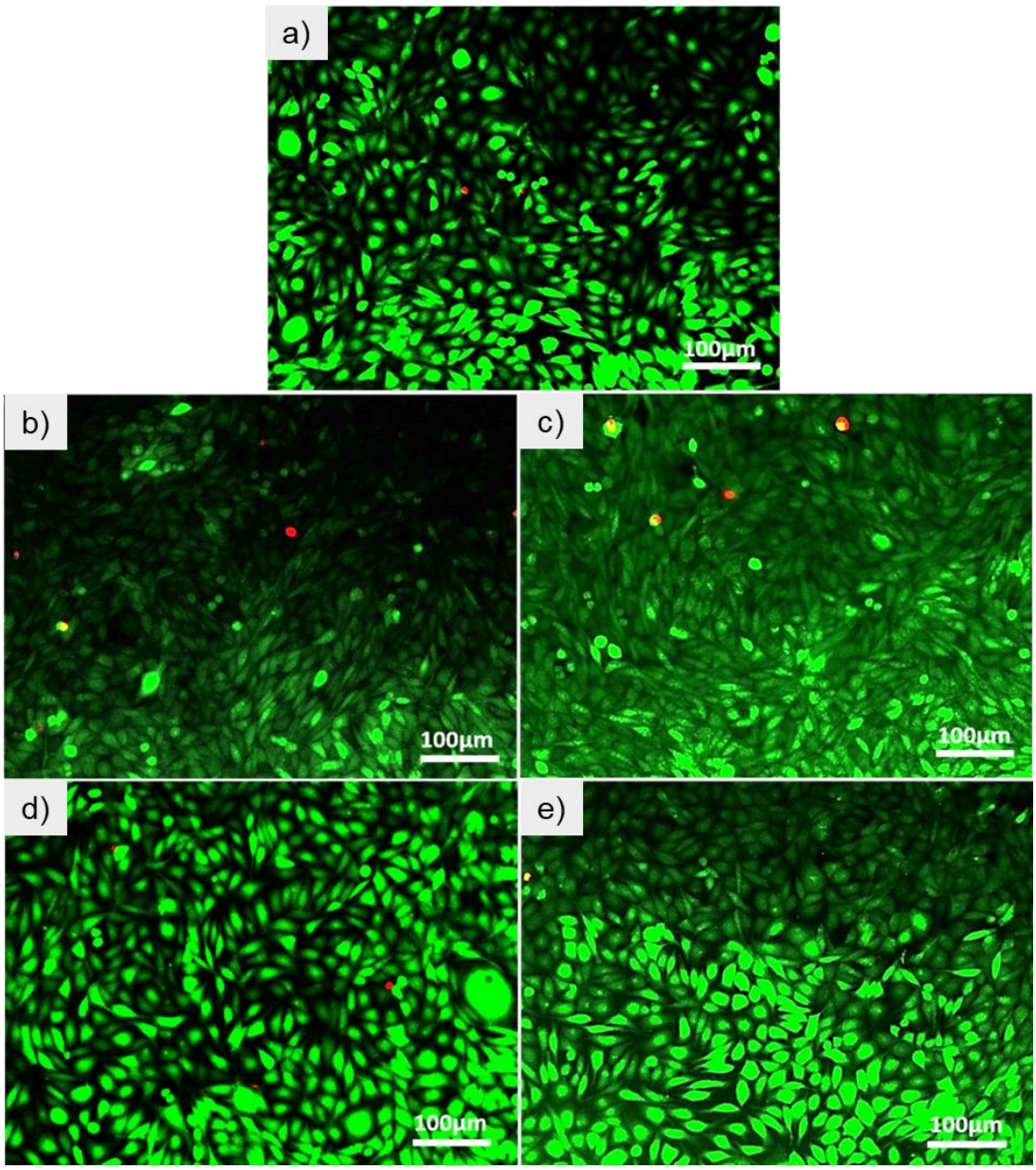

Figure 5.12: Live/dead staining test results for a) control, b) PCL Fibres, c) C1 fibre sample, c) C2 fibre sample and e) C3 fibre sample.

5.3.5 Antibacterial activity of Cinnamon Extracted Fibres

Antibacterial tests were performed against *E. coli, S. aureus, MRSA* and *E. faecalis* strains over a 24-hour incubation period for the PCL control and cinnamon extracted fibre samples. (**Figure 5.13**) indicates the number of adhered cells of *E. coli, S. aureus, MRSA* and *E. faecalis* strains on the test samples. The results showed that C1, C2 and C3 samples decreased the bacterial cell numbers by up to 2 orders of magnitude (log 2 / 100 times). The

sample groups; C1, C2 and C3 showed statistically significant decreases (* $p < 0.05$) in the bacterial cell viability in contrast to the PCL control group for *E. coli* (gram negative), *S. aureus (*gram positive)*, MRSA (*gram positive) and *E. faecalis (*gram positive). The antibacterial test results showed that the bacterial cell numbers on the PCL control groups were $6.1x10^8$ cfu/mL, $1.2x10^8$ cfu/mL, $8.7x10^8$ cfu/mL and $3x10^8$ cfu/mL for *S. aureus*, MRSA, *E. coli* and *E. faecalis*, respectively. The cinnamon extracted bandage-like fibrous sample groups exhibited statistically significant decreases as follow; C1: $3x10^6$ cfu/mL, C2: $2.7x10^6$ cfu/mL, C3: $5x10^6$ cfu/mL for *S. aureus,* C1:$7.2x10^6$ cfu/mL, C2: $3.1x10^6$ cfu/mL, C3: $3.7x10^6$ cfu/mL for MRSA*,* C1: $2x10^8$ cfu/mL, C2: $1.7x10^8$ cfu/mL, C3: $9x10^7$ cfu/mL for *E. coli* and C1:$2x10^7$ cfu/mL, C2: $3.6x10^7$ cfu/mL, C3: $3.8x10^7$ cfu/mL for *E. faecalis.* It has been shown that all the sample groups exhibited a statistically significant reduction in bacterial cell viability compared to the PCL control group. On the other hand, there is no observable significant difference was between the C1, C2 and C3 sample groups against any of the bacterial species, this could mean that even at the lowest concentration, there is enough active ingredient to cause an antibacterial effect.

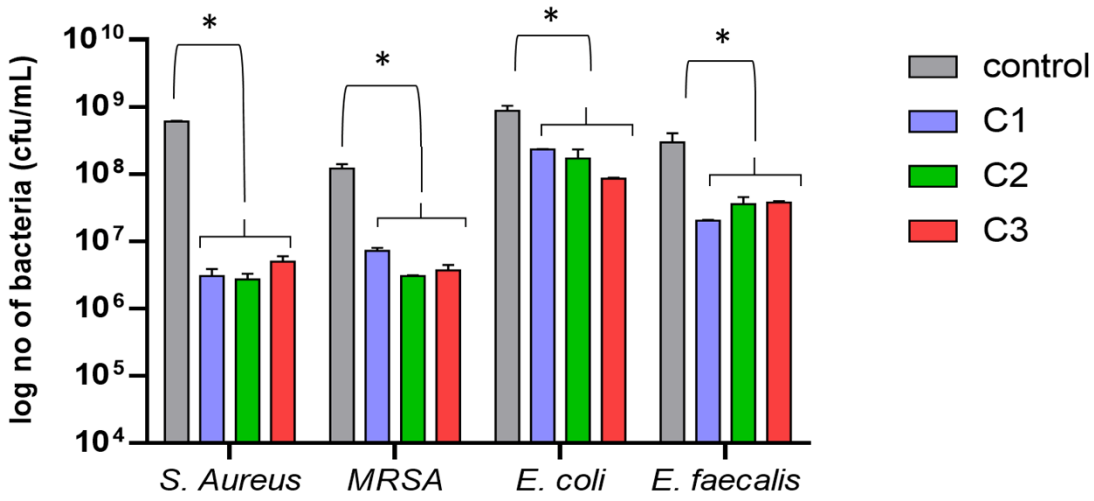

Figure 5.13: Antibacterial test results for control (virgin PCL), C1, C2 and C3 samples against S. aureus, MRSA, E. coli and E. faecalis bacteria species (* $p < 0.05$).

Antibacterial test results were also investigated microscopically via SEM (**Figure 5.14**). SEM micrographs support the results obtained by the antibacterial test results. (**Figure 5.14 A-E-I-M**) shows the PCL control group against S*. aureus, MRSA, E. coli* and *E. faecalis* strains, respectively. In these micrographs (**Figure 5.14 A-E-I-M**) shows that bacterial species adhere to the fibre structures at higher numbers compared to the C1, C2 and C3 sample groups for each tested bacterial species. Additionally, in the control groups, the adhered bacterial cells managed to colonise, but the cells on C1, C2 and C3 sample groups showed random and rare colonies with fewer cell numbers than which have been shown in (**Figure 5.14 B-C-D-F-G-H-N-O-P**)

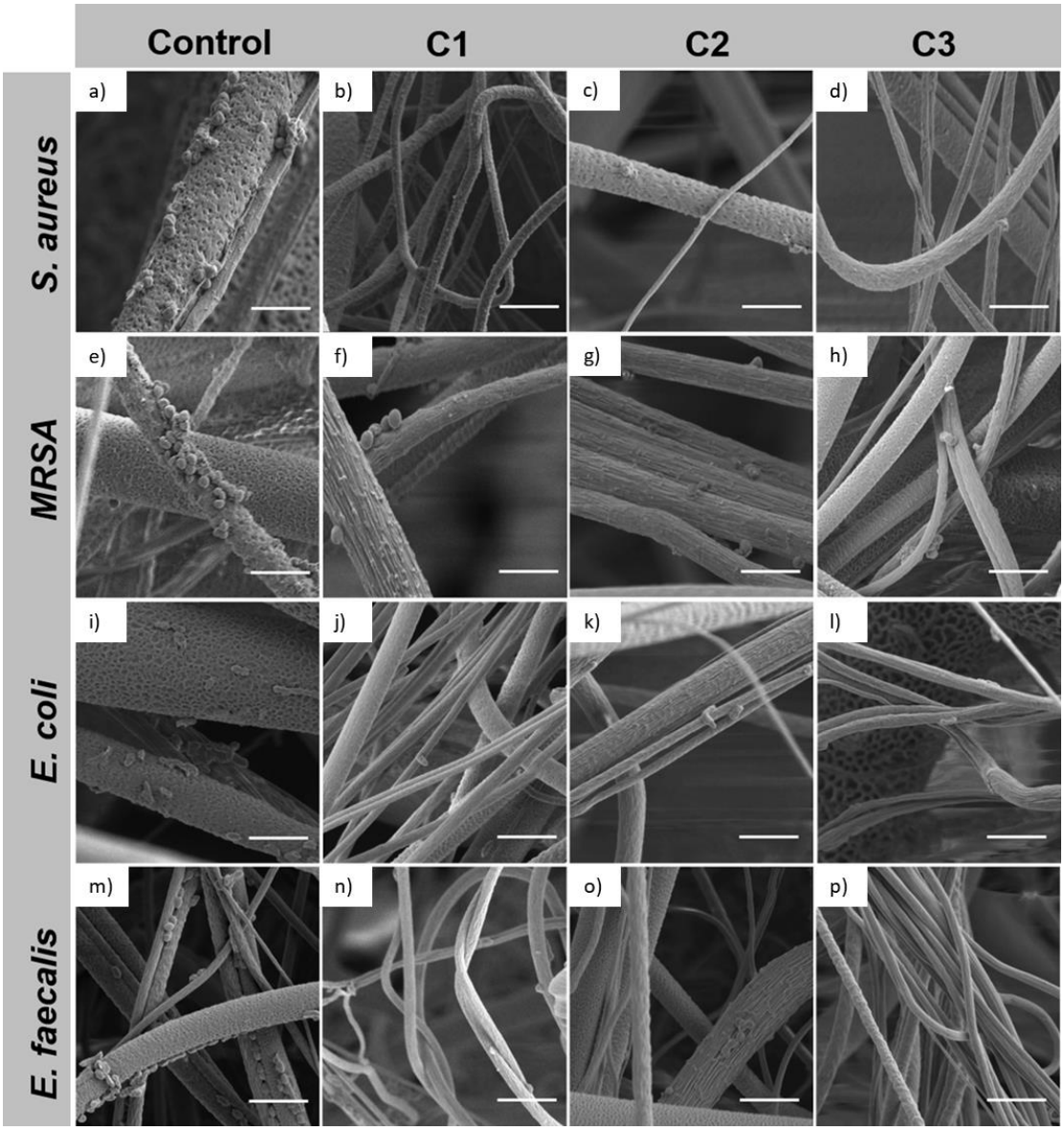

Figure 5.14: Antibacterial test results captured by scanning electron micrographs for the control (virgin PCL), C1, C2 and C3 samples against S. aureus, MRSA, E. coli and E. faecalis species. For each micrograph, the scalebar corresponds to 5 µm.

The results showed that cinnamon extract containing PCL fibres successfully exhibited antibacterial activity for both gram-negative and gram-positive species. Additionally, *E. coli, a* gram-negative species, showed a statistically significant decrease in the viable cell number but was not as great when compared to the gram-positive species. This result can be explained by the differences between the cell membranes of the bacterial species. Since the bacterial membrane of gram-negative species are thicker than the positive

counterparts as they have the lipopolysaccharide peptidoglycan cell membrane [494]. The antibacterial mechanism of cinnamon is via disruption of the bacterial cell wall and subsequent penetration through the cell wall to demolish the cytoplasmic membrane [495, 496]. The antibacterial activity of cinnamon has long been studied in the literature, especially concerning food and cosmetic applications [497, 498]. Cinnamon-extracted and other spice-extraction methods have not been translated into the production of polymeric biodegradable bandages before. Synthetic compounds can have detrimental environmental impacts in the long run such as the large necessity for crude oil, toxic run-off and non-degradable release mechanisms. The work here validates the viable means of producing antibacterial biomaterials that have high antimicrobial efficacy, whilst remaining within safety limits and offering to be more environmentally responsible and cytocompatible than synthetic approaches.

Chapter 6 : Advancements in Manufacturing Technologies and Materials Selection

6.1 Bandage Production with Novel Manufacturing Approaches

6.1.1 Bandage Production

The produced bandages and patches were analysed under high magnification microscopy to understand the fibre morphology which is closely related to its function as a bandage in a wound healing environment. The PCL fibres (**Figure 6.1**) acted as the bulk portion of the bandages, which wouldn't necessarily come into contact with the open wound, but high-quality fibres would be beneficial in maintaining a good wound environment.

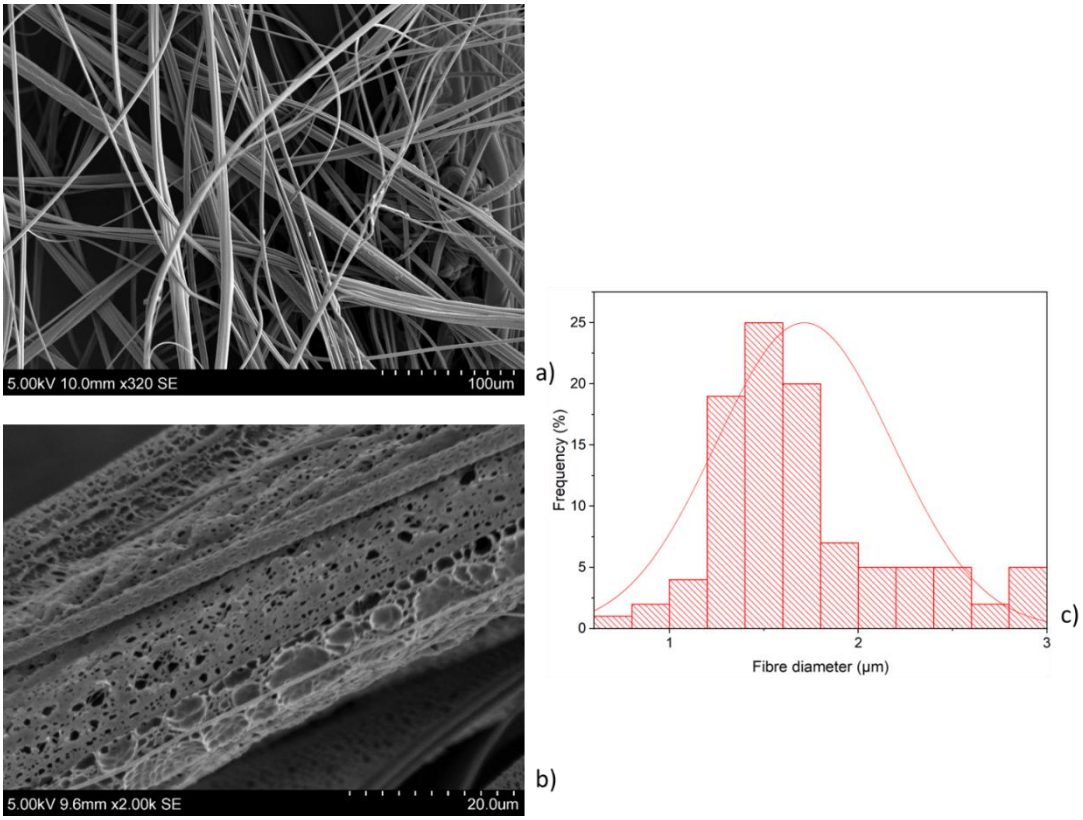

Figure 6.1: a), b) high magnification scanning electron micrographs of PCL fibrous bandages; c) fibre diameter distribution graph for the corresponding micrographs.

The bulk material of the produced bandages was produced using PCL which has many favourable properties for its applications in wound healing. Functional wound dressings should be able to separate the wound site from the external environment whilst being able to promote haemostasis and limit tissue oedema through external compression [499]. PCL is a flexible, biodegradable and biocompatible polymer that can tolerate the forces that occur at a wound site whilst also being non-toxic to cells of responding to the trauma caused by injury [12, 500, 501].

The images from (**Figure 6.1**) show the microstructure of the produced PCL bandages. It can be seen that the resulting fibres are very thin and have an average fibre diameter of 1.71 ± 0.47 µm. The significance of having low diameter fibres are that they have a very high surface area to volume ratio which can be useful in cellular interactions at the wound site where additional binding sites can be made available [502]. Also, from the fibre distribution

graph of (**Figure 6.1**)**,** it is evident that these fibres are very uniform in their thicknesses which will allow for predictable results from patient to patient.

From the structure of these bandages, it can be seen that the profile of these bandages appear cross-woven, this structure not only reinforces the strength and flexibility of the bandages but the perforations allow for exudate to flow in and out of the area surrounding the wound site, an essential consideration of wound healing materials [486]. The flexibility and tensile strength of PCL is significant for its use as a bandage, high tensile strength allows the material to withstand the strains the bandage will endure as a dressing, whilst also being flexible enough to be applied to uneven surfaces such as the knee. From closer inspection of the PCL fibres, it is seen that the fibres contain many nanopores on the surface which is a result of rapid solvent evaporation [121]. Having pores further increases available surface area of the fibres (**Figure 6.1 b**), additionally pore size can influence the rate of cell proliferation and migration on wound healing, which can determine the length of the recovery period [503].

The PCL bandages presented here offer potential use as non-adhesive and non-absorbent wound dressings which will prevent the adhesion of the bandages on the wound bed that can cause pain and damage upon removal. Furthermore, these bandages are semi-occlusive, meaning that they can maintain a moist wound environment which has been shown to enhance wound healing [499, 504, 505]. Given that these bandages are also biodegradable, in the event of epidermal growth into the bandages, the fibres will act as an external scaffold and can later be degraded as a function of time, avoiding any potentially harmful removal.

6.1.2 Collagen and Chitosan Patches

The active fibrous patch was fabricated by using PEO as the carrier polymer and contained 17% collagen and 7% chitosan by total mass. These fibres can be directly spun onto the bandages using templates to ensure a uniform and level deposition. These patches (**Figure 6.2**) come directly into contact with

the wound environment and so the fibre morphology is a key aspect of cellular interaction and wound healing.

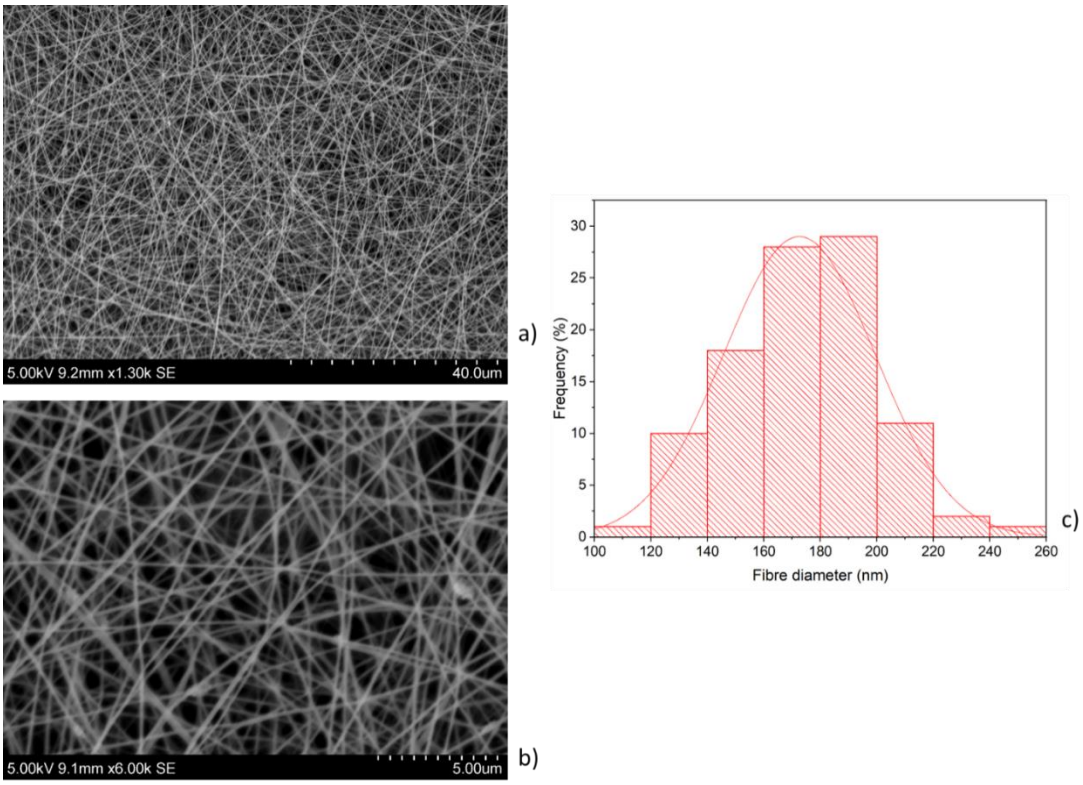

Figure 6.2: a), b) high magnification scanning electron micrographs of: PEO fibres loaded with collagen and chitosan within the polymer matrix; c) fibre diameter distribution graph for the corresponding micrographs

Having an active area that will come into contact with the wound site, avoids the use of expensive materials in the bulk bandage and allows for special constituents to be used only in the necessary area. The incorporation of collagen into a wound site has been shown to promote favourable attachment and proliferation of cells such as fibroblasts and keratinocytes which can help to accelerate wound healing and demonstrate a better healed final result [30, 506]. Additionally, the combination of chitosan and collagen into the active site is set to encourage higher quality and rate of wound healing. Chitosan is used as a healing accelerator in veterinary medicine, where it can enhance the functions of the inflammatory cells of the wound response, as well as enhance the production of macrophages, growth factors and fibroblasts [507-509].

The produced fibrous patch made of PEO is shown in (**Figure 6.2**)**.** The average diameter for these fibres is 173 ± 27 nm, proving that they are incredibly thin and uniform in their distribution. Furthermore, the structure of these fibres resembles the extracellular matrix, the cross-woven morphology allows multiple layers where cells can attach and proliferate. Extracellular matrix plays a crucial role in facilitating wound healing, where its components such as collagen, elastin and other glycoproteins regulate functions such as protein synthesis and degradation which is crucial in the repair process [510, 511]. The included collagen will act as a collagen reserve which can promote cells of the wound healing process such as fibroblasts, macrophages and keratinocytes to infiltrate and continue the recovery stages. The chitosan within the patch also can promote rapid healing, these two components work together for optimal wound recovery. Both components, collagen and chitosan are completely biocompatible and are easily degraded into safe products in the body. The carrier polymer (PEO) is also water-soluble, allowing to keep the patch moist in a wound environment.

Having small diameter fibres allows not only for a high surface area but in this case, allows for a small mesh size of the patch. This will keep the wound bed isolated from the external environment and help reduce cases of infections for the patients. Furthermore, chitosan naturally exhibits good antimicrobial properties, which only adds value for use as wound healing bandages [512-514].

6.1.3 Collagen, Chitosan and Antimicrobial Nanoparticles Patches

Additional fibrous patches were created containing collagen and chitosan, but also antimicrobial nanoparticles (**Figure 6.3**). With the addition of antimicrobial nanoparticles, it is expected that the bandages will have a higher level of antimicrobial action and help prevent infections in wound healing environments. These fibres were also spun using PEO as the carrier polymer and contained 19% collagen, 13% chitosan and 1% antimicrobial nanoparticles by mass. This composition contained the highest mass of collagen and chitosan together to form fibres, due to their effect on the solution

conductivity, these two components are difficult to form together in large quantities [515].

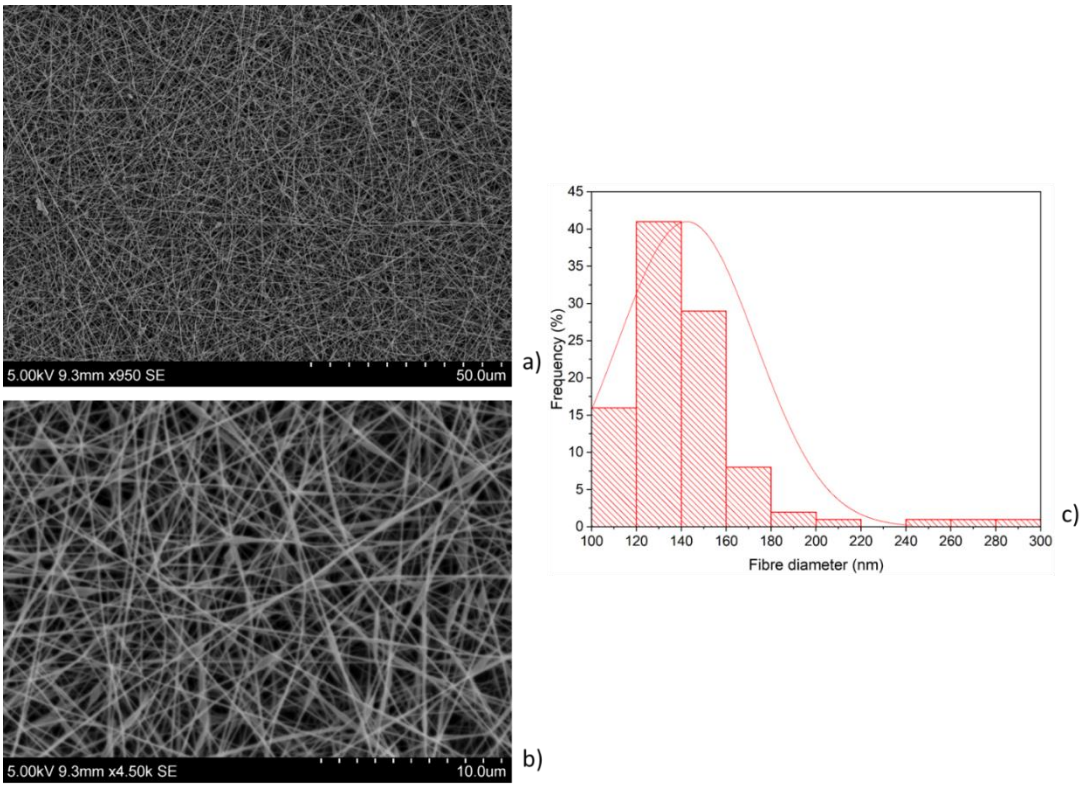

Figure 6.3: a), b) high magnification scanning electron micrographs of: PEO fibres loaded with collagen, chitosan and antimicrobial nanoparticles; c) fibre diameter distribution graph for the corresponding micrographs.

Antimicrobial nanoparticles containing metallic particles of antimicrobial metals such as copper, zinc and silver have been successfully used in applications with very high kill rates [394, 516, 517]. The addition of these nanoparticles within the active patch allows for extensive protection against pathogens which serve to cause infections or cause disruption to cellular interactions during wound healing.

The produced fibrous patch had an average fibre diameter of 142 ± 31 nm, proving once again that these patches are capable of being produced into very fine structures with a high degree of uniformity. The structure of these fibres again closely resembles that of the extracellular matrix which should allow the cells to attach and proliferate accordingly to continue the wound healing

process. The closely packed nature of these fibres will serve as a protective barrier for infections against the wound site, coupled with the ability of the AMNP to mechanically kill the invading pathogens, these patches have great potential as antimicrobial wound care materials. Furthermore, the ability to incorporate additives such as AMNP opens the possibility to add compounds within the patch that will contribute to a much more effective healing process.

6.2 Gyratory Fibre Production with an Updated Vessel Design

The updated design (P1) was compared to the original vessel design (P0), (**Figure 3.3**) shows a comparison in their size and design. Differences were expected to be seen in the fibre formation due to the differences in mass (35g for P1 and 53g for P0), dimensions of the vessels (600 x 300 mm for P0 vs 660 x 340 mm for P0) and the pronounced curvature of the wall for the P1 design.

As has been already established, the physical properties of a polymer solution have a direct effect on how it is manipulated under the various forces of the pressurised gyration vessel. In this study, the same solvent was used, and similar concentrations of the polymer were also, to make the results more comparable. (**Table 7**) shows the physical properties of these polymer solutions, in particular the surface tension and viscosity which can be used to elucidate some of the differences in fibre morphology following the spinning process.

Table 7: Solution properties of the three polymer solutions used in this study, all dissolved in chloroform.

Polymer Solution	Surface Tension (mN m^{-1})	Viscosity (mPa s)
PCL (15%)	36.7 ± 0.2	3575 ± 56
PLA (15%)	51.2 ± 0.3	4235 ± 36
PMMA (20%)	28.7 ± 0.1	680 ± 21

PCL, PLA and PMMA polymer solutions were spun with the P0 pot and the P1 pot, the SEM micrographs given in (**Figure 6.4**) highlight the general fibre morphology and also the fibre diameter distribution. Comparing P0 with P1, there are both differences in fibre morphology and their corresponding diameters. At zero additional gas pressure, PCL fibres show a remarkable improvement in their thicknesses, uniformity and alignment as can be seen in (**Figure 6.4 a)** and **g)**). With the updated P1 design, the fibres are seen to become highly uniaxially aligned, which can make them especially suitable for nerve tissue engineering applications and in cellular guidance for wound healing applications [518, 519]. The average fibre diameter and their uniformity have also dropped significantly from 7.5 ± 2.4 μm to 3.5 ± 1.3 μm. This difference is likely due to the aforementioned differences in the pot designs. The updated pot is over a third lighter in its mass, allowing the motor to achieve its maximum velocity in a shorter timeframe. It has been noted that the elongated start-up time of the motor is the cause for non-uniformity in the fibre production due to lower rotational speeds having a lower centrifugal force impacting onto the polymer solution, thus producing thicker fibres. The lower mass of the P1 pot allows for higher rotational speeds to be achieved, producing thinner overall fibres.

Further comparing PLA and PMMA fibres spun at zero additional pressure with both pot designs, differences are consistently seen in the reduction of average fibre diameter and its corresponding uniformity. The average fibre diameter for PLA fibres drops from 8.1 ± 4.0 μm to 6.4 ± 3.7 μm and the average fibre diameter for the PMMA fibres drops slightly from 1.4 ± 0.9 μm to 1.3 ± 0.7 μm. The drop in fibre diameter for the PMMA fibres is not significant, indicating that this low viscosity solution is already operating at its limit in the gyration vessel and a further reduction in diameter will require much larger changes in centrifugal force. Thinner fibres are highly desirable in many applications due to the increase in surface area to volume ratio. PCL and PLA polymer solutions generally produce thicker fibres due to the much higher viscosities, however by using updated vessel designs, the diameter of these fibres can be reduced.

The fibres from the P1 pot differ in the extent of their alignment. P1 produced fibres are significantly more uniaxially aligned for all the tested polymer solutions when no additional gas pressure is applied. However, further differences in fibre morphology are not observed. For example, all the fibre samples still possess surface nanopores, which is a direct result of using a volatile solvent such as chloroform. Also, the PMMA fibres retain their bead-on-string morphology, likely due to their very low surface tension which can cause irregular ejection of the polymer solution as the polymer easily escapes the vessel orifices, even at lower rotational speeds [520].

At no additional gas pressure into the vessel, the forces acting onto the polymer solution will act on the liquid-air interface where the air remains more or less constant in volume inside the vessel without a direct means for replenishment. Therefore, the impact on additional applied gas pressure is crucial in understanding the implications of pressurised gyration on the two pot designs. (**Figure 6.5**) shows the SEM micrographs of all the tested polymers at 0.1 MPa of additional gas pressure.

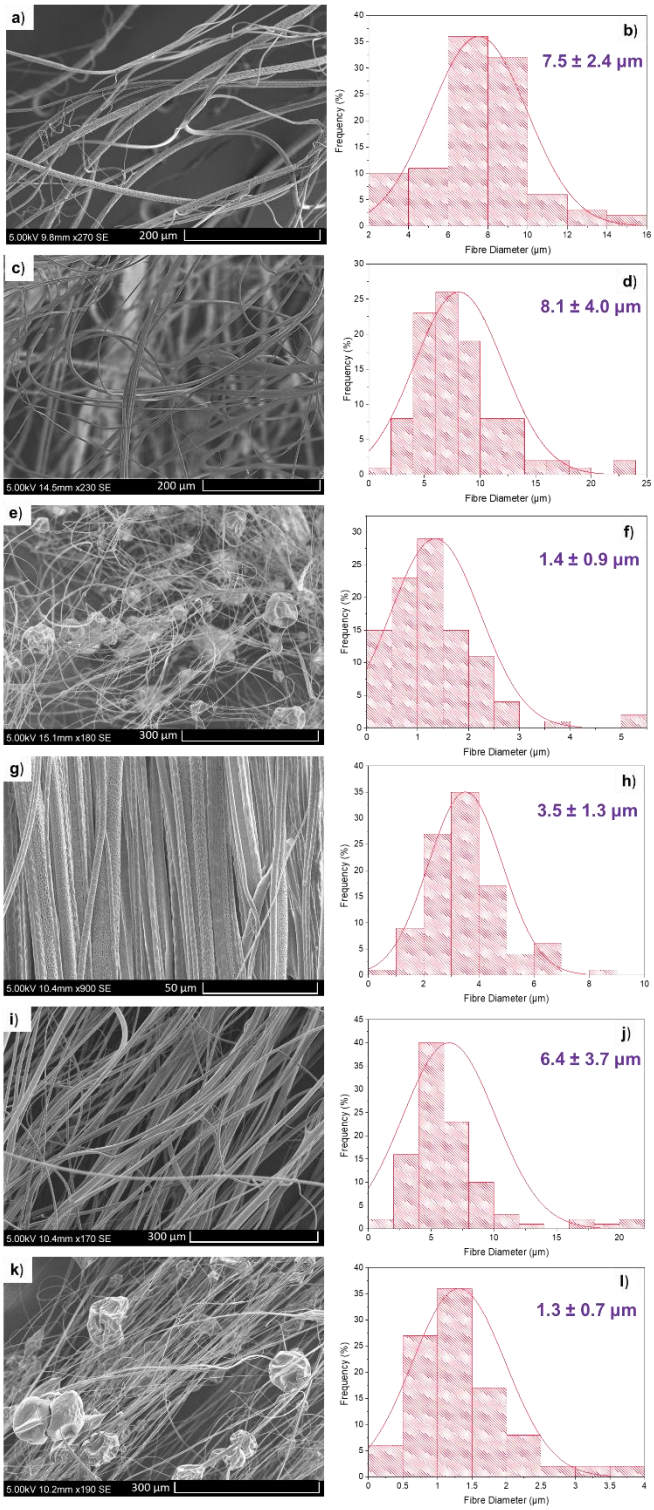

Figure 6.4: SEM micrographs of: a) PCL, c) PLA and e) PMMA fibres spun at 0.0 MPa additional gas pressure with the P0 pot design, g) PCL, i) PLA and k) PMMA fibres spun at 0.0 MPa additional gas pressure with the P0 pot design. b),d), f), h), j) and l) are fibre diameter distributions to the corresponding SEM micrographs.

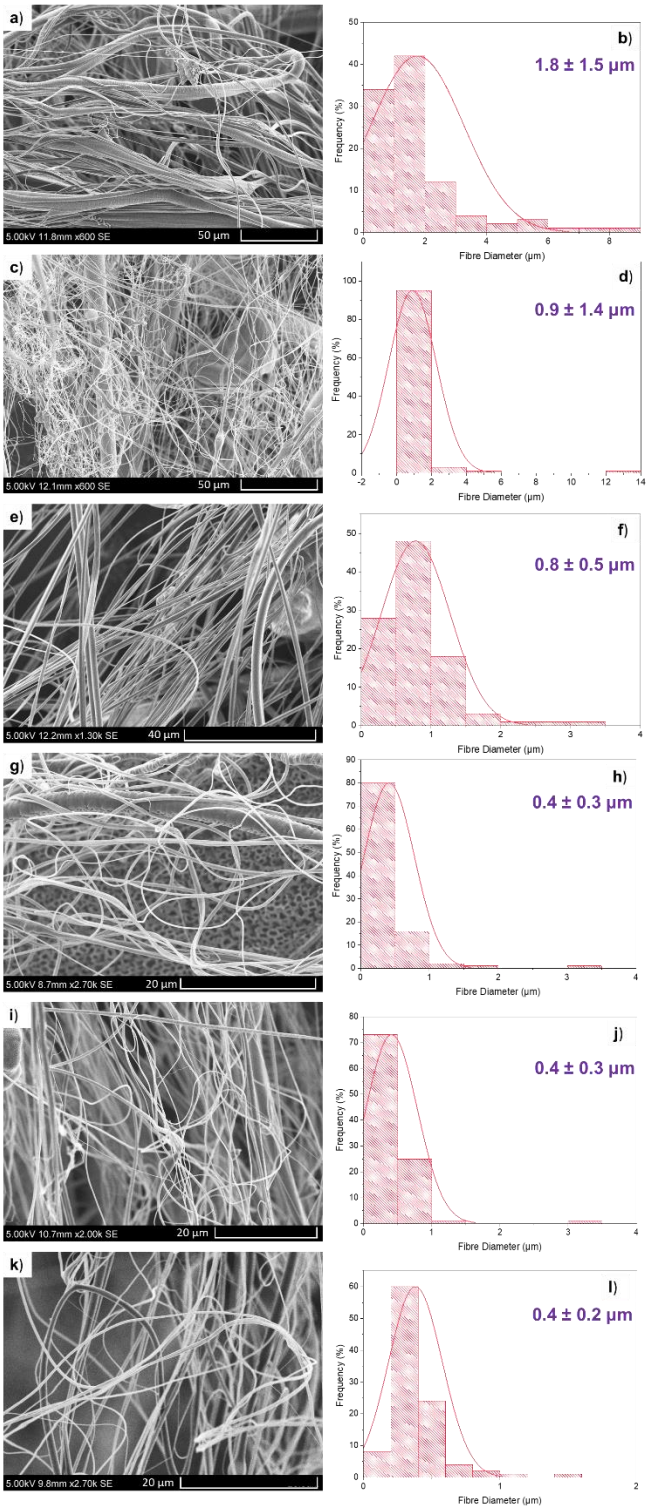

Figure 6.5: SEM micrographs of: a) PCL, c) PLA and e) PMMA fibres spun at 0.1 MPa additional gas pressure with the P1 pot design, g) PCL, i) PLA and k) PMMA fibres spun at 0.1 MPa additional gas pressure with the P0 pot design. b),d), f), h), j) and l) are fibre diameter distributions to the corresponding SEM micrographs.

Comparing the PCL fibres spun at additional gas pressure, we can again see discernible differences in the fibre diameter and distribution. (**Figure 6.5 a)** and **g)**) show PCL fibres which drop significantly in fibre diameter from 1.8 ± 1.5 μm to 0.4 ± 0.3 μm. The addition of gas pressure does cause a significant decline in average fibre diameter for the PCL fibres, even for the P0 pot, showing again that high viscosity solutions can be made to produce thinner fibres with better management of the air-liquid interactions. The P1 pot manages to reduce the average diameter further as compared to the P0 pot, likely due to the curved walls handling the manipulation of the air inside the vessel more uniformly. PLA fibres are thinner also with the P1 design compared to the P0 design, dropping from 0.9 ± 1.4 μm to 0.4 ± 0.3 μm. However similar to beforehand, PMMA fibres do not show any significant differences in diameter, likely due to the already low viscosity and surface tension of the solutions.

The infusion of the gas pressure has an effect on the alignment of the fibres. All samples appear to have similar degree of alignment, which is to say that they are mostly uniaxial, with some random settling of fibres. The addition of gas pressure levels out the differences between the alignment of both pot designs. In order to achieve more aligned fibres, the collector has to be redesigned to allow for uniaxially aligned fibres.

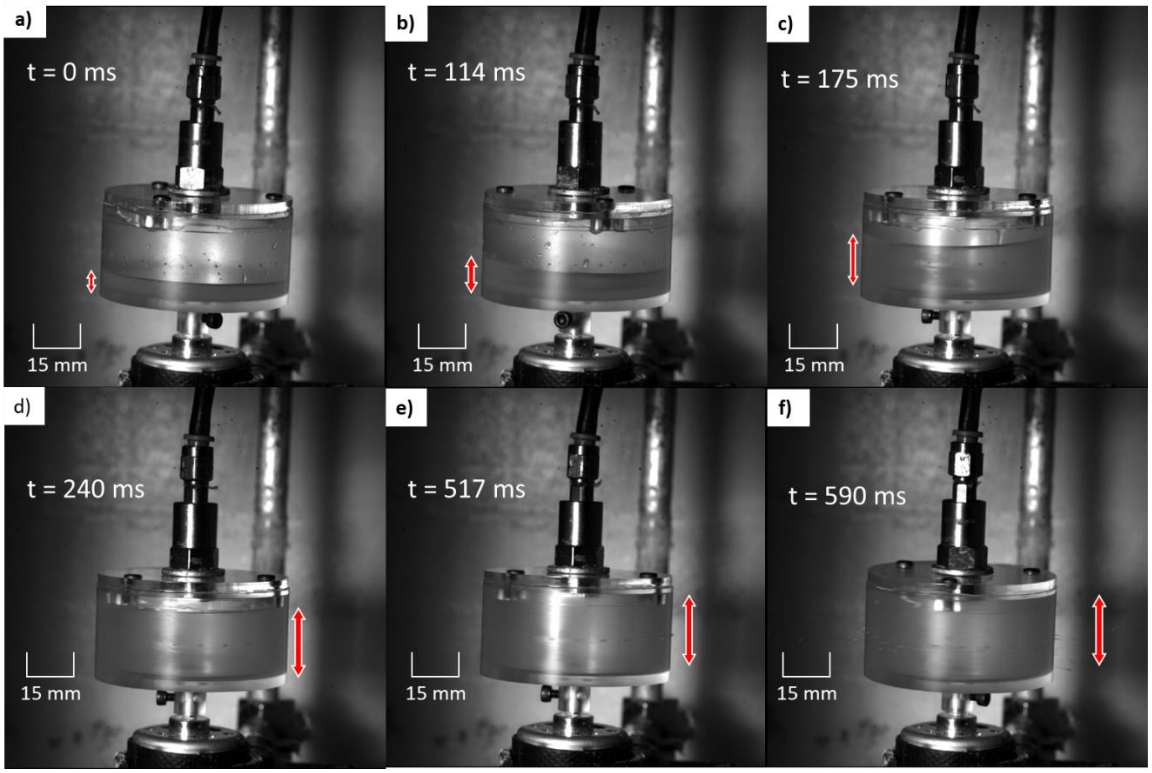

Figure 6.6: High speed video camera snapshots of a transparent gyration pot with the original P0 design. a) – f) shows 6 frames from when t=0 after the gyration motor starts to t= 590 ms when the fibre generation begins.

The increased height of the P1 pot as compared to the P0 pot can impact the performance of fibre production. For testing the internal kinematics of the polymer solution within the original P0 vessel, a transparent version was made out of acrylic and a high-speed camera was utilised to capture the interior interactions with the solution. It can be seen that a liquid-air interaction occurs in the pot, as the motor spins, there is an interaction between the air inside the vessel and the polymer solution, manipulating the solution, the greater the amount of air in the vessel, the higher the resultant forces ono the polymer solution. A larger volume therefore can be useful in producing thinner fibres, if the trade-off is not an increase in mass. The red arrows in (**Figure 6.6**) show the altitude of the polymer solution at various time points. At t=0 ms, the ratio of air to the solution is high, therefore the gyration of the vessel will cause a focus of forces at the liquid-air interface. The initial fill volume of the vessel, therefore, is required to be low for more optimised fibre production as the air

interacting with the polymer solution is responsible for its manipulation into a polymer jet, after overcoming its surface tension. At t= 114ms, we can see that the height of the polymer solution is increasing, still, at this point, the rotational speed of the motor is low, but it forces the polymer solution towards the wall. At t=175ms the polymer solution rises further, forced along the walls due to the centrifugal force. It should be noted that the air inside the vessel more or less remains at the same volume but is centred in the middle due to the various forces acting on it. The air can only decrease significantly in volume if there is enough force inside the vessels to compress it and allow it to leave the orifices. The exiting of the gas through the orifices also acts to expel the polymer solution out, however, at t=175ms, there is inadequate energy to overcome the surface of the polymer solution, responsible for preventing the escape of liquid.

At t=517 ms, the solution has risen the full length of the walls, but the surface tension of the polymer solution prevents it from escaping through the orifices. At t=590ms, the threshold limit of centrifugal force has exceeded the surface tension of the polymer solution and it begins to leave the orifice in the form of polymer jets. These jets in turn dry in the surrounding environment to produce fibres used for various applications. The high-speed camera footage shows that the height of the gyration pot is important for optimal production of fibres as it allows for a larger air: liquid ratio. Additionally, the curved walls of the P1 design are pivotal in uniform fibre production as kinetic energy is lost when the energy from the gyration motion forces the solution up the walls; in the P1 design, kinetic energy is maintained as the walls follow a naturally curved profile, similar to the earth’s globe. The globular shape of the P1 design could deal with vibrations more efficiently, as the P0 design can suffer from vibrations and movement when the polymer solution hits the walls as a result of the various forces, as mentioned before, the kinetic energy is preserved due to the curved walls.

6.3 Advanced Material Selection for Novel Wound Healing Approaches

The advancement of technological approaches to design and production can only progress the development of healthcare-related biomaterials so much without the constant discovery of novel materials and material combinations. To excel in this field, there is a necessity to investigate the promising properties of innovative materials which promise to be a suitable replacement for current standards.

Graphene is a monatomic sheet of carbon atoms that is found tightly packed in a hexagonal crystal lattice [521]. Graphene sheets are found to have new and unique properties such as being able to absorb a larger than normal fraction of incident white light (photoacoustic absorption of 2.3%), having very high thermal conductivity between 4840 to 5300 W/mK, the electrical conductivity of up to 2000 S/cm and a Young's modulus of over 1 TPa [10, 522, 523]. Because of these excellent properties relating especially to its optical, thermal, electrical and mechanical features, graphene is potentially a superior replacement medium for current industrial application standards, such as in semiconductors, electromagnetic shielding, healthcare, high-bandwidth wiring systems, fibre optics, material reinforcement and even heat dissipation for advanced hardware cooling [524-526].

Graphene oxide has recently been found to be antibacterial at certain concentrations, opening up the possibility to be used in wound dressings [527]. The antibacterial potential of graphene is of particular interest to many areas of biomedical engineering and wound healing because it has the potential to apply a long-lasting antibacterial effect. Traditionally, antibiotics rely on chemical disruptions to the cell wall of the pathogen which can prove to be infective in the long term due to resistant strains which rapidly adapt to develop defences for these chemical attacks. However, graphene and its derivatives have the innate ability to provide a mechanical deterrent to viruses and other microbes where its dagger-like protrusions can rupture pathogenic cell walls whilst being harmless to the larger cells found in the body. It is very difficult to

adapt to a physical force which kills microbes and therefore this technology has huge potential in wound healing and as coatings in commonly touched surfaces.

Porous graphene (PG), has recently been discovered to have refined properties compared to graphene due to the mesoporous nature and high specific surface area, which allows for diffusion of ions and molecules [528-530]. Highly porous graphene nanosheets are comprised of few-layered graphene sheets which benefit from high specific surface area, super hydrophobicity, optical transparency, good chemical stability and oxidation resistance [531]. In this section, porous graphene (PG) has been incorporated into a polycaprolactone polymer hybrid fibrous scaffold to target wound healing with a non-conventional approach [532].

6.3.1 Characterisation of Fibres

The production of PG-loaded fibres relies heavily on the produced polymer solutions. With higher loading of PG, solution behaviour is expected to deviate as the solution becomes more saturated by the dispersed PG. The PG sheets and the polymer were left to dissolve in tandem, allowing for the polymer chain to fully incorporate with the PG dispersion, for this reason, solution properties will have a discernible effect on the fibre morphology. Without the addition of PG, the average surface tension of the PCL solution was 27.8 mN/m, which is due to using chloroform as the solvent and which is in agreement with other studies [200, 533]. The addition of PG to the polymer solution results in a rise of surface tension from 27.8 to over 35 mN/m, this is likely due to the very high surface energy of carbon-based materials which increase the net inward cohesive force at the surface of the polymer solution [534, 535]. There is a slight increase in surface tension of the solutions with higher loading of PG, again likely due to the higher amount of high surface energy materials in the solution.

The concentration of the polymer solution often determines its viscosity, which is typically a proportional increase and therefore rises with higher

concentrations [536]. Addition of PG to the PCL solution results in the reduction of viscosity. This is a phenomenon that is not commonly seen; the increase in concentration generally leads to an increase in viscosity. One explanation for the reduction in polymer viscosity could be due to the presence of radical degeneration from the PG, this is when produced radicals react with the polymer backbone, resulting in the reduction of molecular weight [537]. A study into the viscosity of graphene oxide nanoparticles dispersed in water did not observe the reduction of viscosity with an increase in graphene concentration [538]. The study concluded that the viscosity was due to particle concentration and temperature, this suggests that the reduction in viscosity is due to the interaction of the PCL polymer backbone and PG. The unusually low viscosity of graphene has also been theorised to be due to the presence of electronic turbulence. The unique aspect ratio and dimensions of graphene nanoparticles allow them to behave irregularly compared with other nanoparticles [539]. Graphene nanoparticles reduce the intermolecular interaction within the solution, this could be attributed to the sliding of the nanoparticles which reduce the friction and therefore the measured viscosity. Another study found that by increasing the concentration of reduced graphene oxide, the resulting solution had a 3% reduction of its surface tension followed by a reduction in apparent viscosity [540]. The addition of PG into the polymer solution may also act as a secondary fluid which improves the hydrophobicity of the particles, this results in an increase in free water in the suspension that significantly reduces the viscosity and yield stress [541]. It is observed that higher loading of PG significantly reduces the viscosity of the polymer solution and at 5 wt%, the viscosity is less than half that of the original PCL solution.

High magnification images of the produced fibres allow for the study of fibre diameter distribution, fibre topography and alignment. (**Figure 6.7**) shows SEM micrographs of both the macro view of the fibre strands and higher magnification images of the fibre surface. From these images, diameter distribution histograms have been deduced which also show the uniformity of the fibres at concentrations.

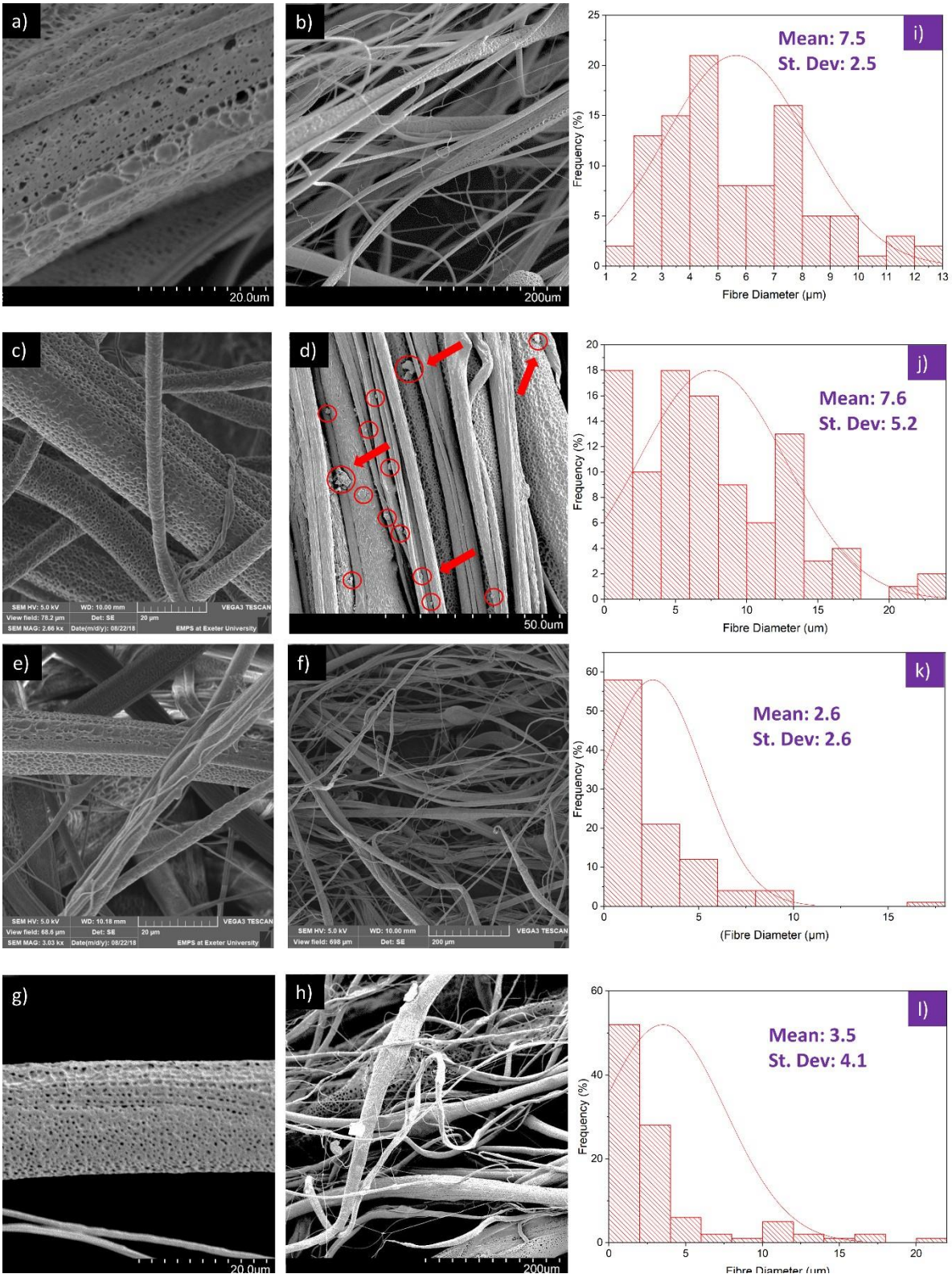

Figure 6.7: Scanning electron micrograph images of fibres; a), b) 15% pristine PCL fibres without the incorporation of PG, c), d) 3 wt% PG incorporated fibres showing surface porosity and unidirectional

alignment, red circles and arrows indicate the presence of surface particles e), f) 4 wt% PG incorporated fibres showing surface topography and random orientation alignment and g, h)) 5 wt % PG incorporated fibres with surface and full view, all images come with accompanying diameter distribution graphs, i), j), k) and l). For each graph, 100 fibre strands were measured at random.

Morphological features of fibres are largely due to the PCL-PG solution properties and the working parameters of the production process. Higher rotational speeds lead to a greater extension of the emerging polymer jet which leads to thinner deposited fibres [542]. The fibres presented here were all spun under the same working conditions to ensure that differences in morphology were due to solution characteristics only. Pristine PCL fibres had an average fibre diameter of 7 μm, owing to their high molecular weight and viscosity. (**Figure 2.1 a,b**), revealed that the fibres are mostly aligned unidirectionally which can be a benefit in electrical and optical systems where unidirectional reinforcement increases the front-to-back strength, but also in wound regeneration of nerve cells which require conduit-like guidance [543-545]. At 3 wt% PG, the fibre diameter remains similar to that of the pristine PCL fibres, and this is caused by the similarity in viscosity values.

As the viscosity of a polymer solution decreases, a downward trend of reduced fibre diameters is observed [546]. The 4 wt% fibres had a significantly lower viscosity and also had a substantially lower fibre diameter. At lower viscosities, there are fewer polymer chain entanglements and thus the emerging polymer jet is thinner [78]. However, at 5 wt% the fibres presented a slight increase in the average diameter, this could be due to the build-up of additional PG layers on the fibre surface, or the inconsistencies afforded by the low solution viscosity and polymer chain entanglement on the forming technique. Lower fibre diameters are favoured in wound healing applications as there is a higher available surface area for cellular interaction and guidance for reepithelisation.

All the fibres shown here have been observed to have a porous surface. These pores are the result of using a volatile compound (chloroform) as the solvent. As the chloroform evaporates rapidly, it causes a temperature difference on

the fibre surface which leads to condensation of droplets that then evaporate to leave behind nano to micro pores [121]. These pores can greatly increase the surface area to volume ratio making them suitable for applications in hydrogen storage materials for example, where the higher surface area will increase the hydrogen absorption capacity [547]. The pores can also provide a cellular niche for the attachment of many key cells of the wound response such as fibroblasts and other dermal cells. Furthermore, (**Figure 3d**) shows the 3 wt% fibres with particles on the surface. as indicated by red arrows and circles. These particles correspond with the micrographs of the PG, meaning that some of the graphene has been dispersed onto the surface of the fibre, potentially advantageous as biosensor components and in producing antimicrobial surfaces [4, 548-552].

The PG have pores in the size range of 3-5 nm and these characteristics have been discussed previously [399]. The fibres also contain surface pores due to solvent evaporation as discussed above and these pores were found to be about 500 nm in diameter, in some instances the pores penetrate deep into the fibre [121]. The surface pores are therefore beneficial in exposing the PG layers to the environment, which is useful in antimicrobial applications [553, 554].

6.3.2 Chemical Composition of Fibres

The Raman spectrum of the pristine PCL fibres is displayed in (**Figure 6.8**). Raman active bands and their corresponding positions are listed in (**Table 8**). CH_2 antisymmetric and symmetric stretching bands are known to be apparent at 2920 and 2868 cm^{-1}. The characteristic bands of PCL are seen at 1725 cm^{-1} and 1110 cm^{-1} and are designated to vC=O and vCOC, which reveal polymer crystallisation. A weak band at 1725 cm^{-1} and a strong band at 1735 cm^{-1} represent the crystalline and amorphous nature of PCL, as shown in (**Table 8**) [555]. A region of 1287–1306 cm^{-1} is assigned to coupled CH_2 wagging vibrations. Bands at 1440 (δCH_2) and 915 (vC–COO) cm^{-1} reveal the crystalline nature of PCL [556]. The decrease in band intensities at 1725 (vC =O; cryst.), 1442 (δCH_2; cryst.) and 1067 cm^{-1} (vCOC; cryst.) reveal the

development of amorphous segments near the surface [556, 557]. The band expansion within an amorphous nature and respective reduction in crystallinity represent the disordered morphology of PCL.

Table 8: Collected Raman bands (cm^{-1}) and their corresponding assignments for PCL-based graphene nanocomposite at 532 nm laser excitation [555-557].

PCL-Porous graphene-based composite Raman bands [cm^{-1}]			**Band assignment**
PCL-PG 3%	**PCL-PG 4%**	**PCL-PG 5%**	
869	877	872	ν(C–COO); amorph
956	957	950	ν(C–COO);
1099	1097	1090	ν(COC); amorph
1198	1287	1285	ω(CH_2); cryst
1306	1305	1309	ω(CH_2); cryst & amorph
1350	1356	1348	δ(CH_2)
1440	1446	1448	δ(CH_2); cryst
1576	1576	1616	δ(CH_2)
1728	1729	1731	ν(C═O); cryst
1733	1730	1736	ν(C═O); amorph
2893	2893	2875	ν(CH_2)
2930	2930	2929	C–H stretching ν(CH_2)

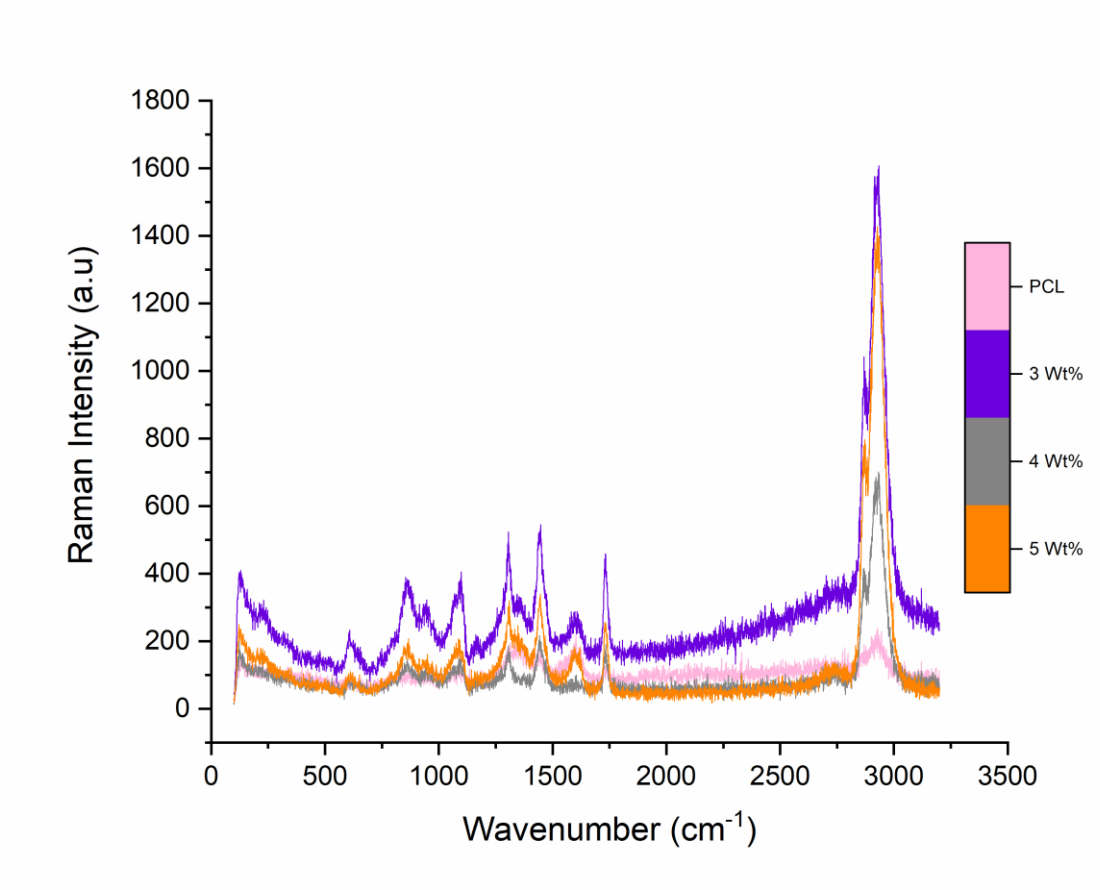

Figure 6.8: Raman spectra of 3,4 and 5 wt% PG-PCL composite fibres.

Raman spectroscopy showed distinct differences in crystallinity between the pristine PCL and the PG composite fibres. The characteristic graphene G-band peak at 1587 cm^{-1} using a 532nm excitation laser illustrates that the 3wt% and 4wt% PG composite fibres contain a single layer of graphene along their surface [558, 559]. As the G peak experiences a shift with additional layers of graphene, it is expected that 5wt% PG composite fibres contained more than a single layer of graphene, also supported by its larger apparent thickness [560]. Considering the changes expected in sp^2 hybridisation of PG during the fabrication process of composite fibres with pressurised gyration, Raman spectroscopy was used to study the defective structures of composite fibres. Raman spectra revealed that there is a shift in the vibrational bands of graphene, clearly showing that the graphene layers are in contact with the polymer. Furthermore, the considerable shift in the 2D Raman peak demonstrates that the composites were robust and that no interfacial issues were encountered.

XRD peaks of different concentrations of PG within the fibres revealed that the (002) peak of PG-loaded fibres was extended and had a decreased mode, showing that composites were comprised of single-layered graphene (**Figure 6.9**) [561]. The diffraction patterns of the composites show characteristic peaks of graphene and demonstrate that PG could play a role as an agent for polymer crystallisation.

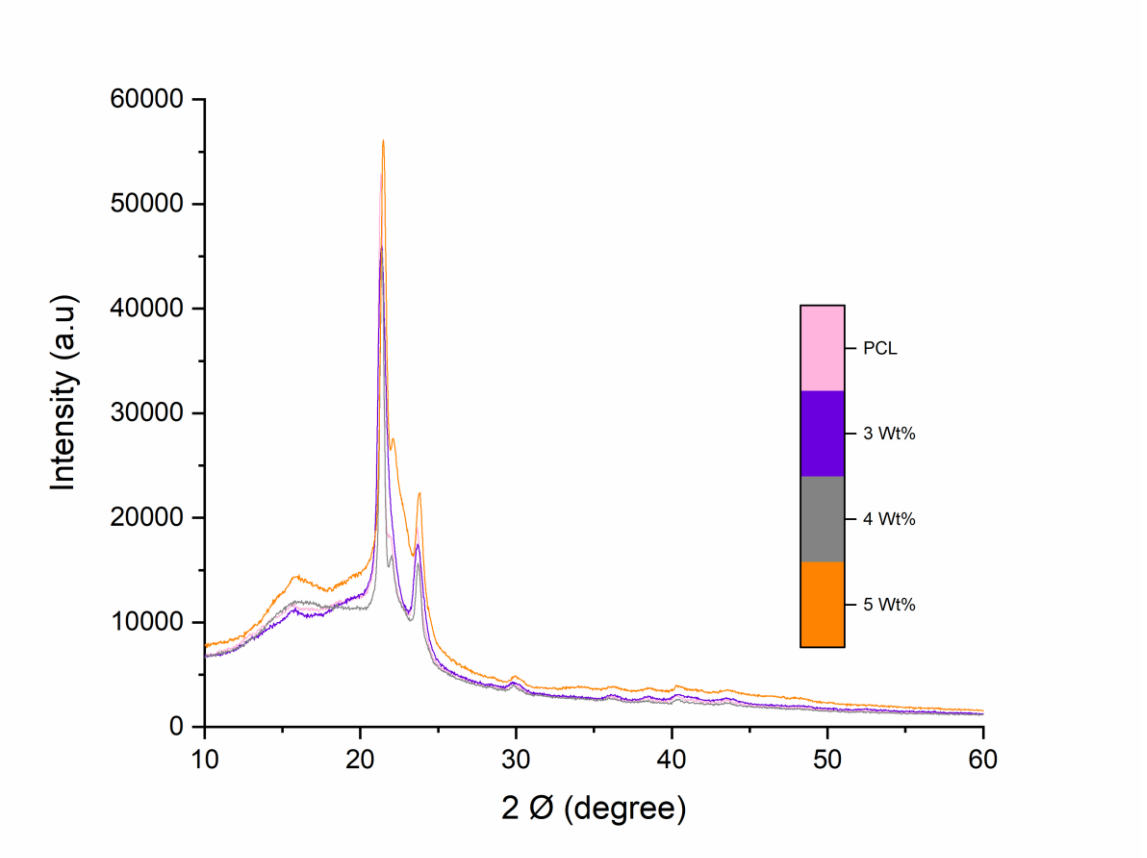

Figure 6.9: Fourier Transform Infrared (FTIR) spectra comparing the chemical compositions of pristine PCL fibres along with 3, 4 and 5 wt% PG-PCL fibres.

The FTIR spectrum of PG has been reported previously [399]. The distinct peaks of PG were at 1735 and 1072 cm^{-1} conforming to the C=O and C–O–C stretching vibrations from carbon and epoxy functional groups, respectively [401, 562]. (**Figure 6.10**) demonstrates the FTIR spectra of PCL and PG-loaded PCL. PCL showed a peak near 3500 cm^{-1} and a strong band at 1745 cm^{-1}, corresponding to hydroxyl and ester functional groups, respectively. The other distinct peaks of PCL were asymmetric and symmetric CH_2 bonds

corresponding to bands at 2940 and 2860 cm^{-1}, respectively [563]. The FTIR spectra of PG-loaded PCL showed a significant sharpness at 3500 cm^{-1} referring to OH groups coming from PG molecules and reduction in the intensity at 1700 cm^{-1} and confirmed the increase of PG molecule covalent coupling onto the surface of PCL [564]. FTIR has been used to analyse the interconnected features of PG-polymer composite fibres and to study the cross-linking of functional groups such as OH, CO, COC and other epoxy groups from PG edges to fibres. PG-fibres demonstrate the reordering of bonding in their networks. FTIR analysis of fibres further demonstrates the robustness of fibres and also the cross-linking of PG to fibres at correct ratios.

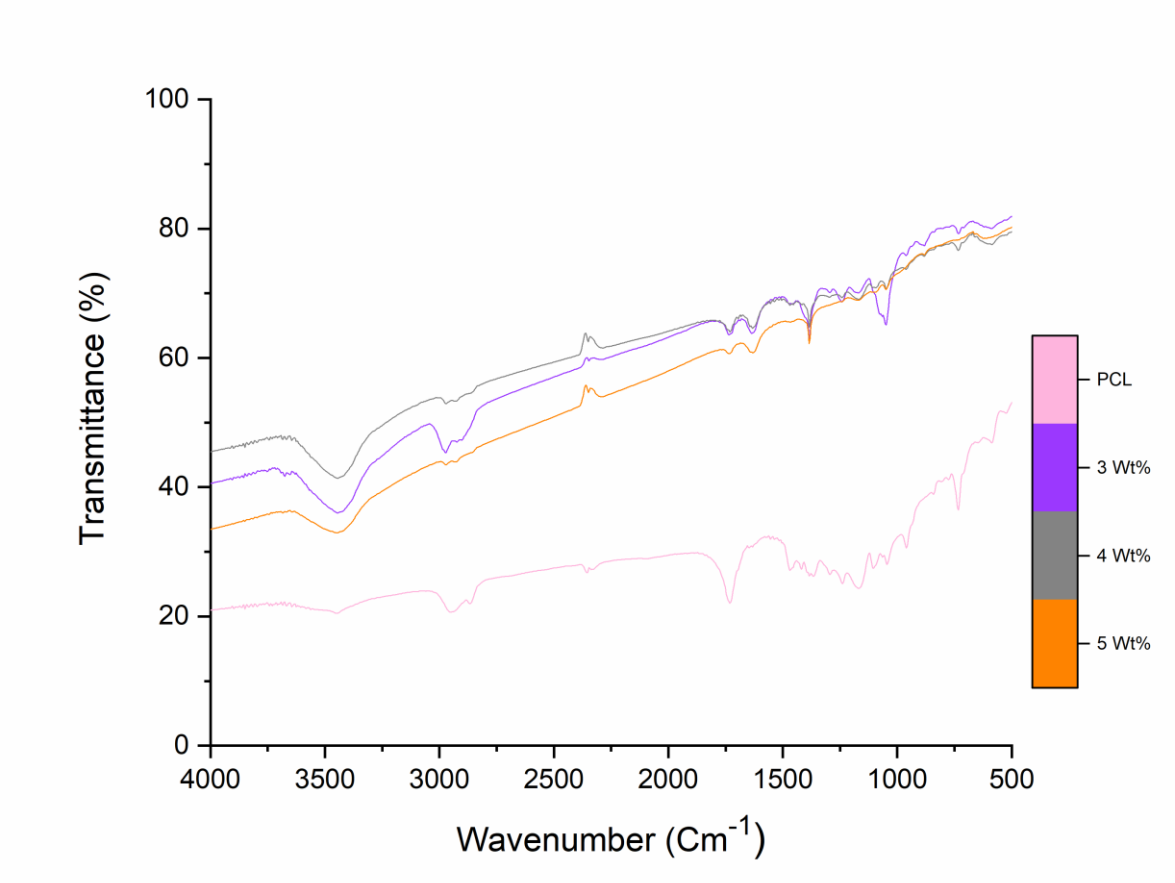

Figure 6.10: Fourier Transform Infrared (FTIR) spectra comparing the chemical compositions of pristine PCL fibres along with 3, 4 and 5 wt% PG-PCL fibres.

The combination of the analysis techniques showed that PG was successfully incorporated into the PCL solution and was able to form fibres. These assemblies, as seen from SEM images, were correctly identified as fibres that differed in fibre diameter distribution ranges but ultimately all had surface pores. Raman studies and XRD analysis alluded to the single-layer formation of graphene being present on the fibres. FTIR spectroscopy confirmed the presence of graphene on the composite samples and established that higher loading of PG in the polymer solutions lead to higher and more successful incorporation of graphene into the fibres. These graphene-based composite fibres could be utilised to release and store pharmaceuticals, genetic material, biological molecules, and can be used in biosensing, the treatment of many diseases, also these can be used in wound healing and to treat viral infections. The antimicrobial properties of these constructs have not yet been tested for, but this work shows the benefit of such fibres in wound healing.

Chapter 7 : Conclusions and Future work

7.1 Conclusions

Having an in-depth understanding of the manufacturing processes that can deliver materials-based healthcare is crucial in producing functional biomaterials for wound healing. In this thesis, the aim was to carry out experimental research into which factors influence fibre production and the subsequent production of bioactive wound-healing fibrous constructs. In this section, some concluding remarks are given for each experimental segment.

7.1.1 The effects of Solution and Working Parameters in Fibre Production

7.1.1.1. The effect of polymer solution solubility on fibre morphology

With any solution-based fibre manufacturing technology such as electrospinning and pressurised gyration, the final fibre morphology is heavily dependent on how the polymer solution was prepared. The effect of solubility is therefore a key component to consider when designing fibrous products. As different solvents and polymers have varying levels of compatibility with their solubility parameters, this can have a large effect on how the polymer solution is formed, the degree of polymer chain entanglement and even its physical characteristics.

The choice of solvent is always a compromise between the solubility of the solute and its environmental impact, where solvents with high solubilising power, may be more toxic. A single polymer such as polycaprolactone will be soluble in a wide range of organic solvents, but each solvent will vary greatly in properties such as volatility, vapour pressure and solubility parameters. The viscosity and surface tension values of the final polymer solution, as a result, differ based on the choice of solvent. This difference in the physical properties of the polymer solution will affect the fibre morphology. Solvents with low volatility resulted in less-aligned fibres, due to the increased time required for

evaporation. This knowledge of the polymer-solvent systems allows for the prediction of fibre diameter and morphology which has huge implications in biomedical applications.

7.1.1.2. The effect of polymer physical properties on fibre morphology

The choice of solvent as mentioned before affects the physical properties of any given polymer solution. However, other factors can also influence the surface tension and viscosity, which include the concentration of the polymer solution, the molecular weight of the polymer and the degree of polymer chain entanglement. There is a direct relationship between the viscosity of the polymer and the average diameter of the final fibres. An increase in polymer chain entanglement causes an increase in solution viscosity, a minimum level of entanglement is required for fibre formation, but beyond this, fibres are produced thicker. During the fibre manufacturing process, more viscous polymer solutions require greater energy to form the polymer jet, so at any given working condition, the jet will thin less, resulting in thicker fibre production.

Additionally, the surface tension of the polymer solution can have a marked impact on final fibre morphology. This value can be determined by the choice of solvent. During pressurised gyration, the centrifugal force and the applied gas pressure must exceed the surface tension of the polymer solution for the polymer jet to be formed, in electrospinning this force is the applied electrical voltage. A polymer solution with a higher surface tension value will therefore resist these forces to a greater degree and will typically yield on average, thicker fibres. It was also found that the surface tension of the polymer solution affects bead-on-string morphology as well as the vapour pressure affecting surface nano pores. It is therefore beneficial to both measure and study the effects of the polymer's physical properties, to make informed decisions in the design of custom-made fibres.

7.1.1.3. The effect of solvent choice on fibre morphology

Five different solvents were used to dissolve polycaprolactone at identical concentrations in the work and the resulting fibres were analysed for their

morphology. Each solvent produced fibres with distinctive properties. Fibres made from DMF and Toluene as the solvent showcased a highly beaded nature with very fine interconnected fibres. DCM and chloroform both have very similar surface tension values and thus produce similar morphologies when spun, as DCM is more volatile but similar in chemistry, the resulting fibres are thinner due to the rapid evaporation. Fibres spun with THF as the solvent display very fine and mostly unidirectionally aligned fibres, but also exhibit ribbon-like structures.

There is also a large discrepancy in the average fibre diameter of the different polymer solutions when the solvent is changed. For example, chloroform-produced fibres produced the thickest fibres by a large margin, whilst the less volatile solvents such as DMF and Toluene produced the thinnest fibres. Therefore, the volatility of the solvent, as well as the solubilising power of the solvent is important in the resulting fibre morphology. Whilst lower volatility can lead to an increased duration for polymer jet thinning, the solvents ability to produce polymer chain entanglements will determine the effective viscosity of the polymer solution. This knowledge and experimentation of solvent choice ultimately empower the fibre manufacturer to make decisions that will allow them to tailor-make their fibrous products.

7.1.1.4 The effect of applied gas pressure on fibre morphology

Pressurised gyration incorporates an additional applied gas pressure to overcome the surface tension and viscous forces of the polymer solution. Gas pressure allowed thinner fibres to be formed with this process, although higher pressures did not necessarily always lead to thinner fibres. At high pressures using organic solvents, the pressure can cause the polymer jet to widen, causing slightly thicker and fewer uniform fibres. This effect is not usually seen with water-based systems where the increase in applied pressure typically causes the average fibre diameter to reduce.

Gas pressure also significantly reduced the bead-on-string morphology in the polymer systems used in this work. This discovery allows fibres to be made from polymer solutions that would otherwise only produce highly-beaded structures, such as with electrospinning. Gas pressure is therefore an

important working parameter that allows for increased control over the final fibre morphology. The study of the effects of the applied gas pressure allows for the discovery of novel fibre morphologies.

7.1.1.5 Effect of binary and ternary polymer blends

As we have established that the polymer solution plays a vital role in fibre formation, polymers can be blended to display composite behaviours which provide extra control over fibre morphology and its mechanical properties in any intended biomedical application. The comprehensive investigation into blends of important biomedical polymers such as PLA and PCL for use in healthcare and wound healing applications shows the optimal composition for yield, morphology and bacterial cellulose content in bandage-like fibrous scaffolds. The results presented in this work highlight the possibility to achieve high loading of bacterial cellulose through binary and ternary polymeric composite systems.

By creating blends of PLA-PCL fibres, we can create a more suitable system in terms of yield and mechanical properties. It was found that the desired mechanical properties of important biomedical polymer could be increased by introducing polymer blends. For example, a 50:50 blend of PCL and PLA showed a double in ultimate tensile strength than just using PCL or PLA alone. It was also found that the stiffness of a polymer can be adjusted by introducing varying parts of PCL or PLA in the polymer blend. The work here demonstrates a promising outlook for the future of composite polymer blends and the effects of using binary and ternary systems for wound healing constructs with advanced manufacturing techniques.

7.1.2 Bandage production using natural materials

7.1.2.1 Antibacterial activity of Honey

Various forms of honey possess many health benefits which are not only limited to them exhibiting potent antimicrobial abilities. In this work, Black Forest Honeydew honey and Manuka honey was tested against *S. epidermidis* and *E. coli* bacterial species to discern their antibacterial efficacy against both

gram-positive and gram-negative strains. It was found that composite bandage-like fibres could be formed when these honey sources were combined with polycaprolactone polymer and spun by pressurised gyration. These composite fibres were then tested for their antibacterial ability. Both Black Forest Honeydew honey and Manuka honey showed bactericidal effects as indicated by the increased proportion of dead cells following incubation. It was found that at higher loadings of honey in the composite fibres, the bactericidal effect increased significantly. Overall, Manuka honey display higher levels of antibacterial activity and was thus selected as the focus of the study to produce and assess Manuka honey bandage-like composite fibres. This work confirms that honey has potent antibacterial abilities and by producing honey-polymer composite fibres, we can control the extent of its effectiveness against common infections.

7.1.2.2. Honey composite bandage-like fibres

Manuka Honey was chosen for its use as an antibacterial agent in wound healing constructs. Novel Manuka honey-PCL composite fibrous meshes were successfully prepared by pressurised gyration. These fibrous structures could act as a bandage to mechanically protect the wound environment whilst simultaneously proving an antibacterial setting. Pressurised gyration proved to be a successful route to mass-produce honey fibrous meshes able to be incorporated into bandages, these constructs have the benefit of high antibacterial activity, pro wound healing capabilities and a very high available surface area for cellular interactions. FTIR spectra of the different fibre samples confirm the presence of Manuka honey in the composite bandage-like fibres.

As the concentration of honey increased in the polymer solution from 0-30% (v/v), the viscosity increased significantly. Honey is well known to be a highly viscous substance and was not an exception in these polymer blends. However, although the viscosity of the resulting polymer solutions was very high, this had a reducing effect on the diameter of the produced fibres. The average diameter for the 10% honey composite fibres was 437 ± 21 nm, this unexpected steep and sudden drop in fibre diameter does not coincide with

normal trends where the increase in polymer viscosity leads to thicker formed fibres. The highly thick solution could have reduced the available orifice aperture of the gyration pot to subsequently cause thinner fibres to be extruded from the orifices. Therefore, the produced composite bandage-like fibres demonstrated much thinner fibres than the polycaprolactone fibres alone. The results here show that composite behaviour can be more unpredictable and that at a certain viscosity, the fibres produced may begin to be formed thinner, due to a reduction in orifice aperture size.

7.1.2.3 Antimicrobial ability of cinnamon

As with honey, cinnamon is another edible substance that displays antimicrobial properties. In this work, cinnamon was extracted with chloroform and made into a polycaprolactone polymer solution to be made into bandage-like fibres with pressurised gyration. The antifungal capability of cinnamon alone and the fibre samples was tested against *C. albicans* where inhibition areas were used to determine the effectiveness of each anti-fungal substance. All cinnamon-containing samples were found with a clear inhibition zone surrounding them, which indicated that these fibrous meshes were able to prevent the inward growth of *C. albicans.* By increasing the concentration of cinnamon extract within the fibres, even at the same weight, there is an increase in antifungal strength. From the results presented with the cinnamon work, it is apparent that the gyro spun cinnamon-extract-containing bandages have a strong anti-fungal effect. Compared with the negative control (Virgin PCL), there is a far greater inhibition area associated with these fibres. Cinnamon-loaded fibres had a strong anti-fungal activity that lasted more than 3 weeks, something that could not have been achieved if not in the fibre form. This work opens up the possibility for crude unpurified extracts of natural materials to be used in wound care and other anti-microbial filtering applications.

We also see that cinnamon-extract containing polymeric fibrous biomaterials can deliver significant antibacterial properties against *S. aureus*, MRSA, *E. coli* and *E. faecalis* species. These species frequently contribute to and cause

common hospital-acquired infections, which increases in prevalence in open wound environments, surgical operations, hernia and infected interocutaneous fistula.

7.1.2.4 Cytotoxicity of cinnamon bandage-like fibres

There is a concern when a substance has inherent antimicrobial ability, it may pose toxicity to the native cells of the body. Cytotoxicity tests showed that there is no toxic effect for either the virgin PCL gyro spun fibres nor the cinnamon-extracted fibres. It was observed that virgin PCL fibres showed 88.1 ± 6.7 % cell viability compared to the negative control (100 % cell). According to the ISO10993-5 standard, the cytotoxicity limit is 70 % cell viability where all our samples have results above this threshold value.

The spice-extract containing bandage-like materials do not display significant cytotoxicity and can thus be safely used as bandage materials to cover wounds and prevent infections, as a filter material for masks or even as a biomaterial. The production method and the tailorable nature of the production methods allow for precise control in manufacturing, leading to fibrous scaffold materials which can sustain the requirements of a good antibacterial biomaterial environment. Thinner diameter fibres can be produced to increase the available surface area for bioactivity and the release of beneficial pharmaceutical or medicinal ingredients. The ease of use, value and rapid manufacturing parameters will be the key to outstanding potential. The advantages of these natural cinnamon extract containing bandages are vast and pose as a contender to the future of bioactive biomaterials with a fibre-based architecture.

7.1.3 Advancements in Manufacturing Technologies and Materials Selection

7.1.3.1 Novel approaches to bandage production

This study has focused on two main fibre production techniques, pressurised gyration and electrospinning. Each technology will have its distinct advantages over the other, but the stagnation of development and discovery of novel techniques will only be a detriment to the manufacturing of advanced wound healing materials. To have greater control over fibre production, product yield and product characteristics, novel approaches to producing fibres or 3-dimensional meshes should be pursued.

For example, there have been many adaptations to the original electrospinning design to create setups with multiple needles for core-sheath designs, rotating collectors and increased control over specific working parameters. In the case of pressurised gyration, since 2013, there have been many improvements such as producing a system capable of producing core-sheath structures, melt gyration and pressure-coupled infusion gyration. This work, therefore, highlights the importance in the continual development of fibre manufacturing techniques and the symbiotic relationship it has with biomedical engineering.

7.1.3.2 Collagen and chitosan patches

As the population size increases, there is a greater number of people who require wound care, whether that being small cuts or large chronic wounds. The fact remains that there is an open market for bandages that can offer both wound acceleration and prevent infection. Most importantly, these bandages should be able to be produced at a large scale to lower prices to the end consumer. Strong, flexible bandages made of polycaprolactone have been successfully produced with a bioactive patch containing collagen, chitosan and antimicrobial nanoparticles. The resulting bandages contain the important bioactive materials, collagen and chitosan, whilst also providing a great cell niche for attachment, migration and proliferation of the cells of the wound response. With the additional incorporation of antimicrobial nanoparticles, these bandages prove to be highly suitable for bacterial rejection into the wound site.

Here I have shown a successful combination of two widely cited laboratory manufacturing techniques that can produce highly customisable bandages. The manufacturing of these materials shown here can be achieved with a high degree of automation, allowing for lower prices to be delivered to the targeted healthcare market. By utilising the strengths of each technique, higher production rates can be achieved, whilst also ensuring a highly reproducible intended mechanism of action for the bandages. Gyration techniques generally have a higher production rate, whilst electrospinning systems allow for very fine, uniform and precise fibre deposition. This manufacturing combination also has the potential for scalability as the bandages can be transported to a mechanical conveyor belt and the number of electrospinning needles can be increased for scalability. By ensuring that there is a constant supply of bandages from the gyration system, there can be many needles placed far apart from each other to exclude needle interferences. This new manufacturing combination has the potential to allow for the large-scale production of novel and advanced wound healing products.

7.1.3.3 Gyratory fibre production with an updated design

Work on the updated design for the pressurised gyration vessel (P1) has shown that small but thoughtful changes in the design of vital components can have a marked effect on the final fibre production. The updated design allows for finer and more uniform fibres to be produced from high viscosity polymer solutions. The average fibre diameter and their uniformity dropped significantly from the different design iterations. This difference is likely due to the aforementioned differences in the pot designs. The updated pot is over a third lighter in its mass, allowing the motor to achieve its maximum velocity in a shorter timeframe. It has been noted that the elongated start-up time of the motor is the cause for non-uniformity in the fibre production due to lower rotational speeds having a lower centrifugal force impacting onto the polymer solution, thus producing thicker fibres. The lighter mass of the pot allows for higher rotational speeds to be achieved, producing thinner overall fibres.

Designs such as this need to continually be made to excel in the field of materials-based healthcare for wound healing and other applications.

7.1.3.4 Conclusions

The originality in my research is that I have specifically contributed to the production of polymeric fibres using multiple techniques such as electrospinning and pressurised gyration, where I have optimised and improved upon their production efficiency by taking into consideration, how they operate as well as how different polymer systems work with these technologies. I have designed and implemented a fibre-production assembly which produces low-cost bioactive bandages that is able to focus on cost-effectiveness whilst maximising the bioactivity of the bandages. I have furthermore used multiple advanced characterisation techniques to assess the produced fibres and have personally conducted some antimicrobial testing to assess the efficacy of the fibrous products. Moreover, I have developed a new class of bandages which utilises extractions of highly abundant and environmentally friendly natural materials such as cinnamon to produce long-lasting antimicrobial protection with low cytotoxicity. These contributions are beneficial to understanding the link between manufacturing, engineering, and the real-world applications of such polymeric structures. This work therefore showcases an in-depth study into the proposed future direction which would be beneficial for biomedical engineering, focusing on sustainable and environmentally friendly production techniques and materials processing to make healthcare more accessible to the masses.

The novel discovery of materials becomes increasingly difficult but novel material combinations are almost limitless. By incorporating materials such as graphene which have many advantageous properties, there can be a forward shift in new approaches in wound care that may not seem obvious at first. There must therefore always be an encouragement for novel material combinations such as the porous graphene and polycaprolactone composite fibres shown in this work. In summary, this work shows the viability of using

polymeric fibre production techniques to produce scaffolds that can be used for advanced wound healing.

7.2 Future work and Limitations

The discoveries from this project show a wealth of knowledge surrounding the materials science and engineering behind producing functional biomaterials that are suitable for healthcare. From this extensive report, it has been elucidated how one may produce optimised fibrous scaffolds for these applications, however, the work is not complete, and it should provoke further research and development. Examples of potential further studies are detailed below.

7.2.1 Analyse non-major working parameters

Although the major working parameters such as solution flow rate, applied electrical voltage, rotation speed and applied gas pressure were investigated, there remain other non-essential parameters that can affect the final fibre morphology. For example, the collection temperature and relative humidity can greatly influence the evaporation time of the polymer solution and the subsequent fibre morphology. If this work were to be continued, there would be a thorough investigation of how temperature and relative humidity effects the polymer jet thinning during fibre formation in manufacturing techniques such as electrospinning and pressurised gyration.

Furthermore, parameters such as polymer fill volume may affect the fibre formation mechanism, as having more or less polymer solution volume within the gyration vessel results in a differing balance at the liquid-air interface. A large polymer volume within the vessel restricts the air intake, reducing the impact of centrifugal force on the polymer, this can result in thicker fibres being produced or droplets being formed. By experimenting with different polymer fill volumes and different infusion rates, we can increase the control over final fibre morphology.

Collection methods greatly determine final fibre morphology. In electrospinning, having a rotating mandrel, for example, allows highly uni-axially aligned fibres to be created. Collector designs, therefore, allow for even more control over fibre size and permit novel structures to be created. In further work, collector designs can be created and analysed to produce bandage-like fibrous structures which can be made to be more suitable for wound healing. Additionally, the collection chamber can be modified to include vacuum or partial vacuum systems, to establish the effects of such a collection environment on fibre morphology and suitability for advanced wound healing applications.

7.2.2 Develop polymer systems avoiding organic solvents

Organic solvents such as dichloromethane, chloroform and Dimethylformamide used in this work are great at dissolving important biomedical polymers such as polycaprolactone and poly(lactic acid). However, the use of such organic solvents poses toxicity concerns for humans and animals, whilst also having a detrimental impact on the environment. For these reasons, the use of organic solvents should be reduced and alternative methods to dissolve polymers into more environmentally friendly solvents should be explored. In this work, poly(ethylene oxide) was used with electrospinning, this is a water-soluble polymer that does not require harsh solvents to dissolve it. If further work were to be carried out, there would be a greater emphasis on discovering and utilising novel and existing polymers that are either water-soluble or able to dissolve in less harsh solvents such as ethanol and acetone.

It is important to consider the biocompatibility and biodegradability of any polymer which will be used as a biomaterial in a health care setting. Although most, if not all of the polymers used in this work are both biocompatible and biodegradable, they may not be bioresorbable. A bioresorbable polymer can be degraded within the body and its subsequent breakdown molecules can be properly disposed of by the body via natural means. For example, poly(lactic acid), is broken down into lactic acid, which is found naturally in the body and thus can be broken down by the metabolic system. This being said, there

should be a deeper focus on bioresorbable polymer which in healthcare and wound healing settings make removal or revision surgeries much less complicated.

7.2.3 Extensive mechanical testing

Although there was an analysis of the mechanical properties of binary and ternary polymer systems in this work, further mechanical testing can be beneficial in understanding the physical characteristics of polymers in composite form. Additional tests such as tensile testing where the elastic modulus can be calculated from the initial part of the slope from stress-strain graphs can serve to better understand the mechanical properties of the produced bandage-like fibres. Dynamic mechanical properties can also be obtained to study the viscoelastic behaviour of the fibrous scaffolds; allowing for the determination of complex modulus as the temperature of the polymeric fibres or the frequency of the stress are varied. Dynamic mechanical properties thus lead to variations in the complex modulus which can be used to locate the glass transition temperature of the tested material.

Additionally, atomic force microscopy could be used in further studies, this technology obtains a very high-resolution image of a sample by utilising a small cantilever that probes the surface. Using atomic force microscopy, you can obtain surface maps of samples down to the low nanometre range and can further be used to measure the mechanical properties of samples such as obtaining values for a sample's Young's modulus. Advanced mechanical testing, we can make sure that the produced scaffolds exhibit the desired mechanical properties which are required for wound healing and other biomedical applications.

7.2.4 Further chemical and morphological testing

Although SEM has been used extensively in this work to obtain high magnification images of the fibrous samples, other imaging techniques could be utilised in upcoming work. For example, transition electron microscopy can be used where the fibres are specially pre-prepared, but the resulting image may benefit from a higher overall resolution as the electrons pass through the

sample, instead of being reflected from the surface, as with scanning electron microscopy. Transition electron microscopy allows for near-atomic resolution of structures which can be used to further analyse the complete topography and morphology of the polymeric samples used in this work.

Focused ion beam is an imaging technique that is used widely in the semiconductor industry and materials science to obtain high-resolution images of surface patterning. Focused ion beam is very similar to SEM but instead of using a focused beam of electrons it used a focused beam of ions. This technology can be used for cross-sectional analysis of fibre samples to determine the internal structure. Cross-sectional analysis can provide additional data to the internal structure of the produced bandage-like structures and can be beneficial in predicting cellular interactions and possible wound healing benefits.

Supplementing the imaging of the fibres, further chemical analysis could be undertaken to confirm the uptake of bioactive ingredients of the bandage-like scaffolds. For example, Raman spectroscopy which is a spectroscopic technique used to determine vibrational modes of molecules can be used to provide the structural fingerprints of the constituent molecules, confirming the presence of bioactive substances. Furthermore, energy-dispersive X-ray spectroscopy may also be used in conjunction with SEM to provide an elemental analysis of the samples to confirm the presence of certain elements in question. Via the chemical and morphological analysis of the produced polymeric fibres, there can be more confidence in the intended and desired effects inside a wound healing environment.

7.2.5 Further discovery of natural materials which have antimicrobial effects

This work showcases many naturally occurring materials which exhibit a potent antimicrobial effect such as cinnamon and honey. The benefits of using naturally occurring materials are that they are highly abundant, often less toxic than synthetic alternatives and their waste products are more environmentally friendly. However, there remains many more tried and testing, naturally

occurring materials and spices which should be analysed further to develop new strategies against the emerging concern of antimicrobial resistance.

In the continual pursuit of naturally antibacterial materials, compounds can be isolated and synthesised which offer new mechanisms of antimicrobial action which will prove to be effective against resistant strains. Nautically occurring spices have several hundreds of constituent compounds which can work in tandem to provide a unique antimicrobial effect. For this reason, isolating pure compounds can often demonstrate a less effective method of antimicrobial action. Therefore, work on utilising naturally occurring materials in their full state or extracted from may serve to facilitate highly-effective antimicrobial strategies for wound healing and other aspects of biomedical engineering.

7.2.6 Further discovery of natural materials with healthcare benefits

As mentioned above, naturally occurring materials in their full form and extracted form can benefit from antimicrobial abilities, but they also demonstrate many different healthcare benefits, useful in wound healing materials. For example, honey and other naturally occurring materials exhibit properties in being anti-cancer, anti-thrombotic, anti-inflammatory, anti-diabetic, cholesterol-reducing, anticarcinogenic, neutralisation of reactive oxygen species, antioxidant and many other health benefits. The exact mix of constituent compounds could be working together to provide the pro-health effects.

The discovery of further natural materials can therefore serve to allow wound healing bandages to be manufactured with greater a higher quality wound healing response. Natural materials are both abundant and highly biocompatible, allowing for advancement in wound management technologies. Specific compounds can even be extracted into solution form and mass-produced into polymeric structures which will have many applications in biomedical engineering. The long-lasting effects of extractions, as shown in this work could open up countless opportunities.

7.2.7 Antimicrobial tests

The antimicrobial properties of naturally occurring materials were investigated against Gram-negative and Gram-positive microorganisms and have shown positive preliminary results. The limitations in this work are that these organisms seldom act as a lone species in infection and thus cannot be representative of all real-world infection scenarios. Furthermore, not all conditions in the laboratory can effectively simulate hospital-acquired infections such as ventilation of the room, hygiene of patient, ambient conditions and exposure to external stimuli such as doctors and nurses. Although all lab testing is limited, live trials may serve as the most representative for actual antimicrobial and pro-wound healing activities.

In further tests, a greater variety of bacteria and fungi will be used against the fibrous scaffolds to determine the antimicrobial efficacy of the bandages against a range of pathogens to better understand how different and effective these compounds are at aiding microbial death. In addition, the antimicrobial tests could be performed in various environments such as in a range of differing humidity, different nutrient conditions and in shake flasks. The environment may have a large effect on antimicrobial action. Within a wound environment, for example, the actual conditions can be drastically different, and you would have to account for factors such as blood movement, pH levels and cellular interaction.

7.2.8 Mechanism of Action

Although great antimicrobial abilities have been shown, it is still unknown how these antimicrobials can reduce the microbial population, both in fibre form and on their own. Possible theories have been postulated and some may be known, but until we can completely discern how the antimicrobial action works in fibre form, we cannot fully optimise the constructs. Future work in this regard

will be to study biochemistry and utilise high magnification technologies to detail crucial events in the antimicrobial phases.

Using high-resolution imaging and other techniques, we can try to assess the membrane of dead microbial cells. For example, common antimicrobial mechanisms of action are via the rupturing of the pathogen's cell wall. Determination of cell wall integrity can point to mechanical disruption of the cell wall. Other modes of antimicrobial mechanism of action are via the inhibition of the pathogen's vital protein synthesis, interference of the nucleic acid synthesis, inhibition of certain metabolic pathways and death via the use of reactive oxygen species. In determining the mechanism of action, we can better predict the longevity of the antimicrobial effects as pathogens can rapidly evolve to evade many of these chemical mechanisms.

7.2.9 Further Purification and Isolation Studies

Naturally occurring materials such as honey and cinnamon have shown great promise in this thesis. However, it is still not known what principal component cause the antimicrobial or pro-wound healing effect. It may be that many components work which in tandem to create a perfect combination. However, isolation and purification can lead to the synthesis and mass utilisation of these useful materials.

It would also be useful to understand the key components which cause the antimicrobial or the health-benefiting effects. This is because there may exist certain compounds which will have a slightly toxic effect on the body's native cells. Isolation of bioactive compounds can also serve to develop the understanding of chemical compounds and their effects on healthcare; this can therefore be utilised to advance the wound-healing market and in the manufacture of advanced wound care materials.

7.2.10 Wound Healing Models

In the studies relating to this thesis, the wound healing ability of the materials was assessed based on their physical structure, material properties,

cytotoxicity of wound healing cells and their proliferation. These studies are limited in their ability to be completely representative of the complete process of wound healing, which is known to be highly complex. Future work on these materials should be aimed at physical wound healing models such as artificial skin, scratch tests, mice wound healing models and other innovative methods of simulating human wounds.

7.2.11 Further Development of Fibre Forming Technologies

The novel combination of pressurised gyration and electrospinning presented in this work shows the leveraging of strengths from different techniques to produce functional materials with an emphasis on ease and cost savings. However, the limitations of this study were mostly time-constrained and further development into an automated assembly of producing bioactive bandages will need to be carried out. This work is already being carried out in addition to the design and implementation of updated manufacturing components to advance the field of manufacturing and biomaterials.

In future studies, work will be carried out to incorporate two or more of these manufacturing techniques into a single unified and automated hybrid technology, to produce advanced wound healing bandages that aim to reduce the final cost of pro-wound-healing bandages. Current manufacturing of such materials proves to be costly as they require expensive bioactive materials, but by utilising specifically targeted deposition of bioactive substances, the reduction of cost can be translated down to the consumer and the healthcare providers.

7.2.12 Materials Discovery and Novel Combinations

As alluded to at the end of this study, the work carried out in this thesis focuses on the tailored production of functional polymeric materials and the pursuit for materials discovery and composites is always required. The antimicrobial nature of the produced porous graphene-PCL fibrous constructs was not investigated, as graphene oxide has previously shown antibacterial activity at lower concentrations, it is not out of the question that these bandages would

be able to fight off infection. Further work into incorporating and discovering materials with valuable properties must continue and is one of the only ways science and technology can keep pace with an ever-developing landscape of human needs and desires.

References

[1] Posnett J, Gottrup F, Lundgren H, Saal G. The resource impact of wounds on health-care providers in Europe. Journal of wound care 2009;18(4):154-61.

[2] Gould L, Abadir P, Brem H, Carter M, Conner-Kerr T, Davidson J, DiPietro L, Falanga V, Fife C, Gardner S, Grice E, Harmon J, Hazzard WR, High KP, Houghton P, Jacobson N, Kirsner RS, Kovacs EJ, Margolis D, McFarland Horne F, Reed MJ, Sullivan DH, Thom S, Tomic-Canic M, Walston J, Whitney JA, Williams J, Zieman S, Schmader K. Chronic wound repair and healing in older adults: current status and future research. Journal of the American Geriatrics Society 2015;63(3):427-38.

[3] Lipsky BA, Hoey C. Topical Antimicrobial Therapy for Treating Chronic Wounds. Clinical Infectious Diseases 2009;49(10):1541-9.

[4] Matharu RK, Porwal H, Ciric L, Edirisinghe M. The effect of graphene–poly(Methyl methacrylate) fibres on microbial growth. Interface Focus 2018;8(3):20170058.

[5] Matharu RK, Charani Z, Ciric L, Illangakoon UE, Edirisinghe M. Antimicrobial activity of tellurium-loaded polymeric fiber meshes. Journal of Applied Polymer Science 2018;135(25):46368.

[6] Coleman BD. On the strength of classical fibres and fibre bundles. Journal of the Mechanics and Physics of Solids 1958;7(1):60-70.

[7] Pettersson T, Hellwig J, Gustafsson P-J, Stenström S. Measurement of the flexibility of wet cellulose fibres using atomic force microscopy. Cellulose 2017;24(10):4139-49.

[8] Sinclair R. Chapter 1 - Understanding Textile Fibres and Their Properties: What is a Textile Fibre? In: Sinclair R, editor Textiles and Fashion. Woodhead Publishing; 2015, p. 3-27.

[9] Wu T, Zhang J, Wang Y, Li D, Sun B, El-Hamshary H, Yin M, Mo X. Fabrication and preliminary study of a biomimetic tri-layer tubular graft based on fibers and fiber yarns for vascular tissue engineering. Materials Science and Engineering: C 2018;82:121-9.

[10] Nair BP, Vaikkath D, Mohan DS, Nair PD. Fabrication of a microvesicles-incorporated fibrous membrane for controlled delivery applications in tissue engineering. Biofabrication 2014;6(4):045008.

[11] Kosmider K, Scott J. Polymeric nanofibres exhibit an enhanced air filtration performance. Filtration & Separation 2002;39(6):20-2.

[12] Serrano MC, Pagani R, Vallet-Regí M, Peña J, Rámila A, Izquierdo I, Portolés MT. In vitro biocompatibility assessment of poly(ε-caprolactone) films using L929 mouse fibroblasts. Biomaterials 2004;25(25):5603-11.

[13] Guex AG, Kocher FM, Fortunato G, Körner E, Hegemann D, Carrel TP, Tevaearai HT, Giraud MN. Fine-tuning of substrate architecture and surface chemistry promotes muscle tissue development. Acta Biomaterialia 2012;8(4):1481-9.

[14] Luo CJ, Stoyanov SD, Stride E, Pelan E, Edirisinghe M. Electrospinning versus fibre production methods: from specifics to technological convergence. Chemical Society Reviews 2012;41(13):4708-35.

[15] Bhardwaj N, Kundu SC. Electrospinning: A fascinating fiber fabrication technique. Biotechnology Advances 2010;28(3):325-47.

[16] Heseltine PL, Ahmed J, Edirisinghe M. Developments in pressurized gyration for the mass production of polymeric fibers. Macromolecular Materials and Engineering 2018;0(0):1800218.

[17] Gago J, Carretero O, Filgueiras AV, Viñas L. Synthetic microfibers in the marine environment: A review on their occurrence in seawater and sediments. Marine Pollution Bulletin 2018;127:365-76.

[18] Raskin I, Ribnicky DM, Komarnytsky S, Ilic N, Poulev A, Borisjuk N, Brinker A, Moreno DA, Ripoll C, Yakoby N, O'Neal JM, Cornwell T, Pastor I, Fridlender B. Plants and human health in the twenty-first century. Trends in Biotechnology 2002;20(12):522-31.

[19] Gu J-D. Microbiological deterioration and degradation of synthetic polymeric materials: recent research advances. International Biodeterioration & Biodegradation 2003;52(2):69-91.

[20] Asghari F, Samiei M, Adibkia K, Akbarzadeh A, Davaran S. Biodegradable and biocompatible polymers for tissue engineering

application: a review. Artificial Cells, Nanomedicine, and Biotechnology 2017;45(2):185-92.

[21] Majdalawieh AF, Carr RI. In Vitro Investigation of the Potential Immunomodulatory and Anti-Cancer Activities of Black Pepper (Piper nigrum) and Cardamom (Elettaria cardamomum). Journal of Medicinal Food 2010;13(2):371-81.

[22] Wang P-C, Zhao S, Yang B-Y, Wang Q-H, Kuang H-X. Anti-diabetic polysaccharides from natural sources: A review. Carbohydrate Polymers 2016;148:86-97.

[23] Czaja W, Krystynowicz A, Bielecki S, Brown RM, Jr. Microbial cellulose--the natural power to heal wounds. Biomaterials 2006;27(2):145-51.

[24] Wang C, Wu S, Jian M, Xie J, Xu L, Yang X, Zheng Q, Zhang Y. Silk nanofibers as high efficient and lightweight air filter. Nano Research 2016;9(9):2590-7.

[25] Angelova N, Hunkeler D. Rationalizing the design of polymeric biomaterials. Trends in Biotechnology 1999;17(10):409-21.

[26] Marston HD, Dixon DM, Knisely JM, Palmore TN, Fauci AS. Antimicrobial Resistance. JAMA 2016;316(11):1193-204.

[27] Chen J-P, Chang G-Y, Chen J-K. Electrospun collagen/chitosan nanofibrous membrane as wound dressing. Colloids and Surfaces A: Physicochemical and Engineering Aspects 2008;313-314:183-8.

[28] Shalumon KT, Anulekha KH, Nair SV, Nair SV, Chennazhi KP, Jayakumar R. Sodium alginate/poly(vinyl alcohol)/nano ZnO composite nanofibers for antibacterial wound dressings. International Journal of Biological Macromolecules 2011;49(3):247-54.

[29] Mayet N, Choonara YE, Kumar P, Tomar LK, Tyagi C, Du Toit LC, Pillay V. A Comprehensive Review of Advanced Biopolymeric Wound Healing Systems. Journal of Pharmaceutical Sciences 2014;103(8):2211-30.

[30] Rho KS, Jeong L, Lee G, Seo B-M, Park YJ, Hong S-D, Roh S, Cho JJ, Park WH, Min B-M. Electrospinning of collagen nanofibers: Effects on the behavior of normal human keratinocytes and early-stage wound healing. Biomaterials 2006;27(8):1452-61.

[31] Schneider A, Wang XY, Kaplan DL, Garlick JA, Egles C. Biofunctionalized electrospun silk mats as a topical bioactive dressing for accelerated wound healing. Acta Biomaterialia 2009;5(7):2570-8.

[32] Khorshidi S, Solouk A, Mirzadeh H, Mazinani S, Lagaron JM, Sharifi S, Ramakrishna S. A review of key challenges of electrospun scaffolds for tissue-engineering applications. Journal of Tissue Engineering and Regenerative Medicine 2016;10(9):715-38.

[33] Altun E, Aydogdu Mehmet O, Koc F, Crabbe-Mann M, Brako F, Kaur-Matharu R, Ozen G, Kuruca Serap E, Edirisinghe U, Gunduz O, Edirisinghe M. Novel Making of Bacterial Cellulose Blended Polymeric Fiber Bandages. Macromolecular Materials and Engineering 2018;303(3):1700607.

[34] Mahalingam S, Edirisinghe M. Forming of polymer nanofibers by a pressurised gyration process. Macromolecular Rapid Communications 2013;34(14):1134-9.

[35] El-Newehy MH, Al-Deyab SS, Kenawy E-R, Abdel-Megeed A. Nanospider technology for the production of nylon-6 nanofibers for biomedical applications. J Nanomaterials 2011;2011:Article 9.

[36] Edwards HGM, Farwell DW, Webster D. FT Raman microscopy of untreated natural plant fibres. Spectrochimica Acta Part A: Molecular and Biomolecular Spectroscopy 1997;53(13):2383-92.

[37] Morton WE, Hearle JWS. Physical Properties of Textile Fibres: Fourth Edition. Physical Properties of Textile Fibres: Fourth Edition 2008:1-776.

[38] Fisher CH. History of Natural Fibers. Journal of Macromolecular Science: Part A - Chemistry 1981;15(7):1345-75.

[39] Sharifi F, Sooriyarachchi AC, Altural H, Montazami R, Rylander MN, Hashemi N. Fiber Based Approaches as Medicine Delivery Systems. ACS Biomaterials Science & Engineering 2016;2(9):1411-31.

[40] Wendel JF, Brubaker C, Alvarez I, Cronn R, Stewart JM. Evolution and Natural History of the Cotton Genus. In: Paterson AH, editor Genetics and Genomics of Cotton. New York, NY: Springer US; 2009, p. 3-22.

[41] Hosseini Ravandi SA, Valizadeh M. 2 - Properties of fibers and fabrics that contribute to human comfort. In: Song G, editor Improving Comfort in Clothing. Woodhead Publishing; 2011, p. 61-78.

[42] Andrawes KZ, McGown A, Kabir MH. Uniaxial strength testing of woven and nonwoven geotextiles. Geotextiles and Geomembranes 1984;1(1):41-56.

[43] Pourmohammadi A. 19 - Nonwoven materials and joining techniques. In: Jones I, Stylios GK, editors. Joining Textiles. Woodhead Publishing; 2013, p. 565-81.

[44] Ellison CJ, Phatak A, Giles DW, Macosko CW, Bates FS. Melt blown nanofibers: Fiber diameter distributions and onset of fiber breakup. Polymer 2007;48(11):3306-16.

[45] Laufman H, Eudy WW, Vandernoot AM, Harris CA, Liu D. Strike-through of moist contamination by woven and nonwoven surgical materials. Annals of Surgery 1975;181(6):857-62.

[46] Pause B. Nonwoven Protective Garments with Thermo-Regulating Properties. Journal of Industrial Textiles 2003;33(2):93-9.

[47] Schaff AJ, Ogale AA. Tensile Viscoelastic Properties of Spunbonded Nonwoven Polypropylene Backing. Textile Research Journal 1991;61(7):386-92.

[48] Wang C-C, Chen C-C. Anti-bacterial and swelling properties of acrylic acid grafted and collagen/chitosan immobilized polypropylene non-woven fabrics. Journal of Applied Polymer Science 2005;98(1):391-400.

[49] Patel MS, Asch DA, Volpp KG. Wearable Devices as Facilitators, Not Drivers, of Health Behavior Change. JAMA 2015;313(5):459-60.

[50] Adabi M, Naghibzadeh M, Adabi M, Zarrinfard MA, Esnaashari SS, Seifalian AM, Faridi-Majidi R, Tanimowo Aiyelabegan H, Ghanbari H. Biocompatibility and nanostructured materials: applications in nanomedicine. Artificial Cells, Nanomedicine, and Biotechnology 2017;45(4):833-42.

[51] Gupta BS, Edwards JV. 3 - Textile materials and structures for topical management of wounds. In: Rajendran S, editor Advanced Textiles for Wound Care (Second Edition). Woodhead Publishing; 2019, p. 55-104.

[52] Lee YE, Wadsworth LC. Fiber and web formation of melt-blown thermoplastic polyurethane polymers. Journal of Applied Polymer Science 2007;105(6):3724-7.

[53] Soltani I, Macosko CW. Influence of rheology and surface properties on morphology of nanofibers derived from islands-in-the-sea meltblown nonwovens. Polymer 2018;145:21-30.

[54] Lee Y, Wadsworth LC. Structure and filtration properties of melt blown polypropylene webs. Polymer Engineering & Science 1990;30(22):1413-9.

[55] Wei QF, Mather RR, Fotheringham AF, Yang RD. Evaluation of nonwoven polypropylene oil sorbents in marine oil-spill recovery. Marine Pollution Bulletin 2003;46(6):780-3.

[56] Balogh A, Farkas B, Farago K, Farkas A, Wagner I, Van Assche I, Verreck G, Nagy ZK, Marosi G. Melt-blown and electrospun drug-loaded polymer fiber mats for dissolution enhancement: a comparative study. Journal of Pharmaceutical Sciences 2015;104(5):1767-76.

[57] Gou Z, McHugh AJ. Two-dimensional modeling of dry spinning of polymer fibers. Journal of Non-Newtonian Fluid Mechanics 2004;118(2):121-36.

[58] Imura Y, Hogan RMC, Jaffe M. 10 - Dry spinning of synthetic polymer fibers. In: Zhang D, editor Advances in Filament Yarn Spinning of Textiles and Polymers. Woodhead Publishing; 2014, p. 187-202.

[59] Chen S, Schueneman G, Pipes RB, Youngblood J, Moon RJ. Effects of Crystal Orientation on Cellulose Nanocrystals–Cellulose Acetate Nanocomposite Fibers Prepared by Dry Spinning. Biomacromolecules 2014;15(10):3827-35.

[60] Ozipek B, Karakas H. 9 - Wet spinning of synthetic polymer fibers. In: Zhang D, editor Advances in Filament Yarn Spinning of Textiles and Polymers. Woodhead Publishing; 2014, p. 174-86.

[61] Mirabedini A, Foroughi J, Wallace GG. Developments in conducting polymer fibres: from established spinning methods toward advanced applications. RSC Advances 2016;6(50):44687-716.

[62] Paul DR. A study of spinnability in the wet-spinning of acrylic fibers. Journal of Applied Polymer Science 1968;12(10):2273-98.

[63] Heinrich K, Jung H. New Concepts in para-Aramid Fibers. Textile Research Journal 1992;62(12):771-5.

[64] East GC, Qin Y. Wet spinning of chitosan and the acetylation of chitosan fibers. Journal of Applied Polymer Science 1993;50(10):1773-9.

[65] Liu H, Xu W, Zou H, Ke G, Li W, Ouyang C. Feasibility of wet spinning of silk-inspired polyurethane elastic biofiber. Materials Letters 2008;62(12):1949-52.

[66] Agarwal S, Jiang S. Nanofibers and Electrospinning. In: Kobayashi S, Müllen K, editors. Encyclopedia of Polymeric Nanomaterials. Berlin, Heidelberg: Springer Berlin Heidelberg; 2014, p. 1-15.

[67] Jiang T, Carbone EJ, Lo KWH, Laurencin CT. Electrospinning of polymer nanofibers for tissue regeneration. Progress in Polymer Science 2015;46:1-24.

[68] Hartman RPA, Brunner DJ, Camelot DMA, Marijnissen JCM, Scarlett B. Electrohydrodynamic Atomization In The Cone–Jet Mode Physical Modelling Of The Liquid Cone And Jet. Journal of Aerosol Science 1999;30(7):823-49.

[69] Yalcinkaya B, Yener F, Jirsak O, Cengiz-Callioglu F. On the Nature of Electric Current in the Electrospinning Process. Journal of Nanomaterials 2013;2013:10.

[70] Krupa A, Tomasz Sobczyk A, Jaworek A. Surface Properties of Plasma-Modified Poly(vinylidene fluoride) and Poly(vinyl chloride) Nanofibres. Fibres and Textiles in Eastern Europe 2014;104:35-9.

[71] Baji A, Mai Y-W, Wong S-C, Abtahi M, Chen P. Electrospinning of polymer nanofibers: Effects on oriented morphology, structures and tensile properties. Composites Science and Technology 2010;70(5):703-18.

[72] Li D, Xia Y. Electrospinning of Nanofibers: Reinventing the Wheel? Advanced Materials 2004;16(14):1151-70.

[73] He J-H, Wan Y-Q. Allometric scaling for voltage and current in electrospinning. Polymer 2004;45(19):6731-4.

[74] Katti DS, Robinson KW, Ko FK, Laurencin CT. Bioresorbable nanofiber-based systems for wound healing and drug delivery: Optimization of

fabrication parameters. Journal of Biomedical Materials Research Part B: Applied Biomaterials 2004;70B(2):286-96.

[75] Luo CJ, Stride E, Edirisinghe M. Mapping the Influence of Solubility and Dielectric Constant on Electrospinning Polycaprolactone Solutions. Macromolecules 2012;45(11):4669-80.

[76] Sill TJ, von Recum HA. Electrospinning: applications in drug delivery and tissue engineering. Biomaterials 2008;29(13):1989-2006.

[77] Bosworth LA, Downes S. Acetone, a Sustainable Solvent for Electrospinning Poly(ε-Caprolactone) Fibres: Effect of Varying Parameters and Solution Concentrations on Fibre Diameter. Journal of Polymers and the Environment 2012;20(3):879-86.

[78] Husain O, Lau W, Edirisinghe M, Parhizkar M. Investigating the particle to fibre transition threshold during electrohydrodynamic atomization of a polymer solution. Materials Science and Engineering: C 2016;65:240-50.

[79] Guerrero J, Rivero J, Gundabala VR, Perez-Saborid M, Fernandez-Nieves A. Whipping of electrified liquid jets. Proceedings of the National Academy of Sciences 2014;111(38):13763.

[80] Ko J, Mohtaram NK, Ahmed F, Montgomery A, Carlson M, Lee PCD, Willerth SM, Jun MBG. Fabrication of poly (ϵ-caprolactone) microfiber scaffolds with varying topography and mechanical properties for stem cell-based tissue engineering applications. Journal of Biomaterials Science, Polymer Edition 2014;25(1):1-17.

[81] Huang C, Chen S, Lai C, Reneker DH, Qiu H, Ye Y, Hou H. Electrospun polymer nanofibres with small diameters. Nanotechnology 2006;17(6):1558-63.

[82] Nuansing W, Ninmuang S, Jarernboon W, Maensiri S, Seraphin S. Structural characterization and morphology of electrospun TiO2 nanofibers. Materials Science and Engineering: B 2006;131(1):147-55.

[83] Wu W-Y, Ting J-M, Huang P-J. Electrospun ZnO Nanowires as Gas Sensors for Ethanol Detection. Nanoscale Research Letters 2009;4(6):513.

[84] Son WK, Youk JH, Lee TS, Park WH. The effects of solution properties and polyelectrolyte on electrospinning of ultrafine poly(ethylene oxide) fibers. Polymer 2004;45(9):2959-66.

[85] Tambralli A, Blakeney B, Anderson J, Kushwaha M, Andukuri A, Dean D, Jun HW. A hybrid biomimetic scaffold composed of electrospun polycaprolactone nanofibers and self-assembled peptide amphiphile nanofibers. Biofabrication 2009;1(2):025001.

[86] Yang E, Shi J, Xue Y. Influence of electric field interference on double nozzles electrospinning. Journal of Applied Polymer Science 2010;116(6):3688-92.

[87] Zhang S, Karaca BT, VanOosten SK, Yuca E, Mahalingam S, Edirisinghe M, Tamerler C. Coupling Infusion and Gyration for the Nanoscale Assembly of Functional Polymer Nanofibers Integrated with Genetically Engineered Proteins. Macromolecular Rapid Communications 2015;36(14):1322-8.

[88] Hong X, Edirisinghe M, Mahalingam S. Beads, beaded-fibres and fibres: Tailoring the morphology of poly(caprolactone) using pressurised gyration. Materials Science and Engineering: C 2016;69(Supplement C):1373-82.

[89] Mahalingam S, Ren GG, Edirisinghe MJ. Rheology and pressurised gyration of starch and starch-loaded poly(ethylene oxide). Carbohydrate Polymers 2014;114:279-87.

[90] Ahmed J, Matharu RK, Shams T, Illangakoon UE, Edirisinghe M. A comparison of electric-field-driven and pressure-driven fiber generation methods for drug delivery. Macromolecular Materials and Engineering 2018:1700577.

[91] Edirisinghe M, Duncan C, Suntharavathanan M, Bahijja Tolulope R-A. Exploitation of Pressurised Gyration as an Innovative Manufacturing Route for Nanofibrous Structures. Research Councils UK 2014.

[92] Raimi-Abraham BT, Mahalingam S, Davies PJ, Edirisinghe M, Craig DQM. Development and Characterization of Amorphous Nanofiber Drug Dispersions Prepared Using Pressurized Gyration. Molecular Pharmaceutics 2015;12(11):3851-61.

[93] Brako F, Raimi-Abraham B, Mahalingam S, Craig DQM, Edirisinghe M. Making nanofibres of mucoadhesive polymer blends for vaginal therapies. European Polymer Journal 2015;70:186-96.

[94] Daristotle JL, Behrens AM, Sandler AD, Kofinas P. A Review of the Fundamental Principles and Applications of Solution Blow Spinning. ACS Applied Materials & Interfaces 2016;8(51):34951-63.

[95] Bognitzki M, Frese T, Steinhart M, Greiner A, Wendorff JH, Schaper A, Hellwig M. Preparation of fibers with nanoscaled morphologies: Electrospinning of polymer blends. Polymer Engineering & Science 2001;41(6):982-9.

[96] Stojanovska E, Canbay E, Pampal ES, Calisir MD, Agma O, Polat Y, Simsek R, Gundogdu NAS, Akgul Y, Kilic A. A review on non-electro nanofibre spinning techniques. RSC Advances 2016;6(87):83783-801.

[97] Matharu RK, Charani Z, Ciric L, Illangakoon Upulitha E, Edirisinghe M. Antimicrobial activity of tellurium-loaded polymeric fiber meshes. Journal of Applied Polymer Science 2018;0(0):46368.

[98] Li M, Zhang J, Zhang H, Liu Y, Wang C, Xu X, Tang Y, Yang B. Electrospinning: A Facile Method to Disperse Fluorescent Quantum Dots in Nanofibers without Förster Resonance Energy Transfer. Advanced Functional Materials 2007;17(17):3650-6.

[99] Sampson SL, Saraiva L, Gustafsson K, Jayasinghe SN, Robertson BD. Cell Electrospinning: An In Vitro and In Vivo Study. Small 2014;10(1):78-82.

[100] Vasita R, Katti DS. Nanofibers and their applications in tissue engineering. International journal of nanomedicine 2006;1(1):15-30.

[101] Chattopadhyay R. 1 - Introduction: types of technical textile yarn. In: Alagirusamy R, Das A, editors. Technical Textile Yarns. Woodhead Publishing; 2010, p. 3-55.

[102] Choi SW, Jo SM, Lee WS, Kim YR. An electrospun poly(vinylidene fluoride) nanofibrous membrane and its battery applications. Advanced Materials 2003;15(23):2027-32.

[103] Demczyk BG, Wang YM, Cumings J, Hetman M, Han W, Zettl A, Ritchie RO. Direct mechanical measurement of the tensile strength and elastic

modulus of multiwalled carbon nanotubes. Materials Science and Engineering: A 2002;334(1):173-8.

[104] Doillon CJ, Dunn MG, Bender E, Silver FH. Collagen Fiber Formation in Repair Tissue: Development of Strength and Toughness. Collagen and Related Research 1985;5(6):481-92.

[105] Baie SH, Sheikh KA. The wound healing properties of Channa striatus-cetrimide cream — tensile strength measurement. Journal of Ethnopharmacology 2000;71(1):93-100.

[106] Takao Y, Chou TW, Taya M. Effective Longitudinal Young's Modulus of Misoriented Short Fiber Composites. Journal of Applied Mechanics 1982;49(3):536-40.

[107] Schulgasser K. Fibre orientation in machine-made paper. Journal of Materials Science 1985;20(3):859-66.

[108] Wong VW, Akaishi S, Longaker MT, Gurtner GC. Pushing Back: Wound Mechanotransduction in Repair and Regeneration. Journal of Investigative Dermatology 2011;131(11):2186-96.

[109] Wipff P-J, Rifkin DB, Meister J-J, Hinz B. Myofibroblast contraction activates latent TGF-beta1 from the extracellular matrix. The Journal of cell biology 2007;179(6):1311-23.

[110] Branco da Cunha C, Klumpers DD, Li WA, Koshy ST, Weaver JC, Chaudhuri O, Granja PL, Mooney DJ. Influence of the stiffness of three-dimensional alginate/collagen-I interpenetrating networks on fibroblast biology. Biomaterials 2014;35(32):8927-36.

[111] Liverani L, Killian MS, Boccaccini AR. Fibronectin Functionalized Electrospun Fibers by Using Benign Solvents: Best Way to Achieve Effective Functionalization. Frontiers in Bioengineering and Biotechnology 2019;7(68).

[112] Lin J, Tian F, Shang Y, Wang F, Ding B, Yu J. Facile control of intra-fiber porosity and inter-fiber voids in electrospun fibers for selective adsorption. Nanoscale 2012;4(17):5316-20.

[113] Lien S-M, Ko L-Y, Huang T-J. Effect of pore size on ECM secretion and cell growth in gelatin scaffold for articular cartilage tissue engineering. Acta Biomaterialia 2009;5(2):670-9.

[114] Loh QL, Choong C. Three-Dimensional Scaffolds for Tissue Engineering Applications: Role of Porosity and Pore Size. Tissue Engineering Part B: Reviews 2013;19(6):485-502.

[115] Karageorgiou V, Kaplan D. Porosity of 3D biomaterial scaffolds and osteogenesis. Biomaterials 2005;26(27):5474-91.

[116] Sung H-J, Meredith C, Johnson C, Galis ZS. The effect of scaffold degradation rate on three-dimensional cell growth and angiogenesis. Biomaterials 2004;25(26):5735-42.

[117] Chevalier E, Chulia D, Pouget C, Viana M. Fabrication of porous substrates: A review of processes using pore forming agents in the biomaterial field. Journal of Pharmaceutical Sciences 2008;97(3):1135-54.

[118] Frey MW, Li L. Electrospinning and Porosity Measurements of Nylon-6/Poly(ethylene oxide) Blended Nonwovens. Journal of Engineered Fibers and Fabrics 2007;2(1):155892500700200103.

[119] Wang Z, Zhao C, Pan Z. Porous bead-on-string poly(lactic acid) fibrous membranes for air filtration. Journal of Colloid and Interface Science 2015;441(Supplement C):121-9.

[120] Dalby MJ. Topographically induced direct cell mechanotransduction. Medical Engineering and Physics 2005;27(9):730-42.

[121] Illangakoon EU, Mahalingam S, Matharu KR, Edirisinghe M. Evolution of Surface Nanopores in Pressurised Gyrospun Polymeric Microfibers. Polymers 2017;9(10).

[122] Yoo HS, Kim TG, Park TG. Surface-functionalized electrospun nanofibers for tissue engineering and drug delivery. Advanced Drug Delivery Reviews 2009;61(12):1033-42.

[123] Eichhorn SJ, Sampson WW. Statistical geometry of pores and statistics of porous nanofibrous assemblies. Journal of The Royal Society Interface 2005;2(4):309-18.

[124] Gopal R, Kaur S, Feng CY, Chan C, Ramakrishna S, Tabe S, Matsuura T. Electrospun nanofibrous polysulfone membranes as pre-filters: Particulate removal. Journal of Membrane Science 2007;289(1):210-9.

[125] Schaub NJ, Britton T, Rajachar R, Gilbert RJ. Engineered Nanotopography on Electrospun PLLA Microfibers Modifies RAW

264.7 Cell Response. ACS Applied Materials & Interfaces 2013;5(20):10173-84.

[126] Johnson CD, D'Amato AR, Puhl DL, Wich DM, Vesperman A, Gilbert RJ. Electrospun fiber surface nanotopography influences astrocyte-mediated neurite outgrowth. Biomedical Materials 2018;13(5):054101.

[127] Ziemba AM, Lane KP, San Segundo IM, D'Amato AR, Mason AK, Sexton RJ, Casajus H, Gross RA, Corr DT, Gilbert RJ. Poly-l-lactic acid-co-poly(pentadecalactone) Electrospun Fibers Result in Greater Neurite Outgrowth of Chick Dorsal Root Ganglia in Vitro Compared to Poly-l-lactic Acid Fibers. ACS Biomaterials Science & Engineering 2018;4(5):1491-7.

[128] Galli C, Passeri G, Ravanetti F, Elezi E, Pedrazzoni M, Macaluso GM. Rough surface topography enhances the activation of Wnt/beta-catenin signaling in mesenchymal cells. Journal of Biomedical Materials Research: Part A 2010;95(3):682-90.

[129] Lee MR, Kwon KW, Jung H, Kim HN, Suh KY, Kim K, Kim K-S. Direct differentiation of human embryonic stem cells into selective neurons on nanoscale ridge/groove pattern arrays. Biomaterials 2010;31(15):4360-6.

[130] Aviss KJ, Gough JE, Downes S. Aligned electrospun polymer fibres for skeletal muscle regeneration. European Cells & Materials 2010;19:193-204.

[131] Truong YB, Glattauer V, Lang G, Hands K, Kyratzis IL, Werkmeister JA, Ramshaw JAM. A comparison of the effects of fibre alignment of smooth and textured fibres in electrospun membranes on fibroblast cell adhesion. Biomedical Materials 2010;5(2):025005.

[132] Stähli P, Custer R, van Mier JGM. On flow properties, fibre distribution, fibre orientation and flexural behaviour of FRC. Materials and Structures 2008;41(1):189-96.

[133] Shang S, Yang F, Cheng X, Walboomers XF, Jansen JA. The effect of electrospun fibre alignment on the behaviour of rat periodontal ligament cells. European Cells & Materials 2010;19:180-92.

[134] Johnson J, Nowicki MO, Lee CH, Chiocca EA, Viapiano MS, Lawler SE, Lannutti JJ. Quantitative analysis of complex glioma cell migration

on electrospun polycaprolactone using time-lapse microscopy. Tissue Eng Part C Methods 2009;15(4):531-40.

[135] Krifa M, Hammami MA, Wu H. Occurrence and morphology of bead-on-string structures in centrifugal forcespun PA6 fibers. The Journal of The Textile Institute 2015;106(3):284-94.

[136] Liu Y, He J-H, Yu J-y, Zeng H-m. Controlling numbers and sizes of beads in electrospun nanofibers. Polymer International 2008;57(4):632-6.

[137] Lin T, Wang H, Wang H, Wang X. The charge effect of cationic surfactants on the elimination of fibre beads in the electrospinning of polystyrene. 2004;15(9):1375-81.

[138] Lee J-H. Gas sensors using hierarchical and hollow oxide nanostructures: Overview. Sensors and Actuators B: Chemical 2009;140(1):319-36.

[139] Trask RS, Bond IP. Biomimetic self-healing of advanced composite structures using hollow glass fibres. Smart Materials and Structures 2006;15(3):704-10.

[140] Wang H, Ma D, Huang X, Huang Y, Zhang X. General and controllable synthesis strategy of metal oxide/TiO2 hierarchical heterostructures with improved lithium-ion battery performance. Scientific Reports 2012;2:701.

[141] Jeong G, Kim JG, Park MS, Seo M, Hwang SM, Kim YU, Kim YJ, Kim JH, Dou SX. Core-shell structured silicon nanoparticles@TiO2-x/carbon mesoporous microfiber composite as a safe and high-performance lithium-ion battery anode. ACS Nano 2014;8(3):2977-85.

[142] Meneghello G, Parker DJ, Ainsworth BJ, Perera SP, Chaudhuri JB, Ellis MJ, De Bank PA. Fabrication and characterization of poly(lactic-co-glycolic acid)/polyvinyl alcohol blended hollow fibre membranes for tissue engineering applications. Journal of Membrane Science 2009;344(1):55-61.

[143] Wen X, Tresco PA. Fabrication and characterization of permeable degradable poly(dl-lactide-co-glycolide) (PLGA) hollow fiber phase inversion membranes for use as nerve tract guidance channels. Biomaterials 2006;27(20):3800-9.

[144] Russell PSJ, Hölzer P, Chang W, Abdolvand A, Travers JC. Hollow-core photonic crystal fibres for gas-based nonlinear optics. Nature Photonics 2014;8(4):278-86.

[145] Wang X, Drew C, Lee S-H, Senecal KJ, Kumar J, Samuelson LA. Electrospun Nanofibrous Membranes for Highly Sensitive Optical Sensors. Nano Letters 2002;2(11):1273-5.

[146] Hubbell JA. Biomaterials in Tissue Engineering. Bio/Technology 1995;13(6):565-76.

[147] Khan AH, Jiang X, Surwase S, Gultekinoglu M, Bayram C, Sathisaran I, Bhatia D, Ahmed J, Wu B, Ulubayram K, Edirisinghe M, Dalvi SV. Effectiveness of Oil-Layered Albumin Microbubbles Produced Using Microfluidic T-Junctions in Series for In Vitro Inhibition of Tumor Cells. Langmuir 2020;36(39):11429-41.

[148] Lannutti J, Reneker D, Ma T, Tomasko D, Farson D. Electrospinning for tissue engineering scaffolds. Materials Science and Engineering: C 2007;27(3):504-9.

[149] Chen ZG, Wang PW, Wei B, Mo XM, Cui FZ. Electrospun collagen–chitosan nanofiber: A biomimetic extracellular matrix for endothelial cell and smooth muscle cell. Acta Biomaterialia 2010;6(2):372-82.

[150] Mo XM, Xu CY, Kotaki M, Ramakrishna S. Electrospun P(LLA-CL) nanofiber: a biomimetic extracellular matrix for smooth muscle cell and endothelial cell proliferation. Biomaterials 2004;25(10):1883-90.

[151] Hu Y, Grainger DW, Winn SR, Hollinger JO. Fabrication of poly(alpha-hydroxy acid) foam scaffolds using multiple solvent systems. Journal of Biomedical Materials Research 2002;59(3):563-72.

[152] Geng X, Kwon O-H, Jang J. Electrospinning of chitosan dissolved in concentrated acetic acid solution. Biomaterials 2005;26(27):5427-32.

[153] Kim TG, Park TG. Surface Functionalized Electrospun Biodegradable Nanofibers for Immobilization of Bioactive Molecules. Biotechnology Progress 2006;22(4):1108-13.

[154] Hussain A, Collins G, Yip D, Cho CH. Functional 3-D cardiac co-culture model using bioactive chitosan nanofiber scaffolds. Biotechnology and Bioengineering 2013;110(2):637-47.

[155] Mullender M, El Haj AJ, Yang Y, van Duin MA, Burger EH, Klein-Nulend J. Mechanotransduction of bone cellsin vitro: Mechanobiology of bone tissue. Medical and Biological Engineering and Computing 2004;42(1):14-21.

[156] Abrams GA, Goodman SL, Nealey PF, Franco M, Murphy CJ. Nanoscale topography of the basement membrane underlying the corneal epithelium of the rhesus macaque. Cell and Tissue Research 2000;299(1):39-46.

[157] Norman JJ, Desai TA. Methods for fabrication of nanoscale topography for tissue engineering scaffolds. Annals of Biomedical Engineering 2006;34(1):89-101.

[158] Ma PX. Scaffolds for tissue fabrication. Materials Today 2004;7(5):30-40.

[159] Leong KF, Chua CK, Sudarmadji N, Yeong WY. Engineering functionally graded tissue engineering scaffolds. Journal of the Mechanical Behavior of Biomedical Materials 2008;1(2):140-52.

[160] Cowin SC. Bone mechanics handbook. CRC press; 2001.

[161] Kreke MR, Huckle WR, Goldstein AS. Fluid flow stimulates expression of osteopontin and bone sialoprotein by bone marrow stromal cells in a temporally dependent manner. Bone 2005;36(6):1047-55.

[162] Rossi S, Sandri G, Caramella CM. Buccal drug delivery: A challenge already won? Drug Discovery Today: Technologies 2005;2(1):59-65.

[163] Utembe W, Potgieter K, Stefaniak AB, Gulumian M. Dissolution and biodurability: Important parameters needed for risk assessment of nanomaterials. Part Fibre Toxicol 2015;12:11.

[164] Huang Y, Dai W-G. Fundamental aspects of solid dispersion technology for poorly soluble drugs. Acta Pharmaceutica Sinica B 2014;4(1):18-25.

[165] Serajuddin AT. Solid dispersion of poorly water-soluble drugs: early promises, subsequent problems, and recent breakthroughs. Journal of Pharmaceutical Sciences 1999;88(10):1058-66.

[166] Qiu LY, Bae YH. Polymer Architecture and Drug Delivery. Pharmaceutical Research 2006;23(1):1-30.

[167] Celebioglu A, Uyar T. Electrospun formulation of acyclovir/cyclodextrin nanofibers for fast-dissolving antiviral drug delivery. Materials Science and Engineering: C 2021;118:111514.

[168] Wang L, Chang M-W, Ahmad Z, Zheng H, Li J-S. Mass and controlled fabrication of aligned PVP fibers for matrix type antibiotic drug delivery systems. Chemical Engineering Journal 2017;307:661-9.

[169] Chou S-F, Woodrow KA. Relationships between mechanical properties and drug release from electrospun fibers of PCL and PLGA blends. Journal of the Mechanical Behavior of Biomedical Materials 2017;65:724-33.

[170] Siegel SJ, Kahn JB, Metzger K, Winey KI, Werner K, Dan N. Effect of drug type on the degradation rate of PLGA matrices. European Journal of Pharmaceutics and Biopharmaceutics 2006;64(3):287-93.

[171] Cam ME, Hazar-Yavuz AN, Cesur S, Ozkan O, Alenezi H, Turkoglu Sasmazel H, Sayip Eroglu M, Brako F, Ahmed J, Kabasakal L, Ren G, Gunduz O, Edirisinghe M. A novel treatment strategy for preterm birth: Intra-vaginal progesterone-loaded fibrous patches. International Journal of Pharmaceutics 2020;588:119782.

[172] Shen X, Yu D, Zhu L, Branford-White C, White K, Chatterton NP. Electrospun diclofenac sodium loaded Eudragit® L 100-55 nanofibers for colon-targeted drug delivery. International Journal of Pharmaceutics 2011;408(1):200-7.

[173] Sun L, Liu Z, Tian H, Le Z, Liu L, Leong KW, Mao H-Q, Chen Y. Scalable Manufacturing of Enteric Encapsulation Systems for Site-Specific Oral Insulin Delivery. Biomacromolecules 2019;20(1):528-38.

[174] da Silva Júnior WF, de Oliveira Pinheiro JG, Moreira CDLFA, de Souza FJJ, de Lima ÁAN. Chapter 15 - Alternative Technologies to Improve Solubility and Stability of Poorly Water-Soluble Drugs. In: Grumezescu AM, editor Multifunctional Systems for Combined Delivery, Biosensing and Diagnostics. Elsevier; 2017, p. 281-305.

[175] Ahmed J, Harker A, Edirisinghe M. COVID-19: Facemasks, healthcare policies and risk factors in the crucial initial months of a global pandemic. Medical Devices & Sensors 2020:e10120.

[176] Gopal R, Kaur S, Ma Z, Chan C, Ramakrishna S, Matsuura T. Electrospun nanofibrous filtration membrane. Journal of Membrane Science 2006;281(1):581-6.

[177] Sparks T, Chase G. Section 7 - Filter Selection, Process Design, Testing, Optimization and Troubleshooting Guidelines. In: Sparks T, Chase G, editors. Filters and Filtration Handbook (Sixth Edition). Oxford: Butterworth-Heinemann; 2016, p. 383-413.

[178] Gorgojo P, Karan S, Wong HC, Jimenez-Solomon MF, Cabral JT, Livingston AG. Ultrathin Polymer Films with Intrinsic Microporosity: Anomalous Solvent Permeation and High Flux Membranes. Advanced Functional Materials 2014;24(30):4729-37.

[179] Soyekwo F, Zhang Q, Gao R, Qu Y, Lin C, Huang X, Zhu A, Liu Q. Cellulose nanofiber intermediary to fabricate highly-permeable ultrathin nanofiltration membranes for fast water purification. Journal of Membrane Science 2017;524:174-85.

[180] Anaissie EJ, Penzak SR, Dignani MC. The Hospital Water Supply as a Source of Nosocomial Infections: A Plea for Action. Archives of Internal Medicine 2002;162(13):1483-92.

[181] Barna Z, Antmann K, Pászti J, Bánfi R, Kádár M, Szax A, Németh M, Szegő E, Vargha M. Infection control by point-of-use water filtration in an intensive care unit – a Hungarian case study. Journal of Water and Health 2014;12(4):858-67.

[182] Walker JT, Jhutty A, Parks S, Willis C, Copley V, Turton JF, Hoffman PN, Bennett AM. Investigation of healthcare-acquired infections associated with Pseudomonas aeruginosa biofilms in taps in neonatal units in Northern Ireland. Journal of Hospital Infection 2014;86(1):16-23.

[183] Illangakoon UE, Mahalingam S, Wang K, Cheong YK, Canales E, Ren GG, Cloutman-Green E, Edirisinghe M, Ciric L. Gyrospun antimicrobial nanoparticle loaded fibrous polymeric filters. Materials Science and Engineering C 2017;74:315-24.

[184] Diegelmann RF, Evans MC. Wound healing: an overview of acute, fibrotic and delayed healing. Frontiers in Bioscience 2004;9:283-9.

[185] Broughton GI, Janis JE, Attinger CE. The Basic Science of Wound Healing. Plastic and Reconstructive Surgery 2006;117(7S):12S-34S.

[186] Hayes TR, Su B. 15 - Wound dressings. In: Bosworth LA, Downes S, editors. Electrospinning for Tissue Regeneration. Woodhead Publishing; 2011, p. 317-39.

[187] Jones VJ. The use of gauze: will it ever change? International Wound Journal 2006;3(2):79-88.

[188] Butcher M. Introducing a new paradigm for bioburden management. Journal of Wound Care 2011;20(Sup3):4-19.

[189] Kai D, Jin G, Prabhakaran MP, Ramakrishna S. Electrospun synthetic and natural nanofibers for regenerative medicine and stem cells. Biotechnology Journal 2013;8(1):59-72.

[190] Schneider M, Claverie J, Graillat C, McKenna TF. High solids content emulsions. I. A study of the influence of the particle size distribution and polymer concentration on viscosity. Journal of Applied Polymer Science 2002;84(10):1878-96.

[191] Tirtaatmadja V, McKinley GH, Cooper-White JJ. Drop formation and breakup of low viscosity elastic fluids: Effects of molecular weight and concentration. Physics of Fluids 2006;18(4):043101.

[192] Olayiwola SO, Dejam M. Mathematical modelling of surface tension of nanoparticles in electrolyte solutions. Chemical Engineering Science 2019;197:345-56.

[193] Eastoe J, Dalton JS. Dynamic surface tension and adsorption mechanisms of surfactants at the air–water interface. Advances in Colloid and Interface Science 2000;85(2):103-44.

[194] Wannatong L, Sirivat A, Supaphol P. Effects of solvents on electrospun polymeric fibers: preliminary study on polystyrene. Polymer International 2004;53(11):1851-9.

[195] Chen BT. Investigation of the solvent-evaporation effect on spin coating of thin films. Polymer Engineering & Science 1983;23(7):399-403.

[196] Megelski S, Stephens JS, Chase DB, Rabolt JF. Micro- and Nanostructured Surface Morphology on Electrospun Polymer Fibers. Macromolecules 2002;35(22):8456-66.

[197] Martin A, Newburger J, Adjei A. Extended hildebrand solubility approach: Solubility of theophylline in polar binary solvents. Journal of Pharmaceutical Sciences 1980;69(5):487-91.

[198] Seedher N, Agarwal P. Various solvent systems for solubility enhancement of enrofloxacin. Indian Journal of Pharmaceutical Sciences 2009;71(1):82-7.

[199] Ponhan W, Maensiri S. Fabrication and magnetic properties of electrospun copper ferrite (CuFe2O4) nanofibers. Solid State Sciences 2009;11(2):479-84.

[200] Fridrikh SV, Yu JH, Brenner MP, Rutledge GC. Controlling the Fiber Diameter during Electrospinning. Physical Review Letters 2003;90(14):144502.

[201] SalehHudin HS, Mohamad EN, Mahadi WNL, Muhammad Afifi A. Multiple-jet electrospinning methods for nanofiber processing: A review. Materials and Manufacturing Processes 2018;33(5):479-98.

[202] Weitz RT, Harnau L, Rauschenbach S, Burghard M, Kern K. Polymer Nanofibers via Nozzle-Free Centrifugal Spinning. Nano Letters 2008;8(4):1187-91.

[203] Raimi-Abraham BT, Mahalingam S, Edirisinghe M, Craig DQM. Generation of poly(N-vinylpyrrolidone) nanofibres using pressurised gyration. Materials Science and Engineering: C 2014;39(Supplement C):168-76.

[204] Hong X, Mahalingam S, Edirisinghe M. Simultaneous Application of Pressure-Infusion-Gyration to Generate Polymeric Nanofibers. Macromolecular Materials and Engineering 2017;302(6):1600564.

[205] Yuan X, Zhang Y, Dong C, Sheng J. Morphology of ultrafine polysulfone fibers prepared by electrospinning. Polymer International 2004;53(11):1704-10.

[206] McClure MJ, Sell SA, Ayres CE, Simpson DG, Bowlin GL. Electrospinning-aligned and random polydioxanone–polycaprolactone–silk fibroin-blended scaffolds: geometry for a vascular matrix. Biomedical Materials 2009;4(5):055010.

[207] Pan H, Li L, Hu L, Cui X. Continuous aligned polymer fibers produced by a modified electrospinning method. Polymer 2006;47(14):4901-4.

[208] Lai PK, Roy J. Antimicrobial and chemopreventive properties of herbs and spices. Current Medicinal Chemistry 2004;11(11):1451-60.

[209] Gibbons A, Aldhous P. Exploring new strategies to fight drug-resistant microbes. Science 1992;257:1036+.

[210] Peter K. Handbook of herbs and spices. Woodhead publishing; 2006.

[211] Rothe M. K. T. Farrell: Spices, Condiments, and Seasonings. Food / Nahrung 1986;30(10):1077-.

[212] Ceylan E, Fung DYC. Antimicrobial Activity Of Spices. Journal of Rapid Methods & Automation in Microbiology 2004;12(1):1-55.

[213] Govindarajan VS. Turmeric--chemistry, technology, and quality. Critical Reviews in Food Science and Nutrition 1980;12(3):199-301.

[214] Shishodia S, Sethi G, Aggarwal BB. Curcumin: Getting Back to the Roots. Annals of the New York Academy of Sciences 2005;1056(1):206-17.

[215] Ruby AJ, Kuttan G, Dinesh Babu K, Rajasekharan KN, Kuttan R. Anti-tumour and antioxidant activity of natural curcuminoids. Cancer Letters 1985;94(1):79-83.

[216] Chattopadhyay I, Biswas K, Bandyopadhyay U, K. Banerjee R. Turmeric and Curcumin: Biological actions and medicinal applications. 2003.

[217] De R, Kundu P, Swarnakar S, Ramamurthy T, Chowdhury A, Nair GB, Mukhopadhyay AK. Antimicrobial activity of curcumin against Helicobacter pylori isolates from India and during infections in mice. Antimicrobial Agents and Chemotherapy 2009;53(4):1592.

[218] Attaguile G, Russo A, Campisi A, Savoca F, Acquaviva R, Ragusa N, Vanella A. Antioxidant activity and protective effect on DNA cleavage of extracts from Cistus incanus L. and Cistus monspeliensis L. Cell Biology and Toxicology 2000;16(2):83-90.

[219] Dimcheva V, Karsheva M. Cistus incanus from Strandja Mountain as a Source of Bioactive Antioxidants. Plants 2018;7(1).

[220] Petereit F, Nahrstedt A, Innerlich B, Luepke NP, Theissen NL, Kemper FH, Winterhoff H. Antiinflammatory Activity of the Traditionally Used Herb of Cistus incanus. 1989.

[221] Wang L, Weller CL. Recent advances in extraction of nutraceuticals from plants. Trends in Food Science & Technology 2006;17(6):300-12.

[222] Barceloux DG. Cinnamon (Cinnamomum Species). Disease-a-Month 2009;55(6):327-35.

[223] Toussaint-Samat M. A History of Food. Wiley; 2009.

[224] Ravindran PN, Nirmal-Babu K, Shylaja M. Cinnamon and Cassia: The Genus Cinnamomum. CRC Press; 2003.

[225] Ziment I. History of the treatment of chronic bronchitis. Respiration 1991;58 Suppl 1:37-42.

[226] Kamath JV, Rana AC, Chowdhury AR. Pro-healing effect of Cinnamomum zeylanicum bark. Phytotherapy Research 2003;17(8):970-2.

[227] Chao LK, Hua KF, Hsu HY, Cheng SS, Liu JY, Chang ST. Study on the antiinflammatory activity of essential oil from leaves of Cinnamomum osmophloeum. Journal of Agricultural and Food Chemistry 2005;53(18):7274-8.

[228] Pham AQ, Kourlas H, Pham DQ. Cinnamon supplementation in patients with type 2 diabetes mellitus. Pharmacotherapy 2007;27(4):595-9.

[229] Simic A, Sokovic MD, Ristic M, Grujic-Jovanovic S, Vukojevic J, Marin PD. The chemical composition of some Lauraceae essential oils and their antifungal activities. Phytotherapy Research 2004;18(9):713-7.

[230] Premanathan M, Rajendran S, Ramanathan T, Kathiresan K, Nakashima H, Yamamoto N. A survey of some Indian medicinal plants for anti-human immunodeficiency virus (HIV) activity. Indian Journal of Medical Research 2000;112:73-7.

[231] Sedighi M, Nazari A, Faghihi M, Rafieian-Kopaei M, Karimi A, Moghimian M, Mozaffarpur SA, Rashidipour M, Namdari M, Cheraghi M, Rasoulian B. Protective effects of cinnamon bark extract against ischemia–reperfusion injury and arrhythmias in rat. Phytotherapy Research 2018;0(0).

[232] Mishra AK, Singh BK, Pandey AK. In vitro-antibacterial activity and phytochemical profiles of Cinnamomum tamala (Tejpat) leaf extracts and oil. Reviews in Infection 2010;1(3):134-9.

[233] Didry N, Dubreuil L, Pinkas M. Antibacterial activity of thymol, carvacrol and cinnamaldehyde alone or in combination. Die Pharmazie 1993;48(4):301-4.

[234] Pei Rs, Zhou F, Ji Bp, Xu J. Evaluation of Combined Antibacterial Effects of Eugenol, Cinnamaldehyde, Thymol, and Carvacrol against E. coli with an Improved Method. Journal of Food Science 2009;74(7):M379-M83.

[235] Zhou F, Ji B, Zhang H, Jiang HUI, Yang Z, Li J, Li J, Yan W. The Antibacterial Effect of Cinnamaldehyde, Thymol, Carvacrol and Their Combinations Against the Foodborne Pathogen Salmonella Typhimurium. Journal of Food Safety 2007;27(2):124-33.

[236] Zumla A, Lulat A. Honey--a remedy rediscovered. Journal of the Royal Society of Medicine 1989;82(7):384-5.

[237] Al-Jabri AA. Honey, milk and antibiotics. African Journal of Biotechnology 2005;4(13).

[238] Bansal V, Medhi B, Pandhi P. Honey--a remedy rediscovered and its therapeutic utility. Kathmandu University Medical Journal (KUMJ) 2005;3(3):305-9.

[239] Efem SE. Clinical observations on the wound healing properties of honey. British Journal of Surgery 1988;75(7):679-81.

[240] Lusby PE, Coombes A, Wilkinson JM. Honey: A Potent Agent for Wound Healing? Journal of Wound Ostomy & Continence Nursing 2002;29(6):295-300.

[241] Bergman A, Yanai J, Weiss J, Bell D, David MP. Acceleration of wound healing by topical application of honey. An animal model. American Journal of Surgery 1983;145(3):374-6.

[242] Al-Waili N, Salom K, Al-Ghamdi AA. Honey for wound healing, ulcers, and burns; data supporting its use in clinical practice. The Scientific World Journal

2011;11:766-87.

[243] Oryan A, Zaker SR. Effects of topical application of honey on cutaneous wound healing in rabbits. Zentralblatt für Veterinärmedizin Reihe A 1998;45(3):181-8.

[244] Cavanagh D, Beazley J, Ostapowicz F. Radical operation for carcinoma of the vulva. A new approach to wound healing. Journal of Obstetrics and Gynaecology of the British Commonwealth 1970;77(11):1037-40.

[245] Ball DW. The Chemical Composition of Honey. Journal of Chemical Education 2007;84(10):1643.

[246] Bizerra FC, Da Silva PI, Jr., Hayashi MAF. Exploring the antibacterial properties of honey and its potential. Frontiers in Microbiology 2012;3:398-.

[247] al Somal N, Coley KE, Molan PC, Hancock BM. Susceptibility of Helicobacter pylori to the antibacterial activity of manuka honey. Journal of the Royal Society of Medicine 1994;87(1):9-12.

[248] Bucekova M, Buriova M, Pekarik L, Majtan V, Majtan J. Phytochemicals-mediated production of hydrogen peroxide is crucial for high antibacterial activity of honeydew honey. 2018;8(1):9061.

[249] Willix DJ, Molan PC, Harfoot CG. A comparison of the sensitivity of wound-infecting species of bacteria to the antibacterial activity of manuka honey and other honey. Journal of Applied Bacteriology 1992;73(5):388-94.

[250] Chirife J, Scarmato G, Herszage L. Scientific basis for use of granulated sugar in treatment of infected wounds. Lancet 1982;1(8271):560-1.

[251] Khan FR, Ul Abadin Z, Rauf N. Honey: nutritional and medicinal value. International Journal of Clinical Practice 2007;61(10):1705-7.

[252] Clark RAF. Basics of Cutaneous Wound Repair. The Journal of Dermatologic Surgery and Oncology 1993;19(8):693-706.

[253] Burdon RH. Superoxide and hydrogen peroxide as cellularly generated life-signals in the balance between proliferation and cell death. In: Cutler RG, Packer L, Bertram J, Mori A, eds. *Oxidative Stress and Aging.* Basel: Birkhäuser Basel; 1995:27-33.

[254] Yoo SK, Huttenlocher A. Innate immunity: wounds burst H2O2 signals to leukocytes. Current Biology 2009;19(14):R553-5.

[255] Cho M, Hunt TK, Hussain MZ. Hydrogen peroxide stimulates macrophage vascular endothelial growth factor release. American Journal of Physiology: Heart and Circulatory Physiology 2001;280(5):H2357-63.

[256] Patino MG, Neiders ME, Andreana S, Noble B, Cohen RE. Collagen: An Overview. Implant Dentistry 2002;11(3):280-5.

[257] McPherson JM, Sawamura S, Armstrong R. An examination of the biologic response to injectable, glutaraldehyde cross-linked collagen implants. Journal of Biomedical Materials Research 1986;20(1):93-107.

[258] Hayashida T, Poncelet A-C, Hubchak SC, Schnaper HW. TGF-β1 activates MAP kinase in human mesangial cells: A possible role in collagen expression. Kidney International 1999;56(5):1710-20.

[259] Franceschi RT, Iyer BS. Relationship between collagen synthesis and expression of the osteoblast phenotype in MC3T3-E1 cells. Journal of Bone and Mineral Research 1992;7(2):235-46.

[260] Fonseca MJ, Alsina MA, Reig F. Coating liposomes with collagen (Mr 50,000) increases uptake into liver. Biochimica et Biophysica Acta 1996;1279(2):259-65.

[261] Maeda M, Tani S, Sano A, Fujioka K. Microstructure and release characteristics of the minipellet, a collagen-based drug delivery system for controlled release of protein drugs. Journal of Controlled Release 1999;62(3):313-24.

[262] Lee CH, Singla A, Lee Y. Biomedical applications of collagen. International Journal of Pharmaceutics 2001;221(1):1-22.

[263] Baranoski S, Ayello EA. Wound dressings: an evolving art and science. Advances in Skin & Wound Care 2012;25(2):87-92; quiz -4.

[264] Fleck CA, Simman R. Modern collagen wound dressings: function and purpose. Journal of the American College of Certified Wound Specialists 2010;2(3):50-4.

[265] Fleck CA, Chakravarthy D. Understanding the Mechanisms of Collagen Dressings. Advances in Skin & Wound Care 2007;20(5):256-9.

[266] Cullen B, Smith R, McCulloch E, Silcock D, Morrison L. Mechanism of action of PROMOGRAN, a protease modulating matrix, for the treatment of diabetic foot ulcers. Wound Repair and Regeneration 2002;10(1):16-25.

[267] Prudden JF, Nishihara G, Baker L. The acceleration of wound healing with cartilage. I. Surgery, Gynecology and Obstetrics 1957;105(3):283-6.

[268] Prudden JF, Migel P, Hanson P, Friedrich L, Balassa L. The discovery of a potent pure chemical wound-healing accelerator. American Journal of Surgery 1970;119(5):560-4.

[269] Davies DH, Hayes ER. Determination of the degree of acetylation of chitin and chitosan. Methods in Enzymology. Academic Press; 1988, p. 442-6.

[270] Ravi Kumar MNV. A review of chitin and chitosan applications. Reactive and Functional Polymers 2000;46(1):1-27.

[271] Muzzarelli C, Muzzarelli RAA. Natural and artificial chitosan–inorganic composites. Journal of Inorganic Biochemistry 2002;92(2):89-94.

[272] Peniche C, Argüelles-Monal W, Peniche H, Acosta N. Chitosan: An Attractive Biocompatible Polymer for Microencapsulation. Macromolecular Bioscience 2003;3(10):511-20.

[273] Dai T, Tanaka M, Huang Y-Y, Hamblin MR. Chitosan preparations for wounds and burns: antimicrobial and wound-healing effects. Expert Review of Anti-Infective Therapy 2011;9(7):857-79.

[274] Muzzarelli R, Biagini G, Pugnaloni A, Filippini O, Baldassarre V, Castaldini C, Rizzoli C. Reconstruction of parodontal tissue with chitosan. Biomaterials 1989;10(9):598-603.

[275] Ishihara M, Ono K, Sato M, Nakanishi K, Saito Y, Yura H, Matsui T, Hattori H, Fujita M, Kikuchi M, Kurita A. Acceleration of wound contraction and healing with a photocrosslinkable chitosan hydrogel. Wound Repair and Regeneration 2001;9(6):513-21.

[276] Ishihara M, Nakanishi K, Ono K, Sato M, Kikuchi M, Saito Y, Yura H, Matsui T, Hattori H, Uenoyama M, Kurita A. Photocrosslinkable chitosan as a dressing for wound occlusion and accelerator in healing process. Biomaterials 2002;23(3):833-40.

[277] Stone CA, Wright H, Clarke T, Powell R, Devaraj VS. Healing at skin graft donor sites dressed with chitosan. British Journal of Plastic Surgery 2000;53(7):601-6.

[278] Minami S, Okamoto Y, Hamada K, Fukumoto Y, Shigemasa Y. Veterinary practice with chitin and chitosan. EXS 1999;87:265-77.

[279] Muzzarelli RA, Mattioli-Belmonte M, Pugnaloni A, Biagini G. Biochemistry, histology and clinical uses of chitins and chitosans in wound healing. EXS 1999;87:251-64.

[280] Paul W, Sharma CP, Tirunal C. Chitosan and Alginate Wound Dressings: A Short Review. Medicine; 2004.

[281] Mi FL, Shyu SS, Wu YB, Lee ST, Shyong JY, Huang RN. Fabrication and characterization of a sponge-like asymmetric chitosan membrane as a wound dressing. Biomaterials 2001;22(2):165-73.

[282] Zhang M, Tan T, Yuan H, Rui C. Insecticidal and Fungicidal Activities of Chitosan and Oligo-chitosan. Journal of Bioactive and Compatible Polymers 2003;18(5):391-400.

[283] Agboh OC, Qin Y. Chitin and Chitosan Fibers. Polymers for Advanced Technologies 1997;8(6):355-65.

[284] Mi F-L, Wu Y-B, Shyu S-S, Schoung J-Y, Huang Y-B, Tsai Y-H, Hao J-Y. Control of wound infections using a bilayer chitosan wound dressing with sustainable antibiotic delivery. Journal of Biomedical Materials Research 2002;59(3):438-49.

[285] Ohkawa K, Cha D, Kim H, Nishida A, Yamamoto H. Electrospinning of Chitosan. Macromolecular Rapid Communications 2004;25(18):1600-5.

[286] Draget KI, Skjåk-Bræk G, Smidsrød O. Alginate based new materials. International Journal of Biological Macromolecules 1997;21(1):47-55.

[287] Lee KY, Mooney DJ. Alginate: Properties and biomedical applications. Progress in Polymer Science 2012;37(1):106-26.

[288] Amici E, Tetradis-Meris G, de Torres CP, Jousse F. Alginate gelation in microfluidic channels. Food Hydrocolloids 2008;22(1):97-104.

[289] Klöck G, Pfeffermann A, Ryser C, Gröhn P, Kuttler B, Hahn H-J, Zimmermann U. Biocompatibility of mannuronic acid-rich alginates. Biomaterials 1997;18(10):707-13.

[290] Sweeney IR, Miraftab M, Collyer G. Absorbent alginate fibres modified with hydrolysed chitosan for wound care dressings – II. Pilot scale development. Carbohydrate Polymers 2014;102:920-7.

[291] Queen D, Orsted H, Sanada H, Sussman G. A dressing history. International Wound Journal 2004;1(1):59-77.

[292] Qin Y. The gel swelling properties of alginate fibers and their applications in wound management. Polymers for Advanced Technologies 2008;19(1):6-14.

[293] Balakrishnan B, Mohanty M, Fernandez AC, Mohanan PV, Jayakrishnan A. Evaluation of the effect of incorporation of dibutyryl cyclic adenosine monophosphate in an in situ-forming hydrogel wound dressing based on oxidized alginate and gelatin. Biomaterials 2006;27(8):1355-61.

[294] Guest JF, Ayoub N, McIlwraith T, Uchegbu I, Gerrish A, Weidlich D, Vowden K, Vowden P. Health economic burden that wounds impose on the National Health Service in the UK. BMJ Open 2015;5(12).

[295] Hosgood G. Stages of Wound Healing and Their Clinical Relevance. Veterinary Clinics: Small Animal Practice 2006;36(4):667-85.

[296] Jamieson GA, Urban CL, Barber AJ. Enzymatic Basis for Platelet: Collagen Adhesion as the Primary Step in Haemostasis. Nature New Biology 1971;234(44):5-7.

[297] Weigel PH, Frost SJ, LeBoeuf RD, McGary CT. The specific interaction between fibrin(ogen) and hyaluronan: possible consequences in haemostasis, inflammation and wound healing. Ciba Foundation Symposium 1989;143:248-61; discussion 61-4, 81-5.

[298] Kurkinen M, Vaheri A, Roberts PJ, Stenman S. Sequential appearance of fibronectin and collagen in experimental granulation tissue. Laboratory Investigation 1980;43(1):47-51.

[299] Ruszczak Z. Effect of collagen matrices on dermal wound healing. Advanced Drug Delivery Reviews 2003;55(12):1595-611.

[300] Xie Z, Paras CB, Weng H, Punnakitikashem P, Su L-C, Vu K, Tang L, Yang J, Nguyen KT. Dual growth factor releasing multi-functional nanofibers for wound healing. Acta Biomaterialia 2013;9(12):9351-9.

[301] Grotendorst GR, Soma Y, Takehara K, Charette M. EGF and TGF-alpha are potent chemoattractants for endothelial cells and EGF-like peptides are present at sites of tissue regeneration. Journal of Cellular Physiology 1989;139(3):617-23.

[302] Eming SA, Brachvogel B, Odorisio T, Koch M. Regulation of angiogenesis: Wound healing as a model. Progress in Histochemistry and Cytochemistry 2007;42(3):115-70.

[303] Broughton G, 2nd, Janis JE, Attinger CE. Wound healing: an overview. Plastic and Reconstructive Surgery 2006;117(7 Suppl):1e-S-32e-S.

[304] Teller P, White TK. The Physiology of Wound Healing: Injury Through Maturation. Perioperative Nursing Clinics 2011;6(2):159-70.

[305] Oxlund H, Christensen H, Seyer-Hansen M, Andreassen TT. Collagen Deposition and Mechanical Strength of Colon Anastomoses and Skin Incisional Wounds of Rats. Journal of Surgical Research 1996;66(1):25-30.

[306] Moriguchi T, Fujimoto D. Crosslink of Collagen in Hypertrophic Scar. Journal of Investigative Dermatology 1979;72(3):143-5.

[307] Bostock RM, Stermer BA. Perspectives on Wound Healing in Resistance to Pathogens. Annual Review of Phytopathology 1989;27(1):343-71.

[308] Sen CK. Wound healing essentials: Let there be oxygen. Wound Repair and Regeneration 2009;17(1):1-18.

[309] Okur ME, Karantas ID, Şenyiğit Z, Okur NÜ, Siafaka PI. Recent trends on wound management; new therapeutic choices based on polymeric carriers. Asian Journal of Pharmaceutical Sciences 2020.

[310] Vowden K, Vowden P. Understanding exudate management and the role of exudate in the healing process. British Journal of Community Nursing 2003;8(Sup5):S4-S13.

[311] Field CK, Kerstein MD. Overview of wound healing in a moist environment. The American Journal of Surgery 1994;167(1, Supplement):S2-S6.

[312] Zahedi P, Rezaeian I, Ranaei-Siadat S-O, Jafari S-H, Supaphol P. A review on wound dressings with an emphasis on electrospun nanofibrous polymeric bandages. Polymers for Advanced Technologies 2010;21(2):77-95.

[313] Mori R, Kondo T, Ohshima T, Ishida Y, Mukaida N. Accelerated wound healing in tumor necrosis factor receptor p55-deficient mice with reduced leukocyte infiltration. The FASEB Journal 2002;16(9):963-74.

[314] Laçin NT. Development of biodegradable antibacterial cellulose based hydrogel membranes for wound healing. International Journal of Biological Macromolecules 2014;67:22-7.

[315] Hu Y, Catchmark JM. In vitro biodegradability and mechanical properties of bioabsorbable bacterial cellulose incorporating cellulases. Acta Biomaterialia 2011;7(7):2835-45.

[316] Wu J, Zheng Y, Yang Z, Lin Q, Qiao K, Chen X, Peng Y. Influence of dialdehyde bacterial cellulose with the nonlinear elasticity and topology structure of ECM on cell adhesion and proliferation. RSC Advances 2014;4(8):3998-4009.

[317] Svensson A, Nicklasson E, Harrah T, Panilaitis B, Kaplan DL, Brittberg M, Gatenholm P. Bacterial cellulose as a potential scaffold for tissue engineering of cartilage. Biomaterials 2005;26(4):419-31.

[318] Torres GF, Commeaux S, Troncoso PO. Biocompatibility of Bacterial Cellulose Based Biomaterials. Journal of Functional Biomaterials 2012;3(4).

[319] Helenius G, Backdahl H, Bodin A, Nannmark U, Gatenholm P, Risberg B. In vivo biocompatibility of bacterial cellulose. Journal of Biomedical Materials Research: Part A 2006;76(2):431-8.

[320] Lin W-C, Lien C-C, Yeh H-J, Yu C-M, Hsu S-h. Bacterial cellulose and bacterial cellulose–chitosan membranes for wound dressing applications. Carbohydrate Polymers 2013;94(1):603-11.

[321] Nakayama A, Kakugo A, Gong JP, Osada Y, Takai M, Erata T, Kawano S. High Mechanical Strength Double-Network Hydrogel with Bacterial Cellulose. Advanced Functional Materials 2004;14(11):1124-8.

[322] Naritomi T, Kouda T, Yano H, Yoshinaga F. Effect of lactate on bacterial cellulose production from fructose in continuous culture. Journal of Fermentation and Bioengineering 1998;85(1):89-95.

[323] Wan YZ, Luo H, He F, Liang H, Huang Y, Li XL. Mechanical, moisture absorption, and biodegradation behaviours of bacterial cellulose fibre-reinforced starch biocomposites. Composites Science and Technology 2009;69(7):1212-7.

[324] Ul-Islam M, Khan T, Park JK. Water holding and release properties of bacterial cellulose obtained by in situ and ex situ modification. Carbohydrate Polymers 2012;88(2):596-603.

[325] Schrecker ST, Gostomski PA. Determining the Water Holding Capacity of Microbial Cellulose. Biotechnology Letters 2005;27(19):1435-8.

[326] Lin S-B, Hsu C-P, Chen L-C, Chen H-H. Adding enzymatically modified gelatin to enhance the rehydration abilities and mechanical properties of bacterial cellulose. Food Hydrocolloids 2009;23(8):2195-203.

[327] Iguchi M, Yamanaka S, Budhiono A. Bacterial cellulose—a masterpiece of nature's arts. Journal of Materials Science 2000;35(2):261-70.

[328] Nishi Y, Uryu M, Yamanaka S, Watanabe K, Kitamura N, Iguchi M, Mitsuhashi S. The structure and mechanical properties of sheets prepared from bacterial cellulose. Journal of Materials Science 1990;25(6):2997-3001.

[329] Vowden K, Vowden P. Wound dressings: principles and practice. Surgery (Oxford) 2017;35(9):489-94.

[330] Queen D, Evans JH, Gaylor JDS, Courtney JM, Reid WH. An in vitro assessment of wound dressing conformability. Biomaterials 1987;8(5):372-6.

[331] Dhivya S, Padma VV, Santhini E. Wound dressings - a review. Biomedicine 2015;5(4):22-.

[332] Broughton G, 2nd, Janis JE, Attinger CE. A brief history of wound care. Plastic and Reconstructive Surgery 2006;117(7 Suppl):6s-11s.

[333] Ovington LG. Hanging wet-to-dry dressings out to dry. Home Healthcare Nurse 2001;19(8):477-83; quiz 84.

[334] Falanga V. Occlusive Wound Dressings: Why, When, Which? Archives of Dermatology 1988;124(6):872-7.

[335] Dinner MI, Peters CR, Sherer J. Use of a semipermeable polyurethane membrane as a dressing for split-skin graft donor sites. Plastic and Reconstructive Surgery 1979;64(1):112-4.

[336] Seaman S. Dressing selection in chronic wound management. Journal of the American Podiatric Medical Association 2002;92(1):24-33.

[337] Brett DW. A review of moisture-control dressings in wound care. Journal of Wound, Ostomy and Continence Nursing 2006;33(6 Suppl):S3-8.

[338] Waycaster C, Milne CT. Clinical and economic benefit of enzymatic debridement of pressure ulcers compared to autolytic debridement with a hydrogel dressing. Journal of Medical Economics 2013;16(7):976-86.

[339] Jandera V, Hudson DA, de Wet PM, Innes PM, Rode H. Cooling the burn wound: evaluation of different modalites. Burns 2000;26(3):265-70.

[340] Tabata Y, Hijikata S, Ikada Y. Enhanced vascularization and tissue granulation by basic fibroblast growth factor impregnated in gelatin hydrogels. Journal of Controlled Release 1994;31(2):189-99.

[341] Dumville JC, Deshpande S, O'Meara S, Speak K. Hydrocolloid dressings for healing diabetic foot ulcers. Cochrane Database of Systematic Reviews 2013(8).

[342] Varghese MC, Balin AK, Carter DM, Caldwell D. Local Environment of Chronic Wounds Under Synthetic Dressings. Archives of Dermatology 1986;122(1):52-7.

[343] Sood A, Granick MS, Tomaselli NL. Wound Dressings and Comparative Effectiveness Data. Advances in Wound Care 2014;3(8):511-29.

[344] Jude EB, Apelqvist J, Spraul M, Martini J, the Silver Dressing Study G. Prospective randomized controlled study of Hydrofiber® dressing containing ionic silver or calcium alginate dressings in non-ischaemic diabetic foot ulcers. Diabetic Medicine 2007;24(3):280-8.

[345] Perumal CJ, Robson M. CASE REPORT Use of a Hydroconductive Dressing to Treat a Traumatic Avulsive Injury of the Face. Eplasty 2012;12:e32-e.

[346] Afshar A, Yuca E, Wisdom C, Alenezi H, Ahmed J, Tamerler C, Edirisinghe M. Next-generation Antimicrobial Peptides (AMPs) incorporated nanofibre wound dressings. Medical Devices & Sensors 2020:e10144.

[347] Ferguson MWJ, O'Kane S. Scar-free healing: from embryonic mechanisms to adult therapeutic intervention. Philosophical

transactions of the Royal Society of London Series B, Biological sciences 2004;359(1445):839-50.

[348] Hantash BM, Zhao L, Knowles JA, Lorenz HP. Adult and fetal wound healing. Frontiers in Bioscience 2008;13:51-61.

[349] Krummel TM, Nelson JM, Diegelmann RF, Lindblad WJ, Salzberg AM, Greenfield LJ, Cohen IK. Fetal response to injury in the rabbit. Journal of Pediatric Surgery 1987;22(7):640-4.

[350] Gauglitz GG, Korting HC, Pavicic T, Ruzicka T, Jeschke MG. Hypertrophic Scarring and Keloids: Pathomechanisms and Current and Emerging Treatment Strategies. Molecular Medicine 2011;17(1):113-25.

[351] Reish RG, Eriksson E. Scar Treatments: Preclinical and Clinical Studies. Journal of the American College of Surgeons 2008;206(4):719-30.

[352] Walmsley GG, Maan ZN, Wong VW, Duscher D, Hu MS, Zielins ER, Wearda T, Muhonen E, McArdle A, Tevlin R, Atashroo DA, Senarath-Yapa K, Lorenz HP, Gurtner GC, Longaker MT. Scarless Wound Healing: Chasing the Holy Grail. Plastic and Reconstructive Surgery 2015;135(3):907-17.

[353] Rhett JM, Ghatnekar GS, Palatinus JA, O'Quinn M, Yost MJ, Gourdie RG. Novel therapies for scar reduction and regenerative healing of skin wounds. Trends in Biotechnology 2008;26(4):173-80.

[354] Burnham JP, Kirby JP, Kollef MH. Diagnosis and management of skin and soft tissue infections in the intensive care unit: a review. Intensive Care Medicine 2016;42(12):1899-911.

[355] Cardona AF, Wilson SE. Skin and Soft-Tissue Infections: A Critical Review and the Role of Telavancin in Their Treatment. Clinical Infectious Diseases 2015;61(suppl_2):S69-S78.

[356] Simoes D, Miguel SP, Ribeiro MP, Coutinho P, Mendonca AG, Correia IJ. Recent advances on antimicrobial wound dressing: A review. European Journal of Pharmaceutics and Biopharmaceutics 2018;127:130-41.

[357] Pawar HV, Tetteh J, Boateng JS. Preparation, optimisation and characterisation of novel wound healing film dressings loaded with

streptomycin and diclofenac. Colloids and Surfaces B: Biointerfaces 2013;102:102-10.

[358] Lan Y, Li W, Guo R, Zhang Y, Xue W, Zhang Y. Preparation and characterisation of vancomycin-impregnated gelatin microspheres/silk fibroin scaffold. Journal of Biomaterials Science, Polymer Edition 2014;25(1):75-87.

[359] Adhirajan N, Shanmugasundaram N, Shanmuganathan S, Babu M. Collagen-based wound dressing for doxycycline delivery: In-vivo evaluation in an infected excisional wound model in rats. Journal of Pharmacy and Pharmacology 2009;61(12):1617-23.

[360] Albrich WC, Monnet DL, Harbarth S. Antibiotic selection pressure and resistance in Streptococcus pneumoniae and Streptococcus pyogenes. Emerging Infectious Diseases 2004;10(3):514-7.

[361] Yang Y, Qin Z, Zeng W, Yang T, Cao Y, Mei C, Kuang Y. Toxicity assessment of nanoparticles in various systems and organs. Nanotechnology Reviews 2017;6(3):279-89.

[362] Azam A, Ahmed AS, Oves M, Khan MS, Habib SS, Memic A. Antimicrobial activity of metal oxide nanoparticles against Gram-positive and Gram-negative bacteria: a comparative study. International journal of nanomedicine 2012;7:6003-9.

[363] Schröfel A, Kratošová G, Šafařík I, Šafaříková M, Raška I, Shor LM. Applications of biosynthesized metallic nanoparticles – A review. Acta Biomaterialia 2014;10(10):4023-42.

[364] Pachón LD, Rothenberg G. Transition-metal nanoparticles: synthesis, stability and the leaching issue. Applied Organometallic Chemistry 2008;22(6):288-99.

[365] Calderone RA, Fonzi WA. Virulence factors of Candida albicans. Trends in Microbiology 2001;9(7):327-35.

[366] Campbell JL, Coyer FM, Mudge AM, Robertson IM, Osborne SR. Candida albicans colonisation, continence status and incontinence-associated dermatitis in the acute care setting: a pilot study. International Wound Journal 2017;14(3):488-95.

[367] Fisher JF, Chew WH, Shadomy S, Duma RJ, Mayhan CG, House WC. Urinary Tract Infections Due to Candida albicans. Reviews of Infectious Diseases 1982;4(6):1107-18.

[368] Nikawa H, Yamashiro H, Makihira S, Nishimura M, Egusa H, Furukawa M, Setijanto D, Hamada T. In vitro cariogenic potential of Candida albicans. Mycoses 2003;46(11-12):471-8.

[369] Ramage G, Martínez JP, López-Ribot JL. Candida biofilms on implanted biomaterials: a clinically significant problem. FEMS Yeast Research 2006;6(7):979-86.

[370] Low W-L, Kenward K, Britland ST, Amin MCIM, Martin C. Essential oils and metal ions as alternative antimicrobial agents: a focus on tea tree oil and silver. International Wound Journal 2016;14(2):369-84.

[371] Eshraghi S, Das S. Mechanical and microstructural properties of polycaprolactone scaffolds with one-dimensional, two-dimensional, and three-dimensional orthogonally oriented porous architectures produced by selective laser sintering. Acta Biomaterialia 2010;6(7):2467-76.

[372] Bordes C, Fréville V, Ruffin E, Marote P, Gauvrit JY, Briançon S, Lantéri P. Determination of poly(ε-caprolactone) solubility parameters: Application to solvent substitution in a microencapsulation process. International Journal of Pharmaceutics 2010;383(1):236-43.

[373] Laturnus F, Haselmann KF, Borch T, Grøn C. Terrestrial natural sources of trichloromethane (chloroform, CHCl3) – An overview. Biogeochemistry 2002;60(2):121-39.

[374] Gribble GW. Natural Organohalogens: A New Frontier for Medicinal Agents? Journal of Chemical Education 2004;81(10):1441.

[375] Cappelletti M, Frascari D, Zannoni D, Fedi S. Microbial degradation of chloroform. Applied Microbiology and Biotechnology 2012;96(6):1395-409.

[376] Go KS, Kim Y, Real Son S, Kim SD. 1,2-Dichloroethane production by two-step oxychlorination reactions in a fluidized bed reactor. Chemical Engineering Science 2010;65(1):499-503.

[377] Lessells G, Corrigan T. Azeotropic Data on Chlorinated Hydrocarbons. Industrial & Engineering Chemistry Chemical & Engineering Data Series 1958;3(1):43-4.

[378] Vasudevan V, Mushrif SH. Force field parameters for N,N-Dimethylformamide (DMF) revisited: Improved prediction of bulk properties and complete miscibility in water. Journal of Molecular Liquids 2015;206:338-42.

[379] Hansjörg Bipp HK. Formamides. Ullmann's Encyclopedia of Industrial Chemistry. Wiley; 2011.

[380] Fowles J, Boatman R, Bootman J, Lewis C, Morgott D, Rushton E, van Rooij J, Banton M. A review of the toxicological and environmental hazards and risks of tetrahydrofuran. Critical Reviews in Toxicology 2013;43(10):811-28.

[381] Specht J, Murray L. Jet ink compositions containing tetrahydrofuran solvent. Google Patents; 1979.

[382] Gao S, House W, Chapman WG. NMR/MRI Study of Clathrate Hydrate Mechanisms. The Journal of Physical Chemistry B 2005;109(41):19090-3.

[383] Boor JW, Hurtig HI. Persistent cerebellar ataxia after exposure to toluene. Annals of Neurology 1977;2(5):440-2.

[384] Ogawa H, Koh T, Taya K, Chihara T. Catalysis at the Toluene/Water Interface: Octadecyl Immobilized H-ZSM-5 Catalyst Promoted Hydrolysis of Water-Insoluble Esters. Journal of Catalysis 1994;148(2):493-500.

[385] Madkour AE, Dabkowski JM, Nüsslein K, Tew GN. Fast Disinfecting Antimicrobial Surfaces. Langmuir 2009;25(2):1060-7.

[386] Picheth GF, Pirich CL, Sierakowski MR, Woehl MA, Sakakibara CN, de Souza CF, Martin AA, da Silva R, de Freitas RA. Bacterial cellulose in biomedical applications: A review. International Journal of Biological Macromolecules 2017;104:97-106.

[387] Portela R, Leal CR, Almeida PL, Sobral RG. Bacterial cellulose: a versatile biopolymer for wound dressing applications. Microbial Biotechnology 2019;12(4):586-610.

[388] Ahmed J, Gultekinoglu M, Edirisinghe M. Bacterial cellulose micro-nano fibres for wound healing applications. Biotechnology Advances 2020:107549.

[389] B C N, J H. Antimicrobial Potential of Honey on some Microbial Isolates. Sultan Qaboos University Medical Journal [SQUMJ]; Vol 2, No 2 (2000): October 2000.

[390] Mandal MD, Mandal S. Honey: its medicinal property and antibacterial activity. Asian Pacific journal of tropical biomedicine 2011;1(2):154-60.

[391] Boateng J, Diunase KN. Comparing the Antibacterial and Functional Properties of Cameroonian and Manuka Honeys for Potential Wound Healing-Have We Come Full Cycle in Dealing with Antibiotic Resistance? Molecules 2015;20(9):16068-84.

[392] Altun E, Aydogdu MO, Crabbe-Mann M, Ahmed J, Brako F, Karademir B, Aksu B, Sennaroglu M, Eroglu MS, Ren G, Gunduz O, Edirisinghe M. Co-Culture of Keratinocyte-Staphylococcus aureus on Cu-Ag-Zn/CuO and Cu-Ag-W Nanoparticle Loaded Bacterial Cellulose:PMMA Bandages. Macromolecular Materials and Engineering 2018:1800537.

[393] Altun E, Aydogdu MO, Togay SO, Sengil AZ, Ekren N, Haskoylu ME, Oner ET, Altuncu NA, Ozturk G, Crabbe-Mann M, Ahmed J, Gunduz O, Edirisinghe M. Bioinspired Scaffold Induced Regeneration of Neural Tissue. European Polymer Journal 2019;114(2019):98-108.

[394] Ren G, Hu D, Cheng EWC, Vargas-Reus MA, Reip P, Allaker RP. Characterisation of copper oxide nanoparticles for antimicrobial applications. International Journal of Antimicrobial Agents 2009;33(6):587-90.

[395] Ma L, Gao C, Mao Z, Zhou J, Shen J, Hu X, Han C. Collagen/chitosan porous scaffolds with improved biostability for skin tissue engineering. Biomaterials 2003;24(26):4833-41.

[396] Sionkowska A, Wisniewski M, Skopinska J, Kennedy CJ, Wess TJ. Molecular interactions in collagen and chitosan blends. Biomaterials 2004;25(5):795-801.

[397] Ahmed J, Altun E, Aydogdu MO, Gunduz O, Kerai L, Ren G, Edirisinghe M. Anti-fungal bandages containing cinnamon extract. International Wound Journal 2019;16(3):730-6.

[398] Alenezi H, Cam ME, Edirisinghe M. Experimental and theoretical investigation of the fluid behavior during polymeric fiber formation with and without pressure. Applied Physics Reviews 2019;6(4):041401.

[399] Tabish TA, Memon FA, Gomez DE, Horsell DW, Zhang S. A facile synthesis of porous graphene for efficient water and wastewater treatment. Scientific Reports 2018;8(1):1817.

[400] Khalil AME, Memon FA, Tabish TA, Salmon D, Zhang S, Butler D. Nanostructured porous graphene for efficient removal of emerging contaminants (pharmaceuticals) from water. Chemical Engineering Journal 2020;398:125440.

[401] Tabish TA, Pranjol MZI, Hayat H, Rahat AAM, Abdullah TM, Whatmore JL, Zhang S. In vitro toxic effects of reduced graphene oxide nanosheets on lung cancer cells. Nanotechnology 2017;28(50):504001.

[402] Hedley G. Solubility parameters and varnish removal: a survey. The Conservator 1980;4(1):12-8.

[403] McKee MG, Elkins CL, Long TE. Influence of self-complementary hydrogen bonding on solution rheology/electrospinning relationships. Polymer 2004;45(26):8705-15.

[404] Colby RH, Fetters LJ, Funk WG, Graessley WW. Effects of Concentration and Thermodynamic Interaction on the Viscoelastic Properties of Polymer Solutions. Macromolecules 1991;24(13):3873-82.

[405] J. Vandenburg H, A. Clifford A, D. Bartle K, E. Carlson R, Carroll J, D. Newton I. A simple solvent selection method for accelerated solvent extraction of additives from polymers. Analyst 1999;124(11):1707-10.

[406] Luo CJ, Nangrejo M, Edirisinghe M. A novel method of selecting solvents for polymer electrospinning. Polymer 2010;51(7):1654-62.

[407] Vyazovkin S, Wight CA. Kinetics In Solids. Annual Review of Physical Chemistry 1997;48(1):125-49.

[408] Herrero-Herrero M, Gómez-Tejedor JA, Vallés-Lluch A. PLA/PCL electrospun membranes of tailored fibres diameter as drug delivery systems. European Polymer Journal 2018;99:445-55.

[409] Steinhauser MO. A molecular dynamics study on universal properties of polymer chains in different solvent qualities. Part I. A review of linear chain properties. The Journal of Chemical Physics 2005;122(9):094901.

[410] Gee GAG, Wilson GJ. Intermolecular forces and chain flexibilities in polymers: I. Internal pressures and cohesive energy densities of simple liquids. Polymer 1960;1:456-66.

[411] Wu S. Calculation of interfacial tension in polymer systems. Journal of Polymer Science Part C: Polymer Symposia 1971;34(1):19-30.

[412] Billmeyer Jr FW. Trends in polymer characterization. Journal of Polymer Science: Polymer Symposia 1976;55(1):1-10.

[413] Oosawa F, Asakura S. Surface Tension of High-Polymer Solutions. The Journal of Chemical Physics 1954;22(7):1255-.

[414] van der Gucht J, Besseling NAM, Knoben W, Bouteiller L, Cohen Stuart MA. Brownian particles in supramolecular polymer solutions. Physical Review E 2003;67(5):051106.

[415] Casasola R, Thomas NL, Trybala A, Georgiadou S. Electrospun poly lactic acid (PLA) fibres: Effect of different solvent systems on fibre morphology and diameter. Polymer 2014;55(18):4728-37.

[416] Tam KC, Wu XY, Pelton RH. Poly(N-isopropylacrylamide). II. Effect of polymer concentration, temperature, and surfactant on the viscosity of aqueous solutions. Journal of Polymer Science Part A: Polymer Chemistry 1993;31(4):963-9.

[417] Fong H, Chun I, Reneker DH. Beaded nanofibers formed during electrospinning. Polymer 1999;40(16):4585-92.

[418] Zhang YZ, Feng Y, Huang ZM, Ramakrishna S, Lim CT. Fabrication of porous electrospun nanofibres. Nanotechnology 2006;17(3):901-8.

[419] Hu X, Liu S, Zhou G, Huang Y, Xie Z, Jing X. Electrospinning of polymeric nanofibers for drug delivery applications. Journal of Controlled Release 2014;185(Supplement C):12-21.

[420] Natarajan L, New J, Dasari A, Yu S, Manan MA. Surface morphology of electrospun PLA fibers: mechanisms of pore formation. RSC Advances 2014;4(83):44082-8.

[421] Matthews JA, Wnek GE, Simpson DG, Bowlin GL. Electrospinning of Collagen Nanofibers. Biomacromolecules 2002;3(2):232-8.

[422] Huang Z-M, Zhang YZ, Ramakrishna S, Lim CT. Electrospinning and mechanical characterization of gelatin nanofibers. Polymer 2004;45(15):5361-8.

[423] Koombhongse S, Liu W, Reneker DH. Flat polymer ribbons and other shapes by electrospinning. Journal of Polymer Science Part B: Polymer Physics 2001;39(21):2598-606.

[424] Mahalingam S, Raimi-Abraham BT, Craig DQM, Edirisinghe M. Solubility–spinnability map and model for the preparation of fibres of polyethylene (terephthalate) using gyration and pressure. Chemical Engineering Journal 2015;280(Supplement C):344-53.

[425] O'Connell JP, Prausnitz JM. Thermodynamics of Gas Solubility in Mixed Solvents. Industrial & Engineering Chemistry Fundamentals 1964;3(4):347-51.

[426] Divvela MJ, Joo YL. Discretized modeling of beads-on-a-string morphology from electrically driven, conducting, and viscoelastic polymer jets. Journal of Applied Physics 2017;121(13):134306.

[427] Altun E, Ahmed J, Onur Aydogdu M, Harker A, Edirisinghe M. The Effect of Solvent and Pressure on Polycaprolactone Solutions for Particle and Fibre Formation. European Polymer Journal 2022:111300.

[428] Graessley WW. The entanglement concept in polymer rheology. The Entanglement Concept in Polymer Rheology. Berlin, Heidelberg: Springer Berlin Heidelberg; 1974, p. 1-179.

[429] Shenoy SL, Bates WD, Frisch HL, Wnek GE. Role of chain entanglements on fiber formation during electrospinning of polymer solutions: good solvent, non-specific polymer–polymer interaction limit. Polymer 2005;46(10):3372-84.

[430] Huang M-H, Li S, Vert M. Synthesis and degradation of PLA–PCL–PLA triblock copolymer prepared by successive polymerization of ε-caprolactone and dl-lactide. Polymer 2004;45(26):8675-81.

[431] Li Z, Yin X, Qin J, Zhu L. Preparation and hemocompatibility of electrospun Bacteria Cellulose Sulfate/Polyvinyl Alcohol nanofibrous

composite membrane. IOP Conference Series: Materials Science and Engineering 2018;382:022005.

[432] Aydogdu MO, Altun E, Crabbe-Mann M, Brako F, Koc F, Ozen G, Kuruca SE, Edirisinghe U, Luo CJ, Gunduz O, Edirisinghe M. Cellular interactions with bacterial cellulose: Polycaprolactone nanofibrous scaffolds produced by a portable electrohydrodynamic gun for point-of-need wound dressing. International Wound Journal 2018;15(5):789-97.

[433] Lu L, Wu D, Zhang M, Zhou W. Fabrication of Polylactide/Poly(ε-caprolactone) Blend Fibers by Electrospinning: Morphology and Orientation. Industrial & Engineering Chemistry Research 2012;51(9):3682-91.

[434] Hong X, Harker A, Edirisinghe M. Process Modeling for the Fiber Diameter of Polymer, Spun by Pressure-Coupled Infusion Gyration. ACS Omega 2018;3(5):5470-9.

[435] Vo PP, Doan NH, Kinashi K, Sakai W, Tsutsumi N, Huynh PD. Centrifugally Spun Recycled PET: Processing and Characterization. Polymers 2018;10(6).

[436] Khan TA, Peh KK, Ch'ng HS. Reporting degree of deacetylation values of chitosan: the influence of analytical methods. Journal of Pharmacy & Pharmaceutical Sciences 2002;5(3):205-12.

[437] Matta AK, Rao RU, Suman KNS, Rambabu V. Preparation and Characterization of Biodegradable PLA/PCL Polymeric Blends. Procedia Materials Science 2014;6:1266-70.

[438] Abdellah Ali SF. Mechanical and thermal properties of promising polymer composites for food packaging applications. IOP Conference Series: Materials Science and Engineering 2016;137:012035.

[439] Ostafinska A, Fortelny I, Nevoralova M, Hodan J, Kredatusova J, Slouf M. Synergistic effects in mechanical properties of PLA/PCL blends with optimized composition, processing, and morphology. RSC Advances 2015;5(120):98971-82.

[440] Takayama T, Todo M, Tsuji H. Effect of annealing on the mechanical properties of PLA/PCL and PLA/PCL/LTI polymer blends. Journal of the Mechanical Behavior of Biomedical Materials 2011;4(3):255-60.

[441] Kriel H, D. Sanderson R, Smit E. Single Polymer Composite Yarns and Films Prepared from Heat Bondable Poly(lactic acid) Core-shell Fibres with Submicron Fibre Diameters. Fibres and Textiles in Eastern Europe 2013;100:44-7.

[442] Wu Y-B, Yu S-H, Mi F-L, Wu C-W, Shyu S-S, Peng C-K, Chao A-C. Preparation and characterization on mechanical and antibacterial properties of chitsoan/cellulose blends. Carbohydrate Polymers 2004;57(4):435-40.

[443] White JW, Jr., Subers MH, Schepartz AI. The identification of inhibine, the antibacterial factor in honey, as hydrogen peroxide and its origin in a honey glucose-oxidase system. Biochimica et Biophysica Acta 1963;73:57-70.

[444] Bucekova M, Valachova I, Kohutova L, Prochazka E, Klaudiny J, Majtan J. Honeybee glucose oxidase--its expression in honeybee workers and comparative analyses of its content and H2O2-mediated antibacterial activity in natural honeys. Die Naturwissenschaften 2014;101(8):661-70.

[445] de Graft-Johnson J, Nowak D. Effect of Selected Plant Phenolics on Fe(2+)-EDTA-H_2O_2 System Mediated Deoxyribose Oxidation: Molecular Structure-Derived Relationships of Anti- and Pro-Oxidant Actions. Molecules (Basel, Switzerland) 2016;22(1):59.

[446] Brudzynski K, Abubaker K, Miotto D. Unraveling a mechanism of honey antibacterial action: polyphenol/H(2)O(2)-induced oxidative effect on bacterial cell growth and on DNA degradation. Food Chemistry 2012;133(2):329-36.

[447] Liu X, Li J, Wang Y, Li T, Zhao J, Zhang C. Green tea polyphenols function as prooxidants to inhibit Pseudomonas aeruginosa and induce the expression of oxidative stress-related genes. Folia Microbiologica 2013;58(3):211-7.

[448] Kwakman PHS, te Velde AA, de Boer L, Vandenbroucke-Grauls CMJE, Zaat SAJ. Two Major Medicinal Honeys Have Different Mechanisms of Bactericidal Activity. PloS One 2011;6(3):e17709.

[449] Adams CJ, Boult CH, Deadman BJ, Farr JM, Grainger MN, Manley-Harris M, Snow MJ. Isolation by HPLC and characterisation of the

bioactive fraction of New Zealand manuka (Leptospermum scoparium) honey. Carbohydrate Research 2008;343(4):651-9.

[450] Mavric E, Wittmann S, Barth G, Henle T. Identification and quantification of methylglyoxal as the dominant antibacterial constituent of Manuka (Leptospermum scoparium) honeys from New Zealand. Molecular Nutrition & Food Research 2008;52(4):483-9.

[451] Krymkiewicz N, Dieguez E, Rekarte UD, Zwaig N. Properties and mode of action of a bactericidal compound (=methylglyoxal) produced by a mutant of Escherichia coli. Journal of Bacteriology 1971;108(3):1338-47.

[452] Hayashi K, Fukushima A, Hayashi-Nishino M, Nishino K. Effect of methylglyoxal on multidrug-resistant Pseudomonas aeruginosa. Frontiers in Microbiology 2014;5:180-.

[453] Kalapos MP. The tandem of free radicals and methylglyoxal. Chemico-Biological Interactions 2008;171(3):251-71.

[454] Girma A, Seo W, She RC. Antibacterial activity of varying UMF-graded Manuka honeys. PloS One 2019;14(10):e0224495-e.

[455] Garcia JM, Chambers E, Matta Z, Clark M. Viscosity Measurements of Nectar- and Honey-thick Liquids: Product, Liquid, and Time Comparisons. Dysphagia 2005;20(4):325-35.

[456] De Vrieze S, Van Camp T, Nelvig A, Hagström B, Westbroek P, De Clerck K. The effect of temperature and humidity on electrospinning. Journal of Materials Science 2009;44(5):1357-62.

[457] Mahalingam S, Pierin G, Colombo P, Edirisinghe M. Facile one-pot formation of ceramic fibres from preceramic polymers by pressurised gyration. Ceramics International 2015;41(4):6067-73.

[458] Obregon N, Agubra V, Pokhrel M, Campos H, Flores D, De la Garza D, Mao Y, Macossay J, Alcoutlabi M. Effect of Polymer Concentration, Rotational Speed, and Solvent Mixture on Fiber Formation Using Forcespinning®. Fibers 2016;4(2).

[459] Zhang X, Lu Y. Centrifugal spinning: An alternative approach to fabricate nanofibers at high speed and low cost. Polymer Reviews 2014;54(4):677-701.

[460] Nezarati RM, Eifert MB, Cosgriff-Hernandez E. Effects of Humidity and Solution Viscosity on Electrospun Fiber Morphology. Tissue Engineering Part C: Methods 2013;19(10):810-9.

[461] Ramakrishna S, Fujihara K, Teo W-E, Yong T, Ma Z, Ramaseshan R. Electrospun nanofibers: solving global issues. Materials Today 2006;9(3):40-50.

[462] Tonks AJ, Cooper RA, Jones KP, Blair S, Parton J, Tonks A. Honey stimulates inflammatory cytokine production from monocytes. Cytokine 2003;21(5):242-7.

[463] Werner S, Krieg T, Smola H. Keratinocyte–Fibroblast Interactions in Wound Healing. Journal of Investigative Dermatology 2007;127(5):998-1008.

[464] Martin P. Wound Healing--Aiming for Perfect Skin Regeneration. Science 1997;276(5309):75.

[465] Schultz GS, Wysocki A. Interactions between extracellular matrix and growth factors in wound healing. Wound Repair and Regeneration 2009;17(2):153-62.

[466] He Y, Inoue Y. Novel FTIR method for determining the crystallinity of poly(ε-caprolactone). Polymer International 2000;49(6):623-6.

[467] Elzein T, Nasser-Eddine M, Delaite C, Bistac S, Dumas P. FTIR study of polycaprolactone chain organization at interfaces. Journal of Colloid and Interface Science 2004;273(2):381-7.

[468] Azam NANM, Amin KAM. Influence of Manuka Honey on Mechanical Performance and Swelling Behaviour of Alginate Hydrogel Film. IOP Conference Series: Materials Science and Engineering 2018;440:012024.

[469] Mohd Azam NAN, Amin KAM. The Physical and Mechanical Properties of Gellan Gum Films Incorporated Manuka Honey as Wound Dressing Materials. IOP Conference Series: Materials Science and Engineering 2017;209:012027.

[470] Kasprzyk I, Depciuch J, Grabek-Lejko D, Parlinska-Wojtan M. FTIR-ATR spectroscopy of pollen and honey as a tool for unifloral honey authentication. The case study of rape honey. Food Control 2018;84:33-40.

[471] Persano L, Camposeo A, Tekmen C, Pisignano D. Industrial Upscaling of Electrospinning and Applications of Polymer Nanofibers: A Review. 2013.

[472] Vuong C, Otto M. Staphylococcus epidermidis infections. Microbes and Infection 2002;4(4):481-9.

[473] Heilmann C, Schweitzer O, Gerke C, Vanittanakom N, Mack D, Götz F. Molecular basis of intercellular adhesion in the biofilm-forming Staphylococcus epidermidis. Molecular Microbiology 1996;20(5):1083-91.

[474] Otto M. Staphylococcus epidermidis — the 'accidental' pathogen. Nature Reviews Microbiology 2009;7:555.

[475] Almasaudi SB, El-Shitany NA, Abbas AT, Abdel-dayem UA, Ali SS, Al Jaouni SK, Harakeh S. Antioxidant, Anti-inflammatory, and Antiulcer Potential of Manuka Honey against Gastric Ulcer in Rats. Oxidative Medicine and Cellular Longevity 2016;2016:10.

[476] Visavadia BG, Honeysett J, Danford MH. Manuka honey dressing: An effective treatment for chronic wound infections. British Journal of Oral and Maxillofacial Surgery 2008;46(1):55-6.

[477] Jull AB, Cullum N, Dumville JC, Westby MJ, Deshpande S, Walker N. Honey as a topical treatment for wounds. Cochrane Database of Systematic Reviews 2015(3).

[478] Ulery BD, Nair LS, Laurencin CT. Biomedical Applications of Biodegradable Polymers. Journal of polymer science Part B, Polymer physics 2011;49(12):832-64.

[479] Pilapil VR. Toxic manifestations of cinnamon oil ingestion in a child. Clinical Pediatrics 1989;28(6):276.

[480] Cooper KE. CHAPTER 1 - The Theory of Antibiotic Inhibition Zones. In: Kavanagh F, editor Analytical Microbiology. Academic Press; 1963, p. 1-86.

[481] Hong S-H, Ismail IA, Kang S-M, Han DC, Kwon B-M. Cinnamaldehydes in Cancer Chemotherapy. Phytotherapy Research 2016;30(5):754-67.

[482] Akiyama H, Fujii K, Yamasaki O, Oono T, Iwatsuki K. Antibacterial action of several tannins against Staphylococcus aureus. Journal of Antimicrobial Chemotherapy 2001;48(4):487-91.

[483] Gill AO, Holley RA. Mechanisms of Bactericidal Action of Cinnamaldehyde against Listeria monocytogenes and of Eugenol against L. monocytogenes and Lactobacillus sakei. Applied and Environmental Microbiology 2004;70(10):5750.

[484] Fabio A, Cermelli C, Fabio G, Nicoletti P, Quaglio P. Screening of the antibacterial effects of a variety of essential oils on microorganisms responsible for respiratory infections. Phytotherapy Research 2007;21(4):374-7.

[485] Kannon GA, Garrett AB. Moist wound healing with occlusive dressings. A clinical review. Dermatologic Surgery 1995;21(7):583-90.

[486] Hooper SJ, Percival SL, Hill KE, Thomas DW, Hayes AJ, Williams DW. The visualisation and speed of kill of wound isolates on a silver alginate dressing. International Wound Journal 2012;9(6):633-42.

[487] Gautam S, Dinda AK, Mishra NC. Fabrication and characterization of PCL/gelatin composite nanofibrous scaffold for tissue engineering applications by electrospinning method. Materials Science and Engineering: C 2013;33(3):1228-35.

[488] Cox SC, Thornby JA, Gibbons GJ, Williams MA, Mallick KK. 3D printing of porous hydroxyapatite scaffolds intended for use in bone tissue engineering applications. Materials Science and Engineering: C 2015;47:237-47.

[489] Fumal I, Braham C, Paquet P, Piérard-Franchimont C, Piérard GE. The Beneficial Toxicity Paradox of Antimicrobials in Leg Ulcer Healing Impaired by a Polymicrobial Flora: A Proof-of-Concept Study. Dermatology 2002;204(suppl 1)(Suppl. 1):70-4.

[490] Gultekinoglu M, Tunc Sarisozen Y, Erdogdu C, Sagiroglu M, Aksoy EA, Oh YJ, Hinterdorfer P, Ulubayram K. Designing of dynamic polyethyleneimine (PEI) brushes on polyurethane (PU) ureteral stents to prevent infections. Acta Biomaterialia 2015;21:44-54.

[491] Cipitria A, Skelton A, Dargaville TR, Dalton PD, Hutmacher DW. Design, fabrication and characterization of PCL electrospun scaffolds—a review. Journal of Materials Chemistry 2011;21(26):9419-53.

[492] Amiri S, Rahimi A. Poly(ε-caprolactone) electrospun nanofibers containing cinnamon essential oil nanocapsules: A promising technique

for controlled release and high solubility. Journal of Industrial Textiles 2018;48(10):1527-44.

[493] Salehi M, Niyakan M, Ehterami A, Haghi-Daredeh S, Nazarnezhad S, Abbaszadeh-Goudarzi G, Vaez A, Hashemi SF, Rezaei N, Mousavi SR. Porous electrospun poly(ε-caprolactone)/gelatin nanofibrous mat containing cinnamon for wound healing application: in vitro and in vivo study. Biomedical Engineering Letters 2020;10(1):149-61.

[494] Jain A, Bhargava R, Poddar P. Probing interaction of Gram-positive and Gram-negative bacterial cells with ZnO nanorods. Materials Science and Engineering: C 2013;33(3):1247-53.

[495] Zhang Y, Liu X, Wang Y, Jiang P, Quek S. Antibacterial activity and mechanism of cinnamon essential oil against Escherichia coli and Staphylococcus aureus. Food Control 2016;59:282-9.

[496] Borisova M, Gaupp R, Duckworth A, Schneider A, Dalügge D, Mühleck M, Deubel D, Unsleber S, Yu W, Muth G, Bischoff M, Götz F, Mayer C. Peptidoglycan recycling in Gram-positive bacteria is crucial for survival in stationary phase. mBio 2016;7(5):e00923-16.

[497] Julianti E, Rajah KK, Fidrianny I. Antibacterial activity of ethanolic extract of cinnamon bark, honey, and their combination effects against acne-causing bacteria. Scientia pharmaceutica 2017;85(2):19.

[498] Hamidpour R, Hamidpour M, Hamidpour S, Shahlari M. Cinnamon from the selection of traditional applications to its novel effects on the inhibition of angiogenesis in cancer cells and prevention of Alzheimer's disease, and a series of functions such as antioxidant, anticholesterol, antidiabetes, antibacterial, antifungal, nematicidal, acaracidal, and repellent activities. Journal of traditional and complementary medicine 2015;5(2):66-70.

[499] Ng KW, Achuth HN, Moochhala S, Lim TC, Hutmacher DW. In vivo evaluation of an ultra-thin polycaprolactone film as a wound dressing. Journal of Biomaterials Science, Polymer Edition 2007;18(7):925-38.

[500] Tan EPS, Ng SY, Lim CT. Tensile testing of a single ultrafine polymeric fiber. Biomaterials 2005;26(13):1453-6.

[501] Seyednejad H, Gawlitta D, Kuiper RV, de Bruin A, van Nostrum CF, Vermonden T, Dhert WJA, Hennink WE. In vivo biocompatibility and

biodegradation of 3D-printed porous scaffolds based on a hydroxyl-functionalized poly(ε-caprolactone). Biomaterials 2012;33(17):4309-18.

[502] Stevens MM, George JH. Exploring and Engineering the Cell Surface Interface. Science 2005;310(5751):1135.

[503] Parkinson LG, Giles NL, Adcroft KF, Fear MW, Wood FM, Poinern GE. The Potential of Nanoporous Anodic Aluminium Oxide Membranes to Influence Skin Wound Repair. Tissue Engineering Part A 2009;15(12):3753-63.

[504] Atiyeh BS, Ioannovich J, Al-Amm CA, El-Musa KA. Management of acute and chronic open wounds: the importance of moist environment in optimal wound healing. Current Pharmaceutical Biotechnology 2002;3(3):179-95.

[505] Wiechula R. The use of moist wound-healing dressings in the management of split-thickness skin graft donor sites: a systematic review. International Journal of Nursing Practice 2003;9(2):S9-17.

[506] Pilcher BK, Dumin JA, Sudbeck BD, Krane SM, Welgus HG, Parks WC. The Activity of Collagenase-1 Is Required for Keratinocyte Migration on a Type I Collagen Matrix. The Journal of Cell Biology 1997;137(6):1445.

[507] Senel S, McClure SJ. Potential applications of chitosan in veterinary medicine. Adv Drug Deliv Rev 2004;56(10):1467-80.

[508] Mariappan MR, Alas EA, Williams JG, Prager MD. Chitosan and chitosan sulfate have opposing effects on collagen–fibroblast interactions. Wound Repair and Regeneration 2008;7(5):400-6.

[509] Ueno H, Mori T, Fujinaga T. Topical formulations and wound healing applications of chitosan. Advanced Drug Delivery Reviews 2001;52(2):105-15.

[510] Clark RA. Biology of dermal wound repair. Dermatologic Clinics 1993;11(4):647-66.

[511] Maquart FX, Monboisse JC. Extracellular matrix and wound healing. Pathologie Biologie 2014;62(2):91-5.

[512] Campaniello D, Bevilacqua A, Sinigaglia M, Corbo MR. Chitosan: Antimicrobial activity and potential applications for preserving minimally processed strawberries. Food Microbiology 2008;25(8):992-1000.

[513] Cuero RG. Antimicrobial action of exogenous chitosan. EXS 1999;87:315-33.

[514] Zheng L-Y, Zhu J-F. Study on antimicrobial activity of chitosan with different molecular weights. Carbohydrate Polymers 2003;54(4):527-30.

[515] Lima CGA, de Oliveira RS, Figueiró SD, Wehmann CF, Góes JC, Sombra ASB. DC conductivity and dielectric permittivity of collagen–chitosan films. Materials Chemistry and Physics 2006;99(2):284-8.

[516] Chen L, Zheng L, Lv Y, Liu H, Wang G, Ren N, Liu D, Wang J, Boughton RI. Chemical assembly of silver nanoparticles on stainless steel for antimicrobial applications. Surface and Coatings Technology 2010;204(23):3871-5.

[517] Vargas-Reus MA, Memarzadeh K, Huang J, Ren GG, Allaker RP. Antimicrobial activity of nanoparticulate metal oxides against peri-implantitis pathogens. International Journal of Antimicrobial Agents 2012;40(2):135-9.

[518] Sankaran KK, Vasanthan KS, Krishnan UM, Sethuraman S. Development and evaluation of axially aligned nanofibres for blood vessel tissue engineering. Journal of Tissue Engineering and Regenerative Medicine 2014;8(8):640-51.

[519] McDougall S, Dallon J, Sherratt J, Maini P. Fibroblast migration and collagen deposition during dermal wound healing: mathematical modelling and clinical implications. Philosophical Transactions of the Royal Society A: Mathematical, Physical and Engineering Sciences 2006;364(1843):1385-405.

[520] Wee H, Wagoner BW, Kamat PM, Basaran OA. Effects of Surface Viscosity on Breakup of Viscous Threads. Physical Review Letters 2020;124(20):204501.

[521] Girit ÇÖ, Meyer JC, Erni R, Rossell MD, Kisielowski C, Yang L, Park C-H, Crommie MF, Cohen ML, Louie SG, Zettl A. Graphene at the Edge: Stability and Dynamics. Science 2009;323(5922):1705.

[522] Balandin AA, Ghosh S, Bao W, Calizo I, Teweldebrhan D, Miao F, Lau CN. Superior Thermal Conductivity of Single-Layer Graphene. Nano Letters 2008;8(3):902-7.

[523] Wu ZS, Ren W, Gao L, Zhao J, Chen Z, Liu B, Tang D, Yu B, Jiang C, Cheng HM. Synthesis of graphene sheets with high electrical conductivity and good thermal stability by hydrogen arc discharge exfoliation. ACS Nano 2009;3(2):411-7.

[524] Wang G, Shen X, Yao J, Park J. Graphene nanosheets for enhanced lithium storage in lithium ion batteries. Carbon 2009;47(8):2049-53.

[525] Liang J, Wang Y, Huang Y, Ma Y, Liu Z, Cai J, Zhang C, Gao H, Chen Y. Electromagnetic interference shielding of graphene/epoxy composites. Carbon 2009;47(3):922-5.

[526] Wang J, Suzuki R, Ogata K, Nakamura T, Dong A, Weng W. Near-Linear Responsive and Wide-Range Pressure and Stretch Sensor Based on Hierarchical Graphene-Based Structures via Solvent-Free Preparation. Polymers 2020;12(8).

[527] Matharu RK, Porwal H, Ciric L, Edirisinghe M. The effect of graphene–poly(methyl methacrylate) fibres on microbial growth. Interface Focus 2018;8(3).

[528] Alazmi A, El Tall O, Rasul S, Hedhili MN, Patole SP, Costa PMFJ. A process to enhance the specific surface area and capacitance of hydrothermally reduced graphene oxide. Nanoscale 2016;8(41):17782-7.

[529] Du M, Sun J, Chang J, Yang F, Shi L, Gao L. Synthesis of nitrogen-doped reduced graphene oxide directly from nitrogen-doped graphene oxide as a high-performance lithium ion battery anode. RSC Advances 2014;4(80):42412-7.

[530] Tabish TA, Pranjol MZI, Jabeen F, Abdullah T, Latif A, Khalid A, Ali M, Hayat H, Winyard PG, Whatmore JL, Zhang S. Investigation into the toxic effects of graphene nanopores on lung cancer cells and biological tissues. Applied Materials Today 2018;12:389-401.

[531] Paek S-M, Yoo E, Honma I. Enhanced Cyclic Performance and Lithium Storage Capacity of SnO2/Graphene Nanoporous Electrodes with Three-Dimensionally Delaminated Flexible Structure. Nano Letters 2009;9(1):72-5.

[532] Ahmed J, Tabish TA, Zhang S, Edirisinghe M. Porous Graphene Composite Polymer Fibres. Polymers 2021;13(1).

[533] Sun B, Sirringhaus H. Surface Tension and Fluid Flow Driven Self-Assembly of Ordered ZnO Nanorod Films for High-Performance Field Effect Transistors. Journal of the American Chemical Society 2006;128(50):16231-7.

[534] Wang S, Zhang Y, Abidi N, Cabrales L. Wettability and Surface Free Energy of Graphene Films. Langmuir 2009;25(18):11078-81.

[535] Hernandez Y, Nicolosi V, Lotya M, Blighe FM, Sun Z, De S, McGovern IT, Holland B, Byrne M, Gun'Ko YK, Boland JJ, Niraj P, Duesberg G, Krishnamurthy S, Goodhue R, Hutchison J, Scardaci V, Ferrari AC, Coleman JN. High-yield production of graphene by liquid-phase exfoliation of graphite. Nature Nanotechnology 2008;3:563.

[536] Nasouri K, Shoushtari AM, Kaflou A. Investigation of polyacrylonitrile electrospun nanofibres morphology as a function of polymer concentration, viscosity and berry number. Micro & Nano Letters 2012;7(5):423-6.

[537] Nguyen BD, Ngo TK, Bui TH, Pham DK, Dinh XL, Nguyen PT. The impact of graphene oxide particles on viscosity stabilization for diluted polymer solutions using in enhanced oil recovery at HTHP offshore reservoirs. Advances in Natural Sciences: Nanoscience and Nanotechnology 2014;6(1):015012.

[538] Ansón-Casaos A, Ciria JC, Sanahuja-Parejo O, Víctor-Román S, González-Domínguez JM, García-Bordejé E, Benito AM, Maser WK. The viscosity of dilute carbon nanotube (1D) and graphene oxide (2D) nanofluids. Physical Chemistry Chemical Physics 2020;22(20):11474-84.

[539] Müller M, Schmalian J, Fritz L. Graphene: A Nearly Perfect Fluid. Physical Review Letters 2009;103(2):025301.

[540] Cabaleiro D, Estellé P, Navas H, Desforges A, Vigolo B. Dynamic Viscosity and Surface Tension of Stable Graphene Oxide and Reduced Graphene Oxide Aqueous Nanofluids. Journal of Nanofluids 2018;7(6):1081-8.

[541] Xu M, Liu H, Zhao H, Li W. How to Decrease the Viscosity of Suspension with the Second Fluid and Nanoparticles? Scientific Reports 2013;3(1):3137.

[542] Ahmed J, Matharu RK, Shams T, Illangakoon UE, Edirisinghe M. A Comparison of Electric-Field-Driven and Pressure-Driven Fiber Generation Methods for Drug Delivery. Macromolecular Materials and Engineering 2018:1700577-n/a.

[543] Syms RRA, Zou H, Yao J, Uttamchandani D, Stagg J. Scalable electrothermal MEMS actuator for optical fibre alignment. Journal of Micromechanics and Microengineering 2004;14(12):1633.

[544] Wilczynski AP. A basic theory of reinforcement for unidirectional fibrous composites. Composites Science and Technology 1990;38(4):327-37.

[545] Reid AJ, de Luca AC, Faroni A, Downes S, Sun M, Terenghi G, Kingham PJ. Long term peripheral nerve regeneration using a novel PCL nerve conduit. Neuroscience Letters 2013;544:125-30.

[546] Thompson CJ, Chase GG, Yarin AL, Reneker DH. Effects of parameters on nanofiber diameter determined from electrospinning model. Polymer 2007;48(23):6913-22.

[547] Schlapbach L, Züttel A. Hydrogen-storage materials for mobile applications. Materials for Sustainable Energy. Co-Published with Macmillan Publishers Ltd, UK; 2010, p. 265-70.

[548] Krishnan SK, Singh E, Singh P, Meyyappan M, Nalwa HS. A review on graphene-based nanocomposites for electrochemical and fluorescent biosensors. RSC Advances 2019;9(16):8778-881.

[549] Jiang Z, Feng B, Xu J, Qing T, Zhang P, Qing Z. Graphene biosensors for bacterial and viral pathogens. Biosensors and Bioelectronics 2020;166:112471.

[550] Ahmed J. Electrospinning for the manufacture of biosensor components: A mini-review. Medical Devices & Sensors 2020;n/a(n/a):e10136.

[551] Matharu RK, Tabish TA, Trakoolwilaiwan T, Mansfield J, Moger J, Wu T, Lourenço C, Chen B, Ciric L, Parkin IP, Edirisinghe M. Microstructure and antibacterial efficacy of graphene oxide nanocomposite fibres. Journal of Colloid and Interface Science 2020;571:239-52.

[552] Matharu RK, Porwal H, Chen B, Ciric L, Edirisinghe M. Viral filtration using carbon-based materials. Medical Devices & Sensors 2020;n/a(n/a):e10107.

[553] Huang C-L, Lee K-M, Liu Z-X, Lai R-Y, Chen C-K, Chen W-C, Hsu J-F. Antimicrobial Activity of Electrospun Polyvinyl Alcohol Nanofibers Filled with Poly[2-(tert-butylaminoethyl) Methacrylate]-Grafted Graphene Oxide Nanosheets. Polymers 2020;12(7).

[554] Zapata ME, Ruiz Rojas LM, Mina Hernández JH, Delgado-Ospina J, Tovar CD. Acrylic Bone Cements Modified with Graphene Oxide: Mechanical, Physical, and Antibacterial Properties. Polymers 2020;12(8).

[555] Kucher O, Yungerman I, Srebnik S. Coarse-Grained Model for Sequence-Dependent Adsorption of ssDNA on Carbon Nanotubes. The Journal of Physical Chemistry C 2014;118(31):17677-85.

[556] Rahmat M, Hubert P. Carbon nanotube–polymer interactions in nanocomposites: A review. Composites Science and Technology 2011;72(1):72-84.

[557] Wesełucha-Birczyńska A, Świętek M, Sołtysiak E, Galiński P, Płachta Ł, Piekara K, Błażewicz M. Raman spectroscopy and the material study of nanocomposite membranes from poly(ε-caprolactone) with biocompatibility testing in osteoblast-like cells. Analyst 2015;140(7):2311-20.

[558] Fujisawa K, Lei Y, de Tomas C, Suarez-Martinez I, Zhou C, Lin Y-C, Subramanian S, Elías AL, Fujishige M, Takeuchi K, Robinson JA, Marks NA, Endo M, Terrones M. Facile 1D graphene fiber synthesis from an agricultural by-product: A silicon-mediated graphenization route. Carbon 2019;142:78-88.

[559] Lucchese MM, Stavale F, Ferreira EHM, Vilani C, Moutinho MVO, Capaz RB, Achete CA, Jorio A. Quantifying ion-induced defects and Raman relaxation length in graphene. Carbon 2010;48(5):1592-7.

[560] Gupta A, Chen G, Joshi P, Tadigadapa S, Eklund. Raman Scattering from High-Frequency Phonons in Supported n-Graphene Layer Films. Nano Letters 2006;6(12):2667-73.

[561] Zhu Y, Murali S, Stoller MD, Ganesh KJ, Cai W, Ferreira PJ, Pirkle A, Wallace RM, Cychosz KA, Thommes M, Su D, Stach EA, Ruoff RS. Carbon-Based Supercapacitors Produced by Activation of Graphene. Science 2011;332(6037):1537.

[562] Tabish AT, Pranjol ZM, Horsell WD, Rahat AA, Whatmore LJ, Winyard GP, Zhang S. Graphene Oxide-Based Targeting of Extracellular Cathepsin D and Cathepsin L As A Novel Anti-Metastatic Enzyme Cancer Therapy. Cancers 2019;11(3).

[563] Gökalp N, Ulker C, Guvenilir Y. Synthesis of Polycaprolactone via Ring Opening Polymerization Catalyzed by Candida Antarctica Lipase B Immobilized onto an Amorphous Silica Support. 2016.

[564] Benkaddour A, Jradi K, Robert S, Daneault C. Grafting of Polycaprolactone on Oxidized Nanocelluloses by Click Chemistry. Nanomaterials (Basel) 2013;3(1):141-57.